Transcriptional analysis of the host response to HIV-1 infection in $CD4^+$ T lymphocytes and macrophages

Candidate

Name: Ms. Catherine H Wickham

Student number: 12024041

Submitted in fulfilment of the requirements for the degree

Master of Science (Medical Immunology)

In the Faculty of Health Sciences

Department of Immunology

University of Pretoria

Date: June 2019

Supervisor: Prof Michael S Pepper

Co-Supervisor: Dr Chrisna Durandt

Abstract

The human immunodeficiency virus (HIV) is the causative agent of acquired immune deficiency syndrome (AIDS), a condition characterized by depletion of $CD4^+$ T cells and other immune system dysfunctions. Due to its widespread geographic distribution and ease of transmission, HIV has become a serious global healthcare concern. HIV-1 subtype C (HIV-1-C) is of particular interest since it is the most rapidly expanding and is especially prevalent in southern Africa. In addition, HIV-1-C is poorly studied in comparison to other subtypes. Despite HIV being extensively researched, much is still unknown about the host cell response to infection at a molecular level and how this might be exploited for therapeutic intervention. Therefore, the purpose of this study was to use microarray-based transcriptomic analysis to gain an unbiased perspective of the host cell response in $CD4^+$ T lymphocytes and macrophages when exposed to primary HIV-1-C viruses of different tropisms (R5-tropic, X4-tropic, dual-tropic). In order to achieve this overall aim, we first needed to develop and optimize protocols for the culture of primary HIV-1-C strains. A p24 ELISA assay was used to confirm successful viral replication, followed by functional titration using the GHOST reporter cell line. We found that the efficiency of replication of primary viral isolates was highly stochastic. While many of the strains cultured suffered severe losses of infectivity, we managed to produce infective stocks of dual-tropic and X4-tropic isolates. We next aimed to optimize cell culture protocols for $CD4^+$ T lymphocytes and macrophages that would ensure maximal susceptibility to HIV. Since activation of $CD4^+$ T cells is reported to enhance viral replication, we assessed the efficacy of various activation protocols. We found that antibody-mediated activation was highly successful. Flow cytometric analysis revealed increased cell proliferation and CD25 expression. In addition, $CD4^+$ T-cell activation dramatically increased CXCR4 surface expression while CCR5 expression was diminished. Infection experiments with our dual-tropic isolate confirmed that these cells were susceptible to infection. In order to optimize macrophage cell culture conditions, we compared the effects of differentiation under the influence of different growth factors (M-CSF or GM-CSF). Successful differentiation was determined by phenotypic analysis using flow cytometry coupled with a functional phagocytosis assay. Additional analysis of co-receptor expression revealed extremely low levels of CXCR4 and relatively high CCR5 expression in both macrophage populations. The

differentiated macrophages were completely refractory to infection with our dual-tropic isolate, making them unsuitable for further experiments. The final component of the study was the gene expression analysis itself, which was performed using activated $CD4^+$ T lymphocytes exposed to a dual-tropic isolate (CM9). Differential gene expression analysis revealed altered expression patterns in a relatively small but functionally diverse group of genes involved in apoptosis, deubiquitination, transcriptional regulation and immune system functions. Apoptosis and deubiquitination were identified as statistically overrepresented functional pathways in our subsequent GO-based analysis. Comparison of our findings with previous studies performed using HIV-1-B seems to indicate that while many of the genes observed in our study have not specifically been detected previously, they do tend to belong to similar pathways.

Key words: HIV-1-C, $CD4^+$ T lymphocyte, macrophage, transcriptome, virus-host interaction, microarray, gene expression, viral culture, immunophenotyping, co-receptor

Declaration of Authenticity

I hereby declare the work herein contained to be my own, original work, and that any contributors are appropriately acknowledged. Furthermore, I declare that all source material is cited appropriately, and to my knowledge, neither I nor any declared contributors are aware of any plagiarism in the following work.

Contributor	**Contribution**
Ms C H Wickham	Laboratory work, data analysis and write up of dissertation
Prof M S Pepper	Conceptualization of project, project overview, editing of dissertation
Dr C Durandt	Project overview, editing of dissertation, assistance in laboratory

I hereby submit the following title as my own work, and confirm that all contributors (if any) are listed in the above table.

Title of work:

Transcriptional analysis of the host response to HIV-1 infection in CD4+ T lymphocytes and macrophages

(MSc Dissertation)

Date: 15 August 2019

Name: Catherine Heather Wickham

Signature:

Acknowledgements

First and foremost, I would like to thank my supervisor Prof Pepper for his constant support and encouragement throughout this project. Through all the trials and tribulations, you always believed we would find a way and made us believe it too. Thank you for every progress meeting where I went in dispirited and left feeling inspired. I would also like to thank my co-supervisor Dr Chrisna Durandt, for her endless good advice and willingness to help me troubleshoot my experiments, for her tireless work though many a long night so that I could collect data, and finally for all the flow cytometry lessons along the way.

My most heartfelt thanks go to the members of our HIV Team without whom this work could never have been done: Candice, for your considerable force of will which pulled all of us along and your wonderfully weird sense of humour; Juanita, for your dedication and sharp (sometimes painful) wit; and of course our team leader, Chrisna, for keeping us all on track. A special thank you also goes to Dr Samantha Nicholson, who was invaluable in setting up the BSL2+ lab and laying the foundation for our HIV protocols.

Thank you to the rest of my colleagues at the ICMM, particularly “Captain” Candice for always keeping our ship sailing smoothly, Elize in her self-appointed role of office cheerleader and distributor of emergency hot chocolate, Mqondisi for helping me to smile in the chaos, and to Carina for lending a sympathetic ear to the HIV Team’s woes and cheering us up with motivational art and cute dog pics. Thanks to all of you for making our office such a special place to work.

I would like to thank to the staff at the Clinical Research Unit for their willingness to help in collecting blood donations with efficiency and professionalism. Thanks also to the donors, who, although they remain anonymous, are appreciated all the same.

We are very grateful to the other research groups and collaborators which offered their advice and assistance, particularly Prof Lynn Morris at the NICD for providing us with starter HIV cultures and Dr Janine Scholefield at the CSIR for donating some of her GHOST cell stocks.

Finally, I wish to thank (and apologize to) Bonnie, Terry, and Graham Wickham, as well as my friends, who have been subjected to numerous project-related rants and have patiently responded with nothing but encouragement. You have all helped me in so many different ways, and I love you all so much.

Table of Contents

Table of Figures

List of Tables

Table of Equations

List of Abbreviations, Symbols and Units

Abbreviation	Description
7-AAD	7-Aminoactinomycin D
AHR	Aryl hydrocarbon receptor
AIDS	Acquired Immune Deficiency Syndrome
AKR7A2	Aldo-keto reductase family 7, member A2
AP-1	Activator protein 1
APC	Allophycocyanin
APC-Cy7	Allophycocyanin-Cyanine 7
APE 1	Apurinic/apyrimidinic endonuclease 1
APOBEC3	Apolipoprotein B mRNA editing enzyme, catalytic polypeptide-like 3
APOD	Apolipoprotein D
ATP	Adenosine triphosphate
AUC	Area under the curve
BAK	Bcl-2 antagonist/killer
Bax	Bcl-2-associated X
Bcl-2	B-cell lymphoma 2
Bcl-6	B-cell lymphoma 6
Bcl-x	B-cell lymphoma x
BP	Bandpass
BSL2+	Biosafety Level 2+
BTN3A3	Butyrophilin, subfamily 3, member A3
BV 510	Brilliant Violet™ 510
BV 605	Brilliant Violet™ 605
BV 711	Brilliant Violet™ 711
C9orf3	Bhromosome 9 open reading frame 3
CAL	Calibration (factor)
CAR	Chimeric antigen receptor
cART	Combination antiretroviral therapy
Cas9	CRISPR associated protein 9
CCL	C-C motif chemokine ligand
CCR	C-C chemokine receptor
CCR5	C-C chemokine receptor type 5
CD	Cluster of differentiation
CDC25	Cell division cycle 25
CDK1	Cyclin-dependent kinase 1
CDK9	Cyclin-dependent kinase 9
cDNA	Complementary DNA
CIDEC	Cell death-inducing DFFA-like effector C

CLTA-4	Cytotoxic T-lymphocyte-associated protein 4
CRISPR	Clustered regularly interspaced short palindromic repeats
cRNA	Complementary RNA
CSIR	Council for Scientific and Industrial Research
CTRC	Chymotrypsin C (caldecrin)
CXCL	C-X-C motif chemokine ligand
CXCR	C-X-C chemokine receptor
CXCR4	C-X-C chemokine receptor type 4
DAPI	4’,6-diamidino-2-phenylindole
DC	Dendritic cell
DEG	Differentially expressed gene
DMEM	Dulbecco's modified Eagle's medium
DMSO	Dimethyl sulfoxide
DN	Double-negative
DNA	Deoxyribonucleic acid
dNTP	Deoxyribonucleotide triphosphate
DOA	Day of assay
DOI	Day of infection
DP	Double-positive
ds	Double-stranded
dTTP	Deoxythymidine triphosphate
dUTP	Deoxyuridine triphosphate
E. coli	*Escherichia coli*
EDTA	Ethylenediaminetetraacetic acid
eIF4E	Eukaryotic translation initiation factor 4E
ELISA	Enzyme-linked Immunosorbent Assay
ER	Endoplasmic reticulum
FABP5	Fatty acid binding protein 5
FACS	Fluorescence-activated cell sorting
FAM26F	Family with sequence similarity 26, member F
FBS	Foetal bovine serum
FITC	Fluorescein isothiocyanate
FMO	Fluorescence Minus One
Foxp3	Forkhead box P3
FS	Forward scatter
FS-A	Forward scatter area
FS-H	Forward scatter height
GADD45	Growth arrest and DNA damage 45
GATSL2	GATS protein-like 2
GFP	Green Fluorescent Protein
Glut	Glucose transporter

GMCL1	Germ cell-less, spermatogenesis associated 1
GM-CSF	Granulocyte-macrophage colony-stimulating factor
GO	Gene Ontology
GPR15	G protein-coupled receptor 15
GWAS	Genome-wide association studies
HIST	Histone
HIV	Human immunodeficiency virus
HIV-1-B	HIV-1 subtype B
HIV-1-C	HIV-1 subtype C
HLA	Human leukocyte antigen
HOS	Human Osteosarcoma
HOXB4	Homeobox B4
HRP	Horseradish peroxidase
HSC	Haematopoietic stem cell
HSP90	Heat-shock protein 90
ICOS	Inducible co-stimulator
IFN	Interferon
Ig	Immunoglobulin
IGHMBP2	Immunoglobulin mu binding protein 2
IGLC	Immunoglobulin lambda constant
IGLJ	Immunoglobulin lambda joining
IGLV	Immunoglobulin lambda variable
IL	Interleukin
IL-2 GM	IL-2 growth medium
IL-2R	Interleukin-2 receptor
INF	Interferon
IRF	Interferon regulatory factor
ISG	Interferon-stimulated gene
ITFG1	Integrin alpha FG-GAP repeat containing 1
iTreg	Induced regulatory T (cell)
IVT	In vitro transcription
JAK-STAT	Janus kinase signal transducer and activator of transcription
KCNK4	Potassium channel, two pore domain subfamily K, member 4
KIR3DL	Killer cell immunoglobulin-like receptor, three domains, long cytoplasmic tail
KO	Krome Orange
LEAF	Low-endotoxin Azide-free
Lin	Linear
lncRNA	Long non-coding RNA
Log	Logarithmic
LP	Longpass
LPS	Lipopolysaccharide

LRRC8C	Leucine rich repeat containing 8 family, member C
LTR	Long terminal repeat
M group	Major group
MAP3K8	MAP kinase kinase kinase 8
M-CSF	Macrophage colony-stimulating factor
MDM	Monocyte-derived macrophage
MDM2	Mouse double minute 2 homolog
MFI	Median Fluorescence Intensity
MHC	Major histocompatibilty complex
MIP-1α	Macrophage inflammatory protein 1α
MIP-1β	Macrophage inflammatory protein 1β
MIR	MicroRNA encoding gene
miRNA	MicroRNA
MLR	Mixed lymphocyte reaction
MOI	Multiplicity of infection
mRNA	Messenger RNA
MYT1	Myelin transcription factor 1
N group	New group
NFAT	Nuclear factor of activated T-cells
NF-κB	Nuclear factor kappa-light-chain-enhancer of activated B cells
NICD	National Institute for Communicable Diseases
NIPA1	Non imprinted in Prader-Willi/Angelman syndrome 1
NK	Natural killer (cell)
NKT	natural killer T (cell)
NLR	Nucleotide-binding oligomerization domain-like receptor
nTreg	Natural regulatory T (cell)
O group	Outlier group
OAS	Oligoadenylate synthetase
OR	Olfactory receptor
PBMNC	Peripheral blood mononuclear cell
PBS	Phosphate buffered saline
PCR	Polymerase Chain Reaction
PDCL3	Phosducin like 3
PDE3B	Phosphodiesterase 3B, cGMP-inhibited
PE	Phycoerythin
PE-Cy7	Phycoerythrin-Cyanine 7
PHA-L	Phytohemagglutinin-L
PHA-P	Phytohemagglutinin-P
PMN	Polymorphonuclear leukocytes
PP2A	Protein phosphatase 2A
p-TEFb	Positive transcription elongation factor B

PTEN	Phosphatase and tensin homolog
RANTES	Regulated on Activation, Normal T Expressed and Secreted
RDH16	Retinol dehydrogenase 16 (all-trans)
RIN^e	RNA integrity number equivalent
RMA	Robust Multi-array Average
RNA	Ribonucleic acid
RNA-Seq	RNA sequencing
ROC	Receiver operating characteristic
RORγT	Retinoic acid-related orphan receptor γ T
RPMI-1640	Roswell Park Memorial Institute 1640 medium
RPMI-1640	Roswell Park Memorial Institute 1640
RT-PCR	Reverse transcription PCR
S. aureus	*Staphylococcus aureus*
SamHD1	SAM domain and HD domain-containing protein 1
SCN8A	Sodium channel, voltage gated, type VIII alpha subunit
SD	Standard deviation
SEB	Staphylococcal enterotoxin b
SEM	Standard error of the mean
SI	Staining Index
SIV	Simian immunodeficiency virus
SIVagm	SIV derived from African green monkeys
SIVcpz	SIV derived from chimpanzees
SIVsmm	SIV derived from sooty mangabeys/macaques
SLC	Solute carrier family member
SMAD 4	SMAD family member 4
snoRNA	Small nucleolar RNAs
SOD2	Superoxide dismutase 2
Sp1	Specificity protein 1
ss	Single-stranded
SS	Side scatter
STAT	Signal transducer and activator of transcription
TAC	Transcriptome Analysis Console
TAE	Tris-acetate-EDTA
TALENs	Transcription activator-like effector nucleases
TAR	Trans-activating response
TAS2R	Taste receptor, type 2
TBP	TATA-binding protein
TCID50	Tissue Culture Infectious Dose 50
T_{CM}	Central memory T cell
TCR	T cell receptor
TdT	Terminal deoxynucleotidyl transferase

T_{EFF}	Effector T (cell)
T_{EM}	Effector memory T (cell)
Tfh	Follicular helper T (cell)
TGF-β	Transforming growth factor β
Th	Helper T (cell)
TLR	Toll-like receptor
TMB	3,3',5,5'-tetramethylbenzidine
ROS	Reactive oxygen species
TNF	Tumour necrosis factor
TRAJ	T cell receptor alpha joining
TRBV	T cell receptor beta variable
TREX2	Three prime repair exonuclease 2
TRIM16	Tripartite motif containing 16
UDG	Uracil-DNA glycosylase
USP	Ubiquitin specific peptidase
USP17L	Ubiquitin specific peptidase 17-like
UV	Ultraviolet
V3 region/loop	Third hypervariable region/loop
VDC	Vybrant® DyeCycle™
Vol	Volume
VSV-G	Vesicular stomatitis virus G
ZNF	Zinc finger protein

Unit	**Description**
°C	Degrees Celsius
bp	Basepairs
cells/mL	Cells/millilitre
cells/µL	Cells/microlitre
h	Hours
IU	Infectious units
IU/mL	Infectious units/millilitre
kb	Kilobases
Kcal/mol)	Kilocalories/mole
M	Molar
mM	Millimolar
mg/mL	Milligrams/millilitre
min	Minutes
mL	Millilitres
mm3	Cubic millimetres
ng	Nanograms
ng/mL	Nanograms/millilitre

ng/µL	Nanograms/microlitre
nm	Nanometres
nM	Nanomolar
pg/mL	Picograms/millilitre
rpm	Rotations per minute
sec	Seconds
U/mL	Enzyme units/millilitre
V	Volts
µg	Micrograms
µg/mL	Micrograms/millilitre
µL	Microlitres
µm	Micometres

Symbol	**Description**
%	Percent
<	Less than
≥	Greater than or equal to
>	Greater than
α	Alpha
β	Beta
γ	Gamma
Δ / δ	Delta
ε	Epsilon
ζ	Zeta
κ	Kappa
λ	Lambda
R^2	Co-efficient of determination
ΔG	Gibbs free energy
Tm	Primer melting temperature
g	G-Force/ Relative centrifugal force

1

Chapter 1:

Introduction and problem statement

The human immunodeficiency virus (HIV) is a devastating pathogen that has been recognized by global health authorities as one of the world's most serious current public health challenges. The virus targets and destroys immune cells, particularly helper T lymphocytes, which are positive for cluster of differentiation (CD) 4 and are involved in coordinating the responses of almost all immune system cells. The progressive depletion of $CD4^+$ T cells as a result of HIV infection leads to patients becoming severely immunocompromised and results in a greatly increased risk of infection with other pathogens, often with lethal consequences. HIV is readily transmitted through contact with bodily fluids of an HIV-positive individual. Common routes of transmission include sexual intercourse, blood-to-blood contact and mother-to-child transmission. In the early stages of infection, the virus replicates with very few overt symptoms, often leading to further transmission before the patient is aware that they have been infected. This asymptomatic phase can last several years, allowing the virus ample opportunity to reach a large number of potential hosts.

To date, no cure for HIV infection has been found; however, antiretroviral drugs that impose restrictions on viral replication at various points in its life cycle have been successfully developed. Under ideal circumstances, antiretroviral drugs significantly slow the rate of disease progression, allowing patients to live almost as long as uninfected persons. However, antiretrovirals are not without their drawbacks. They can often have serious adverse side effects, leading to poor adherence in some cases. Since they must be taken continually for the rest of the patient's lifespan in order to maintain viral suppression, the cost of this treatment can become a serious burden. The development of drug resistant HIV strains is also a relatively common occurrence, leading to treatment failure. Clearly, alternatives to the currently available treatments are needed. The main goals of much HIV research in recent years has therefore been 1) the development of a preventative vaccine, and 2) the development of a cure that can completely eliminate all trace of infection. These efforts have

been thwarted by the extremely mutable nature of the virus, coupled with its ability to form latent reservoirs in which it is protected from both the immune system of the host and therapeutic agents directed against it.

The failure of conventional approaches in the development of alternative therapies requires us to investigate novel strategies to combat HIV. However, we are still lacking a comprehensive understanding of the complex interactions between HIV and its target host cells upon which to base such strategies. This knowledge would be invaluable for the identification of factors which might be manipulated to benefit the host and to undermine the virus. Efforts have been made to elucidate these interactions at a gene expression level using *in vitro* models, often involving the use of laboratory virus strains and cell lines. An overview of the findings of these studies is presented in **Chapter 2.** However, it is a concern that these models may not adequately capture the complexity of infection of host cells *in vivo* with naturally occurring HIV strains. Furthermore, much of the research that has been done is largely limited to just one viral subtype, namely HIV-1 subtype B (HIV-1-B), due to its prevalence in high income countries. In comparison, the most globally prevalent strain, HIV-1 subtype C (HIV-1-C), has been very poorly characterized. Its effects on the host cell transcriptome remain largely speculative, based on observations from HIV-1-B.

This study aims to address these issues by investigating the effect of infection with primary, patient-derived HIV-1-C strains on the gene expression profiles of the main cellular targets of HIV-1, namely $CD4^+$ T lymphocytes and macrophages. In order to achieve this goal, several preliminary objectives had to be accomplished. First, protocols for the culture of primary HIV-1-C strains had to be developed and optimized in order to produce a high-quality stock of virus for use in gene expression experiments. Methods to successfully detect infected cells also had to be optimized for use with these primary isolates. Work pertaining to viral culture and optimisation of detection methods is presented in **Chapter 3**. Second, pure populations of primary $CD4^+$ T lymphocytes and macrophages, cultured under optimal conditions to enhance susceptibility to infection, were required. **Chapter 4** covers the harvesting, purification and culture of these two cell types, as well as assessment of the effects of various culture conditions on their phenotypic properties and their susceptibility to our HIV-1-C primary isolates. **Chapter 5** describes the final infection and gene expression experiments performed, in which the effects of exposure to these isolates on the transcriptome of the

target cell population were determined by Affymetrix microarray technology. **Chapter 6** comprises a concluding discussion of the results of these experiments and provides some insight into the future directions of this field.

Chapter 2: Literature Review

The host cell response to HIV-1 infection in $CD4^+$ T lymphocytes and macrophages

1. Introduction

HIV was identified as the causative agent of Acquired Immune Deficiency Syndrome (AIDS) in the 1980's (1–3) and has since become a major epidemic with global distribution (4,5). HIV is a particular concern in the South African context, since there are approximately 7.5 million individuals currently living with HIV in our country, which corresponds to 13.1% of the total population, according to the latest report from Statistics SA (6). This epidemic continues to contribute significantly to the health burden in South Africa, even though combination antiretroviral therapy (cART) regimens are available. Current cART can improve life-expectancy dramatically by limiting viral replication (7,8). Free access to cART has proven effective in South Africa, with the proportion of AIDS-related deaths dropping from 42.2% in 2004 (when antiretrovirals were made publicly available) to 22.0% in 2018 (6). However, treatment with cART requires life-long use, which places a heavy cost burden on the health sector. Furthermore, antiretrovirals often have adverse effects on the patient (9), and are unable to completely eliminate viral reservoirs (10,11). Poor adherence to cART regimens also contributes to the emergence of resistant viral strains (12,13), which is a serious cause for concern in the management of the HIV epidemic. Therefore, the development of alternative or ancillary strategies in addition to cART would be greatly beneficial.

Attempts to develop a preventative vaccine as an alternative strategy to combat HIV have thus far been unsuccessful. The main reason is the high genetic diversity of HIV, leading to the requirement for an effective vaccine that would enable production of extremely broad-spectrum neutralizing antibodies (14–16). Unfortunately, the primary immunogenic component of the virus particle (the envelope protein) is highly variable, making most antibody responses to HIV strain-specific when using conventional vaccine development

approaches (14–16). Another challenge in the development of more efficient treatment strategies is the ability of HIV to enter a state of latent infection in certain cell types. Productive infection is characterized by integration of the viral genome into the host cell deoxyribonucleic acid (DNA), followed by active transcription of viral genes and production of viral proteins that ultimately leads to the generation of new virions from the host cell. In the case of latent infection, however, the viral genome is integrated but viral gene expression is repressed. In this state, the virus can persist as an inert component of the host cell DNA, protected from both the immune system and any therapeutic agent directed against it, while still retaining the ability to be reactivated at a later stage (10,11,17).

In the past few decades, there has been a concerted global effort to develop an effective, permanent cure for HIV infection. Potential cures can be classified as either “sterilizing” or “functional”, depending on their purpose. A sterilizing cure is one in which complete eradication of all replication competent virus is achieved throughout the body, while a functional cure refers to the establishment of stable, long-term control of viral replication obviating the need for antiretroviral treatment (18). Several strategies have employed various forms of genome editing such zinc-finger nucleases, transcription activator-like effector nucleases (TALENs), and clustered regularly interspaced short palindromic repeats/CRISPR associated protein 9 (CRISPR/Cas9) technologies in an attempt to eradicate or mutate integrated virus in the DNA of host cells (18). Other forms of preventative gene therapy aim to modify host cells to be resistant to further infection, thereby achieving a functional cure (18). Both approaches are currently limited by the difficulty in genetically modifying a large enough number of patient cells to achieve the desired effect. The use of chimeric antigen receptor (CAR) T cells is another emerging cell-based therapy. These engineered cytotoxic T cells, initially developed to eliminate malignant cells in cancer patients, could theoretically be engineered to destroy HIV-infected cells with great specificity (19). The “shock and kill” strategy, on the other hand, is a chemotherapeutic approach which aims to eliminate the viral reservoir through the use of latency reversing agents coupled with potent antiviral therapeutic agents.

While some of the approaches described have shown promise in preliminary studies, they are all still in various stages of development and none have thus far been validated in large-scale clinical trials. There is therefore a critical need to continue to search for effective novel

therapeutic approaches to combat HIV. In order to develop these alternative strategies, we need to have a comprehensive understanding of the interaction between the virus and the host cell. This will allow us to identify potential molecular targets for therapeutic intervention. Such molecular targets would include factors that are essential to HIV's ability to establish successful infection, as well as factors through which the host cell may effectively inhibit viral replication. By gaining a better understanding of these factors, it may eventually be possible to modulate the host cell itself to be immune to infection and potentially to eliminate latent viral reservoirs.

2. The human immunodeficiency virus

2.1. Fundamental biology of HIV

2.1.1. Structure and genomic organization

HIV is taxonomically classified as a retrovirus (family Retroviridae, subfamily Orthoretrovirinae) within the Lentivirus genus (20). The structure of the virion is typical of most lentiviruses, comprising a conical capsid surrounded by a spherical envelope with spiked projections dispersed around the surface (21), (**Figure 2.1**). These projections are composed of the envelope glycoproteins gp120 and gp41 (together known as gp160) which mediate attachment and fusion with host cells (22). The lipid membrane surrounding the capsid is derived from the host cell membrane from which the virion was produced (21), and as such contains several host cell membrane proteins. The membrane is lined with viral p17 matrix proteins, which stabilize the structure of the mature virion and facilitate assembly of viral structural components at the host cell membrane during the formation of new virions (21,22). The viral protease enzyme is packaged in the space between the envelope and the capsid, while the rest of the viral enzymes (reverse transcriptase, integrase) as well as regulatory and accessory proteins, are contained within the capsid along with the viral genome (22). The genome comprises two copies of single-stranded positive sense ribonucleic acid (RNA) molecules, which are coated with p7 nucleocapsid proteins (22,23). These proteins function as chaperones that facilitate correct folding of the RNA (23). The entire virion is approximately 110-130 nm in diameter when fully matured (24).

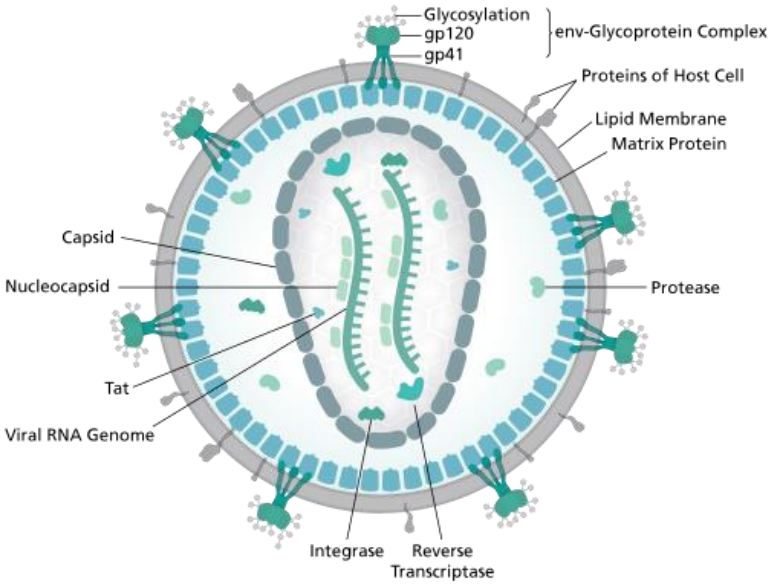

Figure 2.1: Structure of a mature HIV virion. The core of the virus particle is composed of capsid proteins. Enclosed within the capsid are two strands of RNA, coated with nucleocapsid proteins, which function as the viral genome. Most viral enzymes (tat, integrase, reverse transcriptase) are also found within the capsid. The outer envelope of the virion comprises a spherical lipid membrane. Envelope glycoproteins composed of gp120 and gp41 subunits are found on this outer membrane, as well as host proteins derived from the originating host cell. Matrix proteins are arranged along the inner surface of the membrane. The viral protease enzyme resides in the space between the capsid and the envelope. Available from: https://commons.wikimedia.org/wiki/File:HI-virion-structure_en.svg

The genome, which is approximately 9.8 kb in length (25–27), encodes nine genes: *gag, pol, env, tat, rev, nef, vif, vpr* and *vpu/vpx* (22,23,25,28,29) (**Figure 2.2**). *Vpu* is unique to HIV-1, while *vpx* is a feature of HIV-2 strains (30). These genes encode the full complement of viral enzymes, structural proteins and regulatory proteins. The *gag* gene encodes a polyprotein precursor which is cleaved by the viral protease into structural components: p17 matrix protein, p24 capsid protein, p7 nucleocapsid protein, and p6 (21–23,28,29). The *env* gene encodes the Env polyprotein, which is cleaved into surface (gp120) and transmembrane (gp41) envelope glycoprotein subunits (22,23,28,29). The *pol* gene, expressed as part of a Gag-Pol fusion protein, encodes the viral protease, p51 reverse transcriptase (RT) and p31 integrase enzymes as well as p15, which has RNase H activity (28,29,31,32). The regulatory genes *tat* and *rev* encode proteins that control gene expression from the viral genome (22,28,29). The rest of the genes (*nef, vif, vpr, vpu*) are termed accessory genes, since they are not technically essential for viral replication (29,30). However, they do play important

roles in facilitating a favourable environment for replication to occur (29,30). The genome is bounded by long terminal repeat (LTR) elements on either side, which are involved in integration of the viral genome into the DNA of the host cell (29,30,33). The LTR also functions as a promoter sequence for transcription of viral genes (22,29,34).

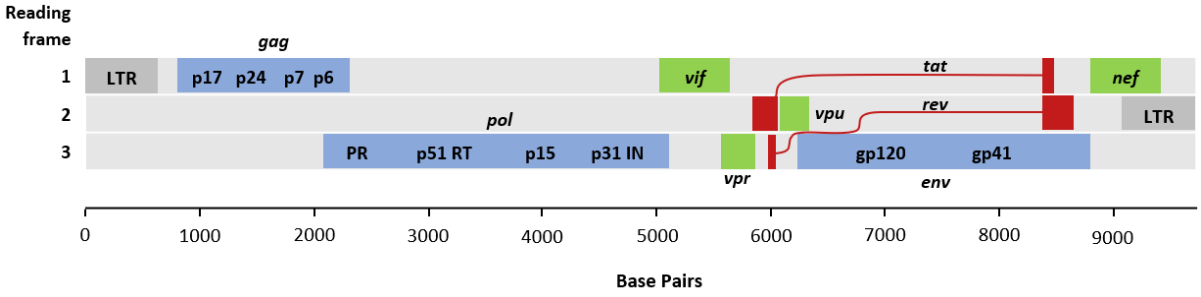

Figure 2.2: Genomic organization of HIV-1. LTR elements border the genome at both the 5' and 3' ends, indicated in grey. Genes encoding structural proteins and essential viral enzymes (*gag*, *pol*, *env*) are indicated in blue. Genes encoding accessory proteins (indicated in green) include *vif, vpr, vpu* and *nef*. The regulatory genes *tat* and *rev* (indicated in red) comprise two exons each, which are spliced together to form their final products. Adapted from an image available from: https://commons.wikimedia.org/wiki/File:HIV-genome.png.

2.1.2. Classification of HIV strains based on genetic diversity

The origins of HIV have been traced to multiple zoonotic transmission events of simian immunodeficiency virus (SIV) from non-human primates to humans in Central and Western Africa (13,25,35). Due to the multifocal nature of these events and the inherent mutability of the viral genome, significant genetic variation exists among HIV strains. This has led to the formation of several sub-groupings based on phylogeny. First and foremost is the distinction between HIV-1 and HIV-2 strains, of which HIV-1 is by far the more pathogenic and prevalent (36,37). As illustrated by the phylogenetic tree in **Figure 2.3**, HIV-1 is most closely related to the SIV strains found naturally in chimpanzees (SIVcpz), while both subtypes of HIV-2 (HIV-2A and HIV-2B) are closely related to SIV derived from sooty mangabeys and macaques (SIVsmm) (13,25). The group of SIV strains derived from the *Chlorocebus* genus of African green monkeys (SIVagm) are also close relatives of both HIV-2 and SIVsmm strains. Within HIV-1, there are three groups: M (major), O (outlier) and N (new) (37,38). Each of these groups are phylogenetically distinct (**Figure 2.3**) and are believed to have arisen from separate transmission events of SIVcpz (13,25,35,39). The HIV-1 M group is responsible for the majority of worldwide HIV infections (35,37). Due to the extensive genetic diversity within this group,

it has been further subdivided into 13 subtypes (A1, A2, A3, A4, B, C, D, F1, F2 G, H, J and K), also known as clades (15,25,40).

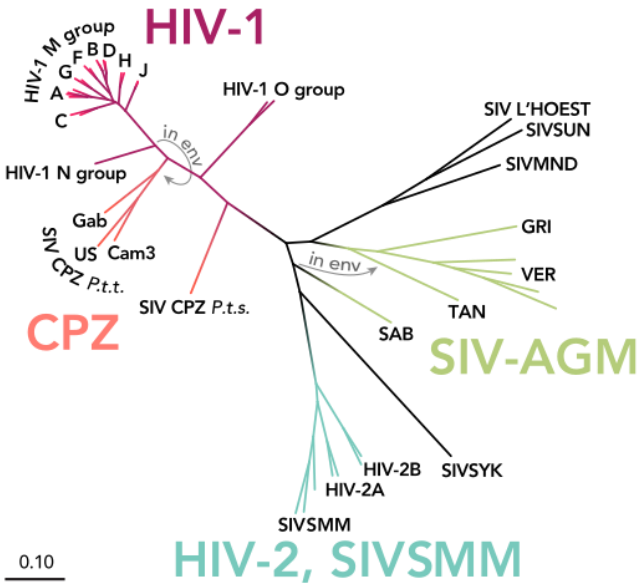

Figure 2.3: Phylogenetic tree of HIV and related SIV strains from various non-human primates. Relative genetic distance is indicated by the scale bar in the lower left corner. CPZ = SIV derived from chimpanzees. Strains from two chimpanzee subspecies, *Pan troglodytes troglodytes* (SIV CPZ P.t.t.) and *Pan troglodytes shweinfuthii* (SIV CPZ P.t.s.) are shown, with three geographically distinct SIV CPZ P.t.t. sub-populations included (Gab, US, Cam3). SIVSMM = SIV derived from sooty mangabeys and macaques. SIV-AGM = SIV derived from African green monkeys. This group includes strains from the following monkey species: TAN = *C. tantalus*, VER = vervet monkey (*C. pygerythrus*), GRI = grivet monkey (*C. aethiops*), SAB = *C. sabaeus.* SIV L'HOEST = SIV derived from L'Hoest's monkey. SIV SUN = SIV derived from sun-tailed monkeys (SIV SUN). SIV MND = SIV derived from mandrills. Available from: https://commons.wikimedia.org/wiki/File:HIV-SIV-phylogenetic-tree_straight.svg

The HIV-1 group M subtypes were historically differentiated based on variation in the sequences of their *gag* and *env* genes (40). While classification is now performed using sequences from all genomic regions (40), most sequence divergence is still detected in the *env* gene (15,37,38,41) which may vary up to 35% between different subtypes and up to 20% within the same subtype (15,41). Recombination can occur within these subtypes, during either superinfection or co-infection with two or more strains (25,38). This has led to the emergence of numerous reported circulating recombinant forms, presently numbered at 97 strains in the Los Alamos HIV sequence database (42). The different HIV-1 group M subtypes have distinct geographic distributions (**Figure 2.4**). HIV-1-B is the dominant form in North America and Europe (38). As such, it has received the most attention for study in these

resource-rich settings. Circulating A/E recombinants are predominant in Southeast Asia (38), while HIV-1-C is most common in sub-Saharan Africa and India (38). HIV-1-C is of particular interest since it is the most rapidly expanding subtype, accounting for 60% of HIV-positive individuals globally (38,43). The reason for the epidemiological success of this clade compared to others remains unclear (43).

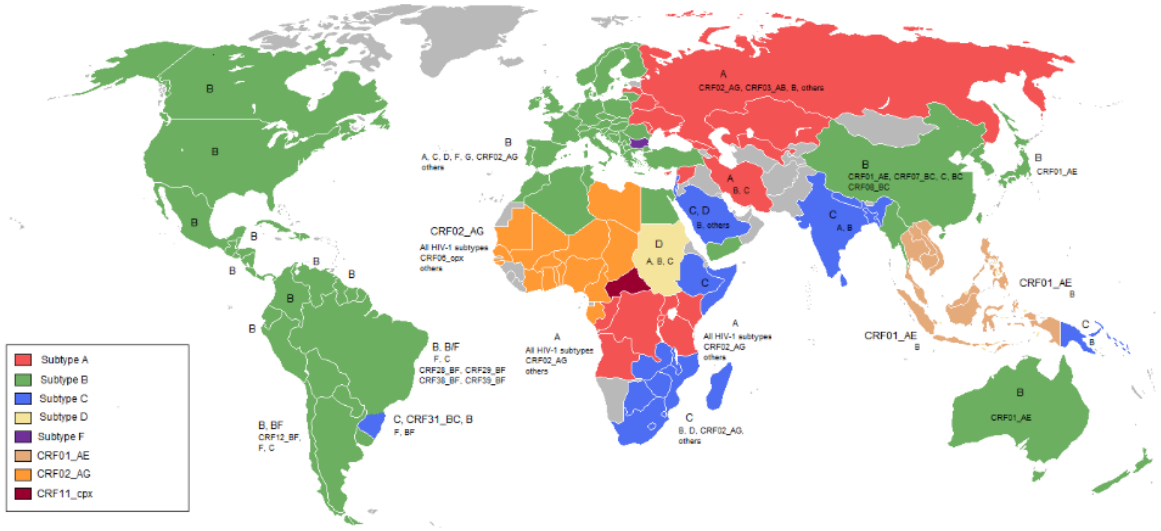

Figure 2.4: Geographic distribution of different HIV-1 group M subtypes. The most prevalent subtype/circulating recombinant form found in each country is indicated on the world map, as per the colour-coded key. Annotations are used to indicate the presence of other prominent subtypes/circulating recombinant forms in some countries. Subtype B clearly predominates in North and South America, Europe, China and Australia, while subtype C is highly prevalent in southern Africa and India. Taken from Santos & Soares (13).

2.1.3. The HIV-1 replication cycle

The replication cycle of HIV, summarised in **Figure 2.5**, is a complex process involving both viral components and numerous host cell proteins. Successful HIV-1 infection is initiated by adherence of a mature, infectious virion to a susceptible host cell expressing the surface marker CD4, such a $CD4^+$ T lymphocyte (22,29). The gp120 domain of the surface envelope glycoprotein (Env) binds to the CD4 receptor (22,29). Subsequent engagement of chemokine co-receptors on the host cell surface, such as C-C chemokine receptor (CCR) type 5 (CCR5) or C-X-C chemokine receptor (CXCR) type 4 (CXCR4), induces conformational changes in the transmembrane envelope glycoprotein gp41 that activate fusion of the viral envelope with the host cell membrane (22,29). The viral capsid enters the host cell cytoplasm and the capsid proteins coating the viral genome are removed (22,29). The exposed RNA genome is then

converted into double stranded DNA by the viral reverse transcriptase enzyme (22,29). The DNA, in combination with several viral and host cell proteins (together termed the pre-integration complex), is transported into the nucleus (22,29). This process is facilitated by the accessory protein Vpr (22,29). Integrase catalyses the cleavage of the host cell DNA and insertion of the viral DNA into the host cell genome (22,29). Once integrated, the viral DNA is referred to as a provirus.

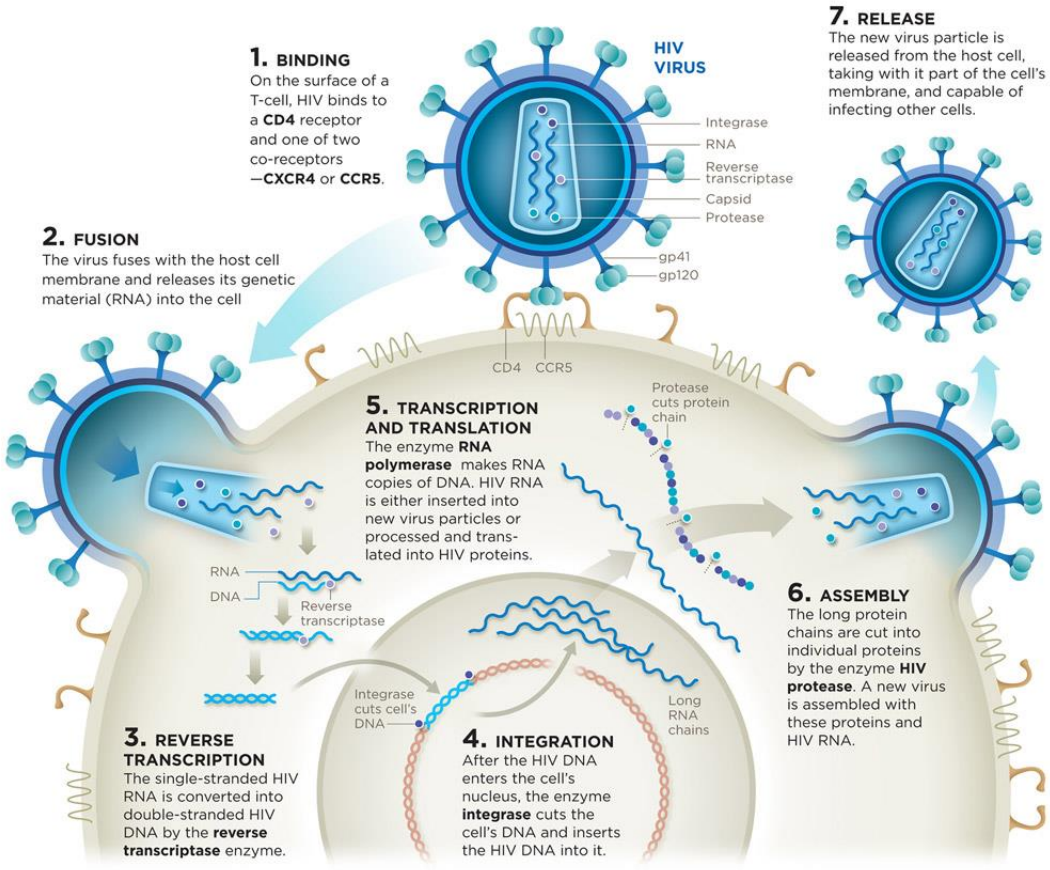

Figure 2.5: The replication cycle of HIV-1 in a susceptible CD4- and CCR5-expressing host cell. The lifecycle of HIV can be summarized in the following stages: 1) binding of the virion to a host cell, 2) fusion of the viral envelope with the host cell membrane and entry of the capsid into the cell, 3) reverse transcription of the RNA genome into DNA, 4) integration of the viral DNA into the host cell genome, 5) transcription and translation of viral genes into viral proteins, 6) assembly of viral proteins into new viral particles which bud off from the host cell membrane. Available from: http://www.5wgraphics.com/img/gallery/5w-sample-020-hiv-lifecycle.jpg

Expression of viral transcripts and protein products from proviral DNA is mediated by the transcriptional and translational machinery of the host cell. The LTR promoter region contains binding sites for multiple cellular transcription factors, such as nuclear factor kappa-light-

chain-enhancer of activated B cells (NF-κB), specificity protein 1 (Sp1), TATA-binding protein (TBP), nuclear factor of activated T-cells (NFAT), and activator protein 1 (AP-1), which are located upstream of the transcription start site (22,29,34,44). Expression of these factors by the host cell therefore facilitates initiation of transcription from the provirus. Transcriptional elongation, on the other hand, is primarily mediated by the viral Tat protein. Tat binds the trans-activating response (TAR) element, an RNA hairpin found at the 5' end of nascent viral transcripts, resulting in stabilisation of the transcription complex and recruitment of host-derived transcription elongation factors, the most important of which is positive transcription elongation factor B (p-TEFb) (22,29,34,45). This interaction drastically increases the efficiency of the RNA polymerase complex, enabling transcription of the entire genome (22,29). Subsequent processing of the resulting viral transcripts via a complex system of differential RNA splicing enables the production of the entire complement of viral gene products.

Transcripts that have undergone varying degrees of splicing differ in the final gene products they are able to encode. The unspliced transcripts of 9.2 kb are used for translation of the Gag and Gag-Pol polyproteins, and are also packaged into newly formed virions where they serve as the genomic RNA (29,33). Another set of incompletely spliced messenger RNA (mRNA) species of approximately 4 kb are produced, which are used for production of the Env polyprotein, as well as the accessory proteins Vif, Vpr and Vpu (29,33). The fully spliced mRNAs (1.8 kb) encode the regulatory proteins Tat, Rev and Nef (29,33). The relative proportions of differentially spliced mRNA isoforms present is determined by the efficiency of the cellular spliceosome enzymes and the relative strengths of the different splice donor and acceptor sequences in the viral transcripts (34). Early in infection, only the fully spliced mRNAs encoding Tat, Rev and Nef are exported to the cytoplasm for translation, while incompletely or unspliced transcripts are degraded in the nucleus. The resulting production of Tat leads to an overall increase in the production of viral transcripts, while the newly translated Rev proteins facilitate transport of incompletely spliced and unspliced mRNAs to the cytoplasm (22,29,33). Therefore, as infection progresses, increased production of Rev enables the transport and subsequent translation of more viral products encoded by the unspliced and partially spliced mRNAs (29,33).

Translation of viral proteins from the various transcripts is carried out by the ribosomes of the host cell (22). Most of the protein products are synthesised in the host endoplasmic reticulum

(ER) by conventional translation from a single open reading frame, with the exception of the Gag-Pol fusion protein which is generated through programmed ribosomal frameshifting (29,34,46). This unusual mechanism is used by several retroviruses to enable translation of a protein across overlapping reading frames, thereby packing more information into a genome of limited size (47). In HIV, ribosomal frameshifting is mediated by the presence of a stem-loop secondary structure in the *gag-pol* transcript and a hexanucleotide "slippery" sequence at the start of the *pol* coding region (34,46). The stem-loop stalls the ribosome over the slippery sequence, which occasionally causes the ribosome to move backwards by one nucleotide. This causes a -1 frameshift, forcing the ribosome into the correct frame for translation of the *pol* coding region and resulting in production of the Gag-Pol fusion protein (34,46). This frameshift occurs in only 5-10% of translating ribosomes, while the majority translate only the Gag coding region (21,34,46).

Assembly of new virions is initiated by movement to and localization of Gag and Gag-Pol polyproteins, accessory proteins (Vif, Vpr and Nef), and the genomic RNA at the cell membrane (21,22,29). The envelope glycoproteins also need to be trafficked to the cell surface for the production of infectious virions. This is hindered by the CD4 molecule, which forms complexes with Env polyproteins in the ER as they are translated, thereby preventing them from being cleaved into functional subunits and incorporated into new virions (22,29). The accessory protein Vpu facilitates release of Env by inducing degradation of CD4 (22,29), enabling transport of Env to the Golgi apparatus where it is cleaved into gp120 and gp41 subunits by host cell proteases (22,29). The subunits are trafficked to the cell surface, allowing their assembly into envelope spikes (22,29). The expression of surface CD4 is inhibited by the activities of Nef, which binds to CD4 and increases the rate at which it is internalized from the plasma membrane (29), thereby preventing further interference with the Env subunits. Once all components of the virus particle are assembled at the cell membrane, the immature virion buds off, taking a portion of the host cell membrane with it. Complete maturation of the virion occurs after budding (21), with the activation of the viral protease leading to cleavage of Gag and Gag-Pol polyproteins into their final protein products, which reassemble to form the components of the mature virion, arranged in distinct layers (21,22,29).

As mentioned previously, HIV can also enter a state of latency in which viral gene expression from the integrated provirus is repressed and no new virions are produced (17,45,48). This is

often due to the induction of transcriptional quiescence in the infected host cell. For instance, in $CD4^+$ T cells, infection is initiated in activated cells which express the transcription factors required for expression of viral genes (17,45). However, if the cell transitions into a resting memory cell state, the lack of these essential transcription factors renders the cellular environment nonpermissive for viral gene expression (17,45,48). The chromatin structure of the surrounding host cell DNA also plays an important role in determining transcriptional activity (17,48). Chromatin can exist as either a loose uncompacted DNA strand, referred to as euchromatin, or as a tightly condensed structure, referred to as heterochromatin. Heterochromatin inhibits gene expression by preventing access of transcription factors, while euchromatin permits active transcription (17,48). Another molecular mechanism which may potentially induce latency is interference from transcription of cellular genes in close proximity to the integrated provirus (17,48). The transcription factors involved in expressing the host cell gene may cause occlusion of the viral promoter or, if the viral genome is integrated in the opposite orientation to the host cell gene, RNA polymerases transcribing in opposite directions may collide resulting in truncation of nascent viral transcripts (17,48). Latency can generally be reversed by providing the latently infected cell with suitable activation stimuli that lift the initial restrictions imposed upon viral gene expression (17,45,48).

2.1.4. Viral tropism

Viral tropism refers to the ability of a virus to infect and replicate within a specific host cell type or tissue. In the case of HIV, tropism is largely determined by the ability of the viral Env protein to interact with co-receptors on the host cell surface which facilitate adherence and fusion with the cell membrane (22,29,49). The specificity of this interaction is determined at a molecular level by the amino acid composition in the third hypervariable (V3) region of the gp120 Env subunit, also called the V3 loop (29,50,51). As mentioned previously, the most common co-receptors which can be utilized by HIV for entry are CCR5 and CXCR4, although several alternate co-receptors such as G protein-coupled receptor 15 (GPR15)/Bob, CXCR6 and CCR3 have also been identified (52,53). HIV-1 strains which use CCR5 and CXCR4 are generally referred to as R5-tropic and X4-tropic respectively, while strains which are capable of using either CCR5 or CXCR4 are referred to as dual-tropic. Differential levels of expression of co-receptors in various cell types therefore affects the efficiency of viral entry into these

cells and determines their susceptibility to infection with strains of different tropisms. The availability of co-receptor on potential host cells can depend on many factors, including host-specific mutations in the co-receptor genes, differential transcriptional regulation and/or RNA splicing, and the quantity of natural ligands for the co-receptor present that may compete with the virus for binding (50).

The tropism of the strain with which a patient is infected is an important diagnostic feature, since it can be correlated with certain characteristic behaviours and may affect treatment efficacy. R5-tropic viruses have the capacity to infect cells of the monocyte/macrophage lineage in addition to $CD4^+$ T lymphocyte subsets, such as memory cells, which express CCR5 in abundance (54–56). R5-tropic viruses generally do not induce syncytium formation, replicate more slowly, and can be recovered from patient cells at all stages of the disease (54,55). X4-tropic strains, on the other hand, preferentially infect $CD4^+$ T cells, especially the naïve subset which has increased expression of CXCR4 (54,56). X4-tropic viruses are generally far more cytopathic than R5 strains, with a tendency to induce formation of syncytia and typically have more rapid replication rates (54). They are generally observed in later stages of infection and are associated with severe depletion of $CD4^+$ T lymphocytes (54,55). Viral tropism also has implications for the selection of appropriate antiretroviral treatment, particularly in the case of entry inhibitors. These drugs function by competitively binding CCR5 (e.g. maraviroc) or CXCR4 (e.g. AMD-3100), thereby selectively preventing entry of R5-tropic or X4-tropic strains respectively.

2.2. Pathogenesis and clinical presentations of HIV infection

The pathogenesis of HIV-1 infection can be attributed to the disruption of intricate cellular networks that leads to systemic dysregulation and dysfunction of the immune system and an associated spectrum of AIDS-defining illnesses. HIV infection occurs in three stages: the initial acute infection, an asymptomatic chronic phase, and finally progression to AIDS. During the acute phase, a few days post-infection, flu-like symptoms may be experienced by the patient as a result of the massive amounts of viral replication and activation of the host immune response (57). Within approximately 6 months post-infection, viremia stabilizes due to the anti-viral activities of the adaptive and innate immune responses and the patient enters the asymptomatic phase wherein viral replication continues, albeit at much lower levels (37). The viral load at this stage is termed the “viral set point”. This chronic infection generally lasts

approximately 10-20 years in individuals without access to cART, during which time $CD4^+$ T lymphocytes are gradually depleted and immune system functions are slowly subverted (37). An HIV-positive individual is diagnosed as having AIDS once the $CD4^+$ T cell count in blood is below 200 cells/mm^3. This stage is associated with the presence of unusual AIDS-defining opportunistic infections and cancers, such as *Pneumocystis jiroveci* infection and Kaposi's sarcoma (37).

The depletion of $CD4^+$ T lymphocytes, which play a central role in mediating immune responses, is the primary reason for the occurrence of AIDS-related illnesses and is mediated by several factors. The viral proteins of HIV are themselves cytopathic to $CD4^+$ T cells as well as their progenitor cells (58). Furthermore, HIV infection renders the cell membrane more permeable and therefore more fragile and susceptible to apoptosis (37) due to continued budding of virions from the cell membrane. The induction of apoptotic pathways is further promoted due to the widespread induction of pro-inflammatory cytokines from virally-mediated immune activation (37,59). Host-mediated immune dysfunctions, such as production of anti-$CD4^+$ autoantibodies (37) and the cytotoxic (60) and autophagic activities (61) of other immune cells directed against $CD4^+$ cells, may exacerbate cell loss. Finally, HIV-associated destruction of bone marrow and lymphoid tissue inhibits restoration of depleted $CD4^+$ T cells, making the eventual decline into complete immunodeficiency inevitable (8).

In addition to its debilitating effect on the immune system, HIV infection can be linked to dysfunctions in almost all other host systems. HIV pathogenesis can manifest haematologically in the form of anaemia, leukopenia, thrombocytopenia or even pancytopenia (62). The causes of these cytopenias are multifactorial, including direct infection of blood cells, inflammation, malnutrition, malignancy, and antiretroviral/chemotherapy administration (62). HIV may also impact on haematopoiesis through direct infection of progenitor cells, or via indirect mechanisms, such as altered cytokine levels, which impact the bone marrow microenvironment (62). HIV-related enteropathy, anorexia, malabsorption, and deficiencies of iron, vitamin B12 and vitamin B9 are frequently observed (62,63). Lipodystrophy is another common co-morbidity associated with HIV infection which is characterized by wasting, redistribution of adipose tissue, dysregulation of lipid metabolism and possible development of insulin resistance (64). HIV may also have neurological effects, manifesting as HIV-associated neurocognitive disorder,

which afflicts 40-70% of infected patients (65). Without treatment, HIV-infected individuals often present with sub-acute dementia, sensory neuropathy and vacuolar myelopathy (54), usually resulting from underlying acute encephalitis (65). cART itself can exacerbate many of these symptoms, with different classes of antiretrovirals having various adverse effects as reviewed by Shibuyama and colleagues (2006) (9). Reverse transcriptase inhibitors have been reported to cause peripheral neuropathy and lipoatrophy; non-nucleoside reverse transcriptase inhibitors have been linked to hepatotoxicity, and protease inhibitors have been associated with wide range of side effects including lipodystrophy, hyperglycemia and gastrointestinal disruption (9).

The rate of viral progression can vary drastically from patient to patient. Based on this, patients can be divided into three major groups: 1) rapid progressors, in which the transition to AIDS occurs within three years following infection and seroconversion; 2) intermediate progressors in which AIDS develops between 3 to 10 years; and 3) long-term non-progressors, in which viral replication is controlled to such an extent that CD4 counts remain stable for many years, even in the absence of antiretroviral therapy (66,67). These progressor phenotypes are correlated to the viral set point, with higher viral set points generally leading to more rapid progression (66,67). In some long-term non-progressors, the viral load is maintained at undetectable levels (below 50 HIV-RNA copies/mL) in which case they are sometimes referred to as “elite controllers” (66). These patients have been extensively studied with the aim of discovering mechanisms to control viral replication in other patients. Another group of interest is HIV-exposed, but uninfected patients. In several of these cases, resistance to infection can be attributed to the presence of the Δ32 mutation in the CCR5 co-receptor gene which inhibits entry of R5-tropic viruses (68). Following the discovery that a bone marrow transplant from a Δ32 homozygous donor to an HIV-positive recipient resulted in the eradication of HIV in the recipient (widely known as the Berlin patient) (69), efforts are currently underway to replicate this cure using gene therapy approaches.

2.3. The role of viral genome diversity and plasticity in the dynamics of HIV infection

The extreme diversity in the HIV-1 genome across different strains is as a result of an extraordinarily high rate of mutation, coupled with short generation times (25). The small genome contributes to rapid viral replication, resulting in an average replication cycle of just

1.2 days (70). Each round of replication produces an enormous number of progeny viruses, leading to an estimated $1x10^{10}$ virus particles being produced per day in the average infected individual (70). *In vitro* mutation rates for HIV-1 have been reported to be in the region of $2x10^{-5}$ mutations per genome per generation (71–73). In a recent study by Cuevas and colleagues (2015), the *in vivo* genome-wide rate of spontaneous mutation in the DNA of peripheral blood mononuclear cells (PBMNCs) was quantified by examining the frequency of premature stop codons (74). This revealed a mutation rate of $4.1x10^{-3}$ per base per cell, a record rate unmatched by any other organism or virus according to the authors of the study (74). A subsequent study by Zanini and colleagues (2017) using whole genome deep sequencing estimated the *in vivo* rate to be $1.2x10^{-5}$ mutations per site per day (75), which was more closely correlated to previous *in vitro* findings.

The high mutation rate is affected by several factors, some intrinsic to the virus itself, and others arising from host cell activities. First, the HIV reverse transcriptase enzyme, which catalyses the conversion of the RNA genome into DNA, has no proofreading ability to repair incorrectly added nucleotides (71,74,76). Second, host cell enzymes belonging to the apolipoprotein B mRNA editing enzyme, catalytic polypeptide-like 3 (APOBEC3) family have been reported to mediate genomic editing, resulting in the induction of base substitution mutations throughout the viral genome (74,77,78). However, this effect is inhibited by the viral accessory protein Vif, which functions by targeting the APOBEC3 enzymes for degradation via the host cell proteasome thereby preventing lethal hypermutation of the viral genome (74,77). Lastly, the viral genome can undergo retroviral recombination when a single cell is infected by two or more different viruses, resulting in co-packaging of two different RNA genomes into progeny viruses (78,79). When the resulting genome is reverse transcribed in the next host cell, the reverse transcriptase switches between both templates leading to production of a chimeric DNA provirus with elements of both parental genomes (78). The rate of retroviral recombination of HIV-1 has been estimated at approximately 1 to 3 recombination events per genome per generation (80,81), or 2% per kilobase per generation (79).

As a result of these mechanisms, each round of HIV-1 replication leads to a wide variety of progeny viruses which have undergone extensive mutation and/or recombination. The varied progeny strains arising from mutation of a parent virus are referred to as viral quasispecies

(82,83). Given the rapid mutation rates in the viral genome and the huge numbers of viruses produced by each infected cell, the numbers of different quasispecies generated in a single patient is immense (25). These quasispecies undergo microevolutionary processes within the environment of their host, leading to selection of the most fit quasispecies, and the rapid emergence of strains adapted to overcoming potential obstacles to further replication (78). The genetic diversity of HIV-1 is therefore key to its ability to evade the immune responses of the host and to adapt rapidly to environmental changes (25,78). This leads to circumvention of treatment strategies and the evolution of resistance to antiretroviral drugs. Furthermore, as mentioned previously, the extremely variable nature of the envelope glycoproteins has stymied the development of effective vaccines, since the probability of developing a vaccine that elicits a sufficiently broad-spectrum response to be able to recognize the multitude of envelope protein mutants present in the HIV-1 population is extremely low (14–16).

A growing body of evidence suggests that the inherent genetic diversity among different HIV-1 subtypes may affect many of their biological properties. This could mean that research performed on model HIV-1-B strains may not be applicable to the non-B strains which are far more prevalent globally. For this reason, this study is focussed on HIV-1-C, with the aim of potentially identifying differences in the host cell responses to infection compared to HIV-1-B. Structurally unique features of HIV-1-C include a greater number of binding sites for NF-κB in the LTR (37), a truncation in the Rev protein, and an insertion of five amino acid residues in the Vpu protein (43), as well as extensive differences in the Env protein (43). The increased number of NF-κB binding sites and the Rev truncation should, in theory, promote increased viral gene expression (43). The protease of HIV-1-C also possesses several amino acid variants compared to subtypes A, B and D, which could affect its function. Indeed, the HIV-1-C protease has been shown to have higher catalytic efficiency than the HIV-1-B protease and has greater diversity in its cleavage sites (43). In contrast, the HIV-1-C reverse transcriptase is less efficient compared to other subtypes (43). This could be the reason for observations made using *in vitro* models, in which subtype C viruses have been demonstrated to have lower replication fitness than other types in both helper T cells and PBMNCs (43).

In addition to subtype-specific differences at a molecular level that can affect replication efficiency, subtypes may differ in other important phenotypic characteristics, such as transmissibility, tropism, virulence and development of drug resistance. Despite having

decreased replication capacity, clade C strains appear to have higher viremia set points during chronic infection and higher virus levels in genital fluids compared to other strains, which may enhance sexual transmission (37). An interesting difference between HIV-1-B and HIV-1-C is the increased tendency of HIV-1-B to undergo tropism switching. HIV-1-B infection is primarily initiated by CCR5-utilizing viruses, which subsequently evolve into dual-tropic strains and finally make the conversion into full X4-tropic viruses via ongoing mutation in the *env* gene with each round of replication (37,49). In contrast, most isolated HIV-1-C strains are R5-tropic at all stages of disease, although X4- and dual-tropic strains have also been observed (37,49,84). Perhaps because of this pattern of co-receptor usage, many HIV-1-C strains appear to be slightly less cytopathogenic than other clades (43). This may further enhance their ability to persist for long periods in an infected host cell and spread to others. Another important difference between subtypes is variations in mutational patterns across the genome that affect the development of resistance to specific antiretroviral drugs through different pathways (13,85,86). This means that certain classes of antiretrovirals may be less effective in the treatment of HIV-1-C strains compared to others.

3. $CD4^+$ T cells and HIV-1 infection

3.1. Fundamental $CD4^+$ T lymphocyte biology

3.1.1. Origin, development and differentiation of $CD4^+$ T lymphocytes

$CD4^+$ T lymphocytes are a specialized population of immune system cells characterized by co-expression of the T cell receptor (TCR) complex, which enables recognition and response to foreign peptides, as well as the CD4 co-receptor. Like all blood cells, they are ultimately derived from haematopoietic stem cells (HSCs) found in the bone marrow (87–89). From this basal cell type, a common lymphoid progenitor cell arises which is able to differentiate into all lymphocyte lineages, including T lymphocytes, B lymphocytes and natural killer (NK) cells (87–91)(**Figure 2.6**). Immature T-cell progenitors migrate from the bone marrow to the thymus. Upon entry into the thymus at the corticomedullary junction, these cells (now termed thymocytes) undergo lineage specification (92). At this stage, the thymocytes are double negative (DN) for both CD4 and CD8 (92). The DN population can be classified into subgroups based on CD44 and CD25 expression. The $CD44^+CD25^-$ (DN1) cells comprise a

heterogenous group that have the potential to differentiate into multiple lymphoid lineages including T cells, NK cells, dendritic cells, macrophages, and B cells (92). The DN1 population can be further subdivided into five subsets (DN1a-e) based on CD117 and CD24 expression (92). Of these subsets, the $CD117^{+}$ groups (DN1a, DN1b) are most likely to undergo specification to the T-cell lineage and become $CD44^{+}CD25^{+}$ (DN2) cells (92).

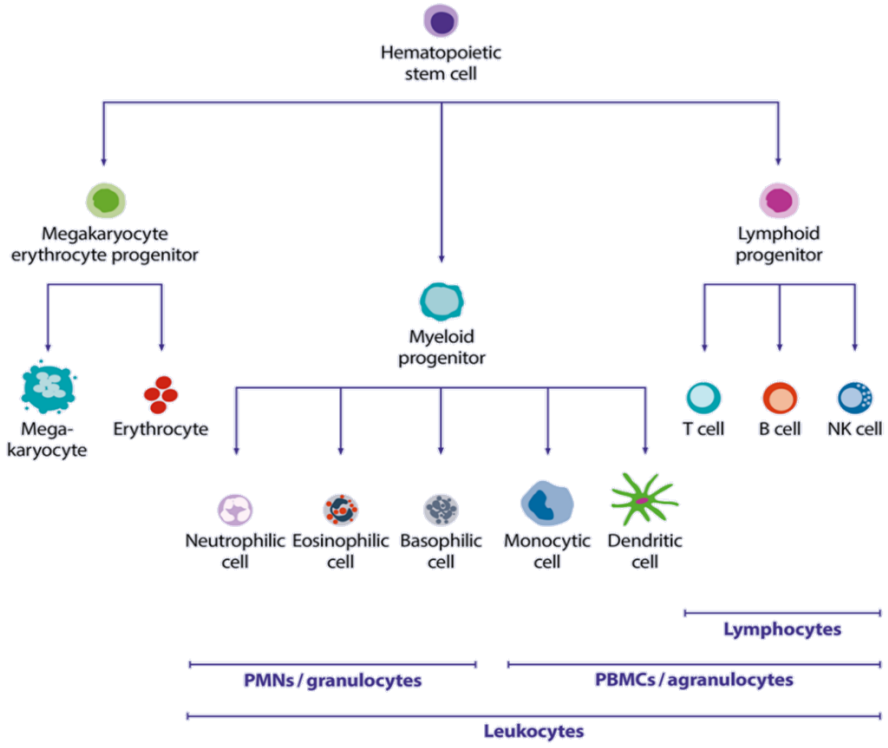

Figure 2.6: Blood cell lineages that arise from hematopoietic stem cells. From the basal haematopoietic stem cell, megakaryocyte erythrocyte, myeloid and lymphoid progenitors arise. The megakaryocyte erythrocyte progenitor can differentiate into either of these two cell types. The myeloid progenitor gives rise to a diverse array of cell types, including granulocytes (neutrophils, eosinophils, basophils) as well as monocytes and dendritic cells. The lymphoid progenitor gives rise to B and T lymphocytes as well as natural killer cells. PMN = polymorphonuclear leukocytes. PBMCs = peripheral blood mononuclear cells. Available from: https://www.miltenyibiotec.com/GB-en/resources/macs-handbook/human-cells-and-organs/human-cell-sources/blood-human.html

The DN2 cells can give rise to both conventional αβ T cells, in which the TCR is composed of TCR-α and TCR-β subunits, as well as the functionally distinct γδ T cell subset, which possesses TCR-γ and TCR-δ subunits (92). DN2 cells migrate through the thymic cortex towards the capsule and undergo rearrangements of the TCR gene segments (92). TCR gene rearrangement is a complex process that is essential for generating variability in the antigen-

binding variable regions of the TCR. At the DN2 stage, only TCR-β, TCR-γ and TCR-δ genes undergo rearrangement (92). Commitment to the αβ T cell lineage occurs with the transition of DN2 cells to the $CD44^{-}CD25^{+}$ (DN3) stage (92). Selection of DN3 cells in which TCR-β rearrangement was successful occurs via the formation of a pre-TCR complex consisting of a temporary pre-TCRα subunit associated with the newly formed β subunit, which protects against apoptotic cell death (92). This process also induces downregulation of CD25, resulting in a transient $CD44^{-}CD25^{-}$ population (DN4) located in the subcapsular region of the thymic cortex (92). The DN4 population subsequently upregulates both CD4 and CD8 to yield a double-positive (DP) population in which TCR-α gene rearrangement occurs (92).

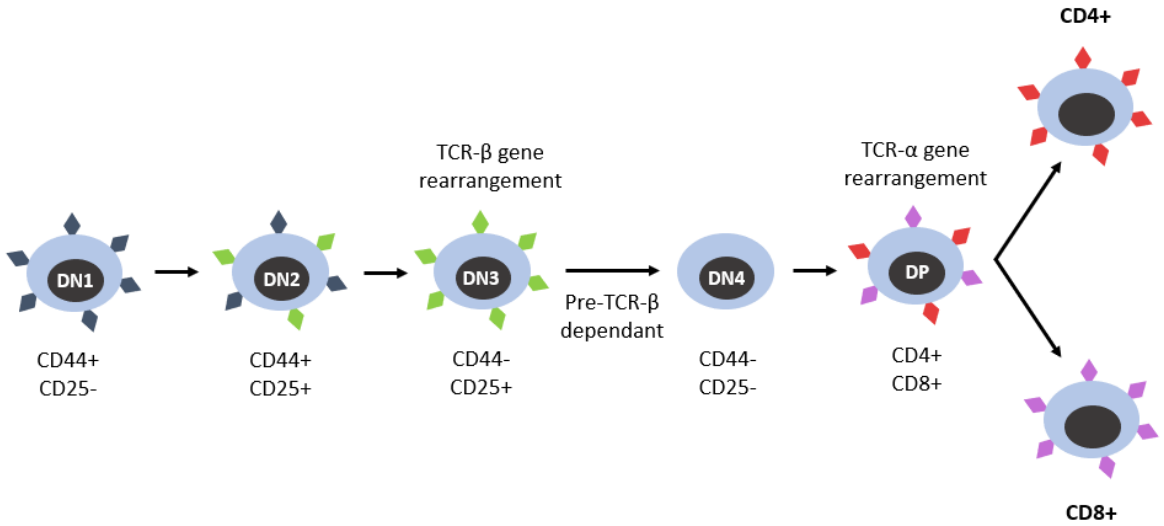

Figure 2.7: Specification of immature thymocytes to the $CD4^{+}$ and $CD8^{+}$ T cell lineages. Immature thymocytes, which are double-negative (DN) for CD4 and CD8, undergo differentiation through $CD44^{+}CD25^{-}$ (DN1), $CD44^{+}CD25^{+}$ (DN2), $CD44^{-}CD25^{+}$ (DN3), and $CD44^{-}CD25^{-}$ (DN4) stages. At the DN3 stage, TCR-β gene rearrangements occur. Only cells possessing successfully rearranged pre-TCR-β receptors survive to become DN4. TCR-α rearrangement occurs once the cells have become double-positive (DP) T cells. Final specification to either the $CD4^{+}$ or $CD8^{+}$ single positive lineages occurs from this DP precursor.

Once specification into the αβ T-cell lineage is completed by progression through the aforementioned stages, DP cells undergo simultaneous positive and negative selection in the cortex of the thymus (92). DP cells interact with self-antigens complexed to either human leukocyte antigen (HLA) class I or class II, which are presented on the cell surfaces of thymic antigen presenting cells (93). Cells with negligible affinity for HLA-antigen complexes die by neglect, due to a failure to induce signalling, while cells that bind with extremely high affinity

are actively destroyed by apoptosis (93). In contrast, cells that bind the HLA-antigen complexes with intermediate affinity are preserved. Thymocytes that survive this selection process are therefore able to respond to HLA-peptide complexes without being overly responsive to self-antigens, which could lead to autoimmune responses. The selected thymocytes become single positive for either CD4 or CD8 and undergo differentiation into either helper ($CD4^+$) or cytotoxic ($CD8^+$) T cell lineages (92,93). Maturation to fully functional naïve T cells, as well as further negative selection against self-reactive cells, occurs in the medulla of the thymus (92,93). Once matured, $CD4^+$ and $CD8^+$ T cells leave the thymus and enter the circulatory system (92,93), where they account for 70% of all peripheral blood lymphocytes (88). It should be noted that, in addition to αβ T cells, several other non-classical T cells also develop in the thymus. These include the aforementioned γδ T cells, as well as natural killer T (NKT) cells and natural regulatory (nTreg) T cells (90–92).

In order to differentiate further, naïve $CD4^+$ lymphocytes of the helper T (Th) lineage must first be activated. Activation is induced upon interaction of the TCR to its cognate antigen, presented by HLA-II which is expressed by professional antigen-presenting cells (90,94). This generally occurs in the secondary lymphoid organs (spleen, lymph nodes, mucosal lymphoid tissue), where large numbers of dendritic cells (DCs), which are the preferred antigen-presenting cell for naïve T cells, are present (90,94). The initial activation signal is augmented by a co-stimulatory signal which is supplied through the interaction of a co-stimulatory receptor with corresponding ligands on the activating antigen-presenting cell (90). CD28 is the most common co-stimulatory receptor found on naïve T cells, although others such as inducible co-stimulator (ICOS), CD27, CD137 and OX-40 may also be used (90). Common co-stimulatory ligands include CD80 and CD86, both of which are found on dendritic cells. Engagement of the TCR with concurrent co-stimulation induces a signal transduction cascade mediated by the CD3 complex associated with the TCR (90,95) that leads to proliferation and differentiation of the activated $CD4^+$ T cell into a clone of effector cells (T_{EFF}) with specificity for the activating antigen (95). Activated effector cells are responsible for migrating to the site of infection and responding to the activating antigen.

$CD4^+$ Th cells may differentiate into one of many functionally distinct effector subsets, depending on the conditions under which activation occurs. To date, the following seven subsets have been identified: Th1, Th2, Th17, Th9, Th22, Tfh (follicular helper T cells) and

induced regulatory T (iTreg) cells (95–98). Differentiation into one of these subsets is primarily determined by the various cytokines present in the activation microenvironment. These cytokines are largely dependent on the type and activation state of the antigen-presenting cell mediating activation (90). Effector T cells are short-lived, lasting only long enough to eliminate the activating pathogen (95). A subset of the progeny produced from proliferation following activation transition into long-lived memory cells, which have the ability to respond rapidly upon re-exposure to the same stimulus (95,99). Memory cells may be found in the secondary lymphoid organs, in which case they are referred to as central memory T cells (T_{CM}) or in the infected tissue, in which case they are referred to as effector memory T cells (T_{EM}) (95). Effector memory T cells can transition back to effector cells with relative ease, while central memory cells can only be reverted upon re-exposure to the same pathogen. T_{EFF}, T_{EM} and T_{CM} $CD4^+$ T cell populations can be identified through differential expression of CD25, CD45RA, CD45RO and CD127 (95) (**Figure 2.8**).

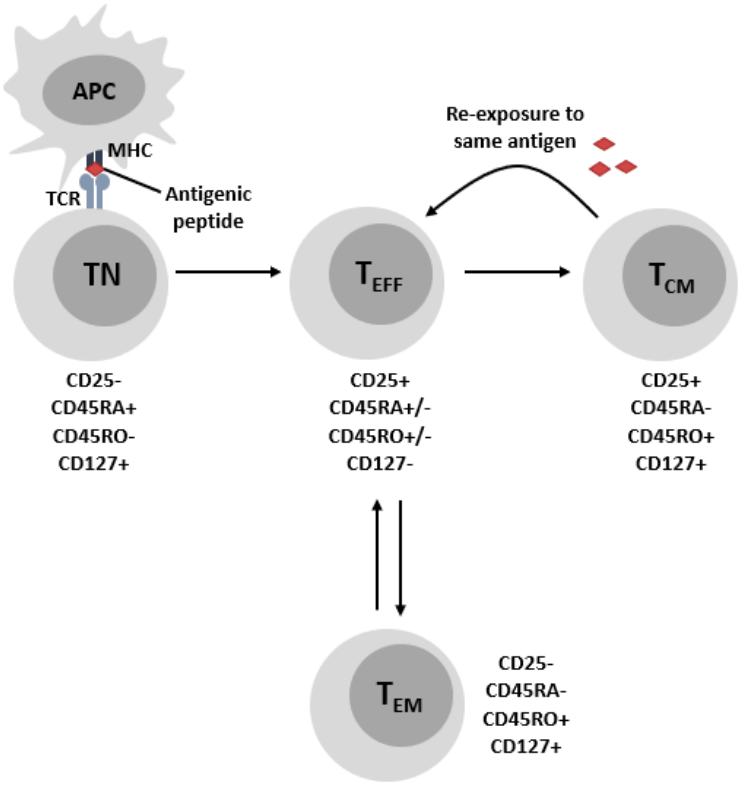

Figure 2.8: Functional differentiation of naïve T cells upon activation. Naïve T cells (TN) are activated into effector T cells (T_{EFF}) upon exposure to an antigen presented by an antigen-presenting cell (APC). Effector T cells can transition into either effector (T_{EM}) or central memory (T_{CM}) T cells. Adapted from Golubovskaya *et al.* (2016) (95).

3.1.2. Functional roles of CD4⁺ T lymphocytes

$CD4^+$ T lymphocytes are considered master regulators of the adaptive immune response, although they also interact closely with cells of the innate immune system. Their primary mode of operation is through the production of specific cytokines and chemokines which coordinate the responses of other immune cells (90,91,96,98). However, they also utilize direct cell-to-cell interactions for the induction of cell-mediated and humoral immune responses, though the activation of $CD8^+$ cytotoxic T lymphocytes and B lymphocytes respectively (88,89). The precise mechanism by which $CD4^+$ T lymphocytes regulate other immune cells is determined by the subset to which they belong (Th1, Th2, Th17, Th9, Th22, Tfh, iTreg), since each subset produces a different set of effector cytokines (**Figure 2.9**). These specialized subsets develop in response to the cytokine environment of the tissues in which they reside. These environmental cues result in the induction of various signal transducer and activator of transcription (STAT) family members which are responsible for triggering expression of lineage-specific genes (90,96,98). The roles of each of the seven $CD4^+$ T lymphocyte subsets derived from the classical Th lineage in modulating immune responses will be discussed in the section to follow.

Th1 cells are generally recognised as a primarily pro-inflammatory $CD4^+$ T cell subset (90,91). They are induced by the cytokines interleukin (IL) 12 and interferon (IFN) γ, which activate signal transduction pathways leading to upregulation of the Th1 master regulator gene, T-bet (90,91,98). The principal cytokines induced by T-bet expression are IFN-γ, tumour necrosis factor β (TNF-β) and IL-2 (90,91,95). A positive feedback loop is thus formed from Th1 cells producing IFN-γ which stimulates further Th1 differentiation (90,91). Th1 cells are particularly important for the response to intracellular pathogens such as *Mycobacterium tuberculosis* (91). The INF-γ they secrete is important for activation of macrophages (91,95) and for increasing expression of Toll-like receptors (TLRs) on innate immune cells (95). IL-2 is important for T lymphocyte activation and is involved in the ability of $CD8^+$ cells to transition to memory cells (91). The dysregulation of Th1 cells has been implicated in several autoimmune diseases and other chronic inflammatory conditions (91).

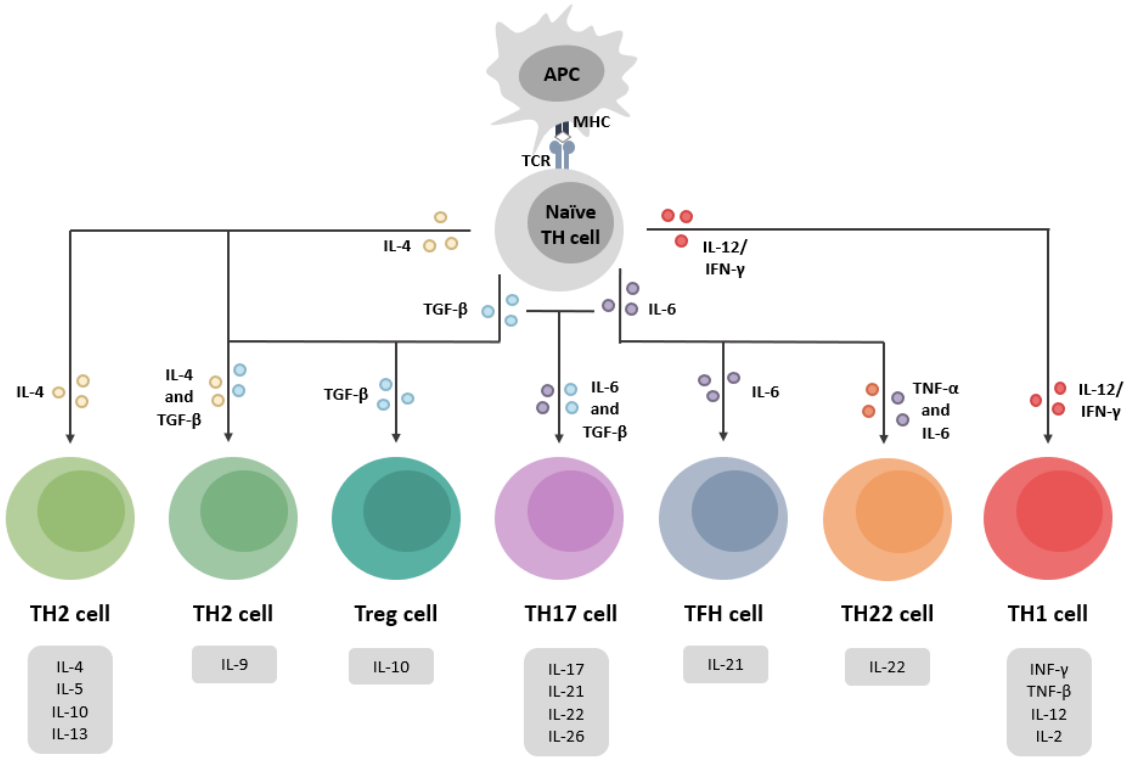

Figure 2.9: Differentiation of naïve T cells into various effector subsets following activation. The cytokines present at the time of activation (indicated as coloured dots) lead to the stimulation of the various effector phenotypes, each of which secrete a specific set of effector cytokines (indicated in the grey boxes).

Th2 cells, on the other hand, tend to release anti-inflammatory cytokines that counteract the activities of Th1 cells. The production of Th2 cells is mediated by IL-4, which induces expression of the master regulator GATA3, via STAT 6 mediated signalling (91). The major cytokines of this subset are IL-4, IL-5, IL-10 and IL-13 (91,98). As for INF-γ in Th1 cells, Th2 cells possess a positive feedback mechanism mediated by IL-4, which is both a product and a differentiation stimulus for this cell type (91). The primary role of Th2 cells is the induction of immune defences against extracellular parasites, such as helminths (91,98). They also play a causative role in allergic reactions and asthma (91,98). IL-4 is critical for B lymphocyte function, as it mediates immunoglobulin class switching (91). IL-5 stimulates eosinophil recruitment to the site of an infection (91), while IL-13 is critical for elimination of helminthic parasites (91).

The Th17 subset, like Th1 cells, is primarily pro-inflammatory although they secrete different effector cytokines. Differentiation into the Th17 subset consists of three stages: 1) initiation by exposure to IL-6 in combination with transforming growth factor β (TGF-β); 2) amplification

due to exposure to IL-21; and 3) stabilization due to sustained IL-23 production (90,97). All the aforementioned cytokines activate STAT 3, leading to expression of Retinoic acid-related orphan receptor γ T (RORγT), which functions as the master regulator of Th17 responses (90,97,98). RORγT-expressing Th17 cells secrete IL-17A, IL-17F, IL-21, IL-22 and IL-26 (90,91,97). The main function of these cells is to control immune responses towards extracellular bacteria and fungi through the activities of their cytokine products (90,91,95). IL-17A is a pro-inflammatory cytokine that induces release of other inflammatory signalling molecules such as IL-6 and IL-8 (90,91). IL-17A and IL-17F are both involved in activation of neutrophils in response to bacterial and fungal pathogens (90,91). IL-21 induces pro-inflammatory responses from $CD8^+$ T cells, B lymphocytes, NK cells and DCs (90,91).

The responses of Th9 cells, which secrete IL-9 as their primary cytokine, were initially attributed the Th2 subset before being recognised as a distinct cell type. This is because the signals leading to Th9 responses overlap significantly with Th2 signals (96). Th9 cells are primed by exposure to IL-4; however, IL-9 production is only induced in the presence of TGF-β (96). Unlike the previously discussed subsets, no master regulator has yet been identified for Th9 cells. However, it has been established that STAT6 (induced as a result of IL-4 stimulation) plays a critical role in priming cells for Th2/Th9 differentiation, while TGF-β induces SMAD proteins that alter the STAT signalling response away from the classical Th2 pathway and ultimately leading to induction of IL-9 (96). The Th9 subset is involved in recruitment of mast cells and eosinophils, the expulsion of helminths, and has also been implicated in the development of allergic diseases (96,98). Th9 cells have been shown to have potent anti-tumour activity, although this seems to be restricted to solid tumours such as melanoma and adenocarcinoma (96). Conversely, Th9 cells have been implicated in promoting other cancers, such as lymphomas (96).

The Th22 subset is characterized by secretion of particularly high levels of its prototypical cytokine, IL-22, and downregulation of cytokines typical of other subsets such as IFN-γ, IL-4 and IL-17 (97,100). Differentiation into this lineage is mediated by engagement of the aryl hydrocarbon receptor (AHR) transcription factor (97,100). Cells which express receptors for IL-22 are generally non-immune cells found at barrier surfaces, such as the skin, gastrointestinal tract and the respiratory system (97,100). IL-22 is implicated in antimicrobial responses, particularly against bacteria such as *Mycobacterium tuberculosis* and *Klebsiella*

pneumoniae (97). For example, in skin keratinocytes, IL-22 causes upregulation of antimicrobial molecules such as β-defensins, psoriasin, and calgranulins (97). This cytokine also appears to be related to viral responses and facilitates viral clearance (97). An interesting side note is that that patients which demonstrate resistance to HIV-1 appear to have elevated IL-22 levels (97). IL-22 also appears to play an important role in wound healing and tissue repair (97).

A relatively high proportion of the total Th cell population belongs to the Tfh subset, which is generally located in lymphoid tissues (97). The primary function of Tfh cells is assisting in the activation and differentiation of B lymphocytes as they mature (98,101). They play an important role in the establishment and maintenance of germinal centres, in which differentiation of naïve B lymphocytes into plasma and memory cells takes place following exposure to antigenic peptides (98,101). They are essential for processes such as isotype switching, somatic hypermutation and affinity maturation, which are crucial for normal B cell development (101). They exert regulatory functions through the secretion of soluble factors such IL-21, IL-4 and C-X-C motif chemokine ligand (CXCL) 4, as well as through direct interaction with B cells (101). Differentiation into this lineage is mediated by IL-6, in the absence of TGF-β (98,101). The expression of the primary effector cytokine, IL-21, is induced by the B cell lymphoma 6 (Bcl-6) transcription factor, which functions as the master regulator for this subset (98,101).

The functions of the Treg subset include suppression the responses of the other subsets through the induction of negative regulatory pathways and the establishment of self-tolerance (91,98). Treg cells can be split into two groups, the naturally occurring nTreg cells, which arise pre-differentiated from the thymus, and the iTreg subset which differentiate upon exposure to cytokine signalling during interaction with an antigen-presenting cell, like the rest of the Th subsets. The differentiation of iTregs from naïve T $CD4^+$ T cells is induced by TGF-β signalling in the absence of pro-inflammatory cytokines (91,98). TGF-β activates SMAD signalling pathways that promote expression of the iTreg master regulator gene, forkhead box P3 (Foxp3) (91,98). Tregs produce suppressive cytokines, including TGF-β, IL-10 and IL-35 (91,95). IL-10 is a potent inhibitor of Th1 differentiation, and also inhibits dendritic cell activities (91). Tregs also supress activation of other T cells by direct cell-to-cell contact, through the action of cytotoxic T-lymphocyte-associated protein 4 (CLTA-4). This ligand binds

to CD80/CD86 on antigen-presenting cells, preventing the induction of CD28-mediated costimulatory signals.

3.2. The response of CD4$^+$ T lymphocytes to infection with HIV-1

The cellular response to infection constitutes a mosaic of HIV-directed events, which promote replication mediated by the activities of viral proteins, and host-directed events which attempt to limit viral replication. In a successful infection, the HIV-directed responses counteract or undermine the defence responses of the host cell, allowing the virus to take control. CD4$^+$ T lymphocytes have long been recognized as being the predominant target for infection by HIV-1, and the progressive depletion of this cell population is a hallmark of HIV pathogenesis (37,102). CD4$^+$ T lymphocytes possess several qualities that make for a highly favourable environment for HIV-1 replication, such as ample surface expression of receptors required for viral entry as well as expression of transcription factors essential for viral replication (22,29). Infection of CD4$^+$ T cells with HIV-1 leads to widespread modulation of cellular processes, including transcriptional and translational regulation, cell cycle regulation, immune functions, cellular metabolism, and stress response mechanisms (44,59,103–107). Ultimately, most cells are unable to withstand the combined effects of the various stresses imposed by the viral onslaught and frequently undergo apoptosis.

A trait that is common to all retroviruses, including HIV-1, is the subversion of the host cell biosynthetic machinery for viral replication. Infected CD4$^+$ T lymphocytes display modulation of a diverse array of transcriptional control networks, as well as alteration of translational and protein trafficking pathways. HIV appears to suppress overall synthesis of host cell mRNA in favour of viral transcript expression (104,106,108,109). This is primarily due to the activities of the viral Tat protein, which functions as an extremely potent transcription factor and co-opts essential host transcription elongation factors to drive viral gene expression (22,29,45). In addition to transcriptional dysregulation, HIV-1-infection is associated with inhibition of host protein translation and dominance of the translation of viral structural proteins (108). This effect can be attributed to the HIV-1-mediated arrest of the cell cycle in the G2/M phase (108). In this phase, translation of cellular transcripts (and fully spliced viral transcripts) is suppressed due to the limited activity of the essential eukaryotic translation initiation factor 4E (eIF4E), a cytoplasmic cap binding protein (108). The unspliced viral mRNAs that encode

late stage viral products are exempt from this limitation, due to retention of nuclear cap binding complex components that allow eIF4E-independent initiation of translation (108). In addition, a study by Kleinman and colleagues (2014) showed that that HIV-1 infection is linked to impaired ribosome biogenesis in the nucleolus, which could lead to further inhibition of translation.

Dysregulation of cell cycle signalling is a marked feature of HIV-1 infection. It has been well established that the accessory protein Vpr is responsible for inducing the characteristic arrest of the cell cycle at the G2/M phase checkpoint, which prevents infected cells from entering mitosis (108,110,111). The currently accepted mechanism by which Vpr affects the cell cycle is through inactivation of cyclin-dependent kinase 1 (CDK1), which is associated with cyclin B and regulates the G2/M transition (111). Vpr does not interact with this complex directly but has been shown to interact with an upstream regulator, protein phosphatase 2A (PP2A) (111,112). PP2A controls phosphorylation of cell division cycle 25 (CDC25) and WEE1, which in turn control activation of CDK1 as positive and negative regulators respectively (111,112). Gene expression studies in HIV-1-infected $CD4^+$ T cells have demonstrated upregulation of WEE1 and other negative regulators of CDK1, such as myelin transcription factor 1 (MYT1) (102,113). Upregulation of 14-3-3 proteins and CHK kinases, which inactivate CDC25, as well as direct modulation of CDC25 itself, have also been reported (102,113). It is important to note that cell cycle arrest can also be initiated by the host cell itself as a response to DNA damage, through the p53 pathway, ultimately leading to the induction of apoptosis (110,113).

Immune activation of $CD4^+$ T lymphocytes plays a central role in the life cycle of HIV-1. As described previously, the expression of HIV genes requires the presence of host cell transcription factors induced as a result of T cell activation for which there are response elements in the viral LTR, such as NF-κB, NFAT and AP-1 (22,29,34,44). It is therefore not surprising that studies examining the transcriptome of HIV-infected $CD4^+$ T cells frequently identify upregulation of both these transcription factors as well as the genes under their control (44,114–116). HIV-1 further exploits these pathways through mechanisms that enhance expression of activation-associated genes. For instance, Nef is recruited into the immunological synapse and promotes expression of NFATc, NF-κB, interferon regulatory factor 1 (IRF) 1, IRF-2, Fos and Jun (114,117). Nef also appears to induce production of the essential Tat cofactor, cyclin-dependent kinase 9 (CDK9), thereby enhancing viral gene

expression further (114). Tat itself can promote activation and proliferation of surrounding bystander cells through upregulation of IL-2 (118,119), thereby providing a continuous pool of new cells to infect.

In addition to promoting inappropriate activation signalling, HIV-1 can have marked effects on other immune effector functions of $CD4^+$ T lymphocytes. HIV-infected patients present with an imbalance in the ratio of pro-inflammatory and anti-inflammatory cytokines produced by the various Th cell subsets (44,120). In general, HIV-infected $CD4^+$ T cells express cytokine profiles consistent with the pro-inflammatory Th1 and Th17 cell subsets, rather than the Th2 type (44). These perturbations in cytokine networks contribute to the overall dysregulation of immune system functioning and chronic immune activation that is often associated with HIV-1 infection. In addition to modulation of cytokine secretion, HIV-1 can mediate the downregulation of HLA class I, thereby preventing the induction of $CD8^+$ T cell and NK cell responses against the infected cell (121,122). HLA-A and HLA-B are affected by Nef (122), while the downregulation of HLA-C is mediated by the activities of Vpu (121,122). Genes relating to motility and chemotaxis also appear to be affected in infected $CD4^+$ T cells (106,107), which may impair their ability to migrate to sites of infection and facilitate immune responses.

$CD4^+$ T cells do, however, possess antiviral mechanisms that are activated as a result of HIV-1 infection, which may ameliorate some of the deleterious effects and slow viral replication. Many transcriptomic studies have identified defence response genes to be functionally enriched in HIV-infected $CD4^+$ T cells, the most important of which are interferons (INFs) and interferon stimulated genes (ISGs) (107,115,123–125). Interferons are innate immune system signalling molecules produced in response to viral/microbial infection (126). The binding of IFNs to their corresponding receptors initiates signalling through the Janus kinase signal transducer and activator of transcription (JAK-STAT) pathway and consequent activation of ISGs (126). ISGs may directly interfere with pathogen functioning, or may enable elimination of the infected cell through induction of p53-dependant apoptosis and exertion of immunomodulatory effects on other immune cells (126). ISGs upregulated in response to HIV-1 generally include those induced by Type I interferons (e.g. INF-α, INF-β), such as Mx proteins, oligoadenylate synthetase (OAS) family members, and interferon regulatory factors, such as IFN-7 (125). Early in the infection process, HIV-infected $CD4^+$ T cells present with

increased expression of INF-α family members and MxB (103,104). Upregulation of interferons and ISGs becomes more pronounced in the chronic phase of infection during which viral replication is more efficiently controlled (107,124,125,127).

HIV-1 has also been shown to modulate diverse aspects of the metabolism of $CD4^+$ T cells, particularly with respect to glucose and lipid metabolic pathways (59,113,128,129). Nef plays a particularly important role in the modulation of cholesterol metabolism, through upregulation of genes involved in cholesterol uptake and intracellular biogenesis (129–131). Cholesterol is an essential component of lipid rafts, which are specialized microdomains of the lipid bilayer of cell membranes (129,130,132). They have been shown to be essential in the viral life cycle, enabling concentration of viral structural components in defined regions during virion assembly and budding (129,130,132) and by acting as platforms for viral entry which facilitate receptor-virus interactions (129,130). Metabolism of lipids other than cholesterol may also be affected by HIV-1 infection. A proteomics-based study identified several proteins involved in enhancing free fatty acid, triglyceride and lipoprotein synthesis, as well as regulation of lipid transport and lipid oxidation that were modulated by HIV infection in a human T cell line (133). These findings corroborate clinical studies in which elevated triglyceride and lipoprotein levels were detected in treatment-naïve HIV patients (134,135). This dysregulation of lipid metabolism leads to the presentation of lipodystrophy in HIV-infected patients, and is exacerbated by several antiretroviral treatments, particularly protease inhibitors (133–135).

Another proposed mechanism of HIV-1 pathogenesis in $CD4^+$ T lymphocytes is metabolic exhaustion that arises as a consequence of interactions between pro-inflammatory activation signals and glucose metabolism. A key gene linked to both increased metabolic activity and HIV-infection is glucose transporter (Glut) 1 (59). This gene mediates the transition from oxidative phosphorylation, carried out in resting T cells, to the less efficient aerobic glycolytic pathway used in activated cells in response to inflammatory signals (59). Since activated $CD4^+$ cells have inherently low energy reserves and predominantly make use of adenosine triphosphate (ATP) in biosynthetic rather than metabolic pathways to support cell proliferation (59), the Glut-1-mediated transition to glycolysis renders them highly susceptible to metabolic exhaustion and eventual cell death (59). In addition to Glut-1, other genes relating to glucose metabolism have been shown to be upregulated by HIV, including

Glut-3, Glut-4, Glut-6 and Hexokinase-1 (128). Modulation of these genes in HIV-infected cells results in abnormally high levels of glucose uptake, which induces oxidative stress. In addition, enhanced glucose uptake is associated with upregulation of CXCR4 expression, allowing for increased entry of X4-tropic strains (59).

As mentioned in the preceding discussion, apoptosis is often the ultimate consequence of infection of $CD4^+$ T lymphocytes. This occurs as a result of multifactorial stresses imposed by the activities of the virus, including dysregulation of normal cellular functions due to cell cycle arrest, genotoxic stress as a result of viral integration, oxidative stress, and metabolic exhaustion. In one of the first transcriptomic studies of HIV-infected $CD4^+$ T cells, Corbeil and colleagues (2001) observed the increased expression of proapoptotic genes belonging to the p53 apoptotic pathway (104). Since then, many other studies have highlighted modulation of apoptotic genes as one of the most pronounced features of the transcriptome of HIV-infected $CD4^+$ T cells (44,105,106,113,136). Frequently reported pro-apoptotic genes that are upregulated upon response to infection include Bcl-2-associated X (Bax) (104,113,116), growth arrest and DNA damage 45 (GADD45) (44,104,125), Fas/Fas ligand (44,136), Bcl-2 antagonist/killer (BAK) (113,125), heat-shock protein 90 (HSP90) (115,136), mouse double minute 2 homolog (MDM2) (44,104), as well as p53 itself (104,113,116,125). The expression of these pro-apoptotic genes leads to the induction of caspases (particularly caspases 2, 3, 6, 7 and 9) which mediate cell death via controlled proteolysis (104,125). HIV-1-infected $CD4^+$ T cells also demonstrate corresponding down-regulation of cell survival and anti-apoptotic genes like B-cell lymphoma 2 (Bcl-2) and B-cell lymphoma x (Bcl-x) (104,136). The induction of apoptotic pathways is a common response to stresses and other intracellular pathogens, induced to prevent replication of damaged and/or infected cells. However, in the case of HIV-1, these mechanisms fail to contain the infection, leading to the ultimate destruction of $CD4^+$ T cells in untreated patients.

4. Macrophages and HIV-1 infection

4.1. Fundamental macrophage biology

4.1.1. Origin, development and differentiation of macrophages

Macrophages comprise a heterogenous population of cells distributed throughout multiple tissues in the body, which, along with monocytes and dendritic cells, form part of the mononuclear phagocyte system (88,89). They are assigned various names depending on their tissue specializations. Macrophages may be found in fat (adipose tissue macrophages), the alveoli of the lungs (alveolar macrophages), in connective tissues (histocytes), in lymph nodes (sinus histiocytes), in the kidneys (intraglomerular mesangial cells), in bone (osteoclasts), in the peritoneal cavity (peritoneal macrophages), in the red pulp of the spleen (sinusoidal lining cells), in the liver (Kupffer cells), and in the brain (microglia) (88,89,137). Macrophages residing in these various tissues are exposed to and profoundly affected by the various cytokines, chemokines, microbial by-products, and other cell types that occur within their specific tissue microenvironments (137,138). Therefore, different types of tissue macrophages possess different phenotypic properties and have the capacity to perform specialized functions (54,137).

The classically described pathway though which macrophages arise is from differentiation of adult HSCs along the myeloid lineage. HSCs give rise to common myeloid progenitors (137), which have the capacity to form megakaryocytes, erythrocytes, granulocytes (including neutrophils, basophils and eosinophils), dendritic cells and monocytes (see **Figure 2.6**). The common myeloid progenitors progress through sequential stages of differentiation, first giving rise to a granulocyte-macrophage progenitor, which is further differentiated into a common macrophage-dendritic cell precursor and finally into monocyte and dendritic progenitors which are fully committed to their respective lineages (137)(**Figure 2.10**). The committed monocyte progenitors mature into functional monocytes, which may be found circulating in the peripheral blood, as well as in the bone marrow and spleen (137). Monocytes can be recruited from the vasculature into various tissue compartments where they undergo differentiation into macrophages (88,89,137,139). The migration of monocytes from the peripheral blood is mediated by the interactions of C-C motif chemokine ligand (CCL) 2 or

CXCL1 with their cognate receptors on monocytes (137). These signalling molecules are released by fibroblasts, epithelial cells and endothelial cells in response to inflammatory signals or microbial products (137).

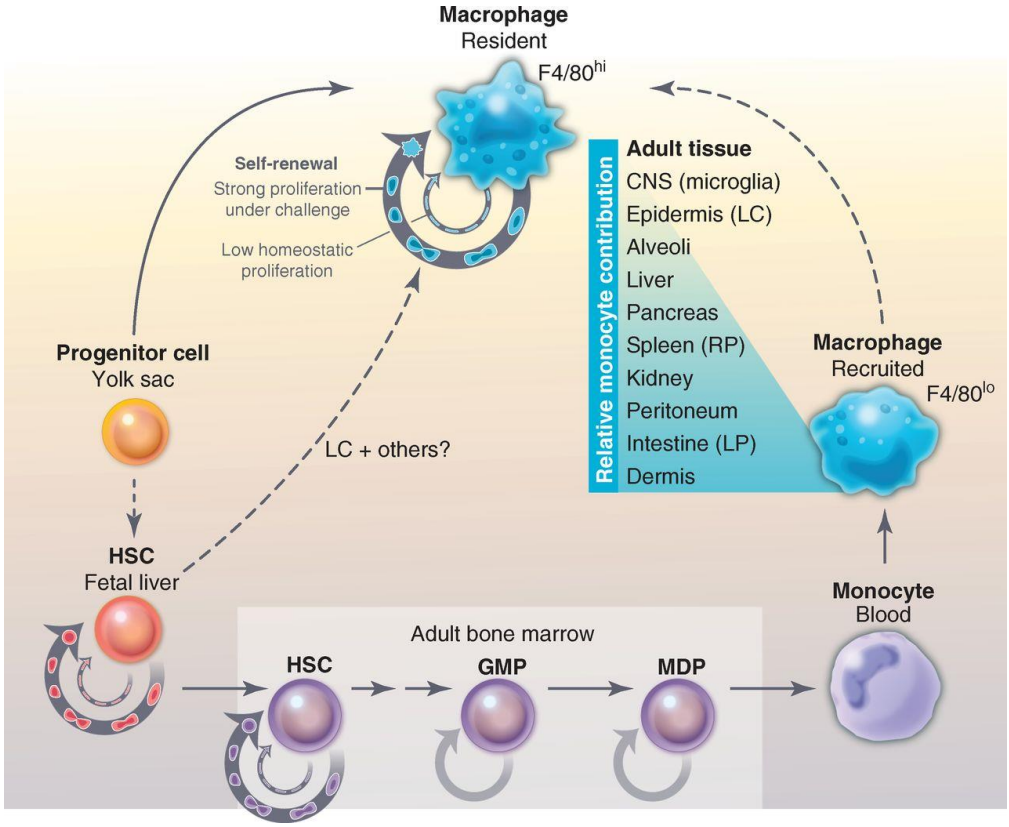

Figure 2.10: Illustration of the various origins of tissue-resident macrophages. Embryonically derived macrophages can arise from undifferentiated haematopoietic cells (hemangioblasts) which are initially present in the yolk sac, or in the fetal liver during later stages of development. In the adult bone marrow, macrophages can arise though differentiation of hematopoietic stem cells (HSC) initially into granulocyte-macrophage progenitor (GMP), then macrophage-dendritic cell progenitor (MDP) stages and finally into peripheral blood monocytes. Monocytes can be recruited into the various tissues indicated (blue shading), where they can differentiate into tissue-resident macrophages. Taken from Sieweke and Allen (2014) (140).

Monocyte-derived macrophages (MDM) are not the only source of macrophages in the various tissues of the body (**Figure 2.10**). Distinct lineages of embryonically derived macrophages also exist that populate tissues before birth. These lineages are derived from haemangioblast precursors produced during embryonic haematopoiesis, which occurs in the yolk sac of the developing embryo and in the fetal liver at later stages of development (137,141). Tissue resident macrophages of these embryonic lineages have recently been shown to have the potential for self-renewal, despite an apparent state of terminal

differentiation (137,140,141). Embryonically derived macrophages play important roles in the clearance of dead cells and tissue remodelling during development and rapid tissue growth (137,141). For instance, microglia in the developing brain are involved in regulation of neuronal patterning, the process by which neurons acquire specific functions based on their spatial position, through direction of either cell survival or programmed cell death (141). In fully developed adult tissues, these cells are mainly involved in maintenance of tissue homeostasis and resolution of inflammation (137,141). The proportions of embryonic to monocyte-derived macrophages varies from tissue to tissue (137,141), adding to the heterogeneity of the macrophage population as a whole.

The two most important growth factors involved in macrophage differentiation are macrophage colony stimulating factor (M-CSF) and granulocyte-macrophage colony stimulating factor (GM-CSF). M-CSF is produced constitutively by multiple cell types throughout the body and promotes proliferation of mononuclear phagocytic cells under homeostatic conditions (137,142). This includes the enhanced production of monocytes via haematopoiesis from the bone marrow, as well as proliferation and self-renewal of tissue-resident macrophages (137). Mature monocytes and macrophages express high levels of the M-CSF receptor. Therefore, when the number of mature cells is sufficiently high, M-CSF is sequestered by binding to its cognate receptor on these cells, and a negative feedback loop is formed that inhibits further differentiation from the bone marrow (137,142). GM-CSF, on the other hand, is mainly produced by activated leukocytes and is involved in enhancing the activation and survival of monocytes and macrophages that have been recruited to sites of infection or inflammation (137,142).

4.1.2. Functional roles of macrophages

Macrophages have many essential roles within the body. First, they are key effector cells of the innate immune system and are involved in the elimination of pathogens, virally-infected cells and cancer cells (54,88,89,143). They are primarily responsible for the recognition, phagocytosis and intracellular killing of invading pathogens (54,88,89,143). In addition, macrophages have the capacity to act as professional antigen-presenting cells, by processing phagocytosed pathogens and presenting the resulting antigenic peptides to other immune cells (54,88,89,143). They can also exert pro-inflammatory responses through the production

of reactive oxygen/nitrogen species and inflammatory cytokines in response to activating signals (54,137,139). In addition to their roles in the immune system, macrophages have important functions in the maintenance of tissue homeostasis though the elimination or repair of damaged cells and tissue matrices (54,137,139). The function exerted by any given macrophage will be dependent on the timing and type of activation signals the cell receives within its microenvironment (**Figure 2.11**).

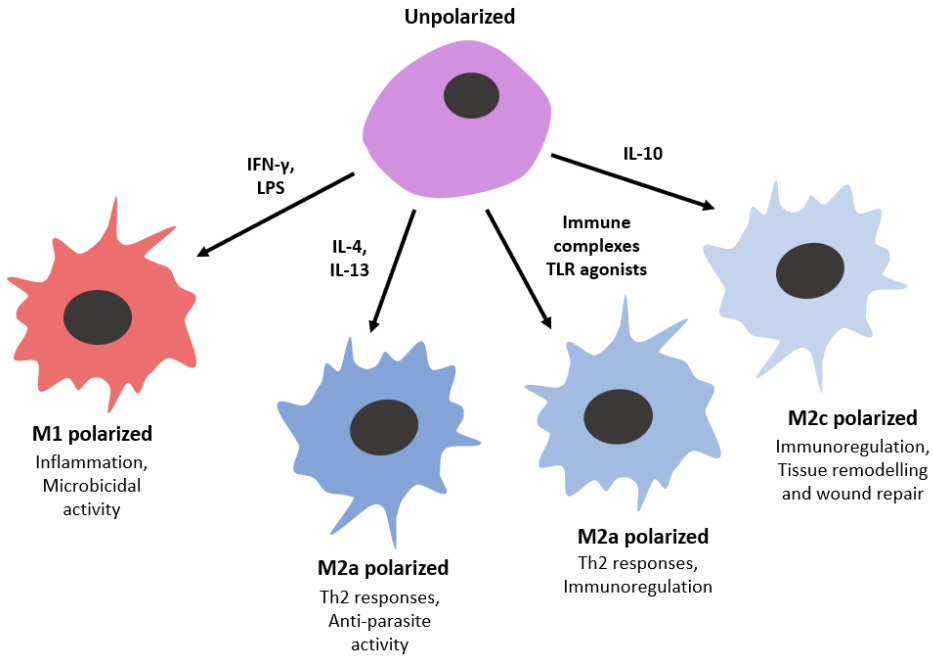

Figure 2.11: Polarization pathways of monocyte-derived macrophages. Depending on the type of stimulus present at the time of activation, unpolarized monocytes can differentiate into macrophage sub-populations with different polarization states (M1, M2a, M2b, or M2c). These differentially polarized macrophages perform specialized functions.

Macrophage polarization was initially described using terms analogous to the classical Th cell subsets. Macrophages with pro-inflammatory functions similar to the Th1 subset were described as M1 polarized, while the opposing anti-inflammatory Th2-like macrophages were designated as M2 (138). These subsets may also be referred to as classically activated (M1) and alternatively activated (M2) macrophages, respectively. M1 macrophages are highly responsive towards bacterial infections, intracellular pathogens and cancer cells. They release inflammatory effector cytokines such as IL-1 β, IL-12, IL-23 and tumour necrosis factor α (TNF-α) as well as reactive oxygen and nitrogen species (138). *In vitro* experiments indicate that M1 macrophages can be induced by exposure to the Th1 cytokines INF-γ and TNF-α, in

combination with TLR or nucleotide-binding oligomerization domain-like receptor (NLR) agonists (144). GM-CSF plays an important role in inducing the proliferation of MDM in response to inflammation and priming them towards an M1-like phenotype (137). However, full polarization requires exposure to the aforementioned pro-inflammatory signals.

Macrophages of the anti-inflammatory M2 program are proposed to represent the default state of macrophages maintained under homeostatic conditions due to the production of M-CSF (137). They are characterized by the secretion of the anti-inflammatory cytokine IL-10, and the expression of scavenger and mannose receptors (138). M2 macrophages comprise a more heterogenous population than M1 macrophages and are thus sub-divided into the following subsets: M2a, M2b and M2c (138). The M2a subset is produced as a result of exposure to IL-4 and/or IL-13, while M2b is induced by stimulation with immune complexes, IL-1 receptor antagonists, or TLR agonists, in the absence of pro-inflammatory stimuli (138). Both M2a and M2b macrophages are involved in driving Th2 type responses, such as the elimination of extracellular parasites, as well as the enhancement of phagocytosis (138). The M2c population is induced by exposure to IL-10, and is involved in suppression of inflammatory responses as well tissue repair and remodelling (138).

4.2. The response of monocyte-derived macrophages to infection with HIV-1

Like $CD4^+$ T lymphocytes, cells of the monocyte/macrophage lineage are important cellular targets of HIV-1 and are among the first cell types to be infected as they are present in tissues that have a high risk of HIV exposure, such as the vaginal mucosa. In addition, macrophages constitutively express both CD4 and CCR5 on their cell surfaces (54,145), although the level of CD4 expression is generally lower than that observed on $CD4^+$ T lymphocytes (56). CXCR4 expression, although not typical, has been reported in primary macrophages and may be used for entry by dual-tropic HIV-1 if expressed (68). An important difference in the response to HIV exposure in macrophages (and other myeloid cells) compared to $CD4^+$ T lymphocytes is that infection is far less cytotoxic (54,146). This is attributed to intrinsic expression of host cell restriction factors in this cell type, such as SAM domain and HD domain-containing protein 1 (SamHD1) and the APOBEC3 family of enzymes (143,147). Freshly isolated peripheral blood monocytes are reported to be highly resistant to infection *in vitro*, and the presence of HIV-1 is only detected in a tiny fraction (0.001%-1%) of monocytes *in vivo* (148–150). Differentiated

macrophages are more susceptible than monocytes to infection by HIV-1, particularly R5-tropic strains (54,147,151). This has been linked to the progressive increase in expression of CCR5 as they mature, as well as concurrent downregulation of the APOBEC3 enzymes (54,147,148).

Although macrophages are resistant to the direct cytopathic effects of HIV infection which occurs in $CD4^+$ T lymphocytes (152), they do develop a wide range of physiological dysfunctions. Like $CD4^+$ T cells, the cell cycle of infected macrophages is dysregulated by the activities of Vpr, resulting in arrest at the G2/M checkpoint as previously described for $CD4^+$ T cells (153,154). However, unlike $CD4^+$ T lymphocytes, infected macrophages persistently fail to undergo apoptosis even when infected with a productively replicating virus (152). Infected macrophages demonstrate a reduction in their primary effector functions such phagocytosis, phagosome-lysosome fusion and antigen presentation (54,152,155) as well as aberrant killing of uninfected $CD4^+$ and $CD8^+$ T lymphocytes (152). Furthermore, they present with abnormal secretion of various cytokines and other signalling molecules, resulting in dysregulation of the activities of other immune cells that respond to these signals (152,154,155). Finally, infected macrophages appear to lose their chemotactic motility and are thereby unable to effectively respond to invading pathogens (154,155).

These alterations in macrophage behaviour as a result of infection have been linked to modulation of the host cell transcriptome. Dysregulated biological pathways include apoptosis (31,32), cell cycling and cell proliferation (31,32), inflammation and immune responses (154), cell motility (154), signal transduction (31,32), energy and protein metabolism (154), cytoskeletal motility (154) and host defence (30,32). The induction of host defences includes the upregulation of well-documented genes encoding antiviral proteins (such as Mx1, Mx2, and OAS1) and other ISGs which are essential for the innate immune response (155). ISGs were found to account for a large proportion of genes modulated in response to HIV-1 exposure in several transcriptomic studies (155–158). Interestingly, a study by Wie and colleagues (2013) found that several known anti-viral ISGs (IFI44, ISG15, and OAS1) were markedly downregulated in primary macrophages which were primed with interferons and then exposed to HIV-1 (159), indicating that HIV-1 possesses mechanisms by which it can undermine interferon-associated antiviral response. It has also been hypothesized that interferon stimulation may in fact be favourable for HIV-1, enabling viral

replication though induction of transcription factors that promote viral gene expression like NFAT, while simultaneously preventing competitive superinfection (155).

A major mechanism by which infected macrophages can mediate systemic changes in other host cells is through the modulation of cytokine and chemokine networks. Infected macrophages tend to produce increased levels of pro-inflammatory cytokines, such as TNF-α, IL-1, IL-6, IL-8 (54). The induction of a pro-inflammatory state is believed to activate HIV replication as well as maintain high levels of viral gene expression through the binding of NF-κB to the viral promoter region (54). Perturbations are also commonly observed in cytokines belonging to the Th2 profile, particularly in levels of IL-10 (54,154). IL-10 is produced in excess by infected macrophages and inhibits both T cell proliferation as well as macrophage activation (54), leading to impaired immunological capacity of the host. HIV-infected macrophages secrete elevated levels of important β-chemokines, such as macrophage inflammatory protein 1α (MIP-1α), macrophage inflammatory protein 1β (MIP-1β) and Regulated on Activation, Normal T Expressed and Secreted (RANTES), all of which are endogenous ligands for the CCR5 co-receptor (54). These chemokines function to enhance the activation of resting $CD4^+$ T cells (54), converting them into ideal targets for infection. Other signalling molecules modulated by HIV infection in both monocytes and macrophages include colony-stimulating factors such as M-CSF (which is increased) and GM-CSF (which is decreased), as well as interferons such as IFN-α and IFN-β (54,155).

As a consequence of this wide range of HIV-induced behavioural dysfunctions and HIV-mediated alterations in the host cell transcriptome, infected macrophages play an important role in the pathogenesis of HIV. First, their permissiveness to infection combined with resistance to apoptosis, and their ability to enter tissue compartments, make macrophages an excellent viral reservoir (54,152). In addition, virus particles have been shown to bud from the intracellular membranes of macrophages, allowing virions to accumulate within the macrophage where they are protected from immune surveillance (160). Macrophages can also function as simultaneous incubators of multiple opportunistic infections, which may exacerbate the pathogenicity of both HIV and the co-infecting pathogen (149,160). This synergistic interaction is often observed during co-infection with *Mycobacterium avium* and *Pneumocystis carinii* (149,160). As mentioned previously, the modification of cytokine profiles in infected macrophage contributes to sustained immune activation and exacerbates the

effects of HIV infection on other cells (54). Infected macrophages may also contribute directly to $CD4^+$ T lymphocyte depletion by participating in the killing of uninfected cells (152). Lastly, macrophage dysfunction has been implicated in the development of HIV- and antiretroviral-related disorders such as atherosclerosis, lipodystrophy and metabolic syndrome (152).

5. Concluding remarks

Years of intensive research have elucidated many aspects of the fundamental biology of HIV and its pathogenesis in disease causation, as outlined in the preceding discussion. We now possess a thorough understanding of the structure and function of all viral components, and the various roles they play in the viral life cycle. We have collected vast resources of clinical data and have developed robust models of disease progression. Phylogenetic and evolutionary studies have revealed the mechanisms by which HIV generates its extraordinary genetic diversity and overcomes obstacles to replication. Despite these insights, we have thus far still not been able to develop a practical solution in terms of either a preventative vaccine or a permanent cure. We believe that the ability to develop such therapeutic interventions hinges on our understanding of the interactions between HIV and its target host cells. In this study we have focussed our attention on $CD4^+$ T lymphocytes and macrophages. Both cell types are complex, comprised of heterogenous subsets which arise under specific conditions to perform specialized immune functions. Previous studies have utilized transcriptomic approaches to assess the effects of HIV-1-B infection in these cell types. In $CD4^+$ T cells, it has been shown that HIV disrupts many cellular pathways including transcriptional and translational regulation, cell cycle, immune functions, and cellular metabolism, ultimately resulting in apoptosis. Infected macrophages are similarly affected in terms of cell cycle regulation and have impaired immune function. Unlike $CD4^+$ T cells, they do not readily undergo apoptosis, making them important viral reservoirs. In this study, we performed transcriptomic analyses using a primary HIV-1-C isolate to determine how these effects may differ from previous findings using HIV-1-B.

Chapter 3:

Virus production, quantification and detection of cells infected with HIV-1-C primary isolates

1. Abstract

A critical prerequisite for studies involving *in vitro* HIV infection is the production of large quantities of infectious viral stock. The first objective of this chapter was thus to optimize viral culture protocols for HIV-1-C isolates of different tropisms (R5-tropic, X4-tropic, dual-tropic). The production of X4-tropic (SW7) and dual-tropic (CM9) isolates was successfully achieved through the modification of existing protocols to suit the replication dynamics of these strains, as measured by analysis of p24 production using a p24 ELISA assay. Due to losses of infectivity, no R5-tropic isolates could be produced. The second objective was to optimize a titration assay using the GHOST reporter cell line and use it to quantify the number of infectious viral particles present in the produced stocks. Optimal timepoints for various stages of the assay were determined and the expression of HIV receptors (CD4, CCR5 and CXCR4) on the surface of the GHOST cells was evaluated by flow cytometry to ensure maximum susceptibility to infection. While CCR5 and CXCR4 were highly expressed, CD4 expression was unstable, requiring isolation of a $CD4^{high}$ GHOST cell population using FACS to allow for further work. Further investigation revealed that CD4 was negatively affected by enzymatic dissociation using trypsin, but that this effect was reduced in the sorted GHOST cells. The final objective of this chapter was to optimize and validate two complementary assays to detect cells infected with our HIV cultures (CM9 and SW7). Our flow cytometric method to detect intracellular p24 in infected GHOST cells using the KC57 monoclonal antibody demonstrated good correlation between HIV positives detected with the antibody and HIV positives detected with the in-built GHOST cell reporter system. Our alternative PCR-based method to detect viral DNA was likewise successful and demonstrated the ability to detect both CM9- and SW7-infected GHOST cells. In summary, despite several setbacks, we were able to produce and quantify two primary HIV-1-C isolates with which to perform our infection

experiments in $CD4^+$ T lymphocytes and macrophages, as well as validate methods to detect infected cells.

2. Introduction

One of the key requirements for *in vitro* HIV studies is the availability of high quality, well characterized virus stock. Several primary HIV-1 isolates of HIV-1-C were obtained from the National Institute for Communicable Diseases (NICD) for this project. However, these initial stocks needed to be further propagated to produce sufficient quantities of infectious virus for experiments to be performed. In order to determine the success of the productions, the viral stocks were quantified and analysed for infectivity. The ability to detect HIV-infected host cells after exposure to the primary HIV isolates was another essential requirement when we performed our experiments. The purpose of this chapter was thus to develop of a set of tools and techniques to enable efficient virus production, accurate quantification and detection of HIV-infected cells with high sensitivity and specificity.

The HIV production method used in this study was originally based on a standard protocol published by the Montefiori Laboratory at Duke University (161). This method makes use of activated PBMNCs obtained from peripheral blood donors which are rich in naturally susceptible host cells (such as $CD4^+$ T lymphocytes, monocytes and dendritic cells). Once infected, these cells have the ability to produce large quantities of viral particles, which are released into the culture supernatant though budding and eventual cell lysis. The virus-rich supernatant is then harvested and used for infection experiments. While this system is a very good model for maintaining physiological relevance, it is important to note that it is uncontrolled in the sense that the virus is free to mutate as it would in a natural host, resulting in the formation of multiple viral quasispecies within one culture (83).

The quantification of the HIV-1-C strains produced in this study was of critical importance, enabling the addition of defined amounts of virus to target cells for infection experiments. There are many different approaches to quantifying HIV in culture, the most basic technique being a tissue culture infectious dose 50 (TCID50) assay, in which the degree of cell death is used as a measure of the quantity of virus present (162). Another approach makes use of genetically engineered cell lines that contain built-in HIV-responsive reporter mechanisms such as GHOST (163) and TZM-bl cells (164). Although these cell lines were developed for co-

receptor usage analysis and neutralizing antibody assays, respectively, methods have been developed to take advantage of the fact that these cells produce an easily detectable HIV-induced signal that can be correlated to the amount of virus used to infect them (165). A third approach is to directly quantify various viral components, such as the amount of p24 capsid protein (e.g. by enzyme-linked immunosorbent assay (ELISA) (162,166)) or the amount of viral nucleic acids present (167,168). Another commonly employed technique is the measurement of reverse transcriptase activity, which serves as a proxy for the amount of virus present (169). For the purposes of infection experiments, it is best to use a method that also gives an indication of the infectivity of the virus, rather than just the quantity. Therefore, for this study, the GHOST cell assay was selected for titration while a p24 ELISA assay was used for confirmation of viral production.

A challenge posed by working with primary virus is the absence of in-built reporter systems able to detect infected target cells. Detection methods for primary isolates therefore generally rely on detecting viral proteins and nucleic acids directly. In this study, a flow cytometric assay for intracellular p24 detection, as well as a simple PCR-based technique, were optimized and validated for use with the HIV-1-C strains available. The intracellular p24 assay makes use of an antibody specific to the viral capsid protein which is added to cells that have been fixed and permeabilized, enabling access to internal cellular compartments (170,171). The bound antibody is detected by flow cytometry, enabling single cell resolution and detection of individual infected cells (170,171).

Flow cytometry is a technique in which the optical and fluorescent characteristics of a single cell (or particle) are measured as they pass in single-file through a laser light source in a highly pressurised fluid stream within a flow cytometer (172). A flow cytometer comprises four integrated systems: 1) a fluidics system for transporting the particles in the sample in a focussed stream, 2) an optics system which includes an excitation component (the laser light source) and a collection component to gather light generated or scattered by the particle, 3) an electronic network which converts the light signal into a voltage pulse proportional to the intensity of the light, and 4) a computer that is able to analyse the collected data (172). Cell populations can be differentiated by the instrument on the basis of their size, complexity and their fluorescent properties (172). Specialized flow cytometers can be used to isolate cell populations of interest based on these characteristics; a technique known as fluorescence-

activated cell sorting (FACS). These instruments, generally called cell sorters, are able to selectively charge particles with user-defined characteristics and deflect the charged particles via electrostatic plates into different collection vessels (172).

3. Materials and Methods

3.1. Propagation of primary HIV-1-C isolates

3.1.1. Viral stocks

Primary HIV-1-C isolates were generously donated by Professor Lynn Morris and her team at the NICD HIV Virology Section, Johannesburg, South Africa. Details regarding the patients from whom these strains were isolated, the primary tropism of the strains and their ability to utilize alternate co-receptors is given in **Table 3.1.** These strains were stored in the form of cell-free viral supernatants at -80°C until used for experiments.

Table 3.1: Details of primary HIV-1-C strains used in this study

Strain Name	Place Isolated	Clinical Category	$CD4^+$ count	Year Isolated	Patient Age*	Primary tropism	Alternate receptor usage	Ref
SW7	Sizwe Hospital Johannesburg	Advanced (AIDS)	10	1999	Adult	X4	None	(173)
CM9	Sizwe Hospital Johannesburg	Advanced (AIDS)	21	1999	Adult	R5X4	Bob, CCR3, CXCR6	(52)
SW20	Sizwe Hospital Johannesburg	Advanced (AIDS)	2	1999	Adult	R5X4	None	(173)
CM1	Sizwe Hospital Johannesburg	Advanced (AIDS)	2	1999	Adult	R5	CXCR6	(173)
Du422	Durban	HIV	409	2000	Adult	R5	Not tested	(174)
Du123F	Durban	Acute	841	2000	Adult	R5	Not tested	(174)
Du156	Durban	HIV	404	2000	Adult	R5	Not tested	(174)
COT1	Cotlands Johannesburg	Acute	1229	1999	Child	R5	Not tested	(175)

*adult refers to patients ≥ 18 years of age

3.1.2. Propagation of primary HIV-1-C isolates in PBMNCs

Frozen stocks of primary isolated PBMNCs (See **Chapter 4** for details regarding isolation) were thawed in Roswell Park Memorial Institute 1640 (RPMI-1640) culture medium (Thermo Fisher Scientific; Waltham, MA, USA). Each cryovial of PBMNCs contained $1x10^7$ cells isolated from a single donor. Multiple vials from two to four different donors (depending on the number of

cells required) were pooled, to account for inter-donor differences in susceptibility to HIV that might interfere with viral production. The thawed cells were centrifuged at 300 x *g* for 10 min and the supernatant was aspirated to remove any residual dimethyl sulfoxide (DMSO) from the freezing medium. The cells were resuspended in RPMI-1640 culture medium supplemented with IL-2 to promote activation and proliferation, termed IL-2 growth medium (IL-2 GM – RPMI-1640, 20% Foetal Bovine Serum [FBS – Thermo Fisher Scientific; Waltham, MA, USA], 2% penicillin/streptomycin [Thermo Fisher Scientific; Waltham, MA, USA], 5% recombinant human IL-2 [Roche; Basel, Switzerland]). The PBMNCs were then plated in either a T-25 or T-75 cell culture flask, depending on the volume used, and incubated at 37°C, 5% CO_2 for 24 hours. After the 24-hour resting period, the medium was changed to IL-2 GM supplemented with 5 µg/mL phytohemagglutinin-P (PHA-P – Sigma-Aldrich; St. Louis, MO, USA), a potent mitogen which stimulates massive immune activation of PBMNCs. The activated PBMNCs were permitted to proliferate for a further 2 days in culture prior to HIV exposure. The volumes of reagents and quantities of cells used was dependant on whether the cells were used for initiating a production cycle, or if they were used to feed an existing culture, as indicated in **Table 3.2**.

Table 3.2: PBMNC activation conditions

Purpose	Total number of cells activated	Volume of IL-2 GM medium used (mL)	Volume of PHA-P added (µL)
Initial infection	$3x10^7$	30	150
Feeding of viral culture	$2x10^7$	20	100

After two days, PHA-activated PBMNCs were collected and centrifuged at 300 x *g* for 10 min. The cell pellet was resuspended in 2 mL of IL-GM to which 1 mL of thawed viral stock was added. This small volume allowed for maximum virus-to-cell contact during the initial exposure. After incubation at 37°C, 5% CO_2 for 2 hours, the HIV-exposed cell suspension was made up to a total volume of 30 mL with RPMI-1640, plated in a T-75 flask and incubated further. During viral production, fresh cells must be periodically added to the culture, since extensive HIV-induced cell death is expected to occur. Therefore, the cultures were fed with PHA-activated PBMNCs every 3 days following virus exposure. On feeding days, both the HIV-infected culture and the PHA-activated PBMNC culture were transferred to 50 mL tubes and

centrifuged at 300 x *g* for 10 min. The respective pellets were resuspended in 1 mL RPMI-1640 each, the two cell suspensions were combined, and the total volume was adjusted to 30 mL.

The culture medium of the HIV-PBMNC co-culture, which contains viral particles released from infected cells, was harvested at 7 or more days post-infection, depending on the isolate used. For productions of isolate SW7, virus was harvested on Day 7, while other isolates were generally harvested at Day 10. During optimization, some harvests were performed at Day 15. On the day of harvest, the contents of the cell culture flask were centrifuged at 300 x *g* for 10 min to collect the PBMNCs into a pellet. The culture supernatant was collected and passed through an MF-Millipore™ 0.45 µm filter (Merck; Darmstadt, Germany) to remove any remaining cells and contaminants. The resulting cell-free supernatant was frozen in both 1 mL and 0.5 mL aliquots at -80°C until use in further experiments. The infected PBMNCs contained in the pellet were resuspended in freezing medium (FBS, 10% DMSO (Sigma-Aldrich; St. Louis, MO, USA), transferred to cryovials and stored at -80°C. This infected PBMNC-HIV co-culture was used as starting material in subsequent viral productions.

3.2. Viral quantification

3.2.1. ELISA-based quantification of p24 viral capsid protein

To determine whether viral productions were successful, the cell-free supernatants were tested using a p24 ELISA assay. ELISA is a well-established method that uses antibodies coupled with an enzymatic reporter system to detect and quantify a protein of interest in a sample (162), in this case viral p24 (**Figure 3.1**). We used the commercially available Lenti-X™ p24 Rapid Titer Kit (Clontech Laboratories; Mountain View, CA, USA) for this assay. Before starting, positive controls were generated by preparing 200 pg/mL and 12.5 pg/mL solutions of the 10 ng/mL p24 Control solution provided with the kit. A working solution of wash buffer was prepared by diluting a 20x stock solution with distilled water and dilutions of the viral supernatants to be tested were made up in RPMI-1640. A negative control consisting of only RPMI-1640 medium was also included.

Samples of 200 µL each were loaded into separate wells of an ELISA plate coated with anti-p24 primary capture antibodies. Lysis buffer (20 µL) was added to each well to lyse the viral particles and release soluble p24. The plate was incubated at 37°C for 60 min to allow binding

of p24 to the primary capture antibodies (**Figure 3.1**). The wells were aspirated and washed 4-6 times with 1x wash buffer using a multichannel pipette. A solution of biotinylated secondary anti-p24 biotin-conjugated antibody (100 µL) was added to each well and the plate was incubated at 37°C for a further 60 min, allowing the secondary antibody to adhere to the plate-bound antibody-p24 complexes (**Figure 3.1**). The antibody solution was removed, and the wells were washed as described previously. A solution of streptavidin-conjugated Horseradish Peroxidase (HRP) was added (100 µL) and allowed to incubate at room temperature for 30 min during which time the HRP reporter enzyme attaches to the antibody complex by biotin-streptavidin interactions (162) (**Figure 3.1**). The secondary antibody solution was removed, followed by another washing step. A solution of 3,3',5,5'-tetramethylbenzidine (TMB) substrate (100 µL) was added to each well and the plate was incubated for 20 min in the dark. The HRP reporter enzyme catalyses the oxidation of the TMB substrate, converting it from a colourless solution to a blue product (**Figure 3.1**). The intensity of the colour change depends on the amount of substrate converted and therefore the amount of antibody-bound enzyme present. The quantity of antibody-bound enzyme present is proportional to the number of secondary antibodies bound to the captured p24 proteins, and thus gives an indication of the amount of p24 present in the sample (162). Stop Solution (100 µL) was added to halt the reaction. This solution is acidic and causes a secondary colour change to yellow. The absorbance of the solution in each well was measured using a PowerWaveX™ spectrophotometer (BioTek; Winooski, VT, USA) at a wavelength of 450 nm.

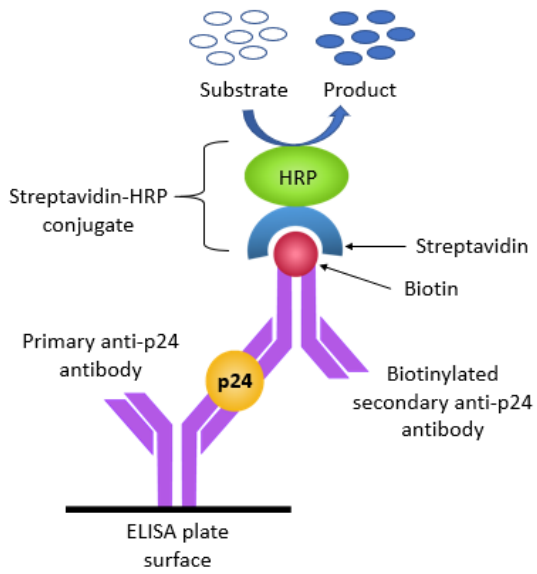

Figure 3.1: Principles of the p24 ELISA assay. The ELISA plate is coated with anti-p24 antibody which captures p24 protein present in the sample. A biotinylated secondary antibody is added, which also binds p24. A reporter enzyme (such as HRP) conjugated to streptavidin binds to the biotinylated antibody. When a suitable substrate (TMB) is provided, the reporter enzyme catalyses a measurable colour change reaction.

For each ELISA plate used in this study, a standard curve was established to relate the absorbance detected in a sample to the absolute quantity of p24 present. Standards of 600, 400, 200, 100, 50, 25, 12.5 and 0 pg/mL p24 were produced from the control solution provided with the kit. The ELISA assay, as described above, was performed on these controls and the values were normalized by dividing the absorbance reading obtained for each standard by the absorbance obtained in the negative control (0 pg/mL p24). An example of the ELISA plate obtained after assaying a set of standards is illustrated in **Figure 3.2**. The normalized values obtained were used to plot a standard curve (**Figure 3.3**). The p24 concentrations of other measured samples can be extrapolated from the standard curve. For example, a sample with a normalized absorbance of 10 has a p24 concentration of 300 pg/mL (indicated by the red arrow in **Figure 3.3**). To perform this extrapolation mathematically, linear regression was performed in Microsoft Excel and the equation of the regression line was determined. This equation is given in the form $y = a + bx$, where y is the normalized absorbance, x is the concentration of p24, a is the intercept on the y-axis and b is the slope of the regression line. The equation can thus be used to solve for the concentration of p24 in a sample (x) once the absorbance value (y) has been obtained. The co-efficient of determination (R^2) is also calculated to give an indication of the strength of the correlation of

the two variables. If R^2 is close to 1, there is a strong correlation and the standard curve can be used to estimate the p24 concentration with confidence.

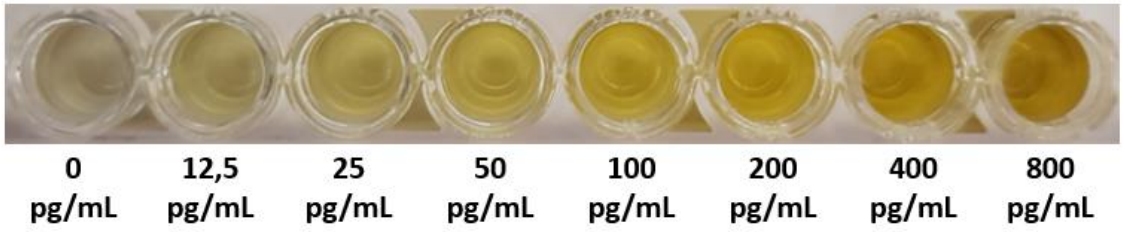

Figure 3.2: Example of a p24 ELISA plate used to produce a standard curve. The intensity of the colour increases as the amount of p24 in the sample increases since the amount of p24 present in the sample at the beginning of the assay is proportional to the amount of antibody-bound reporter enzyme present at the end of the assay. The greater the amount of reporter enzyme present, the more substrate is converted and the more pronounced the colour change reaction will be.

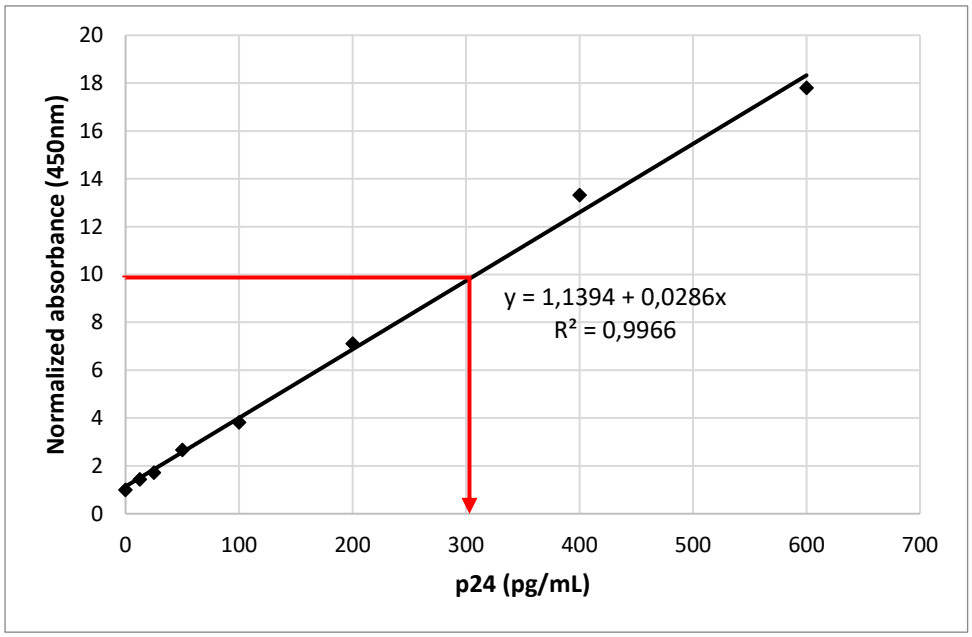

Figure 3.3: Example of a standard curve for the p24 ELISA assay. The normalized absorbance measurements obtained at a wavelength of 450 nm were plotted on the y-axis, while the different concentrations of the p24 standards were plotted on the x-axis. The linear regression line used to correlate the two measures is indicated on the graph in black, as well as the linear regression equation and the R^2 value, which indicates the strength of the association.

3.2.2. GHOST cell functional titration assay

The GHOST cell assay is a technique used to quantify the amount of functional, infectious HIV virus particles present in a sample. Unlike methods such as ELISA, it does not rely on detection

of virus components that may or may not form part of functional virus particles, but rather detects infection at a cellular level. This is achieved using the specially modified GHOST cell line, originally derived from Human Osteosarcoma (HOS) cells (163). These cells have been genetically modified through transduction with multiple constructs to elicit a detectable HIV-specific response upon infection (163). First, they contain an antibiotic-selectable construct which encodes for the HIV receptor molecule, CD4, enabling the viral adherence and entry (163). A range of second generation cell lines have also been engineered to express additional co-receptors, including CCR5, CXCR4, Bob and CXCR6, which can further promote entry of viral isolates with particular tropisms (53). The second critical component is the incorporation of a Green Fluorescent Protein (GFP) reporter construct under the control of a Tat-inducible HIV-2 LTR element that functions as a promoter (163). When HIV enters the cell and infects successfully it induces production of the Tat protein, a potent transcription factor that normally functions to accelerate viral transcription when bound at the LTR of the integrated HIV genome (22). When a GHOST cell becomes infected, the presence of Tat results in induction of transcription from the artificially introduced LTR element and subsequent production of GFP (**Figure 3.4**). The GFP signal can then be detected using techniques such as fluorescence microscopy or flow cytometry.

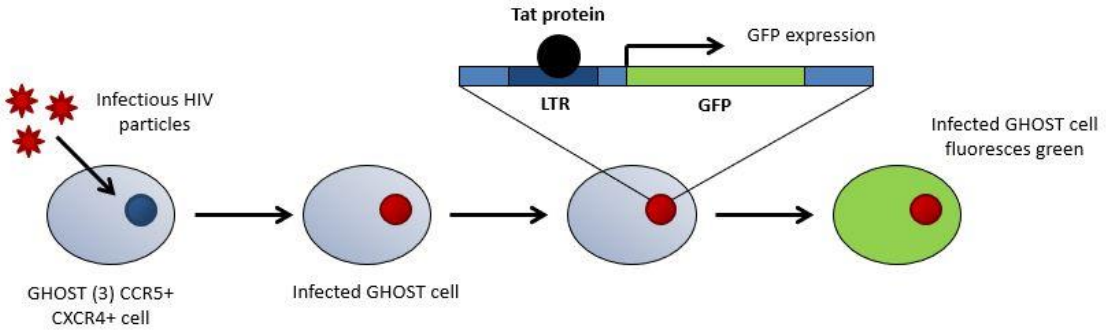

Figure 3.4: Principles of the GHOST reporter cell line. A GHOST cell engineered to express essential receptors for HIV-1 entry (CD4, CCR5 and CXCR4) and transduced with an HIV-responsive GFP construct is exposed to HIV virions. When a cell is infected, the integrated virus directs expression of the Tat protein that binds to the LTR promoter of the construct and activates expression of the GFP reporter gene. This results in translation and expression of GFP and enables the infected cell to fluoresce green.

3.2.2.1. GHOST cell culture

GHOST (3) cells expressing both CCR5 and CXCR4 co-receptors (R5X4) were obtained from the NIH AIDS Reagent Program. For the resuscitation of frozen stocks, cells were thawed through quick transfer of the cryopreserved cells into 30 mL of Dulbecco's modified Eagle's medium (DMEM) supplemented with 10% FBS and 2% penicillin/streptomycin (Thermo Fisher Scientific; Waltham, MA, USA), hereafter termed complete DMEM. To remove residual DMSO that was present in the freezing medium, the suspension was centrifuged at 300 x *g* for 10 min, after which the supernatant was aspirated. The cells were resuspended in 8 mL in selective growth medium consisting of DMEM, 10% FBS, 500 µg/mL G418 (Roche; Basel, Switzerland), 100 µg/mL hygromycin (Biovision Incorporated; Milpitas, CA, USA), 2% penicillin/streptomycin and 1 µg/mL puromycin (Sigma-Aldrich; St. Louis, MO, USA) and plated in a T-75 cell culture. Once GHOST cells have been exposed to this selective medium for at least one passage, most of the cells in culture should express CD4, CCR5, CXCR4 and the LTR-induced GFP-expressing constructs. At this stage, the culture can be changed to complete DMEM for further maintenance of the cell culture.

The GHOST cells were maintained at 37°C, 5% CO_2, changing medium every 3 days until they reached confluence, at which point they were either passaged or used in experiments. To passage, all growth medium was removed from the flask and the culture flasks were rinsed with phosphate buffered saline (PBS, pH 7.4) to remove dead cells and debris. The adherent cells were then dissociated by incubation in 3 mL of 0.25% Trypsin-EDTA (Thermo Fisher Scientific; Waltham, MA, USA) for 5 min at 37°C. After visual confirmation (using a light microscope) that all the cells had been dislodged, an equal volume of complete culture medium was added to inactivate the trypsin. The resulting cell suspension was collected and centrifuged at 300 x *g* for 10 min. The cell pellet was then resuspended in an appropriate volume of medium and counted. The cell concentration was adjusted, and cells were re-plated in T-75 flasks at approximately $2x10^6$ cells per flask.

For certain experiments, Cell Dissociation Solution (Sigma-Aldrich; St. Louis, MO, USA) was used as a non-enzymatic alternative to trypsin. The dissociation solution was pre-warmed to 37°C and 3 mL was added to the to the cell culture flask (T-75) after removing the culture medium and washing with PBS. The cells were incubated at 37°C for 5-10 min, until they could be dislodged with agitation. A further 3 mL of complete DMEM was added to dilute the

Dissociation Solution. The dissociated cells were collected and then centrifuged at 300 x *g* for 10 min. After removing the supernatant, the cells were resuspended in an appropriate volume of complete DMEM.

GHOST cells that were not used immediately for experiments were cryopreserved at approximately $2x10^6$ cells per cryovial. The cell suspension was centrifuged at 300 x *g* for 10 min, the culture medium aspirated, and the pellet resuspended in an appropriate volume of freezing medium (FBS, 10% DMSO). Aliquots (1 mL) of this suspension were transferred to cryovials and stored at -80°C in Mr Frosty™ freezing containers. After at least 24 hours, the frozen cells were transferred to a liquid nitrogen vapour dewar for long-term storage.

3.2.2.2. Enumeration of GHOST cells by flow cytometry

In flow cytometry, size and cellular complexity can be used to identify cells of interest, in this case GHOST cells. These properties are measured as functions of light scatter as the cell passes through the laser of the instrument (**Figure 3.5**). The larger the cell, the more it will disrupt the light from reaching the detector parallel to the light source, resulting in what is called a forward scatter (FS) signal (172). If the cell is highly complex and contains either numerous or large subcellular structures (e.g. granules, multi-lobed nuclei, organelles), the light will be diffracted at an angle when it encounters these structures. This results in side scatter (SS), which is measured by a detector that is perpendicular to the light source (172). In addition to light scatter, a flow cytometer can detect the emitted fluorescence of each cell that passes through the system using a series of optical filters and detectors. In case of GHOST cells, fluorescence will be emitted from GFP produced in response to HIV infection.

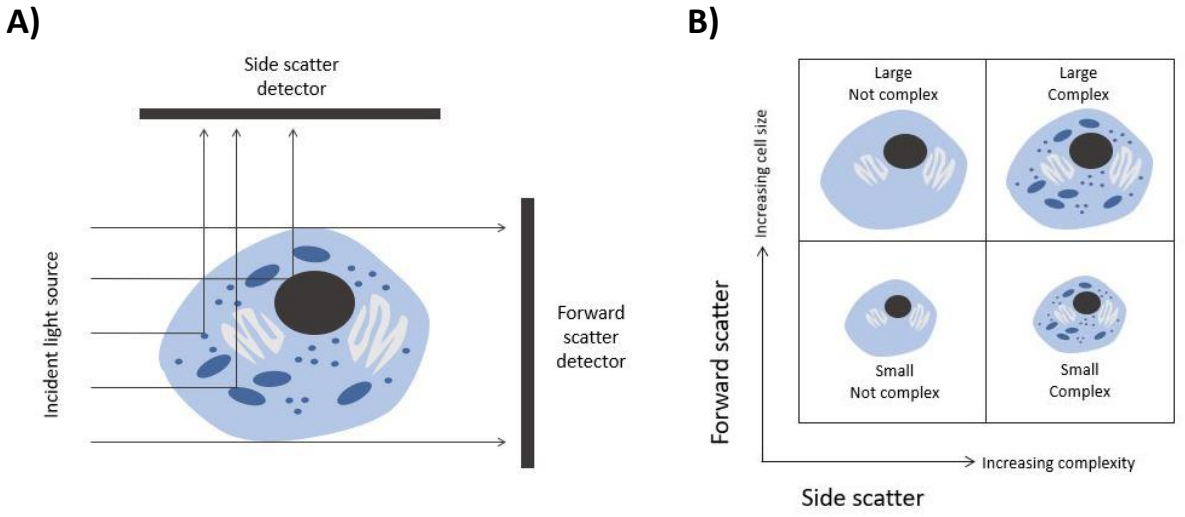

Figure 3.5: The principles of forward scatter and side scatter as used for differentiating cells based on size and complexity in flow cytometry. A) Light from the light source is scattered upon contact with a cell as it passes through the flow cytometer. The degree to which light is scattered in the forward direction depends on the overall size of the cell, while the degree of side scatter is determined by the number/size of intracellular components present that cause the light to diffract. **B)** A plot of forward scatter vs side scatter illustrates how different cell-populations are differentiated from each other based on their morphological features (size and intracellular complexity).

3.2.2.2.1. Sample preparation

A 50 µL aliquot of the GHOST cell suspension was transferred to a flow cytometry tube and stained with 3 µL of 7-Aminoactinomycin D (7-AAD – Beckman Coulter; Miami, FL, USA). 7-AAD is a fluorescent nuclear dye used to assess cell viability. This non-permeable dye is able to cross the cell membranes of cells with compromised membranes and intercalate into double-stranded DNA. Flow-Count™ fluorospheres (Beckman Coulter; Miami, FL, USA) were added to the tube at volume of 50 µL, yielding a proportional ratio of Flow-Count™ beads to cell suspension. Flow-Count™ beads have a known concentration, expressed as a calibration (CAL) factor provided in the product information insert of each batch purchased. The CAL factor is used to calculate the absolute number of cells present in the sample (**Equation 3.1**). An additional 500 µL PBS was added to increase the overall volume of the sample. The cells were then assayed on the Gallios™ flow cytometer (Beckman Coulter; Miami, FL, USA). The laser and filter configurations available on this instrument are described in detail in **Appendix A**.

3.2.2.2.2. Flow cytometry setup and data acquisition

Flow-Count™ fluorospheres are stained with a fluorescent dye with a broad emission spectrum and can be detected in any of the following detection channels: FL1, FL2, FL3 and FL4. A one-parameter Count vs FL3 [Excitation: 488 nm; Emission: 620/30 BP] Log plot was used to identify the Flow-Count™ fluorospheres (**Figure 3.6a**). The FL3 detection channel was selected to avoid interference with the fluorescence from 7-AAD which is optimally detected in the FL4 channel [Excitation: 488 nm; Emission: 695/30 BP]. A second one-parameter plot (FL3 Log vs Time) was created and gated on the region "BEADS" in order to identify intact fluorospheres (**Figure 3.6b**). Disintegrated beads and beads clumped together were excluded (**Figure 3.6b**). GHOST cells were then identified based on their size and cellular complexity in a FS Linear (Lin) versus SS Logarithmic (Log) two-parameter plot (**Figure 3.6c**). The Flow-Count™ beads were gated out of this plot using the "NOT BEADS" Boolean gate. A 7-AAD Log vs FS Lin two-parameter plot, gated on the "GHOST CELLS" region from the previous plot, was used to determine the viable cell population (**Figure 3.6d**). Non-viable cells with compromised membranes become more permeable to 7-AAD and thus have increased fluorescence compared to viable cells. Data was acquired and analysed using Kaluza Flow Cytometry Analysis Software (Version 2.1). The concentration of the cell suspension and the total cell count values were then obtained using the following equations:

Equation 3.1:

$$Cell\ concentration\ (cells/\mu L) = \frac{No.of\ events\ in\ region\ of\ interest}{No.of\ events\ in\ CAL\ region} \times Cal\ factor$$

Equation 3.2:

$$Total\ cells = Cell\ concentration\ (cells/\mu L) \times Cell\ suspension\ volume\ (\mu L)$$

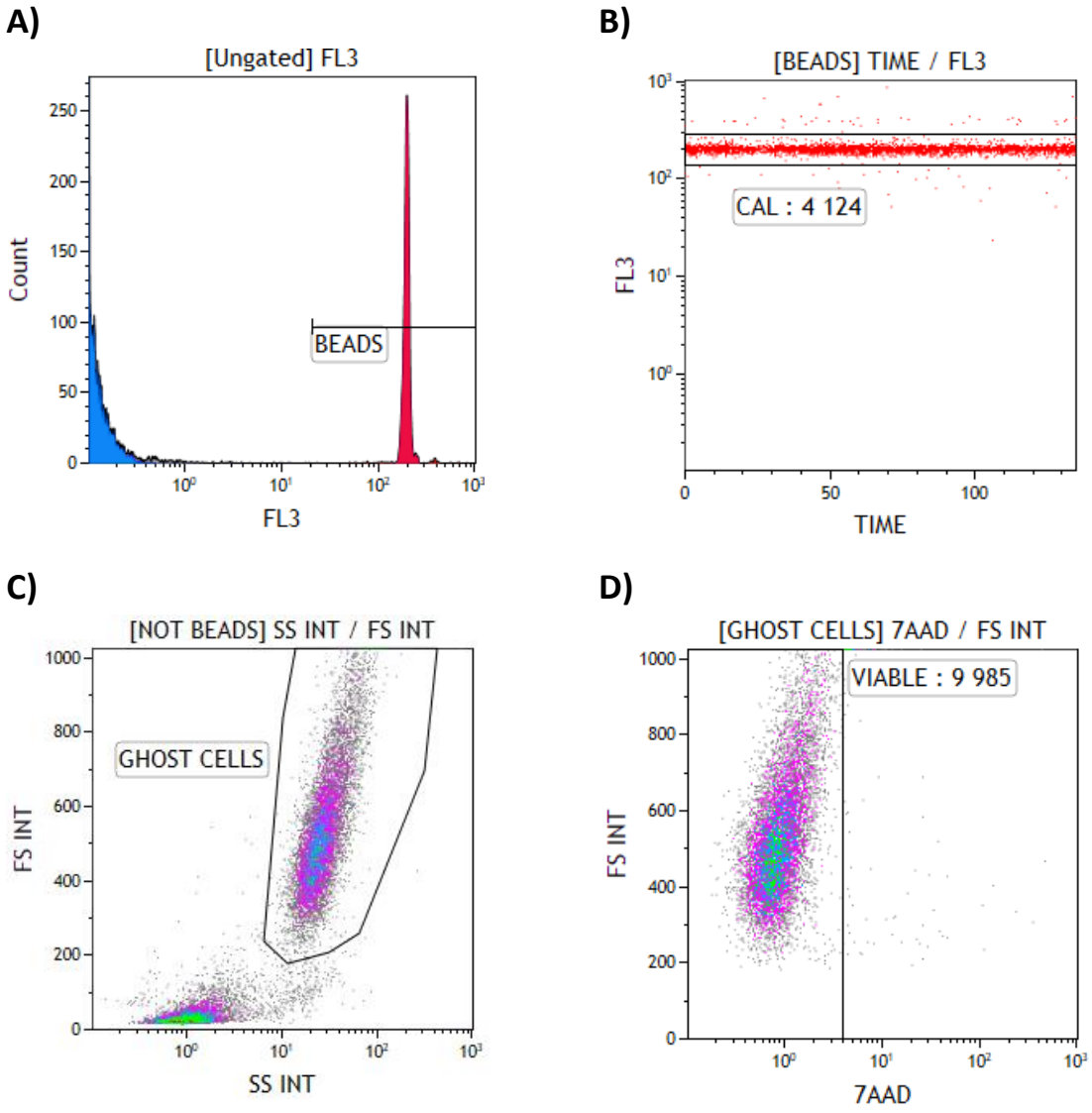

Figure 3.6: Flow cytometry protocol setup for GHOST cell enumeration. A) Flow-Count™ fluorospheres were identified in the FL3 channel as a highly positive peak ("BEADS" region). **B)** An FL3 Log vs Time one-parameter plot, gated on the "BEADS" region, was used to identify the intact fluorospheres, indicated in the region "CAL". **C)** A FS Lin vs SS Log two-parameter plot was used to identify the GHOST cell population, after the Flow-Count™ beads had been gated out with the Boolean gate "NOT BEADS". **D)** A FS Lin vs 7-AAD Log plot gated on the "GHOST CELLS" region was used to determine how many of the GHOST cells were viable. The number of cells in the "VIABLE" region was used in **Equation 3.1** to calculate the concentration of viable GHOST cells present in the sample.

3.2.2.3. Analysis of HIV co-receptor expression by immunophenotyping of GHOST cells

Immunophenotyping is a flow cytometric technique in which antibodies conjugated to fluorochromes are used to detect cells that possess a particular characteristic, such as expression of a particular cell surface protein (172). Cells are stained with the antibody-

fluorochrome conjugate, which binds to an epitope on the cell surface protein (marker) of interest with a high degree of specificity. When the cell passes through the instrument, the fluorochrome is excited by the laser if the light is of the correct excitation wavelength. Following excitation, the fluorochrome returns to its ground state and releases energy in the form of light of a longer emission wavelength (172). The fluorescent signal emitted by an individual cell will be increased in cells that possess higher levels of the cell surface protein and thus were stained with more of the antibody-fluorochrome conjugate (**Figure 3.7**). The antibodies used for flow cytometry are generally monoclonal. This means that they are generated from a single clone of identical B lymphocytes, and therefore will all bind to a single, specific epitope on the target antigen (176). The reactivity of the antibody depends on the species in which it was generated (e.g. mouse, rat, rabbit) and the species from which the target antigen was derived. Antibodies also come in different classes, or isotypes, which are characterized by differences in the constant region segments of the antibody. In mammals, there are five heavy chain (IgA, IgD, IgG, and IgM) and two light chain (κ and λ) isotypes (176).

The inclusion of appropriate controls is essential for immunophenotyping experiments. Cells tend to have a low level of background autofluorescence, the extent of which is dependent on the cell type (177,178). This is generally controlled for by including unstained cell samples to which no fluorochrome has been added (**Figure 3.7**). Non-specific staining is another potential issue. This occurs when the antibody-conjugate binds with low affinity to Fc-receptors on the cell surface (179). Isotype controls are often used to control for non-specific binding. Isotype control antibodies are from the same immunoglobulin class as the target antibody, and are conjugated to the same fluorophore, but do not have the same epitope specificity (178). Therefore, the degree of non-specific binding in the isotype control should ideally be similar to that of the antibody of interest, allowing one to account for any shift in fluorescence intensity it may cause (178).

Another important potential confounding factor in immunophenotyping experiments is spectral overlap. This occurs when the emitted fluorescent signal occurs over a relatively broad range of wavelengths, resulting in fluorescence “spilling over” from the intended channel (based on optimal signal emission) into adjacent detectors resulting in “false positive” signals in the adjacent detectors/channels (180) (**Figure 3.8**). Compensation is an electronic correction that may be applied to remove the unwanted signal (as a percentage of the total

signal) from all detectors into which the signal has spilled over (177). Since spectral overlap can negatively impact the accuracy of immunophenotyping, we performed compensation during data analysis for all experiments in which more than one fluorochrome was used.

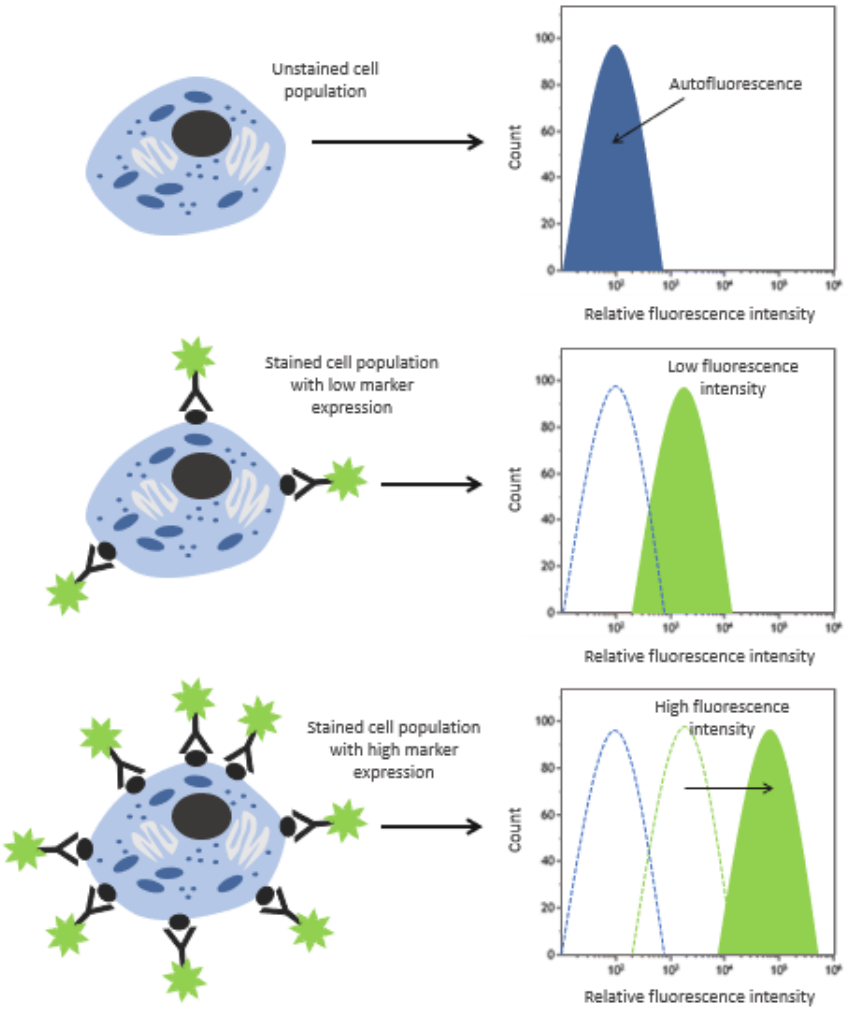

Figure 3.7: Illustration of emitted signal intensity based of different levels of monoclonal antibody binding by individual cells. Signal intensity can be visualized on a one-parameter plot (histogram) illustrating the number of events counted (area under generated peak) for each relative fluorescence intensity value generated. Unstained cells emit a low level of background autofluorescence (indicated in blue) due to the presence of naturally fluorescent cell components. When cells are stained with an antibody-fluorochrome conjugate specific to an epitope present on the cell surface, an additional fluorescent signal is generated (indicated in green). The greater the number of epitopes on a cell, the more antibody-fluorochrome conjugates will be bound, which increases the strength of this fluorescent signal. In general, cells with higher expression levels will thus emit at higher relative fluorescence intensities, resulting in a shift to the right that is indicative of greater positivity.

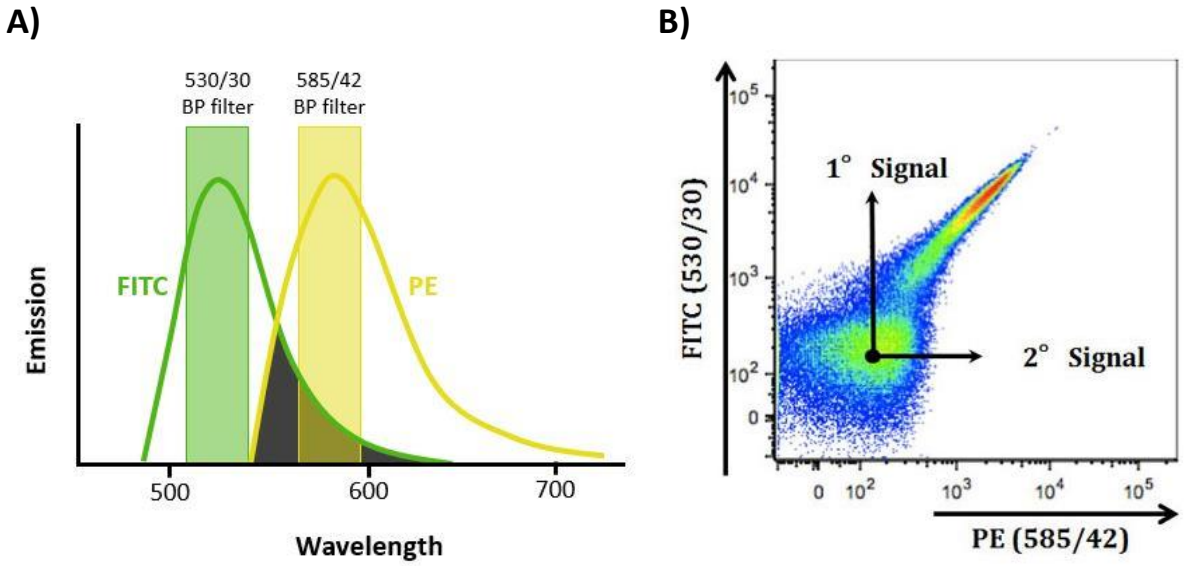

Figure 3.8: Illustration of the principles of spectral overlap using Fluorescein isothiocyanate (FITC) and Phycoerythrin (PE) as examples. A) The emission spectra of FITC and PE are presented on a graph of emitted fluorescence vs wavelength. The range of the two bandpass (BP) filters intended for detection of FITC and PE at their maximum emission wavelengths are superimposed on the graph. Some of the light emitted by FITC will pass through the filter intended to collect light from PE, due to overlap in the two emission spectra (indicated in the dark grey region), resulting in spill-over into the PE channel. **B)** The spill-over signal can be observed using FITC-labelled PBMNCs visualized on a two-parameter plot of FITC vs PE. The 1° Signal indicates the intended positive signal in the FITC channel, while the 2° Signal is a false positive signal in the PE channel as a result of spill-over. (**Figure 3.8b** available from https://bitesizebio.com/13696/introduction-to-spectral-overlap-and-compensation-flow-cytometry-protocol/)

3.2.2.3.1. Sample preparation

Two 100 µL aliquots of the GHOST cell suspension were transferred to flow cytometry tubes. The two samples were stained with either monoclonal antibody conjugates or their corresponding isotypic controls and 7-AAD, as indicated in **Table 3.3**. CCR5 was detected with a Phycoerythrin-Cyanine 7 (PE-Cy7) conjugate, while the CXCR4 antibody was conjugated to the Brilliant Violet™ 605 (BV605) fluorochrome. The cells were incubated for 20 min at room temperature in the dark to allow antibody binding. They were then washed with 1 mL PBS to remove residual unbound antibodies, centrifuged at 300 x *g* for 10 min and resuspended in 500 µL PBS. The samples were analysed on a FACSAria™ Fusion instrument (BD Biosciences; Franklin Lakes, NJ, USA) to determine the co-receptor expression profiles of the cells. The laser and filter configurations used for this instrument are also indicated in **Appendix A.**

Table 3.3: Sample preparation to phenotype co-receptor expression of GHOST cells

TUBE 1		TUBE 2	
Monoclonal antibody	**Volume (µL)**	**Monoclonal antibody**	**Volume (µL)**
CCR5 PE-Cy7	5	PE-Cy7 Isotypic Control	5
CXCR4 BV605	5	BV605 Isotypic Control	5
Viability dye	**Volume (µL)**	**Viability dye**	**Volume (µL)**
7-AAD	5	7-AAD	5

3.2.2.3.2. Flow cytometry setup and data acquisition

Firstly, the viable cells were identified using a SS Log vs 7-AAD Log two-parameter plot (**Figure 3.9a**). The GHOST cells were then identified on a FS Lin vs SS Log plot, gated on the "VIABLE" region, while debris and large cell clumps were excluded (**Figure 3.9b**). CXCR4 and CCR5 expression were analysed by plotting BV605 Log and PE-Cy7 Log against SS Log respectively. These plots were gated on the viable GHOST cell population. The position of the positive gates for these co-receptor plots were defined according to the negative populations cut-off when the samples were stained with the isotypic controls (**Figure 3.9c & Figure 3.9d**). The isotypic controls serve as negative controls which account for non-specific binding of the respective monoclonal antibodies. Data was acquired using BD FACSDiva™ (Version 8.0.1) and analysed using Kaluza Flow Cytometry Analysis Software (Version 2.1).

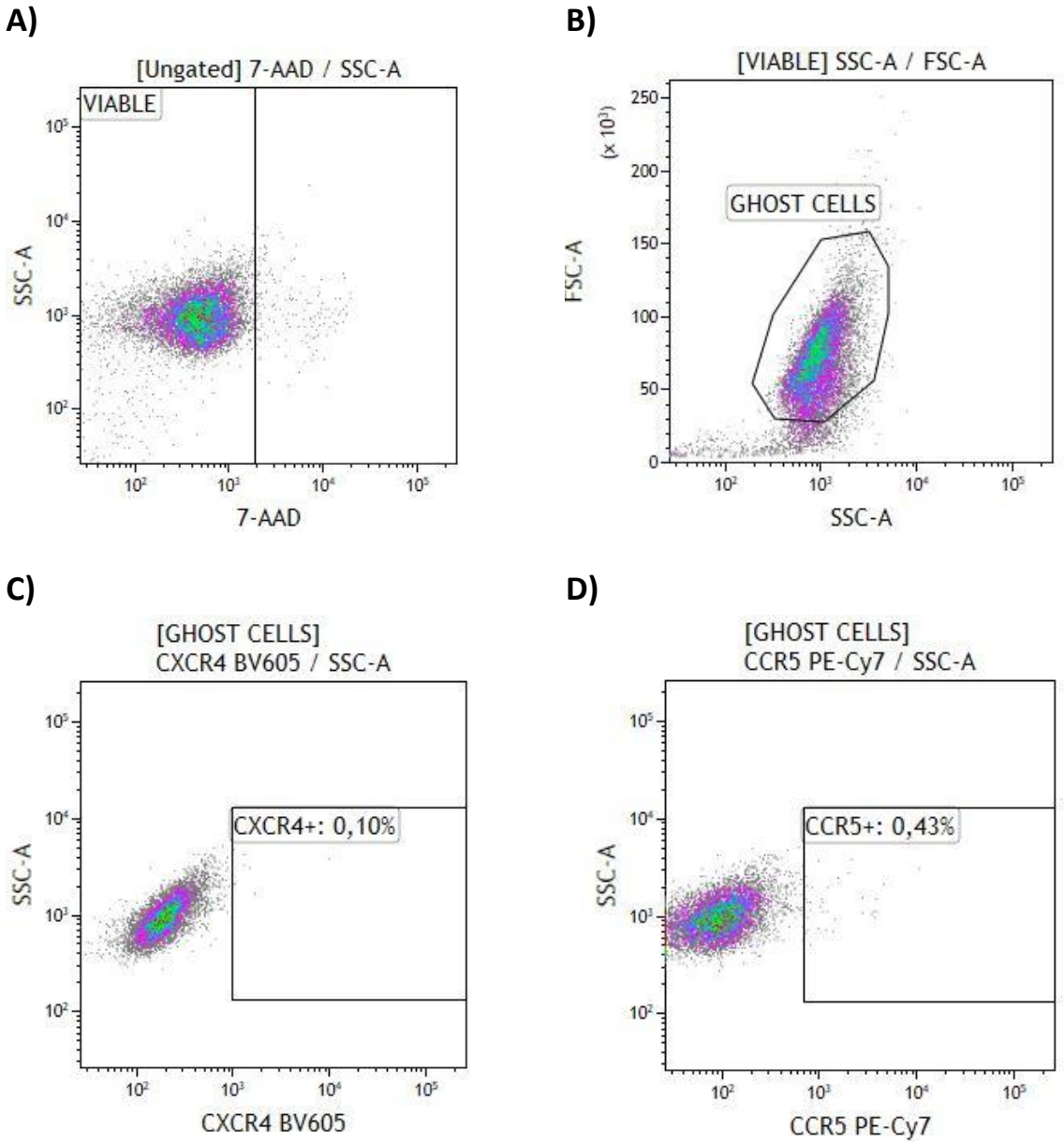

Figure 3.9: Flow cytometry setup for immunophenotyping of co-receptor expression in GHOST cells. A) Cells with intact membranes that stained negative for 7-AAD were first identified using a SS Log vs 7-AAD Log two-parameter plot, indicated in the "VIABLE" region. **B)** The GHOST cells were then identified on a FS Lin vs SS Log plot, gated on the "VIABLE" region. **C)** A SS Log vs CXCR4 BV605 Log two-parameter plot enabled identification of cells that expressed CXCR4 in the "CXCR4+" region. The position of the gate is set using the isotypic control, as indicated here. **D)** A SS Log vs CCR5 PE-Cy7 Log two-parameter plot was used to detect cells expressing CCR5 in the "CCR5+" region. The CCR5-positive region was also set according to the isotypic control. A few cells (events within the CCR5-positive region) displayed high levels of non-specific binding for the isotypic control antibody used. Therefore, the region was set on the edge of the majority of the cells, ignoring the few outliers. The percent non-specific binding observed within the CCR5-poitive region (isotypic control) was subtracted from the CCR5-positive percentage obtained when cells were stained with a monoclonal antibody directed against the CCR5 epitope.

3.2.2.4. Analysis of CD4 expression of GHOST cells

3.2.2.4.1. Sample preparation

Cells were collected from culture flasks using either non-enzymatic Cell Dissociation Solution or trypsin as described in the GHOST cell culture section (**Section 3.2.2.1**). Two 50 µL aliquots of each sample were used to assess CD4 expression. The first aliquot was stained with 3 µL of a CD4 Allophycocyanin (APC) monoclonal antibody in addition to 7-AAD, while the second was stained with the corresponding isotypic control (**Table 3.4**). In some instances, the isotypic control was not available and an unstained control was used instead. Since the cells to be phenotyped were generally seeded for experiments directly after analysis, a count was included as part of the protocol. Flow-Count™ fluorospheres (50 µL) were added to each tube, and 500 µL of PBS was added to the tubes before analysis on the Gallios™ flow cytometer.

Table 3.4: Sample preparation for analysis of CD4 expression of GHOST cells

TUBE 1:		**TUBE 2**	
Monoclonal antibody	**Volume (µL)**	**Monoclonal antibody**	**Volume (µL)**
CD4 APC	3	APC Isotypic Control	3
Viability dye	**Volume (µL)**	**Viability dye**	**Volume (µL)**
7-AAD	3	7-AAD	3

3.2.2.4.2. Flow cytometry setup and data acquisition

As for the enumeration protocol described in **Section 3.2.2.2**, the fluorospheres were first identified in the FL3 channel (**Figure 3.10a**). In the subsequent FS Lin vs SS Log two-parameter plot, the GHOST cells were identified based on their size and complexity (**Figure 3.10b**). Flow-Count™ fluorospheres were excluded from this plot using the Boolean gate "NOT BEADS". From the GHOST cell population, the viable cells were selected using a FS Lin vs 7-AAD Log plot (**Figure 3.10c**). Finally, the CD4 expression of the viable GHOST cell population was analysed using a FS Lin vs CD4 APC Log two-parameter plot, with the position of the positive region being set according to either an isotypic control (**Figure 3.10d**) or an unstained control. CD4 APC is detected in the FL6 channel [Excitation: 638 nm; Emission: 660/20 BP], while 7-

AAD is detected in FL4. Acquired data was analysed using Kaluza Flow Cytometry Analysis Software (Version 2.1).

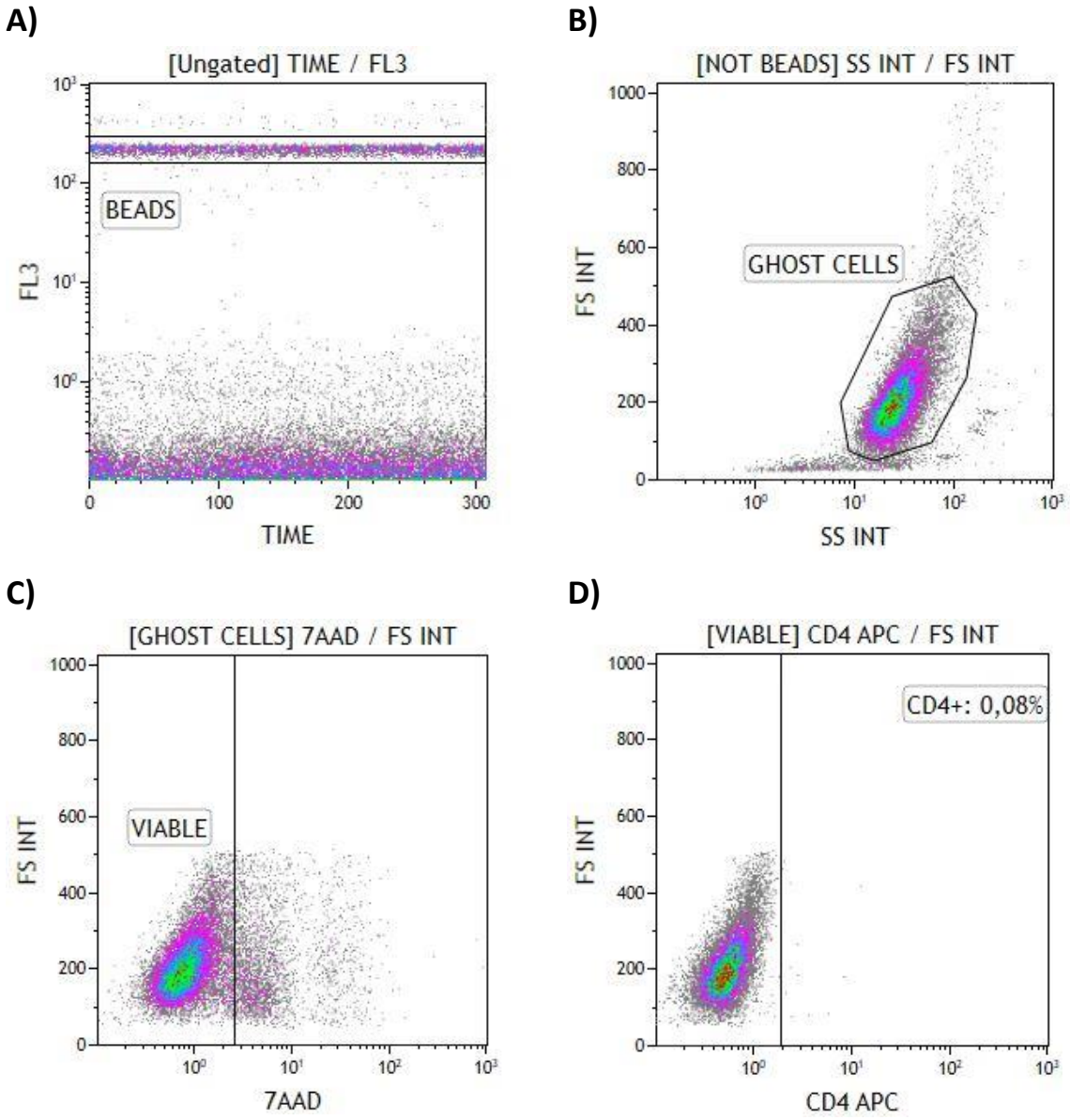

Figure 3.10: Flow cytometry setup for counting and immunophenotyping of CD4 expression of GHOST cells. A) Flow-Count™ fluorospheres are identified in the region "BEADS", using a Log FL3 vs Time two-parameter plot. **B)** A FS Lin vs SS Log two-parameter plot gated using the Boolean gate "NOT BEADS" was used to identify GHOST cells. Cell debris and large clumps were excluded. **C)** A FS Lin vs Log 7-AAD plot enabled detection of viable cells, indicated in the "VIABLE" region. **D)** A two parameter-plot of FS Lin vs Log CD4 APC, gated on the "VIABLE" region was used to analyse CD4 expression. The "CD4+" region was defined according to the position of the negative population using either unstained cell or cells stained with an isotypic control.

3.2.3. Sorting of CD4-positive GHOST cells

Preliminary experiments with GHOST cells seemed to indicate that CD4 expression was highly variable, raising doubts as to whether they were suitable for use. In order to overcome this potential problem, it was decided that GHOST cells with uniformly high CD4 expression should be sorted to be used for future experiments. Several confluent flasks of GHOST cells were used as the starting material. Since it was possible that treatment with trypsin could cause proteolytic cleavage of CD4, the cells were detached from the culture flasks using Cell Dissociation Solution. Cells collected from all flasks were pooled and centrifuged at 300 x *g* for 10 min. Thereafter, they were resuspended in 1mL of complete DMEM for each flask used. For example, if cells were harvested from a total of 4 flasks the cell pellet was resuspended in 4 mL of medium. Cells were stained for 15 min with 5 µL of anti-CD4 APC antibody and 5 µL 7-AAD for each flask used after which the cells were washed twice with PBS. Cells that were both viable (7-AAD negative) and strongly CD4 positive were sorted into a 15 mL tube using the FACSAria™ Fusion cell sorter (**Figure 3.11**). The resulting $CD4^{high}$ GHOST cell population was plated and expanded for two passages into bulk stocks which were stored for future experiments. A second population of cells that expressed CD4 weakly was also sorted for comparison (**Figure 3.11**).

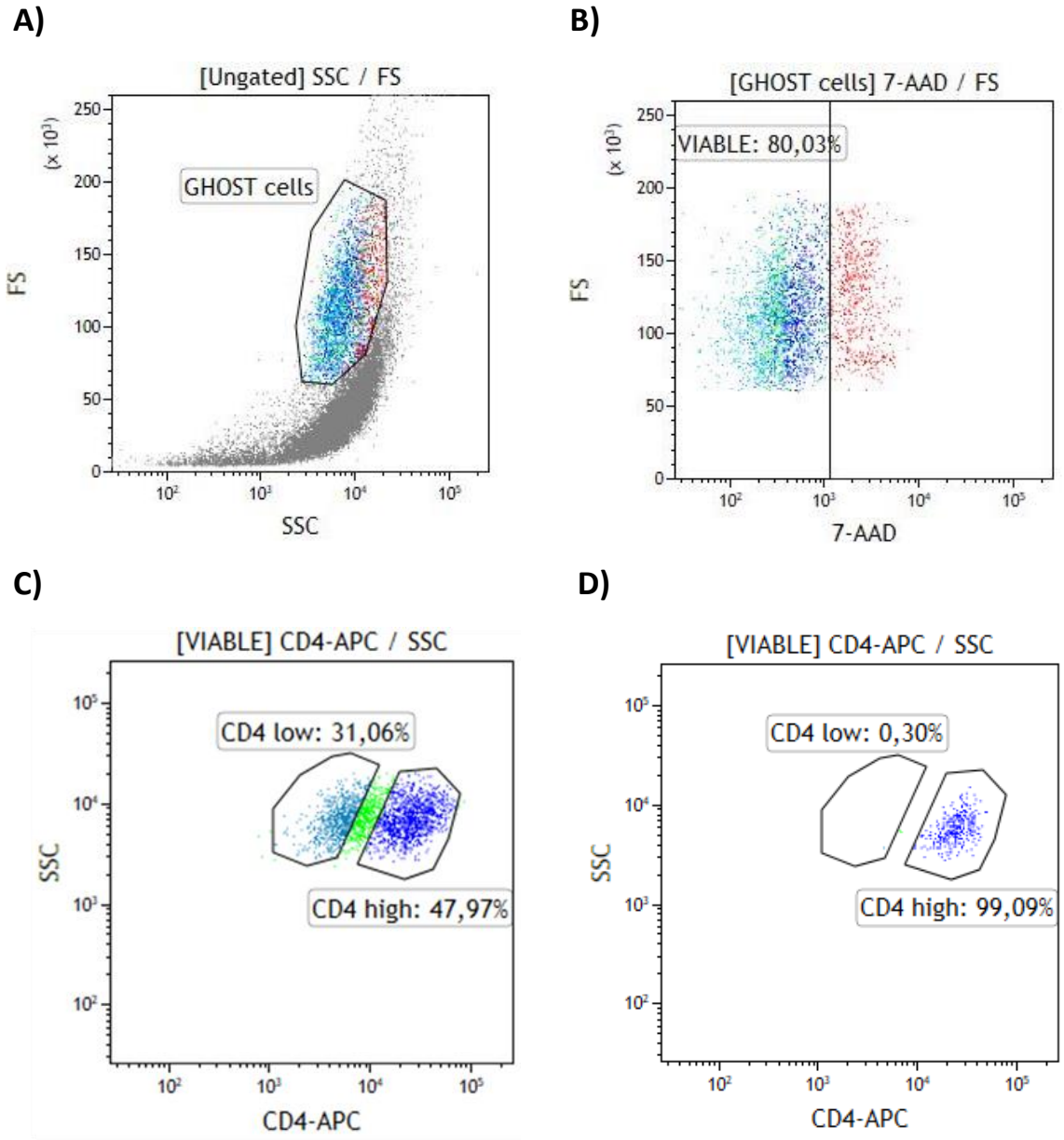

Figure 3.11: Flow cytometry setup for sorting of CD4^{high} GHOST cells. A) Intact cells were identified on a FS Lin vs SS Log two-parameter plot in the region labelled "GHOST cells". **B)** Viable cells negative for 7-AAD were identified on a FS Lin vs Log 7-AAD plot, indicated in the "VIABLE" region. **C)** A two parameter-plot of SS Log vs Log CD4 APC, gated on the "VIABLE" region was used to identify CD4^{high}-expressing and CD4^{low}-expressing populations, which were then sorted into separate tubes. **D)** A post-sort purity check was performed, in which an aliquot of sorted cells was re-analysed immediately using the same protocol. In this example the results are shown for the CD4^{high} population, indicating a sort purity of 99.09%.

3.2.4. RT-PCR of CD4 mRNA in GHOST cells

The Polymerase Chain Reaction (PCR) is an essential molecular tool which is used to determine whether a specific target DNA sequence is present in a cell population of interest by creating numerous copies of the target sequence by *in vitro* DNA replication (181) (**Figure**

3.12). Conventional PCR products can be visualized using a technique called gel electrophoresis (182), the principles of which are illustrated in **Figure 3.13.** Reverse transcription PCR (RT-PCR) is a modification to conventional PCR in which the aim is to amplify an mRNA target. In this case, the mRNA in the starting material is first converted to complementary DNA (cDNA) using a reverse transcriptase enzyme, and then used as a template for a PCR reaction (181).

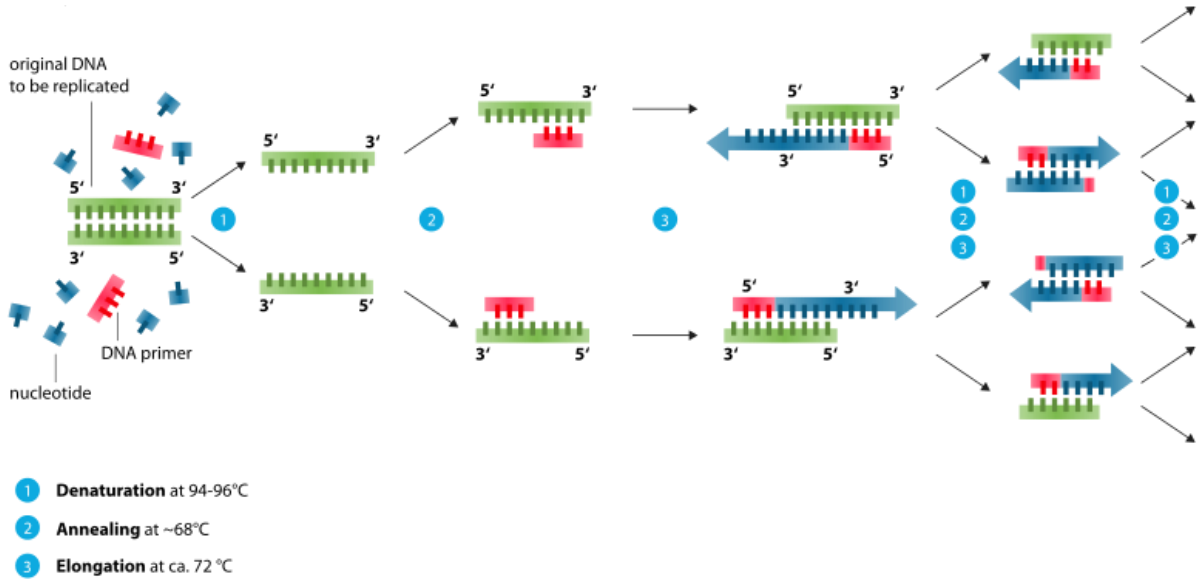

Figure 3.12: Principles of the polymerase chain reaction. Short oligonucleotides called primers are designed to bind to sites flanking the sequence of interest. In the presence of primers and deoxyribonucleotide triphosphates (dNTP) monomers, the template DNA is denatured at high temperatures to separate the two strands (1). When the temperature is reduced, the primes anneal to the template DNA (2). The temperature is raised to 72°C and a thermostable DNA polymerase synthesizes the opposite strand of each template, creating two copies (3). This cycle is repeated for multiple rounds, generating many copies of the target DNA sequence. Available from: https://commons.wikimedia.org/wiki/File:Polymerase_chain_reaction.svg)

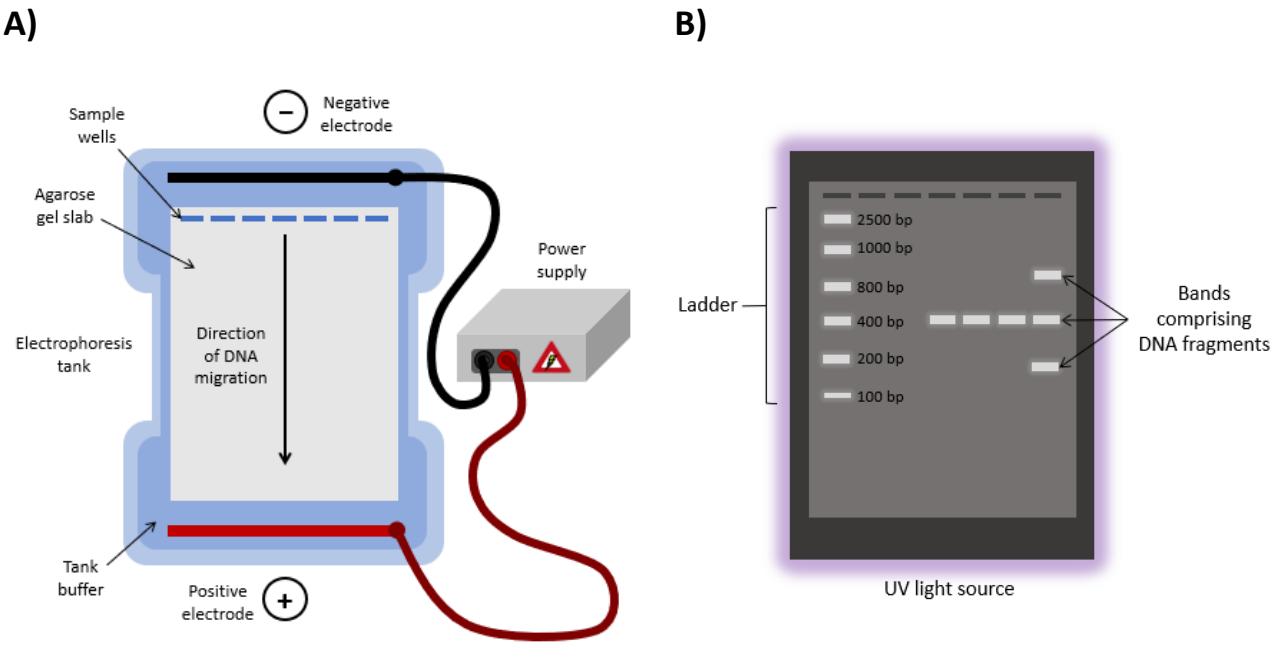

Figure 3.13: Principles of gel electrophoresis. A) A diagram illustrating the experimental setup for gel electrophoresis. Samples containing DNA fragments are loaded into sample wells set into an agarose gel slab. The gel is placed in an electrophoresis tank that is filled with buffer. The two electrodes at either end of the tank are attached to a power supply unit and transmit an electric field through the tank. The samples are loaded near the negative electrode, allowing the DNA to migrate through the gel towards the positive electrode when current is supplied. **B)** The bands of DNA in the samples are visualized using ethidium bromide (often added to the gel itself), which intercalates into the DNA strands and is visible when a UV light is applied. The bands separate based on the size of the DNA fragments. Larger fragments migrate slowly and are thus are found closer to the sample wells, while smaller fragments migrate faster and thus move further through the gel. A ladder, comprising a set of DNA fragments of known size is usually run alongside the samples.

For analysis of CD4 mRNA expression in GHOST cells, $CD4^{high}$ and $CD4^{low}$ (control) GHOST cell populations were sorted using the FACSAria™ Fusion instrument (as per **Section 3.2.3**) and then immunophenotyped for CD4 expression, as described in **Section 3.2.2.4.** The percent $CD4^+$ cells were 91.63% and 35.42% for the high-expressing and low-expressing populations respectively. RNA was isolated from both these GHOST cell populations, as well as from positive (PBMNC, TZM-bl) and negative (HEK293T) control cell types, using the RNeasy® Mini Kit (Qiagen; Hilden, Germany) as per the manufacturer's instructions. The TZM-bl line is a genetically modified HeLa cell line known to stably express high levels of CD4 (164) while the $CD4^+$ T lymphocyte population present in PBMNCs expresses high levels of endogenous CD4. In contrast, the HEK293T cell line does not express CD4 (183,184). The isolated RNA samples were converted to cDNA using the SensiFast™ cDNA Synthesis Kit from Bioline (London, UK).

Reverse transcription reaction mixes were set up on ice, as per **Table 3.5**. The cDNA synthesis reaction was carried out in a GeneAmp™ PCR System 9700 (Thermo Fisher Scientific; Waltham, MA, USA) using the protocol outlined in **Table 3.6**. Both the RNA and cDNA products were analysed using a NanoDrop™ spectrophotometer (Thermo Fisher Scientific; Waltham, MA, USA) to determine the sample concentration and purity.

Table 3.5: Reaction setup for reverse transcription using the SensiFast™ cDNA synthesis kit

Component	**Volume per reaction**
5x TransAmp buffer	4 µL
Reverse transcriptase	1 µL
RNA template	Variable*
Nuclease-free water	Variable**
	Total reaction volume: 20 µL

*The volume was adjusted to allow for the addition of 1 µg of RNA to the reaction.
**The volume of the nuclease-free water was adjusted to ensure a total reaction volume of 20 µL.

Table 3.6: Thermocycling conditions for reverse transcription (SensiFast™ cDNA synthesis kit)

Step	**Temperature**	**Duration**
Primer annealing	25°C	10 min
Reverse transcription	42°C	15 min
Inactivation of reverse transcriptase	85°C	5 min
Hold	4°C	∞

The cDNA products were used as the template for a PCR reaction designed to amplify a small region of the CD4 gene. Previously published primers (185) were used (sequences available in **Appendix B, Table B.2**), however the annealing temperature required optimisation prior to use for experiments (**Appendix B, Figure B.1**). The PCR reactions were set up as indicated in **Table 3.7**, using the KAPA Taq ReadyMix (Kapa Biosystems; Wilmington, MA, USA) and analysed using the GeneAmp™ PCR System 9700. The thermocycling conditions are stated in **Table 3.8**. A positive PCR control reaction using a previously validated primer pair targeting the *Homo sapiens* ribosomal protein L32 pseudogene (sequences available in **Appendix B, Table B.2**) was included to confirm that the reagents and thermocycler were functioning

correctly. GHOST CD4^{high} cDNA was arbitrarily selected as the template for the positive control reaction since GHOST cells, like all the cell types used for this experiment, are of human origin and should possesses the L32 target sequence. A negative PCR control reaction which contained no template DNA was included, also using the L32 primer pair. The resulting products were visualized by gel electrophoresis which was run for 1 hour at 90 V in a 1% agarose (Benchmark Scientific; Edison, NJ, USA) gel made in Tris-acetate-EDTA (TAE) buffer (Thermo Fisher Scientific; Waltham, MA, USA). Band sizes were determined using the Low Range FastRuler™ DNA Ladder (Thermo Fisher Scientific; Waltham, MA, USA).

Table 3.7: Reaction setup for PCR of CD4 using KAPA Taq ReadyMix™

Component	**Volume per reaction**
2X Kapa Taq ReadyMix™	12.5 µL
Forward primer (10 µM)	0.75 µL
Reverse primer (10 µM)	0.75 µL
DNA template	1 µL*
Nuclease-free water	10 µL
	Total reaction volume: 25 µL

*Template DNA concentration was variable

Table 3.8: Thermocycling conditions for PCR of CD4 using KAPA Taq ReadyMix™

Step	**Temperature**	**Duration**	**Number of cycles**
Initial denaturation	94°C	2 min	1
Denaturation	94°C	10 sec	30
Annealing	65°C	10 sec	
Extension	72°C	1 min	
Final extension	72°C	10 min	1
Hold	4°C	∞	-

3.2.5. GHOST cell assay protocol

3.2.5.1. Seeding and quality control of GHOST cells

The complete GHOST cell assay protocol is summarised in **Figure 3.15**. In preparation for the assay, $CD4^{high}$ GHOST cells grown in a T-75 flask were dissociated using non-enzymatic Cell Dissociation Solution, centrifuged at 300 x *g* for 10 min and resuspended in 5 mL complete DMEM. Thereafter, the cells were enumerated and immunophenotyped for CD4 expression by flow cytometry, as per the previously described protocol in **Section 3.2.2.4**. This was done to ensure the cells were expressing consistently high levels of the CD4 receptor, which is critical for HIV entry into the cell. Cells were then seeded in 12-well plates at a density of 150 000 cells/mL in 1 mL DMEM, with a sufficient number of wells being seeded to allow each condition to be assayed in triplicate (**Figure 3.14**). The cells were then cultured for 24 hours before infection.

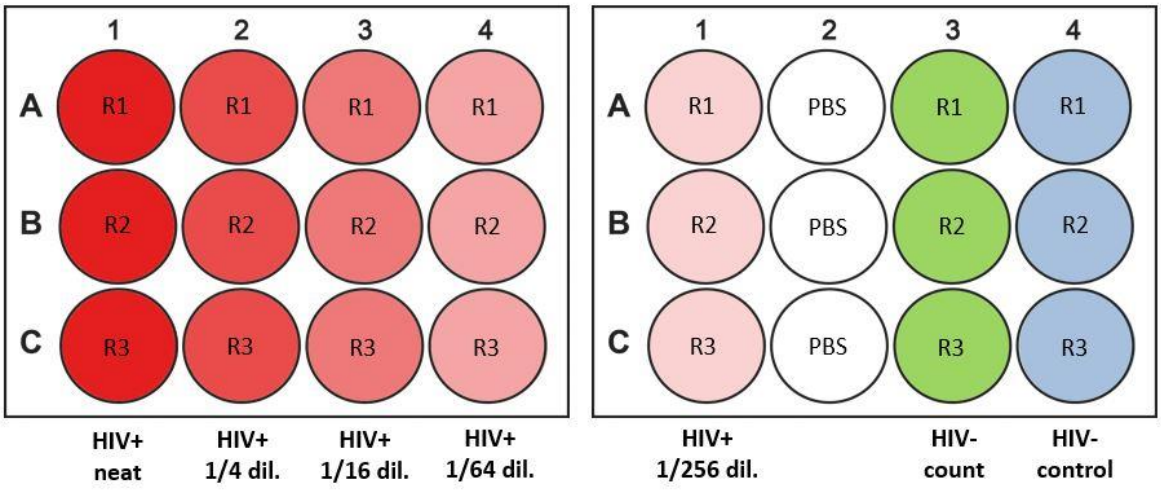

Figure 3.14: Cell culture plate layout of cells seeded for the GHOST cell assay. Two 12-well cell culture plates were used to seed enough wells for three replicates (R1, R2, R3) to be assayed for each condition. The wells to which a dilution series of viral supernatant was added are indicated in shades of red (HIV+). The HIV negative control wells used on Day 3 for GFP analysis are indicated in blue. The HIV negative wells used for obtaining a cell count on Day 1 are indicated in green. The wells to which no cells were added were filled with PBS.

3.2.5.2. Enumeration of GHOST cells

Prior to infection on Day 1 of the assay, the three wells seeded for GHOST cell enumeration (**Figure 3.14**:) were dissociated as described in the GHOST cell culture section (**Section 3.2.2.1**) but using only 200 µL 0.25% Trysin-EDTA to account for the smaller surface area. After

neutralizing the trypsin with 200 µL complete DMEM, the cells were collected, centrifuged at 300 x *g* for 10 min, resuspended in 100 µL PBS and stained with 3 µL 7-AAD. The entire sample was used to obtain an absolute viable cell count on the Gallios™ flow cytometer, as per the GHOST cell enumeration protocol described in **Section 3.2.2.2**. The average cell count obtained from these 3 replicates was used in **Equation 3.3** for the calculation of the functional titre.

3.2.5.3. Infection of GHOST cells

On Day 1 of the assay (24 hours after seeding), the GHOST cells were infected with the virus stock to be titrated. A series of dilutions of the stock was set up in serum-free RPMI-1640 culture medium. The dilutions of virus included were as follows: Neat, 1/4 dilution, 1/8 dilution, 1/16 dilution, 1/64 dilution, 1/256 dilution. An uninfected control, containing only RPMI-1640, was also prepared to determine the background autofluorescence of GHOST cells in the GFP (FL1) channel. Polybrene (Sigma-Aldrich; St. Louis, MO, USA), a cationic polymer that neutralises charge repulsion at the cell membrane, was added to each sample at 20 µg/mL to facilitate viral adhesion. The growth medium in which the GHOST cells were seeded the previous day was removed, and the cells were washed with 1 mL PBS to remove any residual FBS that may interfere with HIV infection. Aliquots of the prepared dilutions were added to the appropriate wells in triplicate (**Figure 3.14**:), using 500 µL per well. The plates were incubated for 2 hours at 37°C, 5% CO_2. Thereafter, each well was supplemented with 500 µL serum-free DMEM and cultured overnight for a further 16 hours. On Day 2 (approximately 48 hours after seeding), the medium in all wells was replaced with 1 mL complete DMEM and the cells were incubated for another 24 hours. Quantification of GFP expression via flow cytometry was carried out on Day 3 (approximately 72 hours post initial seeding) of the assay.

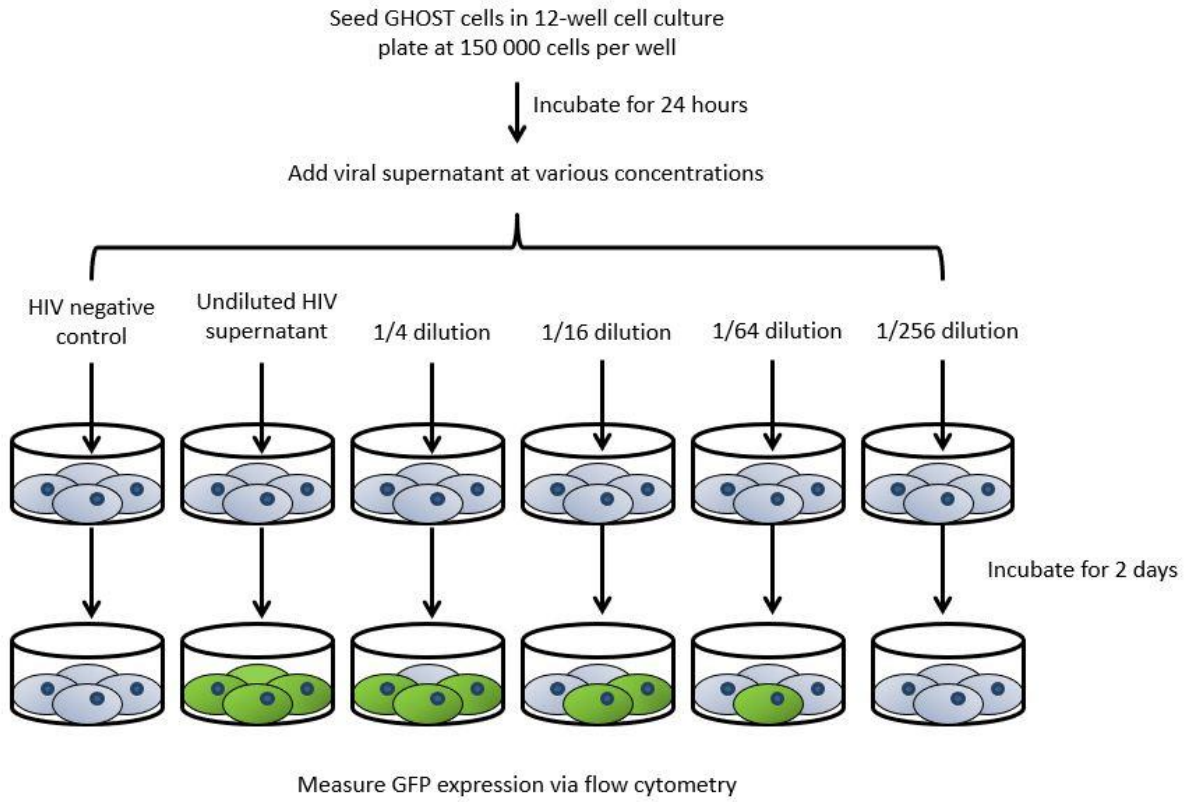

Figure 3.15: Functional titration of HIV-1 strains using the GHOST cell reporter system. Viral supernatant was added to seeded GHOST cells at varying concentrations. A 2-hour incubation period allows infectious virions to infect GHOST cells and initiate GFP expression (illustrated with green cells), which were quantified by flow cytometry after a further 2 days in culture. Viral titre was estimated in terms of infectious units per mL of viral stock using **Equation 3.3** and **Equation 3.4**.

3.2.5.4. Sample preparation for analysis of GFP expression by flow cytometry

The cells in each well were dissociated as previously described and collected in microcentrifuge tubes. After centrifugation at 300 x *g* for 10 min and removal of supernatant, the cells were resuspended in 300 µL IC Fixation Buffer (Thermo Fisher Scientific; Waltham, MA, USA) and incubated for 10 min at room temperature. Fixation of the cells renders them non-infectious and enables them to be safely removed from the Biosafety Level 2+ (BSL2+) facility and run on the flow cytometer. However, this also prevented assessment of cell viability during the analysis since the cells were killed in the process of fixation. The cells were subsequently washed with 1 mL of PBS, then centrifuged at 300 x *g* for 10 min to collect cell pellets. After the cell pellets were resuspended in 400 µL PBS, the cells were analysed on the Gallios™ flow cytometer.

3.2.5.5. Flow cytometry setup and data acquisition

The proportion of GFP-positive GHOST cells in each sample was quantified using a standardized protocol on the Gallios™ flow cytometer. Since GHOST cells are prone to clumping, especially after fixation, doublet discrimination was incorporated into the protocol. Doublet discrimination refers to removal via gating of all cell clumps, resulting in only single cells being analysed. This technique takes advantage of the fact that the voltage pulse generated by the light detector when measuring forward scatter has three characteristics: height, width and area. Height is the maximum intensity of the light signal, width refers to the duration of the signal, while area is the overall amount of light detected during the event. Area is thus a result of the combined effects of width and height. When a single cell is measured all these characteristics should be identical, while a doublet or cell clump will have the same height as a singlet but increased width, and therefore increased area (186) (**Figure 3.16**).

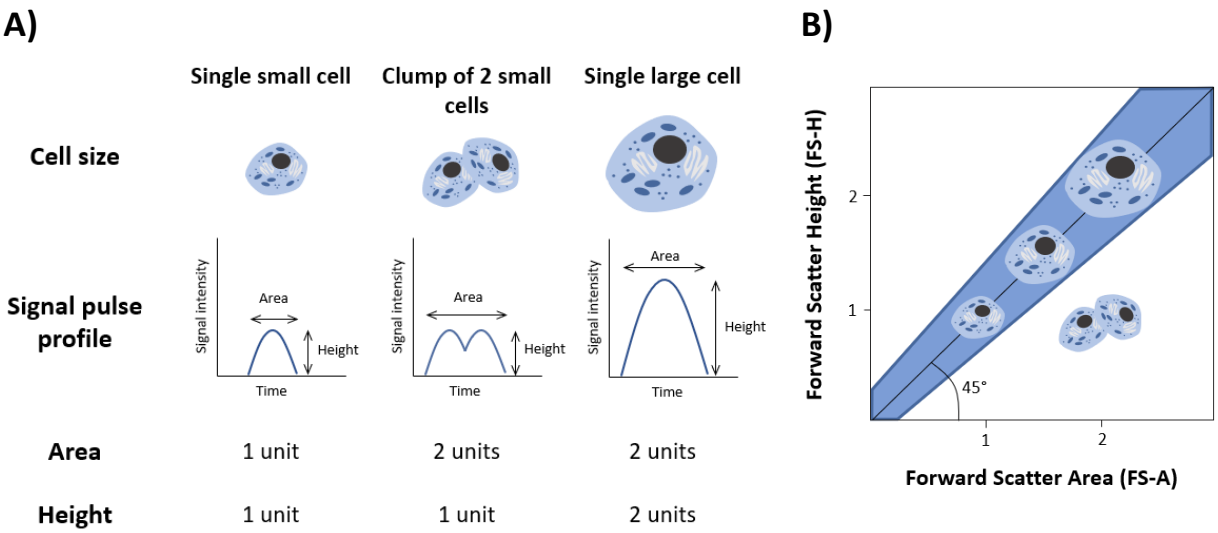

Figure 3.16: Illustration of the use of different forward scatter parameters to distinguish single cells from cell clumps. A) Cells of different sizes will have different FS signal pulse profiles, plotted as the signal pulse intensity vs time. A single cell will always have a 1:1 ratio of FS-Area to FS-Height, whether is it is a small cell (first panel) or a large cell (last panel). A cell clump on the other hand (middle panel) will have the same FS-Height as a single cell of the same size, but since the time taken to pass through the laser is greater, the FS-Area will increase. **B)** When FS-A and FS-H are plotted against each other, the 1:1 proportionality of FS-A to FS-H in the single cells results in a population following a 45° gradient up the plot axes with increasing cell size, indicated in the blue region. Cell clumps on the other hand will fall below this region, since the FS-A values will be larger than the corresponding FS-H value of a single cell of the same size.

The singlet cells were thus identified as a cell population with an approximately one-to-one ratio of Forward Scatter Area (FS-A) to Forward Scatter Height (FS-H), following an approximately linear 45° angle on a FS-A Lin vs FS-H Lin plot (**Figure 3.17a**). Clumps displayed increased FS-A values compared to singlets and fell below the singlet ("B") region when plotted against the FS-H values. The GHOST cells were then identified on a FS Lin vs SS Log plot gated on the singlets ("B") (**Figure 3.17b**). A SS Log vs GFP Log two-parameter plot enabled identification of HIV-positive cells (**Figure 3.17d**). GFP was detected in the FL1 channel [Excitation: 488 nm, Emission: 525/40]). The region indicating GFP positivity was set according to the position of the negative population in the uninfected control (**Figure 3.17c**). Data was acquired and analysed using Kaluza Flow Cytometry Analysis Software (Version 2.1).

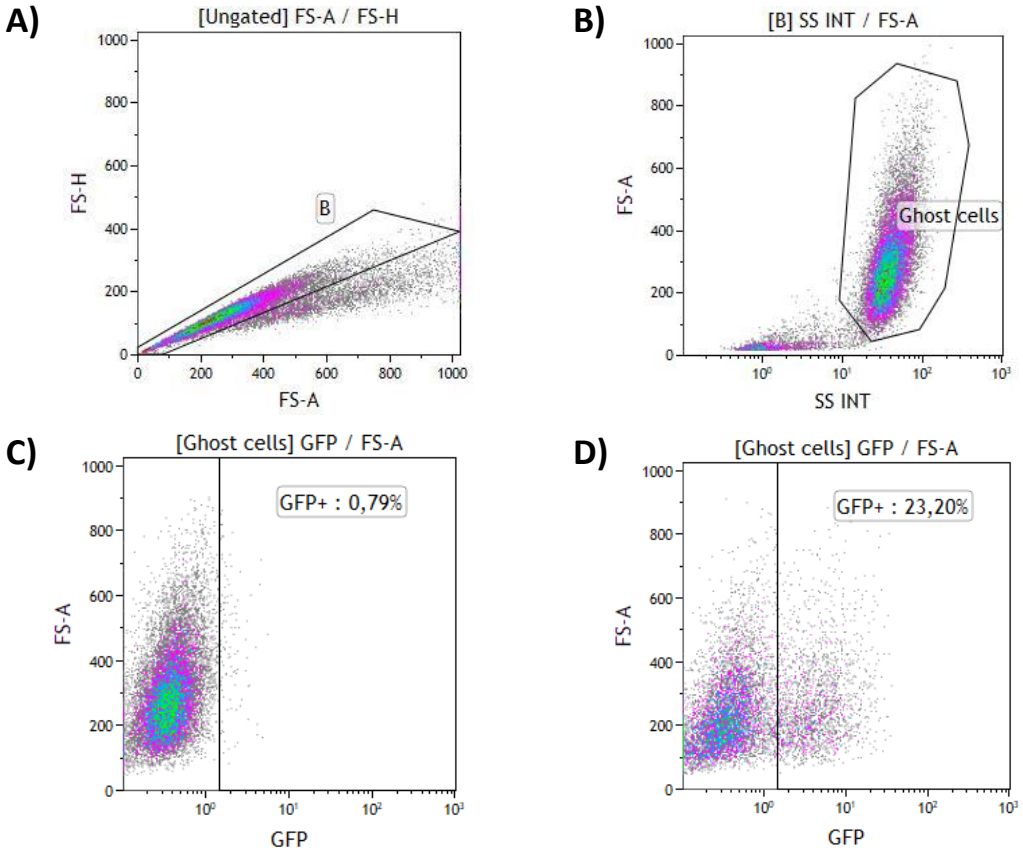

Figure 3.17: Flow cytometry setup for analysis of GFP expression as part of the GHOST cell functional titration assay. A) A FS-H Lin vs FS-A Lin plot was used to exclude any clumps and analyse only single cells downstream. Singlet cells are identified in region "B". **B)** A FS-A Lin vs SS Log plot gated on "B" was used to exclude debris, with the intact cells indicated in the region "Ghost cells". **C)** A FS-A Lin vs GFP Log two-parameter plot gated on "Ghost cells" is used to distinguish HIV-infected cells in the "GFP+" region from the negative cells. The position of this region is set using an HIV-unexposed control, represented in this plot. **D)** HIV-infected cells demonstrate a clear shift towards the right in the FL1 (GFP) channel, allowing for the enumeration of GFP^+ events in the "GFP+" region.

3.2.5.6. Calculation of functional titre

The average percent of GFP-positive cells across the three replicates for each dilution was used in **Equation 3.3** to obtain an estimate of the number of infected cells, which was used as a proxy for the number of infectious viral particles present at the time of infection. If any of the three replicates differed greatly from the other two, causing the standard deviation of the triplicate mean to be greater than 10%, that replicate was considered an outlier and was not used in the calculation. The concentration of infectious viral particles in the stock as a whole was then calculated using **Equation 3.4**, which converts the number of infectious particles per 500 µL (the volume of viral stock used per well in the assay), to the more broadly applicable value of IU/mL. Once IU/mL values were obtained from all dilutions, the three consecutive dilutions that yielded the most similar results were averaged to obtain the final IU/mL used in downstream calculations. An example of this calculation is illustrated in **Table 3.23**.

Equation 3.3:

$$Infectious\ Units\ (IU) = Cell\ count\ \times \frac{(\%\ GFP)}{100} \times\ Dilution\ factor$$

Equation 3.4:

$$IU/mL\ viral\ stock = \frac{IU}{Volume\ per\ well\ (mL)}$$

3.3. Detection of HIV-infected Cells

3.3.1. Detection of intracellular p24 using the KC57 antibody-based assay

3.3.1.1. Sample Preparation

Two sets of samples were used in all experiments: HIV-exposed samples and uninfected controls. Cell suspensions from both sample sets were prepared and counted as per the relevant protocols for each cell type. For optimization purposes, aliquots containing $1x10^6$ GHOST cells were taken, centrifuged at 300 x *g* and resuspended in 100 µL PBS. A fixable viability dye, Zombie Violet™ (Biolegend, San Diego, CA, USA), was added at 1 µL per sample,

if viability was to be assessed. After incubation at room temperature in the absence of light for 15 min, the dye was washed off with 1 mL PBS and resuspended in 100 µL PBS. The stained cells were resuspended in 100 µL PBS, to which 100 µL of IC Fixation Buffer was added. After pulse vortexing to mix, the cells were incubated for 1 hour at room temperature in the dark. The fixed cells were then washed with 2 mL of 1 x Permeabilization Buffer (Thermo Fisher Scientific; Waltham, MA, USA) and centrifuged at 400 x *g* for 5 min. The supernatant was removed, and the wash step repeated. The cells were then resuspended in 100 µL Permeabilization Buffer and stained with 2.5 µL of either KC57 anti-p24 antibody, conjugated to the fluorochrome PE, (Beckman Coulter; Miami, FL, USA) or the corresponding isotypic control. The cells were incubated at room temperature in the dark for 1 hour. Stained cells were washed twice more using Permeabilization buffer and resuspended in a final volume of 500 µL PBS. The final cell suspensions were analysed on the FACSAria™ Fusion cell sorter.

3.3.1.2. Flow cytometry setup and data acquisition

GHOST cells were identified on a FS Lin vs SS Log plot, while excluding clumps and debris as in previous analyses (**Figure 3.18a**). Viability was determined using the fixable viability dye, Zombie Violet™ since 7-AAD cannot be used in fixed cells. The viable population was identified in the Zombie Violet™ negative region, as illustrated in the FS Lin vs Zombie Violet a two-parameter plot (**Figure 3.18b**). A KC57-PE Log vs GFP Log two-parameter plot enabled identification of HIV-positive cells detected through either GFP expression or antibody binding or both (**Figure 3.18c**). The positions of the quadrant regions were set according to the position of the double negative population observed in the uninfected control. This analysis of co-expression allowed assessment of the agreement between the two HIV detection methods. Data was acquired using BD FACSDiva™ (Version 8.0.1) and analysed using Kaluza Flow Cytometry Analysis Software (Version 2.1).

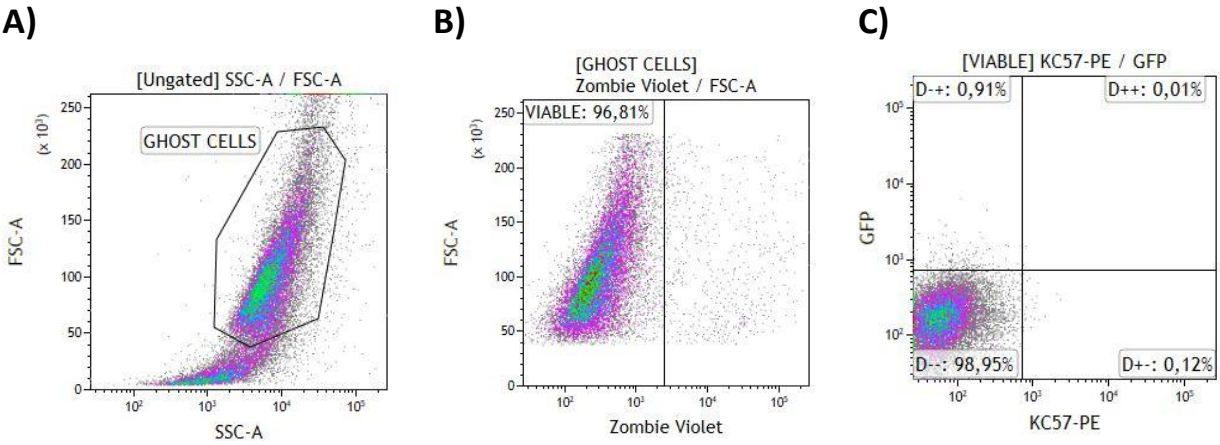

Figure 3.18: Flow cytometry protocol setup for the KC57 assay. A) GHOST cells were first identified in the region "GHOST CELLS" using a FS Lin vs SS Log two-parameter plot. **B)** Viable cells were then identified using a FS Lin vs Zombie Violet Log plot, gated on "GHOST CELLS". **C)** Co-expression of both GFP and intracellular p24 was determined using a GFP Log vs KC57-PE Log two-parameter plot gated on the "VIABLE" region. Cells negative for both were detected in the bottom left quadrant (D--), $KC57^{+}$ GFP^{-} cells were detected in the bottom right (D+-) quadrant, $KC57^{-}$ GFP^{+} cells were detected in the top left (D-+) quadrant, and cells positive for both were detected in the top right (D++) quadrant.

3.3.2. PCR-based detection of viral DNA

3.3.2.1. Primer design

A collection of HIV-1-C genome sequences generated between 2005-2015 was obtained from the Los Alamos National Laboratory HIV database (accessed from: https://www.hiv.lanl.gov/content/index). These sequences were aligned in CLC Main Workbench using the MUSCLE algorithm and a consensus sequence was generated. Primers for amplification of the V3-loop region of the *env* gene as well as for amplification across the LTR and *gag* regions were designed manually using this consensus sequence by Ms Candice Herd (MSc student, Department of Immunology, University of Pretoria). The primers were checked for specificity against the CM9 and SW7 sequences and modified if necessary. The final sequences of the primers used are indicated in **Table 3.9**. The binding sites of the designed primers were checked against the full-length consensus sequence for the HIV-1-C genome with NCBI Primer Blast (accessed from: https://www.ncbi.nlm.nih.gov/tools/primer-blast/), an example of which is shown is **Figure 3.19**. Self-complementarity, melting temperatures and Gibbs free energy (ΔG) metrics were assessed using the online OligoCalc tool (accessed from: http://biotools.nubic.northwestern.edu/OligoCalc.html) (**Figure 3.20**).

All primers were found to have acceptable specificity to the consensus sequence as well as to the isolate-specific sequences. The results of the self-complementarity analysis and examination of physical properties performed in OligoCalc is indicated in **Table 3.10***:*. The primers were synthesized by Inqaba Biotech (Pretoria, South Africa).

Table 3.9: Sequences of primers used for detection of HIV-1-C isolates

Isolate & target region	Primers	Sequence (5' to 3')	Size of amplicon
CM9 LTR/*gag*	**Forward:** LTR fwd6 **Reverse:** ts5'Gag(R) CM9	CCCTCAGATGCTGCATATAAGCAGCTGC TCCTTTAACATTTGCATGGCTGCTTG	983 bp
SW7 LTR/*gag*	**Forward:** LTR fwd6 **Reverse:** ts5'Gag(R)	CCCTCAGATGCTGCATATAAGCAGCTGC TCTTTTAACATTTGCATGGCTGCTTG	978 bp
CM9 V3-loop	**Forward:** V3 fwd6 **Reverse:** V3 rvs1.2	GGACCATGCAATAATGTCAGC GTGTTGTAATTTCTAGGTCCCC	406 bp
SW7 V3-loop	**Forward:** V3 fwd3 **Reverse:** V3 rvs2	GGACCATGCCATAATGTCAGC CCTACCCCCTGCCACATG	551 bp

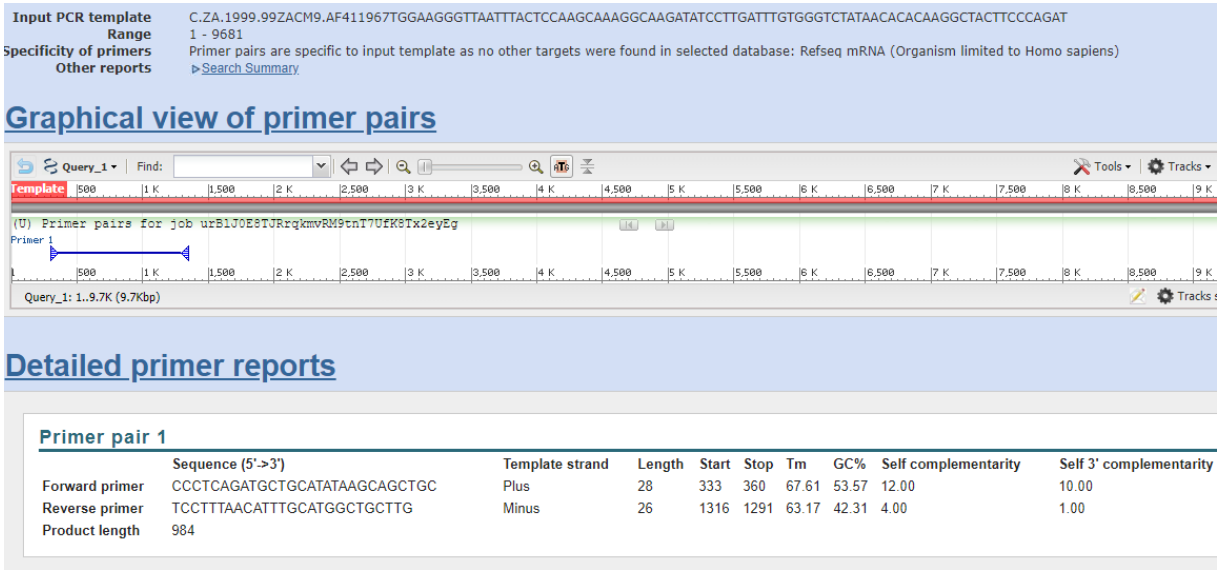

Figure 3.19: Screenshot of the NCBI Primer BLAST output for the CM9 LTR/gag primer pair. The primer pair was predicted to be specific to the HIV-1-C CM9 consensus input sequence, and to have no off-target binding, using the Refseq mRNA database as a reference.

A)

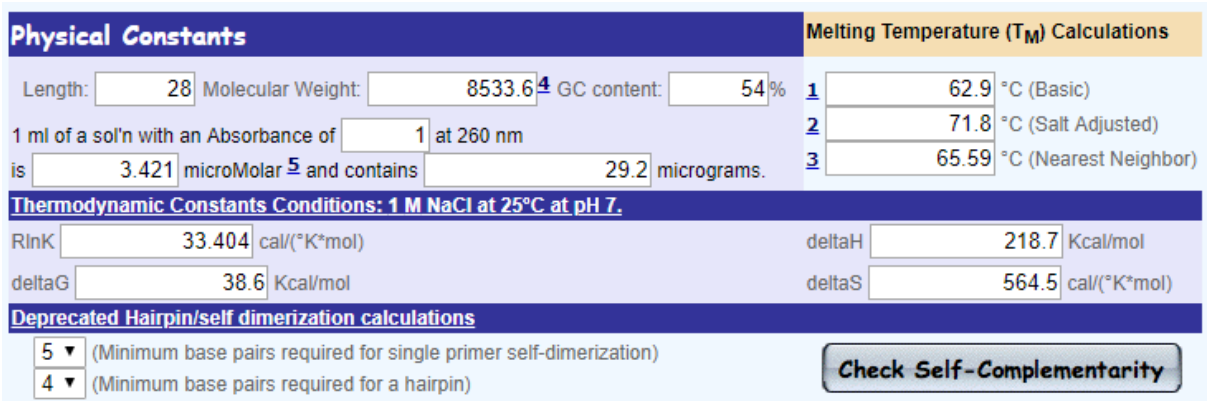

B)

Minimum base pairs required for single primer self-dimerization: 5.
Minimum base pairs required for a hairpin: 4.

Potential hairpin formation :

```
5' CCCTCAGATGCTGCATATAAGCAGCTGC 3'
```

3' Complementarity:
None !

All potential self-annealing sites are marked in red (allowing 1 mis-match):

```
5' CCCTCAGATGCTGCATATAAGCAGCTGC       3'
3'       CGTCGACGAATATACGTCGTAGACTCCC 5'

5'      CCCTCAGATGCTGCATATAAGCAGCTGC  3'
3' CGTCGACGAATATACGTCGTAGACTCCC       5'

5' CCCTCAGATGCTGCATATAAGCAGCTGC       3'
3'    CGTCGACGAATATACGTCGTAGACTCCC    5'
```

Figure 3.20: Screenshots of output from the OligoCalc primer analysis tool for the CM9 LTR/gag forward primer (LTR fwd6). A) Output for analysis of physical constants gives all relevant physical properties of the primer, including GC content, melting temperatures (Tm), Gibbs free energy (delta G), etc. **B)** Output for self-complementarity analysis shows potential hairpin formation, expected 3' self-complementarity, as well as potential sites at which self-annealing of the primer can occur.

Table 3.10: Results of primer analysis using the OligoCalc tool

Primer	Tm (°C)	%GC	ΔG (Kcal/ mol)	Potential hairpin formation	3'comple mentarity	Number and length of self-annealing sites
LTR fwd6	65.59	54	38.6	Yes (4 bp)	None	3 (10 bp, 9 bp, 8 bp)
ts5'Gag(R) CM9	59.11	42	33.7	None	None	None
ts5'Gag(R)	58.05	38	32.8	None	None	None
V3 fwd6	51.73	48	25.8	None	None	None
V3 rvs1.2	49.93	45	26.3	None	None	None
V3 fwd3	53.10	52	26.7	None	None	2 (7 bp, 7 bp)
V3 rvs2	51.88	67	24.5	None	None	None

3.3.2.2. Isolation of DNA from infected GHOST cells

In order to isolate infected GHOST cell template DNA for primer optimization, $CD4^{high}$ sorted GHOST cells were seeded in a 6-well plate and allowed to become confluent. At confluence, the culture medium was removed and 1 mL of either CM9-290118 or SW7-010818 was added to the cells. Serum-free RPMI was used in one well instead of supernatant, which served as a mock-infected control. After a 2-hour incubation period at 37°C, 5% CO_2, the supernatant was supplemented with 1 mL of serum-free DMEM. Following a further incubation overnight for 16 hours, the medium was changed to complete DMEM and the cells were cultured for a further 3 days. On the fourth day post-infection, the HIV-exposed cells were dissociated using trypsin and centrifugation at 300 x *g* for 10 min. DNA was extracted from the cell pellets using the QiaAmp® DNA Mini Kit (Qiagen; Hilden, Germany) as per the manufacturer's protocol for cultured cells.

A second batch of infected GHOST cells was produced using the same method to determine the limit of detection of the LTR/*gag* PCR. However, for this infection cycle, GHOST cells were seeded in T-25 flasks at $1x10^6$ cells per flask and infected using 2 mL of viral supernatant per flask. Isolates CM9-290118 and SW7-010818 were used. An additional T-75 flask of cells was not exposed to HIV and served as an uninfected control. Cells from all flasks were harvested after 3 days in culture. The GFP+ cells in each culture were quantified and used to produce a set of standards containing different concentrations of the respective viruses. This was achieved by sorting the required numbers of GFP positive cells and uninfected cells into 48-

well cell culture plates, using the FACSAria™ Fusion cell sorter, to yield a total of 100 000 cells each as indicated in **Table 3.11.** The sorted cells in each well were collected by centrifugation at 500 x *g* for 10 min and DNA was extracted from the respective cell pellets, using the QiaAmp® DNA Micro Kit (Qiagen; Hilden, Germany) as per the manufacturer's instructions.

Table 3.11: Setup of HIV-infected cell standards used to determine the limit of detection of the LTR/gag PCR reaction

Proportion of infected cells	Number of GFP^+ infected cells	Number of uninfected cells
0.1%	100	99 900
1%	1 000	99 000
5%	5 000	95 000
10%	10 000	90 000
20%	20 000	80 000

3.3.2.3. Amplification of LTR/gag and V3-loop regions by PCR

PCR reactions for amplification of viral DNA in target cells were set up as per **Table 3.12** and analysed using the thermocycling conditions indicated in **Table 3.13.** Additional PCR controls using the L32 primer pair were included – a negative no-template control and a positive PCR control using DNA from uninfected cells as template. The L32 primer pair should be able to amplify from any human genomic DNA template and thus serves to confirm that the reaction conditions are correct. The resulting PCR products were visualized by gel electrophoresis. Electrophoresis conditions were as follows: 40 min to 1 hour at 90 V in a 1% agarose TAE gel. Band sizes were determined using either a Low Range or Middle Range FastRuler™ DNA Ladder (Thermo Fisher Scientific; Waltham, MA, USA).

Table 3.12: Reaction setup for PCR of LTR/gag and V3-loop regions using KAPA Taq ReadyMix™

Component	Volume per reaction
2X Kapa Taq ReadyMix™	12.5 µL
Forward primer (10 µM)	0.75 µL
Reverse primer (10 µM)	0.75 µL
DNA template	1 µL
Nuclease-free water	10 µL
	Total reaction volume: 25 µL

Table 3.13: Thermocycling conditions for PCR of LTR/gag and V3-loop regions using KAPA Taq ReadyMix™

Step	Temperature	Duration	Number of cycles
Initial denaturation	94°C	2 min	1
Denaturation	94°C	10 sec	
Annealing	58.5°C	10 sec	30
Extension	72°C	1 min	
Final extension	72°C	10 min	1
Hold	4°C	∞	-

4. Results

4.1. Propagation of primary HIV-1-C isolates

4.1.1. Optimization of the virus production protocol

During the course of this study, various modifications were made to the original Montefiori protocol based on the behaviour of the primary HIV-1-C isolates in culture (**Figure 3.21**). Initially, three strains were selected for their different tropisms: CM1 (R5-tropic), CM9 (dual-tropic) and SW7 (X4-tropic). During the first production of CM9, aliquots of cell culture supernatant were harvested at Day 7 and Day 10 during the production and tested using a p24 ELISA assay to determine whether viral replication had occurred. It was noticed that, although viral p24 protein was clearly detected in both aliquots, the Day 10 harvest yielded

better results (**Table 3.14**). Therefore, when the next strain (CM1) was produced shortly afterwards, it decided to increase the length of the production. Aliquots were taken at Day 10 and Day 15 for p24 ELISA analysis. Interestingly, the quantity of p24 protein in the Day 10 harvest was higher than the Day 15 harvest (**Table 3.14**), indicating that the increased production time did not improve virus yield. Since the Day 10 harvest produced good yields for both strains, it was decided to harvest only once at Day 10 in future productions, thereby reducing the number of feed cycles to two.

Table 3.14: p24 ELISA results of initial HIV productions using CM1 and CM9 primary isolates

Sample description		Raw absorbance (450 nm)	Normalized absorbance (450 nm)	p24 concentration (pg/mL)
CM9	Blank	0.364	1	-
	Day 7	1.116	3.066	67.36
	Day 10	3.577	9.827	303.76
CM1	Blank	0.322	1	-
	Day 10	3.824	11.876	375.40
	Day 15	2.514	7.807	233.15

In an effort to further increase virus output in the next round of productions, the PBMNC-HIV-1-C co-cultures were split into two separate flasks (**Figure 3.21b**) at the first feed (addition of fresh PBMNCs). Each half was given one feed's worth ($1x10^7$ cells), thus doubling the number of host cells available to the virus. This split-feed strategy generally resulted in higher p24 yields compared to the previous productions(**Table 3.15** and **Figure 3.22**). This was especially true for the CM1 production in which one of the absorbance readings was in fact too high for the spectrophotometer to quantify. However, there is quite a large discrepancy between the yields observed in the two different flasks for each isolate, particularly in CM9 where the p24 yield of the second flask is markedly reduced. This could be because the cultures were kept separate, allowing independent divergence of viral quasispecies with different replication capacities in the different flasks. Therefore, in future productions the two viral cultures were pooled prior to feeding and split once more after the PBMNCs were added to homogenize the viral quasispecies present in each flask.

A) Original protocol

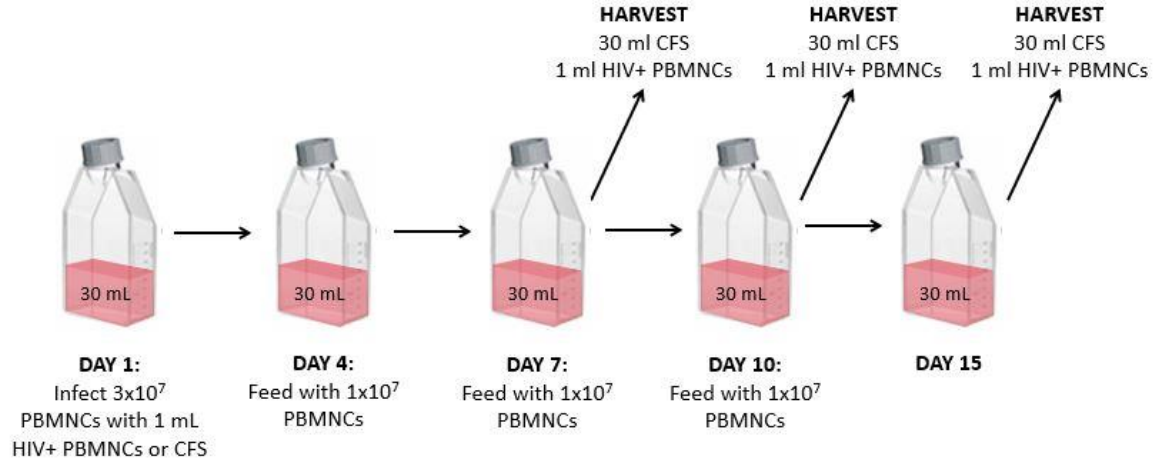

B) Modified protocol

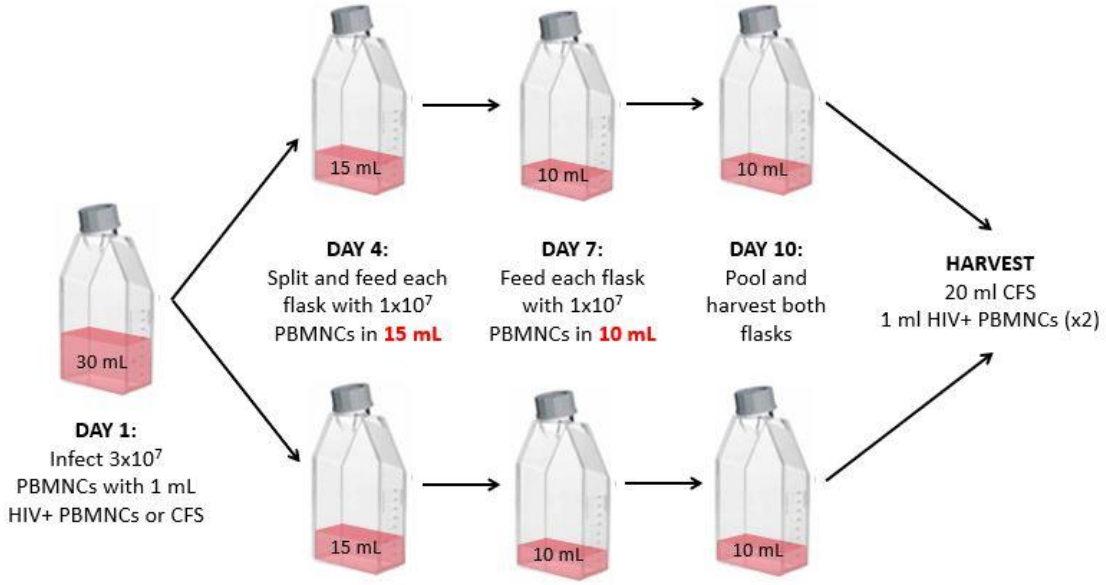

Figure 3.21: Overview of modifications made to the initial HIV production protocol. Production cycles were initiated using $3x10^7$ PHA-activated PBMNCs which were exposed to the viral inoculum. On feeding days, additional activated PBMNCs were added to the cultures. Harvesting involved separating the virus-enriched supernatant from the cells in the co-culture by centrifugation. The supernatant was filtered to remove residual cells, resulting in cell-free supernatant (CFS). The HIV-infected PBMNC pellet remaining once the supernatant has been removed was also harvested in a 1 mL aliquot (HIV+ PBMNCs). **A)** The original production strategy based on the Montefiori protocol uses a single culture flask kept at 30 mL with sequential feeds and harvests. Multiple harvests may be taken, depending on virus output as measured by p24 ELISA. **B)** The modified protocol differs in that the culture was split into two cultures at the first feed on Day 4, with each half being given a full feed's worth of cells. At the second feed on Day 7, the volume of the culture medium was reduced in order to pre-concentrate the virus particles in the supernatant that was harvested on Day 10.

Table 3.15: p24 ELISA results of HIV productions using the split-feed strategy

Sample description	Raw absorbance (450 nm)	Normalized absorbance (450 nm)	p24 concentration (pg/mL)
Blank	0.212	1.000	-
CM1 Day 10 (Flask 1)	3.596	16.962	553.25
CM1 Day 10 (Flask 2)	OUT*	-	-
CM9 Day 10 (Flask 1)	3.984	18.792	617.24
CM9 Day 10 (Flask 2)	0.484	2.283	39.99

*The "OUT" result indicates that the absorbance was outside the measurable range of the spectrophotometer

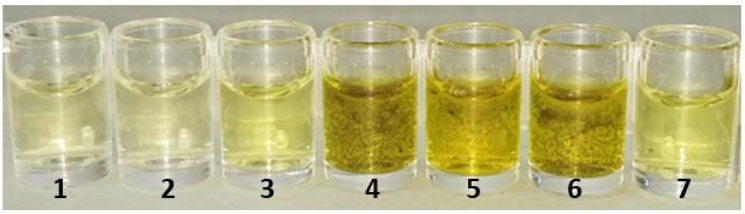

Figure 3.22: ELISA plate used to assay p24 yield in CM1 and CM9 split-feed strategy productions. 1 = Blank, 2 = Positive p24 control 12.5 pg/mL, 3 = Positive p24 control 200 pg/mL, 4 = CM1 Flask 1, 5 = CM1 Flask 2, 6 = CM9 Flask 1, 7 = CM9 Flask 2.

Despite these changes to increase viral production in culture, the concentration of infectious viral particles in the harvested supernatant remained too low to be useful in downstream experiments. Therefore, two further methods were investigated to improve the virus concentration during HIV-1-C viral productions. The first method involved centrifugation of freshly harvested cell-free supernatant at 3 000 x *g* overnight (to collect virus particles towards the bottom of the vessel) and removing the top layer of depleted supernatant. The second method involved reducing the culture volume during the second feed cycle of the production, so that the supernatant would be more concentrated prior to harvesting. In the original protocol, the total culture volume was 30 mL. However, when the split-culture protocol described above was adopted, the volume in each of the two flasks was halved to 15 mL. In the second method, referred to as the pre-concentration method, the final volume of each flask was reduced to 10 mL. Both the methods tested improved the concentration of virus in the CM9 viral supernatant. We found that the simple pre-concentration was more effective than centrifugation, yielding a higher titre in the GHOST cell assay (**Table 3.16**). This step was therefore added to the final modified protocol (**Figure 3.21b**).

Table 3.16: Comparison of GHOST assay results for CM9 productions using different methods for concentration of the viral supernatant

	CENTRIFUGATION		PRE-CONCENTRATION	
Dilution	**Mean % GFP$^+$**	**Mean IU/mL**	**Mean % GFP$^+$**	**Mean IU/mL**
Neat	24.34	$1.10x10^6$	33.81	$1.53x10^6$
1/4 dilution	2.10	$3.80x10^5$	4.94	$8.92x10^5$
1/16 dilution	0.88	$6.36x10^5$	1.47	$1.06x10^6$
Average across dilutions:		**$7,05x10^5$ IU/mL**		**$1.16x10^6$ IU/mL**

4.1.2. Modification of production strategy for an X4-tropic isolate

The adapted production protocol was used successfully for the dual-tropic isolate CM9 as well as for early productions of the R5-tropic CM1 strain. However, the X4-tropic isolate, SW7, proved to be more challenging. During the first production (SW7-110618), it was noticed that extensive cell death had occurred. Observations were done both under the microscope and visually (decrease in the turbidity of the culture). Examination of p24 ELISA results from supernatant harvested at Days 4 and 10, respectively, indicated that while p24 had been produced at Day 4, virus production had dropped to noticeably lower levels by Day 10 (**Table 3.17** and **Figure 3.23a**). It was hypothesized that the X4-tropic primary isolate was more cytotoxic than the dual-tropic and R5-tropic strains produced previously, causing massive cell death during the initial infection and thereby depleting its own host pool. Due to the apparently more rapid infection kinetics of this isolate, it was decided that more frequent feeds with higher cell numbers were required. The protocol was thus shortened to a 7-day production (SW7-240618), with feeds occurring every two days and using double the amount of PBMNCs at each step. A p24 ELISA was performed using supernatant collected at Days 3, 5 and 7, respectively, after applying these modifications. The results indicate that the modifications were successful, with detectable p24 obtained at all time points (**Table 3.17** and **Figure 3.23b**). Maximum yield was observed on Day 7 (**Table 3.17** and **Figure 3.23b**). This success was replicated in a subsequent production (SW7-010818) using the same protocol, but harvesting virus at Day 7 only (**Table 3.16** and **Figure 3.23c**).

Table 3.17: p24 ELISA results of HIV productions for isolate SW7

Production	Sample description	Raw absorbance (450 nm)	Normalized absorbance (450 nm)	p24 concentration (pg/mL)
SW7-110618 (First production)	Blank	0.166	1	-
	Day 4 (1/10 dilution)	0.404	2.434	45.26
	Day 10 (1/10 dilution)	0.24	1.446	10.71
SW7-240618 (Production with modified protocol)	Blank	0.169	1	-
	Day 3 (1/10 dilution)	0.227	1.343	7.13
	Day 5 (1/10 dilution)	0.297	1.757	21.61
	Day 7 (1/10 dilution)	1.099	6.503	187.54
SW7-010818	Blank	0.199	1	-
	Day 7 (1/5 dilution)	3.855	19.372	637.50

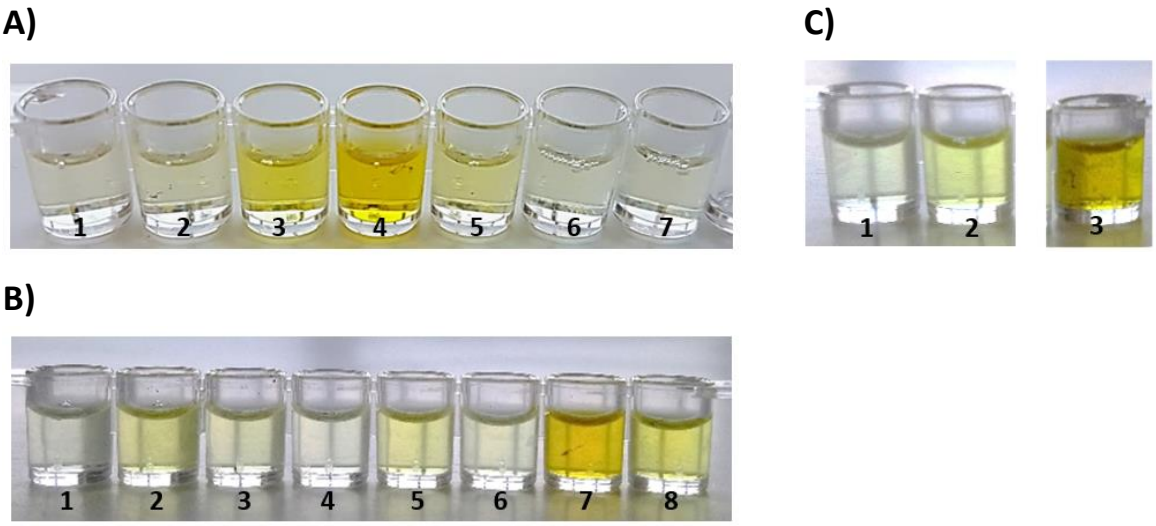

Figure 3.23: ELISA plates used to quantify viral p24 in HIV productions of isolate SW7. A) Results from first production using the standard viral culture protocol. 1 = Blank, 2 = Positive p24 control 20 pg/mL, 3 = Positive p24 control 200 pg/mL, 4 = Day 4 neat, 5 = Day 4 1/10 dilution, 6 = Day 10 neat, 7 = Day 10 1/10 dilution. **B)** Results from the second production using the modified protocol. 1 = Blank, 2 = Positive p24 control 200 pg/mL, 3 = Day 3 neat, 4 = Day 3 1/10 dilution, 5 = Day 5 neat, 6 = Day 5 1/10 dilution, 7 = Day 7 neat, 8 = Day 7 1/10 dilution. **C)** Results from subsequent production to validate the modified protocol. 1 = Blank, 2 = Positive p24 control 200 pg/mL, 3 = Day 7 1/5 dilution.

4.1.3. Screening of R5-tropic strains for use in production

Several attempts were made to produce more infectious R5-tropic virus after the initial successful production round. Despite early successes with CM1 during optimization, this

isolate appeared to lose infectivity with subsequent rounds of production, resulting in the infectious stocks becoming depleted. In order to find a suitable R5-tropic replacement, small-scale productions of five separate R5-tropic strains (CM1, COT1, Du123F, Du156 and Du422) were performed over 3 days using $14x10^6$ activated PBMNCs each, to screen them for their productive potential. On the third day, aliquots of supernatant were harvested for a p24 ELISA, the results of which are presented in **Table 3.18** and **Figure 3.24.** The two isolates in which the most p24 was observed were COT1 and Du156. These two isolates were then taken through full-scale productions, using 5 mL of supernatant from the Day 3 harvest as the viral inoculum. Despite the initial promising p24 results, the full-scale productions were unsuccessful as determined by GHOST cell assays, in which little to no GFP signal was observed (**Figure 3.25**). Even when given the best chance of success, production of an R5-tropic strain from the stocks available proved too challenging to be accomplished in the given time frame for the project and had to be abandoned. Further work was completed using only the dual-tropic and X4-tropic isolates, CM9 and SW7 respectively.

Table 3.18: p24 ELISA results of small-scale R5-tropic HIV productions

Sample description	Raw absorbance (450 nm)	Normalized absorbance (450 nm)	p24 concentration (pg/mL)
Blank	0.199	1	-
CM1-250217	1.006	5.055	136.92
COT1-081002	1.867	9.382	288.20
Du123F-080605	0.676	3.397	78.94
Du156-090499	1.767	8.879	270.63
Du422-240718	0.402	2.020	30.79

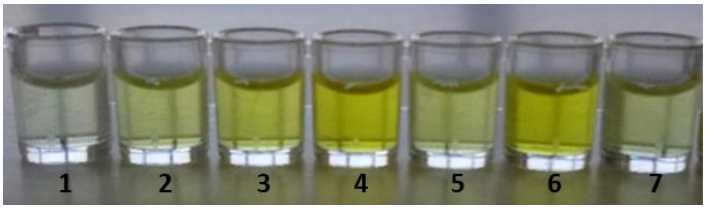

Figure 3.24: p24 ELISA results from small-scale R5-tropic HIV productions. 1 = Blank, 2 = Positive p24 control 200 pg/mL, 3 = CM1, 4 = COT1, 5 = Du123F, 6 = Du156, Du422

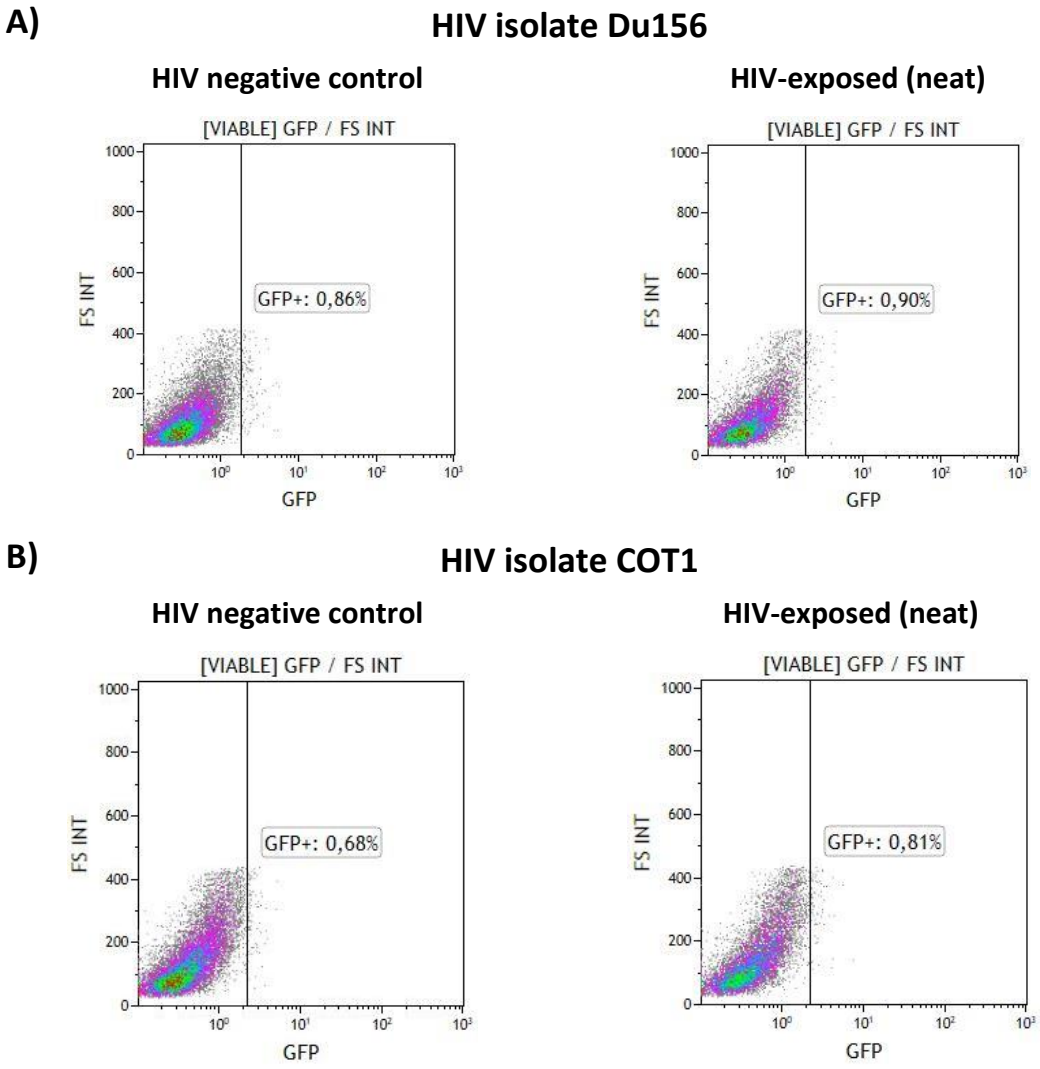

Figure 3.25: GHOST assay results from full scale R5-tropic HIV productions. A) FS Lin vs GFP Log two-parameter plots illustrate the GFP expression observed during the GHOST cell assay for the full-scale production of the R5-tropic isolate Du156. An HIV negative control sample (left) and a sample exposed to undiluted viral stock (right) were selected for illustration purposes, both of which are negative for GFP expression. It was therefore concluded that the virus was non-infectious. **B)** Identical plots from the GHOST cell assay performed using isolate COT1 are presented. As for Du156, there was no evidence of HIV infection in the exposed sample since GFP expression is no different to the HIV negative control.

4.2. Viral quantification

4.2.1. Optimisation of the GHOST cell assay

4.2.1.1. Analysis of CCR5 and CXCR4 expression in GHOST cells

An important quality control step for the GHOST cell assay is to ensure there is enough receptor and co-receptor expression on the cell surfaces to mediate HIV entry. The parental

GHOST cell stock which was expanded and used for all subsequent experiments was immunophenotyped for the HIV co-receptors, CXCR4 and CCR5. Expression levels were high for both, measuring 92.77% and 89.26% for CXCR4 and CCR5, respectively (**Figure 3.26**). This served as a confirmation that the GHOST cells expressed the co-receptors at sufficiently high levels and immunophenotyping of these markers was not repeated on any of the expanded stocks.

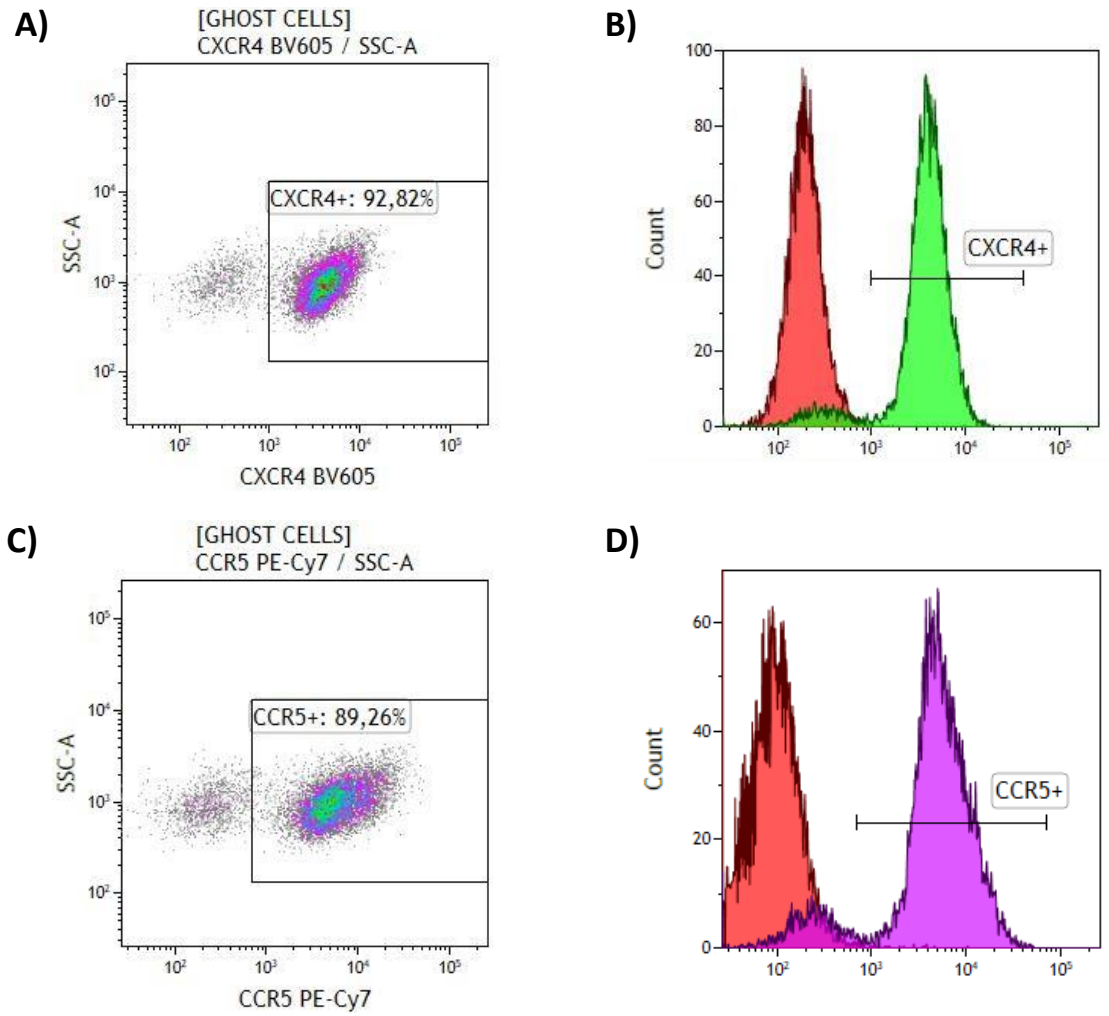

Figure 3.26: Immunophenotyping of GHOST (3) R5X4 stocks for confirmation of HIV co-receptor expression. **A)** A SS vs BV605 two-parameter plot illustrates the proportion of cells expressing CXCR4, in the region "CXCR4+". The negative/positive CXCR4 expression was determined using an appropriate isotypic control **B)** An overlay of a Count vs CXCR4 (BV605) one-parameter plot shows the level of fluorescence observed for the isotypic control (red) compared to the fluorescence observed for the antibody-stained sample (green). **C)** A SS vs PE-Cy7 two-parameter plot illustrates the proportion of cells expressing CCR5, in the region "CCR5+". The negative/positive regions for CCR5 expression were determined using an appropriate isotypic control. **D)** An overlay of a Count vs CCR5 (PE-Cy7) one-parameter plot shows the level of fluorescence observed for the isotypic control (red) compared to the fluorescence observed for the antibody-stained sample (green).

4.2.1.2. Analysis of CD4 expression in GHOST cells

During optimisation experiments, it was noted that the CD4 levels of the initial stocks were considerably lower than expected. GHOST cell cultures at different passages that had been used in our laboratory were immunophenotyped for CD4 expression, including two cultures kindly donated by the Council for Scientific and Industrial Research (CSIR) for comparison (see **Table 3.19** for details of GHOST stocks used). It was hypothesized that the loss of CD4 could be because the cells were treated with trypsin, a proteolytic enzyme. Due to its proteolytic enzyme activity it was possible that trypsin cleaved the CD4 molecule on the GHOST cell surfaces preventing optimal CD4 monoclonal antibody binding during flow cytometric analysis.

The effect of trypsin on CD4 expression by GHOST cells was thus tested in the different cultures listed in **Table 3.19**. The cultures were treated with trypsin and an aliquot was phenotyped to assess baseline expression levels. The remaining cells were seeded in 12-well plates to investigate CD4 recovery over time following exposure to trypsin. The cells were harvested every 24 hours over 4 days using non-enzymatic Cell Dissociation Solution (to prevent any further potential enzymatic cleavage) and phenotyped. Each time point was assayed in duplicate. The results of this experiment are summarised in **Figure 3.27**. The baseline averaged CD4 expression levels were extremely variable, ranging from 30% - 85% (95% CI [21.3%, 77.5%]). However, in all cultures, the levels steadily increase over time, reaching plateaus ranging between 88% - 98% at Day 4 (95% CI [88.7%, 98.9%]). This indicated that trypsin did indeed influence CD4 expression, but the extent appears to be culture specific. Given that GHOST cells should be a relatively homogenous cell line, the extent of variability observed across these biological replicates was concerning.

Table 3.19: Details of GHOST cell cultures used for immunophenotyping of CD4

Culture number	Passage	Date frozen	Source laboratory
BR 1	P4	09-03-2017	ICMM
BR 2	P7	23-07-2017	ICMM
BR 3	P3	29-06-2016	ICMM
BR 4	P14	01-01-2017	CSIR
BR 5	P11	08-09-2014	CSIR

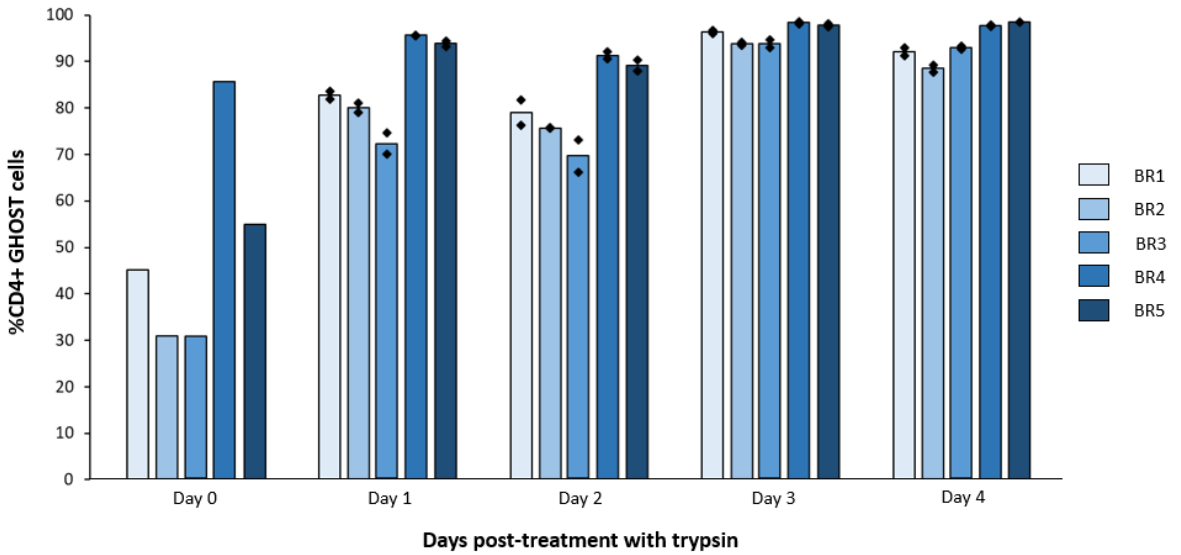

Figure 3.27: Analysis of GHOST cell CD4 expression by flow cytometry. The CD4 expression levels of five different GHOST cell cultures (BR1, BR2, BR3, BR4 and BR5) were assessed every 24 hours for 4 days following treatment with trypsin at Day 0. At each time point, with the exception of Day 0, two replicates were assayed. The average %$CD4^+$ values for each condition were plotted in a bar graph, while the individual values from the two replicates are represented by the black diamond markers over the corresponding bars.

In order to correct the problem of variable CD4 expression and improve the reliability of the GHOST cell assay, a population of GHOST cells expressing high levels of CD4 were isolated from the initial stocks using FACS. A second population on the lower end of the CD4 expression spectrum was also sorted, to be used for comparison with the $CD4^{high}$ cells (see **Figure 3.11**). The CD4 expression of both sorted GHOST cell populations was subsequently analysed to confirm the success of the sort (**Figure 3.28**). The proportion of $CD4^+$ cells was greatly increased post-sort, reaching 96.79%, while the $CD4^{low}$ population was only 57.64% positive.

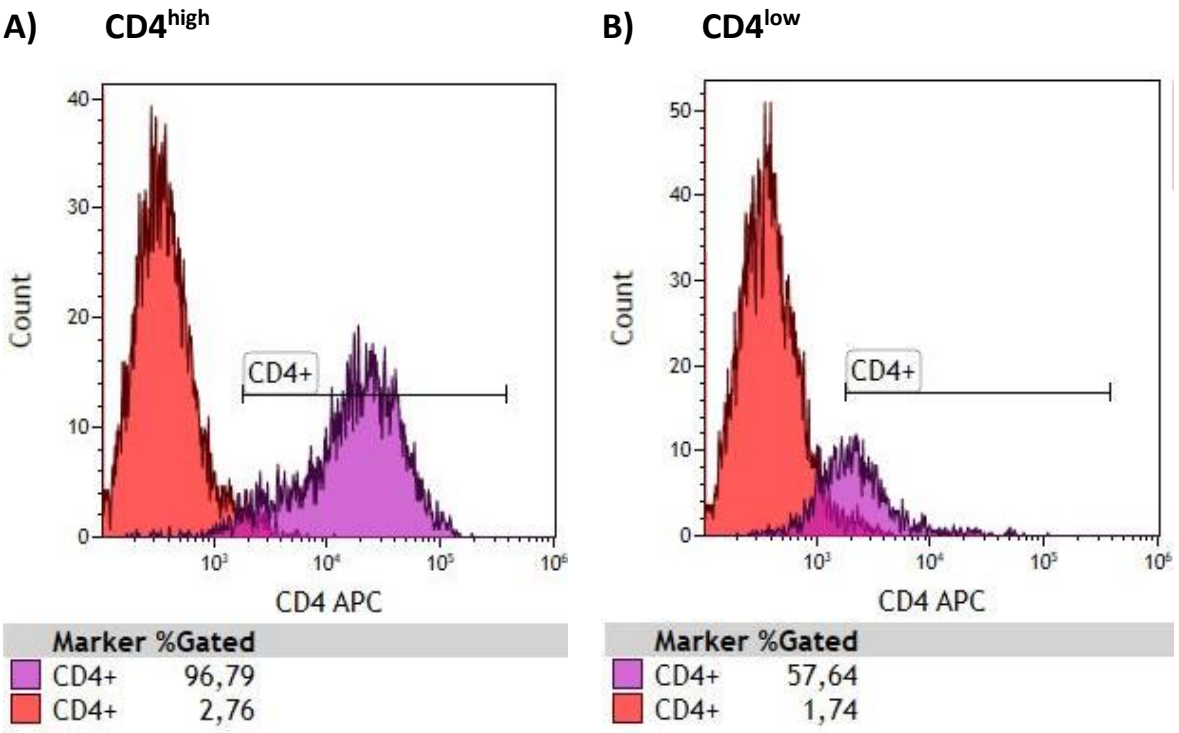

Figure 3.28: Analysis of CD4 expression of sorted GHOST cell populations. Overlay histograms are used to compare the number of events in the CD4 APC channel in unstained (red) vs stained (purple) GHOST cells, using either the **A)** $CD4^{high}$ sorted population or the **B)** $CD4^{low}$ sorted population

The immunophenotyping and CD4 recovery assay was repeated on $CD4^{high}$ sorted GHOST cells, using both enzymatic and non-enzymatic dissociation methods for the baseline measurement. Directly after treatment, the cells treated with trypsin demonstrated a slight decrease in CD4 expression, while the non-enzymatically dissociated cells remained close to 100% $CD4^{+}$ (**Table 3.20**). Thus, our results indicated that trypsin still does have some effect on the sorted cells, but the extent was markedly reduced. As in the CD4 recovery experiment for the unsorted GHOST cells, the time taken for expression of CD4 on the cell surface to return to baseline levels was assayed following treatment with trypsin. Treated cells were seeded in a 6-well plate to allow analysis in duplicate at three time points. Cells were harvested 24-, 48- and 72-hours post-treatment and CD4 expression was analysed by flow cytometry. The percent CD4 positive values for the two replicates at each time point were averaged after analysis.

It was found that CD4 expression returned to pre-treatment levels by 24 hours. Since GHOST cells were exposed to HIV only 24 hours after plating, we reasoned that the initial use of trypsin should not affect the results of the assay when $CD4^{high}$-expressing GHOST cells are

used. However, it was decided that Cell Dissociation Solution should be used instead of trypsin prior to seeding GHOST cells for infection to eliminate any possibility of CD4 reduction. Despite identifying trypsin as a factor influencing CD4 expression, the underlying cause of the variability in expression levels and the response to trypsin was not clear and required further investigation. However, the challenge was circumvented by using the $CD4^{high}$ sorted GHOST cells in future experiments. Using $CD4^{high}$ GHOST cells ensured that the assay was carried out using cells that have consistently high CD4 expression.

Table 3.20: Results of CD4 recovery experiment using sorted $CD4^{high}$ GHOST cells

Time post-treatment	CELLS TREATED WITH CDS*	CELLS TREATED WITH TRYPSIN		
	Average % $CD4^+$	% $CD4^+$ Replicate 1	% $CD4^+$ Replicate 2	Average % $CD4^+$
0 h	97.45	93.44	-	93.44
24 h	-	97.88	98.44	98.16
48 h	-	99.32	99.15	99.23
72 h	-	99.11	98.83	98.97

*CDS = Cell Dissociation Solution

4.2.1.3. Confirmation of CD4 mRNA presence in GHOST cells

Since the initial immunophenotyping results seemed to indicate low expression of CD4 in some cultures, it was decided that it was necessary to check whether CD4 was present at the transcript level. The absence of the mRNA would indicate the absence or loss of functionality of the CD4 construct, while its presence would suggest sub-optimal post-transcriptional modification (such as protein degradation or a failure to produce functional protein from the mRNA). To investigate, reverse-transcriptase PCR was performed on RNA isolated from sorted $CD4^{high}$ and $CD4^{low}$ GHOST cell populations. As a positive control, RNA was also isolated from PBMNCs and TZM-bl cells, since both cell types had demonstrated robust CD4 expression in previous flow cytometric analysis. RNA from HEK293 cells, which are not known to express CD4, was included as a negative control.

From the gel electropherogram of the PCR products (**Figure 3.29**), it is apparent that the GHOST cells do indeed express CD4 transcripts, indicated by the presence of a band which corresponds to the expected size of the amplicon (67 bp). Interestingly, there is no difference between the $CD4^{high}$ and $CD4^{low}$ GHOST cell populations, indicating that the differences in

expression observed at the protein level may be due to some form of post-transcriptional regulation. All controls responded as expected, with the exception of the PBMNC sample which had an additional faint band slightly larger than the expected product. Upon inspection of the binding sites of the primers using NCBI's Primer BLAST, it was noted that the primers fall on either side of a small intron (**Figure 3.30**). Amplification of the unspliced transcript would therefore yield a product of 186 bp, which corresponds to the size of the second band.

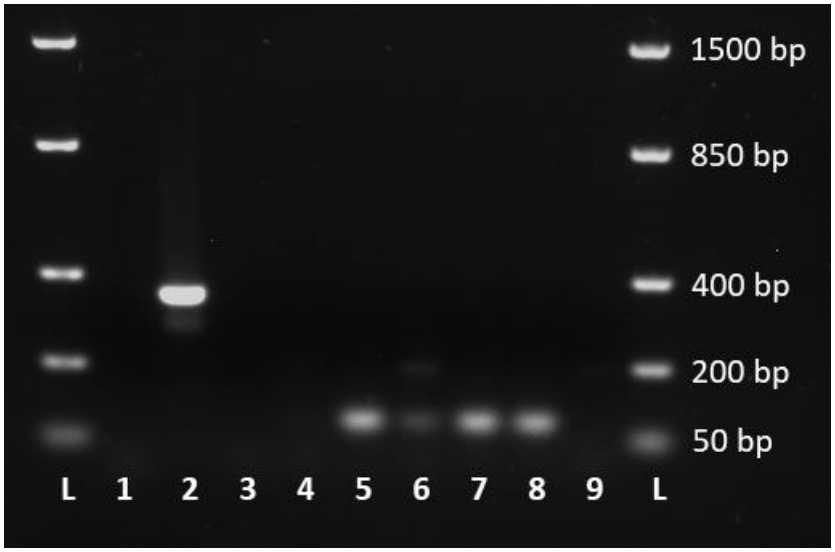

Figure 3.29: Gel electropherogram of CD4 PCR products. L = ladder, 1 = No template PCR control, 2 = L32 positive PCR control, 3 = No template cDNA control, 4 = No reverse transcriptase cDNA control, 5 = TZM-bl cDNA, 6 = PBMC cDNA, 7 = GHOST $CD4^{high}$ cDNA, 8 = GHOST $CD4^{low}$ cDNA, 9 = HEK 293T cDNA.

A)

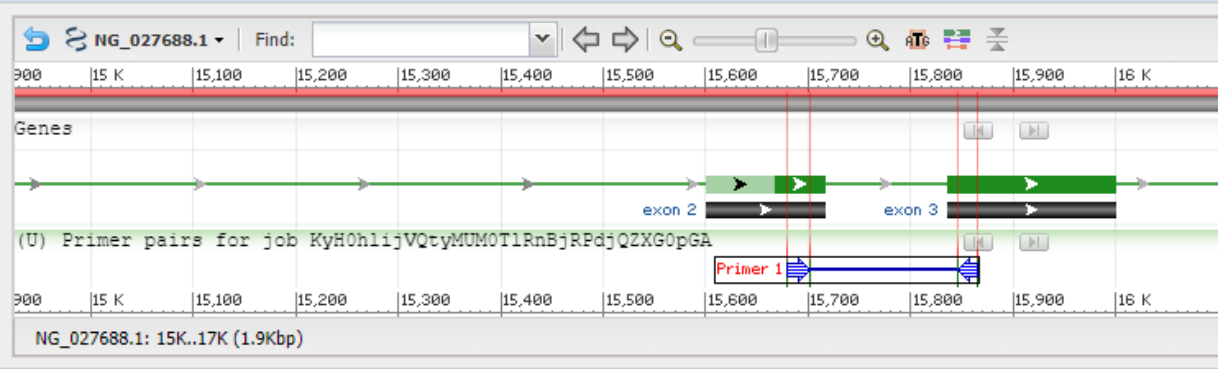

B)

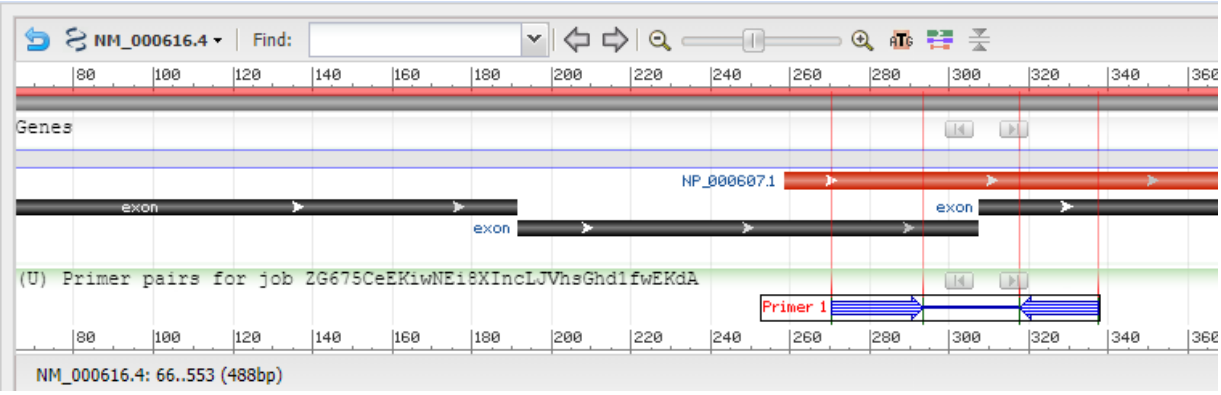

Figure 3.30: Screenshot of CD4 primer binding sites as viewed on NCBI's Primer BLAST website. A) When binding to the unspliced transcript, the primer pair (indicated by blue arrows and labelled "Primer 1") binds on exons 2 and 3 with a small intervening intron being included in the PCR product. **B)** When the transcript has been spliced, the intron is no longer present, resulting in a smaller amplicon being produced.

4.2.1.4. Selection of optimal time points at which to perform cell counts and analyse GFP expression

There is currently no consensus on the best practice for functional titration of primary HIV isolates using the GHOST cell assay that gives consistent, reliable results. Our initial experiments resulted in IU/mL values that were vastly different across different dilutions, which is problematic since the values should theoretically be similar. The aim of the following experiments was thus to determine the conditions that limit variability of the IU/mL across the different dilutions. Two variables were selected for optimization: 1) the optimal day on which the GHOST cell count to be used in **Equation 3.3** (to determine infectious viral units) is obtained and 2) the day on which the GFP expression is analysed by flow cytometry. Since Tat-activated transcription of GFP is initiated soon after viral entry, GFP expression should be detectable from 2 to 3 days after exposure to HIV (187).

Several options for determining cell count were considered based on literature. Many researchers simply use the number of cells seeded as a proxy for the number of cells present during the assay, or simultaneously obtain an absolute count on a flow cytometer during the quantification of GFP expression. The use of the seeding number is not ideal, because it does not account for cell division that occurs in the 24 hours prior to infection and could therefore cause under-estimation of the viral titre (IU/mL) (**Figure 3.31**). Since the premise of the GHOST assay is that one infected cell equals one infectious particle present at the time of exposure, it would be ideal to obtain a measure of the number of infected cells present as soon after the viral stock is added as possible. However, since GFP is not produced immediately, the detection of infected cells is delayed until 2- or 3-days post-infection. During this time, the cells will likely have undergone cell division and the number of infected cells will increase, although the proportion of infected cells should theoretically remain constant due to the inheritance of integrated virus in the progeny cells. If the cell count was taken at the time of GFP expression analysis, this increase in cell number would cause over-estimation of the viral titre because the absolute number of infected cells is no longer be equal to the number of infectious particles present at the time of infection (**Figure 3.31**). An alternate solution is to obtain a cell count on the day of infection and multiply it by the proportion of GFP positive cells obtained on the day of the assay, taking advantage of the fact that the proportion of infected cells remains constant. The absolute number of infected cells calculated in this way should theoretically give a better estimation of the number of infectious virus particles present at the time of infection (**Figure 3.31**).

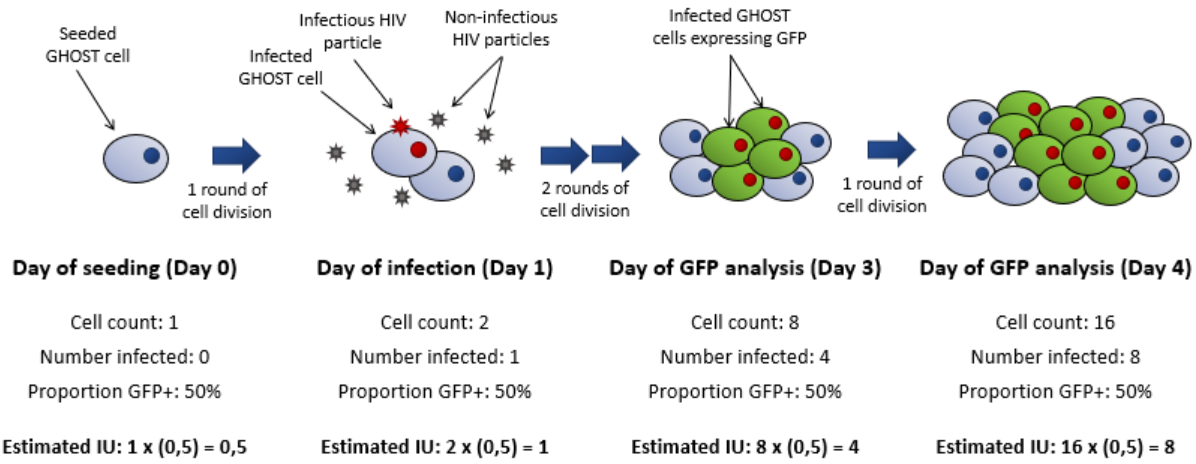

Figure 3.31: Illustration of potential under-estimation or over-estimation of viral titre caused by taking the cell count measurements for the GHOST cell assay on the day of seeding or the day of GFP analysis respectively. In a hypothetical situation, a single GHOST cell is seeded 24 hours prior to infection on Day 0. The rate of cell division is assumed to be 1 round of replication per 24 hours, therefore by the day of infection (Day 1) the cell number has increased to 2. In this example, only one of the virus particles in the viral stock added is infectious, resulting in a single infected GHOST cell. Two further rounds of cell division occurred between Day 1 and Day 3, increasing the cell number to 8. Another round of division occurs between Day 3 and Day 4, thereby bringing the count to 16. The number of infected cells increases proportionally, since the progeny of the initially infected cell will also be infected. The proportion of GFP-expressing infected cells (50%) is measured at either Day 3 or Day 4. The estimated IU is calculated as Cell count x (%GFP^+/100), as per **Equation 3.3** (with no dilution factor applied). The true titre of the viral stock (1 IU) is correctly predicted using the count obtained on Day 1. Using the Day 0 cell count results in under-estimation (0,5 IU) while using cell counts from Day 3 or 4 results in over-estimation (4 IU and 8 IU respectively) due to changes in the total cell count.

In order to characterize the change in cell number due to expansion of the GHOST cells in culture, and to determine whether it is likely to affect the accuracy of the assay, a growth curve was established for the $CD4^{high}$-expressing cells over 4 days. The cells were seeded at 150 000 cells/well in a 12-well cell culture plate for analysis in duplicate at three time points, namely Days 1, 3 and 4 after seeding, and cultured under standard conditions (37°C, 5% CO_2). Cell counts were obtained from two separate wells at the respective time points, and the average of these duplicates was used to plot a growth curve (**Figure 3.32**). Since the sorted $CD4^{high}$ GHOST cell stocks should be homogenous, this experiment was only performed once. From the growth curve, it is apparent that the cell count increases in a logarithmic fashion between Day 1 and Day 3, reaching a plateau by Day 4. Since the changes in cell number are quite dramatic, it is likely to affect the estimation of the titre.

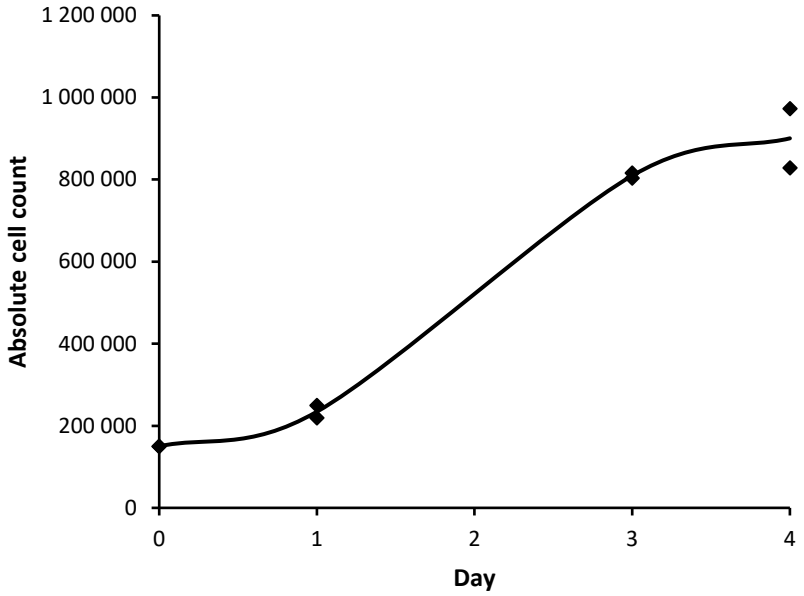

Figure 3.32: Growth curve of GHOST (3) R5X4 cells over 4 days in culture. Counts were taken from duplicate samples at Day 1, Day 3 and Day 4 following seeding at 150 000 cell/mL on Day 0.

A second experiment was designed to test the reproducibility of the functional titres obtained when the cell count was taken on the day of infection (DOI) or the day of the GFP assay (DOA), with the day of the GFP assay being either 48 hours or 72 hours post-infection (i.e. Day 3 or Day 4 of the experiment respectively). Four sets of GHOST cells were seeded at 150 000 cells/well in 12-well cell culture plates to perform assays under the conditions summarised in **Table 3.21**. The assays were carried out using a serial dilution of CM9 cell-free viral supernatant (neat, 1/4, 1/16, 1/64, 1/256) and an uninfected control, as per the standard protocol (**Section 3.2.5.**). The results of this experiment are illustrated in **Figure 3.33**. There is clearly less variability observed across dilutions in the 48 h post-infection dataset, with the most consistent results coming from the DOI dataset (**Figure 3.33a**). The results obtained from the 72 h post-infection dataset appeared to be skewed, with IU/mL increasing dramatically across the dilutions, especially in the DOA dataset (**Figure 3.33b**). The IU/mL value is consistently higher in the assays in which cell count was obtained on the same day as the GFP readings (DOA datasets), indicating possible inflation of the IU/mL based on the increased cell numbers. Taking both these results and the growth curve data into account, it was decided that the count should be performed on the day of infection as this gives the least variability and ensures that the IU/mL is calculated based on the number of cells present at the time of infection, rather than at the time of the GFP assay. It was also decided that GFP expression

should be measured at 48 hours post-infection (Day 3 of the assay), since this appeared to reduce variability in the readings.

Table 3.21: Conditions for GHOST cell optimization experiment

Time of GFP analysis	Day of count	Abbreviation
48 hours post-infection	Day of infection (Day 1)	48 h, DOI
48 hours post-infection	Day of assay (Day 3)	48 h, DOA
72 hours post-infection	Day of infection (Day 1)	72 h, DOI
72 hours post-infection	Day of assay (Day 4)	72 h, DOA

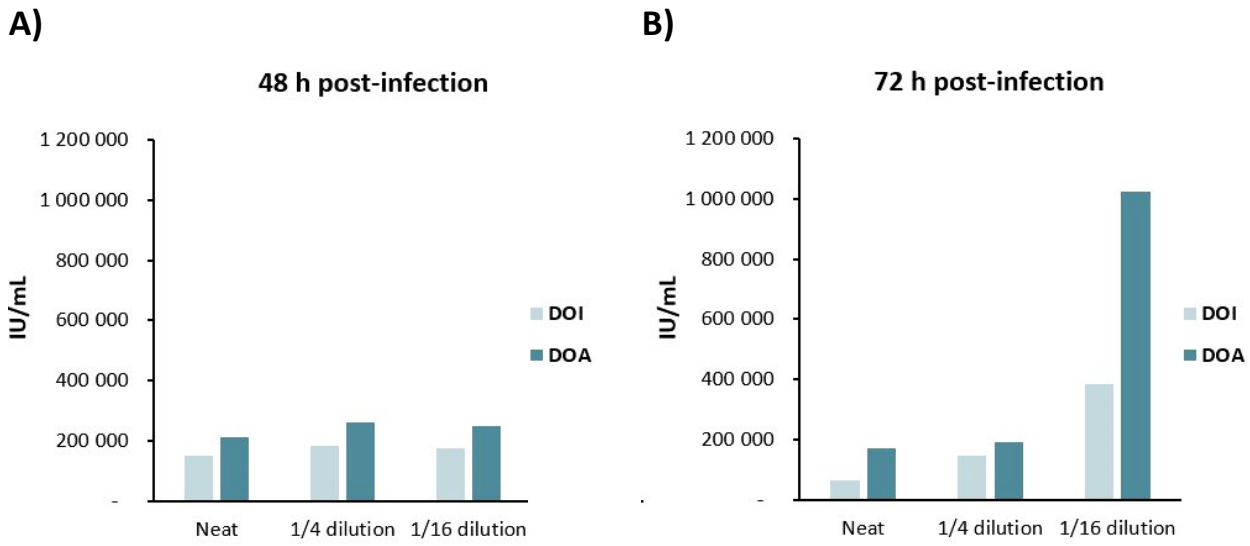

Figure 3.33: Functional titres (IU/mL) calculated from GHOST cell assays using either the day of infection (DOI) or the day of assay (DOA) as the time point at which the cell count was obtained. The day of the assay, on which GFP readings were taken, was either **A)** 48 h post-infection or **B)** 72 h post-infection. No GFP signal was observed past the 1/16 dilution, so these data points have been excluded.

4.2.2. Quantification of HIV isolates used in downstream experiments

The fully optimized GHOST cell assay was, from this point forward, used to obtain a functional titre for the HIV-1-C primary isolates used in further infection and gene expression experiments. The IU/mL values for all isolates produced for which GHOST assays performed are presented in **Table 3.22**. Only the most up-to-date assays using $CD4^{high}$ GHOST cells and the optimized GHOST cell assay are included. An example of the spreadsheet used in the

calculation of the functional titre is presented in **Table 3.23** for isolate CM9-020518, which was used for final gene expression experiments.

Table 3.22: Functional titres of all HIV primary isolates produced as determined by the GHOST cell assay

Tropism	Isolate	Date Harvested	IU/mL
R5-tropic	CM1-250217	2017/02/25	$1.60x10^5$
	CM1-110618	2018/06/11	$2.24x10^5$
R5X4-tropic	CM9-280217	2017/02/28	$5.46x10^5$
	CM9-290118	2018/01/29	$9.47x10^5$
	CM9-020518	2018/05/02	$1.05x10^6$
	CM9-270618	2018/06/27	$3.60x10^5$
X4-tropic	SW7-240618	2018/06/24	$3.04x10^5$
	SW7-110718	2018/07/11	$2.87x10^5$
	SW7-010818	2018/08/01	$4.71x10^5$

Table 3.23: Calculation of functional titre for isolate CM9-020518 using the GHOST cell assay

A: Calculation of GHOST cell counts obtained on Day 1 of the assay (in triplicate)

Sample	Ghost cell count	# Flow-Count™ beads	Cal factor	Cells/µL	µL	Absolute cell count	Mean cell count	SD of mean	SD % of mean
Count R1	5050	2659	1014	1925.80	100	192580			
Count R2	5024	1941	1014	2624.59	100	262459	**223931,40**	32317.91	14%
Count R3	5017	2347	1014	2167.55	100	216755			

B: Calculation of the concentration of HIV-1-C infectious units (IU/mL) using measurements of GFP expression obtained on Day 3 of the assay (in triplicate)

Sample	%GFP	%GFP/100	Mean/ triplicate	Normalized mean	Dilution factor	IU/500µL	IU/mL	Mean IU/mL	SD of IU/mL	SD % of mean
Control R1	0.09	0.0009						**$1.05x10^{6**}$**	$6.28x10^{5}$	59.83%
Control R2	0.08	0.0008	0.000	0.00	0	0	0			
Control R3	0.06	0.0006								
Neat R1*	51.54	0.5154								
Neat R2	62.6	0.626	0.635	0.64	1	142196.44	284392.87			
Neat R3	64.4	0.644								
1/4 R1	25.08	0.2508								
1/4 R2	24.44	0.2444	0.250	0.25	4	224319.54	**448639.09**			
1/4 R3	25.61	0.2561								
1/16 R1	13.17	0.1317								
1/16 R2	14.71	0.1471	0.139	0.14	16	499456.59	**998913.17**			
1/16 R3*	9.65	0.0965								
1/64 R1	6.27	0.0627								
1/64 R2	5.86	0.0586	0.059	0.06	64	850819.88	**1701639.75**			
1/64 R3	5.68	0.0568								
1/256 R1	6.81	0.0681								
1/256 R2	8.45	0.0845	0.080	0.08	256	4612867.34	9225734.67			
1/256 R3	8.88	0.0888								

SD = standard deviation

*Outliers excluded from calculation of mean/triplicate

**Mean calculated using the IU/mL values of the 1/4, 1/16 and 1/64 dilutions (indicated in red)

4.3. Detection of HIV-infected cells

4.3.1. Optimisation of the KC57 antibody-based assay using GHOST cells

The KC57 antibody-based assay is a flow cytometric assay, intended to detect intracellular p24 protein at single-cell resolution, yielding a quantitative estimate of the proportion of infected cells present in the sample. Because of the single-cell resolution, this assay can be used for the detection of events that occur at low frequency, provided enough total events are analysed (171). Furthermore, if a multicolour flow cytometer is available, the expression levels of other cell surface proteins can be assessed in conjunction with HIV detection, by co-staining with other antibodies. The main drawback to the approach is the fact that the cells require fixation prior to analysis, which prohibits the isolation of viable infected cells identified in the assay by FACS for use in downstream experiments. This assay is also not able to determine whether the virus detected is fully replication-competent, or whether it is simply translation-competent and thus able to produce p24 (171). We first optimized the assay using GHOST cells, since they are highly susceptible to infection and contain a HIV-responsive GFP reporter system which functions as an in-built positive control. In later experiments, this assay was applied to $CD4^+$ T lymphocytes and macrophages, as detailed in **Chapter 4**.

In order to confirm that the KC57 antibody was indeed capable of detecting cells infected with our primary HIV-1-C isolates, a KC57 assay was performed on GHOST cells infected with isolate CM9, as well as on unexposed GHOST cells which served as a negative control. For both these conditions, aliquots of the cells were stained with either the KC57 isotypic control, or the KC57 antibody itself. This was done to ensure that shifts in positivity observed were due to HIV infection and not due to non-specific staining. The co-expression profiles of GFP versus KC57 of these samples are presented in **Figure 3.34**. These plots illustrate the concurrent detection of HIV through two independent mechanisms: Tat-dependent GFP expression from the reporter construct and staining of the intracellular viral p24 capsid protein by the KC57 antibody.

A) HIV- isotypic control

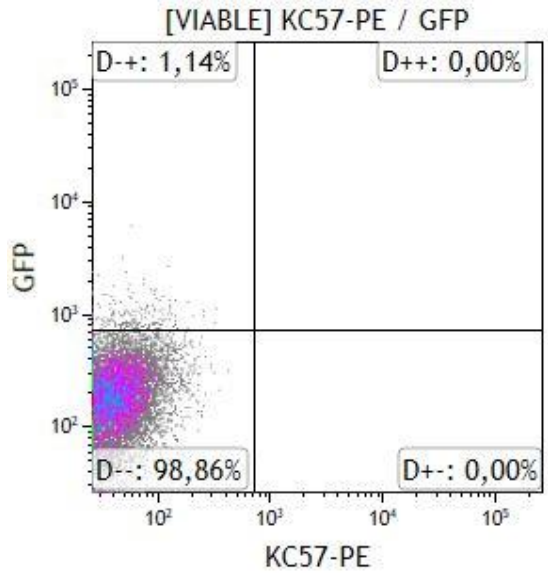

B) HIV- KC57

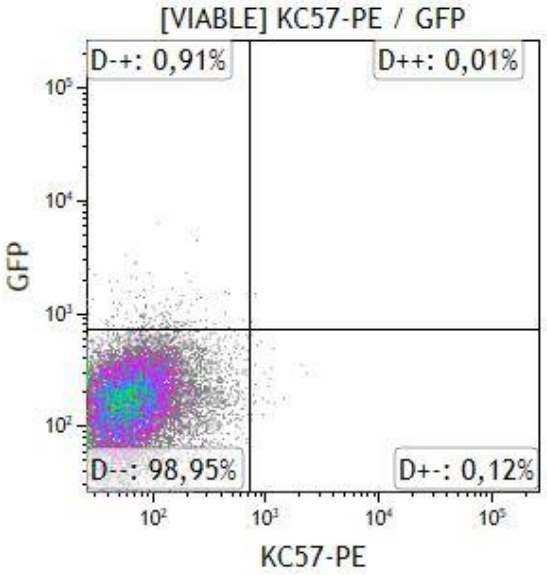

C) HIV+ isotypic control

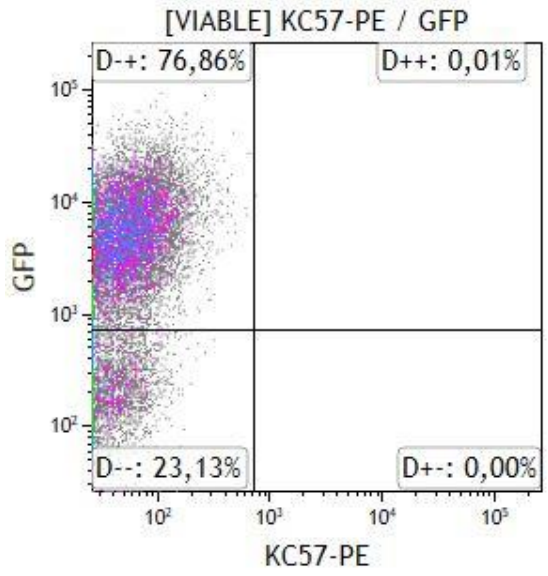

D) HIV+ KC57

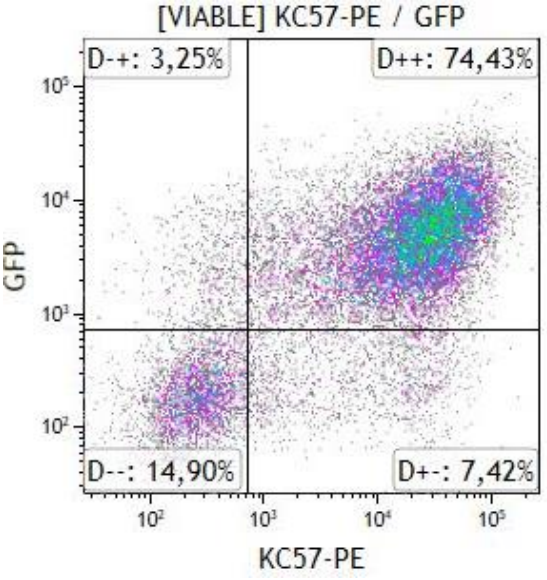

Figure 3.34: Validation and optimization of the KC57 assay using GHOST cells to detect co-expression of GFP and KC57-PE on GFP Log vs KC57-PE Log two-parameter plots. A) Uninfected GHOST cells stained with the isotypic control. **B)** Uninfected GHOST cells stained with the KC57-PE monoclonal antibody. **C)** Infected GHOST cells stained with the isotypic control. **D)** Infected GHOST cells stained with the KC57-PE monoclonal antibody.

From these results, it is clear that the KC57 antibody does indeed detect HIV positive cells, with a high degree of co-expression with GFP observed in the infected antibody-stained sample (**Figure 3.34d**). A small percentage of cells are either GFP-positive but KC57-negative (3.25%) or KC57-positive but GFP-negative (7.42%), indicating that neither of these methods detect all infected cells present. This discrepancy could be due to temporal differences in the

production of the signal used to detect HIV or could simply indicate that the assays have different limits of detection. The profiles shown in **Figure 3.34a** and **Figure 3.34c** indicate that the isotypic control is clearly negative in the PE channel for both the infected and uninfected samples, with only GFP expression increasing in the HIV-infected sample. However, it is important to note that when comparing **Figure 3.34a** and **Figure 3.34b**, which are both from uninfected samples, a shift towards the right of the plot is observed in the KC57-stained sample. This shift is independent of HIV infection, indicating that it is due to the presence of the KC57 antibody itself. Since the isotypic controls do not account for this non-specific shift, it was decided that the use of the isotypic control should be discontinued in future experiments and an uninfected control stained with KC57 should be used to set the position of the $KC57^{+}$ region. The reason for the shift observed for the isotypic control is unknown and requires further investigation.

4.3.2. Optimisation of PCR-based detection of HIV using GHOST cells

As an alternative approach for HIV detection, a simple PCR-based assay was developed to amplify a portion of the HIV genome which is integrated into the host cell DNA. This provides a qualitative method of detecting the virus during the early infection stages of infection when p24 protein is not being produced. This method, like the KC57 assay, was optimized using DNA from GHOST cells since they are highly susceptible to infection and successful infection can easily be confirmed by fluorescence microscopy.

4.3.2.1. Primer optimisation and validation

The four primer pairs listed in **Table 3.9** were validated for PCR using infected GHOST cell DNA, and the optimal annealing temperatures for each were determined (**Appendix B, Figure B.2**). For each primer pair validation, two reactions were set up. For the first reaction, template DNA from GHOST cells infected with the corresponding target HIV isolate was used, while uninfected GHOST cell DNA was used for the second. This allowed for the detection of any non-HIV-specific amplification that may have occurred. Amplification only occurred in HIV-infected samples, with all primer pairs yielding distinct bands of product of the expected length (**Figure 3.35**). Therefore, all these primers were deemed suitable for detection of HIV infection. However, it was decided that only the LTR/gag primer pairs should be used for

detection purposes since the binding site is more conserved and the product is much longer, resulting in increased sensitivity and specificity of the assay.

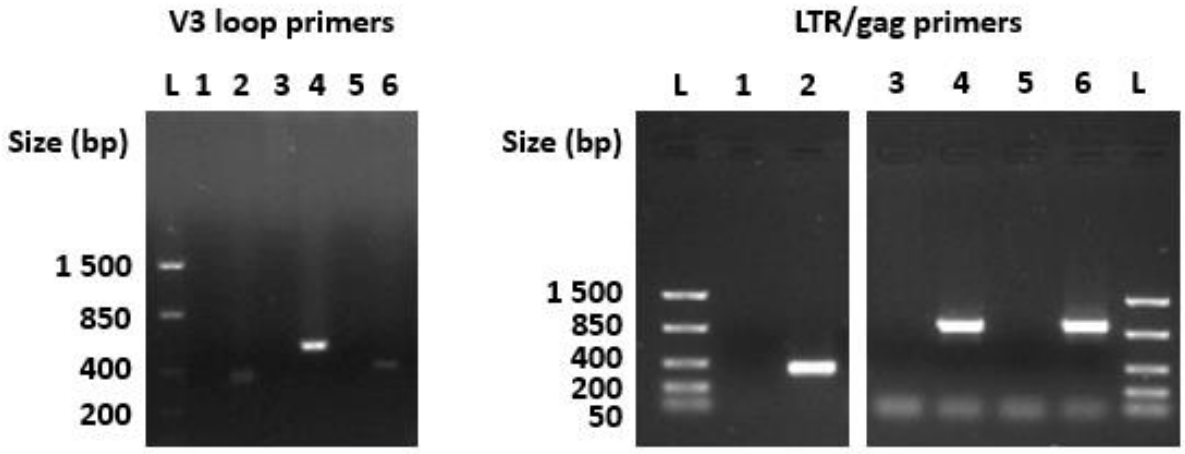

Figure 3.35: Gel electropherograms from primer validation PCRs which were performed for both the V3 loop and LTR/gag regions in HIV isolates, SW7 and CM9. Uninfected GHOST cell DNA was used for the control reactions while DNA from GHOST cells infected with one of the two isolates was used in the HIV positive test reactions. **V3 loop primers:** L = ladder, 1 = No template PCR control, 2 = L32 positive PCR control, 3 = SW7 uninfected, 4 = SW7 infected, 5 = CM9 uninfected, 6 = CM9 infected. **LTR/gag primers:** L = ladder, 1 = No template PCR control, 2 = L32 positive PCR control, 3 = SW7 uninfected, 4 = SW7 infected, 5 = CM9 uninfected, 6 = CM9 infected.

4.3.2.2. Limit of detection

When using primary cells, it is unlikely that a high proportion will become infected upon exposure to HIV, thus the quantity of uninfected host cell DNA will be far greater than the target viral DNA, reducing the efficiency of the PCR reaction. Therefore, in order to use this assay for HIV detection in primary cells instead of GHOST cells, it was critical to determine the limit of detection, i.e. the lowest number of infected cells that will allow reproducible detection of HIV-1-C DNA using PCR. Samples of DNA from a set of standards, using a known proportion of GHOST cells infected with CM9 and SW7 (0.1%, 1%, 5%, 10%, 20%) were used as templates for LTR/*gag* PCR reactions. Gel electrophoresis of the PCR products revealed that the lowest proportion of infected cells at which amplification could be detected is 1% for CM9 and 5% for SW7, with the intensity of the bands increasing as the percentage of infected cells used to generate template DNA increases (**Figure 3.36**). The bands are fainter in SW7

compared to CM9, perhaps indicating a slightly less efficient reaction when using the SW7 LTR/*gag* primer pair, resulting in an increased limit of detection.

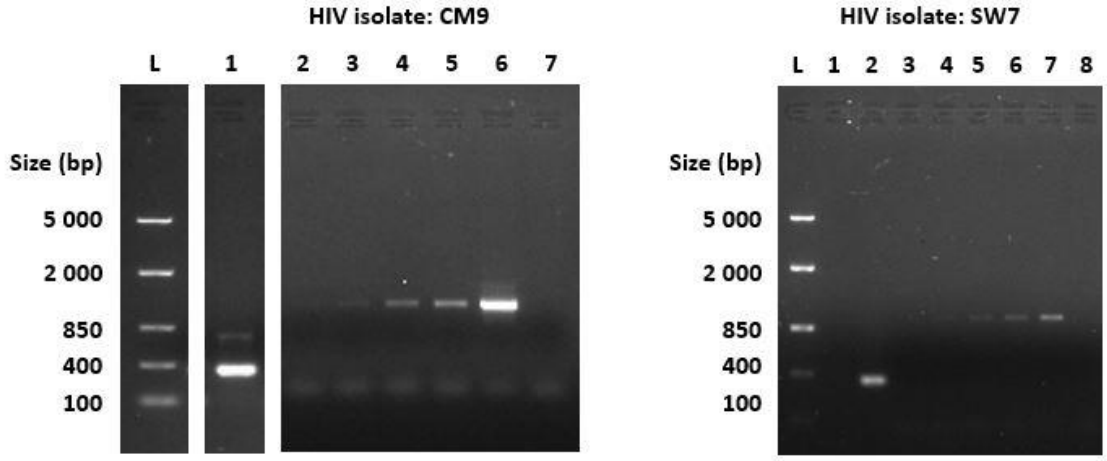

Figure 3.36: Gel electropherograms of PCR products generated during the limit of detection assay using both CM9 and SW7 LTR/gag primer pairs. DNA from GHOST cell standards with varying proportions of cells infected with either SW7 or CM9 were used as template. **CM9:** L = ladder, 1 = L32 positive PCR control, 2 = 0.1% HIV+ GHOST cells, 3 = 1% HIV+ GHOST cells, 4 = 5% HIV+ GHOST cells, 5 = 10% HIV+ GHOST cells, 6 = 20% HIV+ GHOST cells, 7 = HIV- GHOST cell control. **SW7:** L = ladder, 1 = No template PCR control, 2 = L32 positive PCR control, 3 = 0.1% HIV+ GHOST cells, 4 = 1% HIV+ GHOST cells, 5 = 5% HIV+ GHOST cells, 6 = 10% HIV+ GHOST cells, 7 = 20% HIV+ GHOST cells, 8 = HIV- GHOST cell control.

5. Discussion and Conclusions

In vitro propagation of HIV-1 primary isolates poses several unique challenges compared to the production of lentiviral vectors, molecular clones and modified pseudoviruses. Unlike molecular clones, primary isolates cannot be propagated through plasmid replication but must undergo their entire natural life cycle *in vitro*. In direct contrast to clonally replicated viruses, primary virus cultures consist not of one defined type of virus, but a collection of quasispecies that each possess unique sequence variants (82,83). This makes the viral pool as a whole very difficult to characterize and work with but may also provide a more clinically relevant model of infection. The infection efficiency of primary strains is markedly reduced compared to modified strains. For example, Vesicular stomatitis virus G (VSV-G)-pseudotyped viruses have an extremely broad tropism range and are thus not restricted by receptor binding, resulting in improved infection efficiencies (188). There are numerous other factors that can influence whether or not a primary virus will replicate successfully, such as the

amount of host cells available, the susceptibility of those host cells to infection, the response of those cells once infected, the accessory protein content of the virus, its replication rate and the mutability of its genome, to mention a few.

In order to propagate, HIV needs a constant supply of susceptible host cells, which are given at intervals suitable to its replication rate since HIV-1 virions will lose viability within a few hours if they do not have access to a new host cell. If too few cells are provided or they are supplied at intervals too far apart, the virus will likely destroy all the available host cells. On the other hand, if too many host cells are supplied, the virus will become sequestered within the cells and there will no longer be appreciable amounts left in the supernatant to harvest. The ideal feeding regimen is therefore a balance between these two extremes, and most importantly is dependent on the replication kinetics of the viral isolate. This study has demonstrated that different isolates can have very different replication mechanics, and that there is no "one-size-fits-all" protocol. For example, the X4-tropic SW7 isolate caused massive cell death over a very short time, requiring modification to the feeding procedure.

In addition to the number of available host cells, the susceptibility of those cells to infection plays a crucial role in the success of the production. Since this method makes use of primary donated PBMNCs, there are many host factors both environmental and genetic in nature that can alter susceptibility to infection. Since different donors will have varying expression profiles for genes involved in HIV restriction and susceptibility (189), PBMNCs from at least three different donors were used to mitigate the risk that some may be resistant to infection. In addition, the PBMNCs from all donors used in HIV productions were immunophenotyped for expression of the co-receptors CCR5 and CXCR4 (See **Chapter 4**), to screen for any anomalies such as a donor homozygous for the CCR5 Δ32 mutation which would completely inhibit entry of R5-tropic HIV strains (189). Activation of the PBMNC pool prior to infection is another step that ensures maximum susceptibility, as it is well established that HIV preferentially infects activated $CD4^+$ T lymphocytes (190–193). Although all possible precautions were taken to ensure maximum susceptibility, it is unfortunately not feasible to control all the variables involved in this production system.

A further complication is the fact that the HIV genome is highly prone to mutation, primarily due to the notorious infidelity of its reverse transcriptase (83). As it replicates, errors will be introduced into the genome which cannot be rectified due to the lack of any proofreading

ability (74). In addition, the genome may be subject to editing by cellular enzymes of the APOBEC3 family which induce widespread base substitutions (74). These factors contribute to the instability of the HIV genome, increasing the likelihood that the progeny from an infectious virus will mutate and be rendered non-infectious in some way (83). The fact that HIV continues to persist from one generation to the next is purely a numbers game, made possible by the production of massive quantities of virions by each infected cell. Even though only a small fraction of these are likely to be infectious, there are still enough in terms of absolute numbers to enable the next replication cycle. In a primary viral culture setting, what this means is that the overall infectivity of the strain will fluctuate unpredictably from one round of replication to the next. Furthermore, it is not guaranteed that other properties of the strain, such as its tropism or virulence, will remain consistent. This fundamental aspect of HIV biology is in fact what enables the virus to evade the host immune system and adapt rapidly to its environment (74), but the resulting lack of predictable behaviour makes long-term primary viral culture incredibly challenging in a laboratory setting.

The quantification component of this chapter has highlighted both the utility of the methods chosen, as well as some of their limitations. The p24 ELISA method is a well-established technique for HIV detection and quantification which is favoured for its simplicity and ease of application. However, as mentioned earlier, it does not exclude virus particles that possess p24 but are non-infectious and is thus not a useful titration method for infection experiments. This method is often used as a check during virus productions to ensure that replication is ongoing, for which it is very appropriate. In this study it did not serve as a good predictor of successful replication when used to assess the R5-tropic strains for their production potential. However, this is not necessarily a reflection on the robustness of the assay but is more likely due to the unpredictable nature of the primary HIV-1-C isolates.

After extensive optimization, troubleshooting and quality control, the GHOST cell assay appears to be suitable for use in viral quantification; however, while working with these cells a few key issues were noted. The lack of consistency in CD4 expression in cultures at different passages suggests that the construct may not be entirely stable. The NIH AIDS Reagent Program recommends that GHOST cells should not be used in experiments above 10-15 passages. The inconsistencies we experienced might be precisely for this reason, since they were from stocks previously used in our laboratory and were of unknown starting passage.

Based on the findings in this study, it seems advisable to check all GHOST cell stocks for CD4 and co-receptor expression prior to use, since any deficiency in receptor expression could lead to underestimation of viral titre. This study has also illustrated that trypsin, which is used routinely for GHOST cell culture, may have an impact on the expression of CD4. This is important to keep in mind when planning future infection experiments with GHOST cells since it may interfere with susceptibility to infection.

A few assumptions were made during the execution of the GHOST cell assay that may not always hold true. The first assumption is that the proportion of infected cells remains constant in the period between exposure and measuring GFP expression. While in theory the integrated virus and previously synthesized GFP present in the cytoplasm should pass to progeny cells that are produced in the days following infection, this may not always occur in practice and has not been fully investigated. Furthermore, the assay takes place over three days. New infections may have occurred during this period and there is a possibility that the newly infected cells could already be expressing GFP (187), resulting in an overestimation of the infectious units. The second assumption made is that one infected cell equals one infectious particle. This assumption does not make allowance for the possibility of multiple virus particles infecting a single cell, but the likelihood of such an occurrence is small and it should not have much impact on the overall result.

One of the most important prerequisites for a method to quantify HIV isolates for infection experiments is that it must be able to discriminate between infectious and non-infectious virus particles. Methods that failed to meet this criterion, such as PCR-based detection, p24 quantification and reverse transcriptase activity analysis, were therefore not considered for use in this study. Of the methods which do give a functional measure of infection, the most commonly employed is the classical TCID50 assay which uses cell death as a measure of infection (162). However, this method can be problematic if used to quantify a strain with low cytotoxicity since the infected cells may not be killed, leading to under-estimation of the amount of virus present. Reporter cell lines circumvent this problem since the signal produced is a direct consequence of HIV infection rather than a downstream effect like cell death, making the GHOST cell assay a better choice. Cell lines other than GHOST cells may also be used for quantification, such as the TZM-bl line – a HeLa cell derivative transduced to express both CD4 and CCR5 as well as Tat-responsive firefly luciferase and *Escherichia coli* (*E. coli*) β-

galactosidase reporter constructs (164). The benefit of using GHOST cells compared to TZM-bl cells and other lines is that multiple variants with different co-receptor constructs are readily available.

Detection of HIV-infected cells, when working with primary virus that lacks any kind of reporter mechanisms, was a challenging yet essential component of our infection studies. The flow cytometry-based KC57 assay is a well-established technique that is well suited to detecting productively infected cells that are actively producing the p24 protein (170,171). In this study, it has been clearly demonstrated that intracellular staining with the KC57 antibody shows good correlation with GFP positivity in infected GHOST cells. The sensitivity of this method can also be greatly improved with the incorporation of concurrent fluorescent *in situ* RNA hybridization to detect the HIV *gag-pol* RNA (171). The developers of this technique, Baxter *et al*, report detection of 0.5 to 1 double-positive infected cells per million $CD4^+$ T cells (171). Another key benefit of this flow cytometric approach is the potential to combine HIV detection with analysis of expression patterns of other cell surface proteins, making it a highly versatile research tool (171). This modification to the classic assay should therefore be seriously considered for future experiments, particularly when using primary cells which generally have lower susceptibility to infection than GHOST cells.

Like the KC57 assay, the PCR-based assay developed for this study appears to have been successful based on the validation performed using infected GHOST cells. The use of customized primers specific to the LTR/*gag* regions of the clade C strains used for this study has ensured specific and sensitive amplification. Although the PCR was optimized as far as time and resources allowed, we feel that the sensitivity of the assay could be improved. The limit of detection was measured at approximately 1% for CM9 and 5% for SW7, which may not be sufficient for detection in primary $CD4^+$ T lymphocytes and macrophages. The assay is also only qualitative and would need to be adapted to a real-time PCR in order to give a quantitative measure of HIV infection. Another potential limitation of this type of PCR is that it does not discriminate between integrated and non-integrated viral DNA which has implications for determining whether the cell was successfully infected or not. The gold-standard for detection of integrated viral DNA is the *Alu*-HIV PCR which involves the use of a primer pair which binds to a well-conserved portion of the virus genome (*gag* or the LTR) as well as to the repetitive *Alu* sequence which is found scattered throughout the human

genome. This configuration only permits amplification when both the human and viral sequences are in close proximity, which occurs as a result of viral integration (194–196). However, if a simple indication of HIV presence or absence is all that is required, then a conventional PCR assay, such as the one used in this study, is sufficient.

Despite the many challenges encountered, three main outcomes were achieved in this chapter. Firstly, we were able to produce two primary HIV-1-C isolates with a sufficiently high titre to perform downstream infection experiments. The production strategies for these two isolates, CM9 (dual-tropic) and SW7 (X4-tropic), have been optimized according their strain-specific replication mechanics, and reproducibly used for several rounds of production. Secondly, the GHOST cell assay has been fully optimized for use with these isolates, with modifications made to account for the generally lower infectivity of primary cultures and to reduce intra-assay variability. Furthermore, the GHOST cells themselves have been extensively quality controlled, and validated in terms of CD4 and co-receptor expression. Finally, two independent HIV detection mechanisms have been validated for use with these primary isolates using GHOST cells: 1) the KC57 intracellular p24 assay and 2) the LTR/*gag* PCR assay. The viral isolates and the methods used to detect them were therefore deemed ready for use in infection experiments with the natural target cells of HIV: $CD4^+$ T lymphocytes and macrophages.

6. Key Findings

The main goal of this chapter was to develop viral culture techniques optimized for primary HIV-1-C isolates. An important point arising from our optimization experiments was that the mutability of the HIV genome creates many challenges when propagating primary viral isolates. We found that the production protocol had to be modified to fit the unique replication dynamics of each isolate and that some isolates may undergo complete loss of infectivity, as demonstrated in our R5-tropic strains. Despite these challenges, we managed to produce infectious stocks of isolates CM9 (dual-tropic) and SW7 (X4-tropic). For titration of our viral stocks, we elected to use the GHOST cell assay since this also gives a measure of infectivity. The assay required extensive optimisation. First, when CD4, CXCR4 and CCR5 cell surface expression was examined, the levels of CD4 expression was found to be suboptimal necessitating the sorting of a $CD4^{high}$ population to allow for further work. It was also noted

that CD4 expression can be negatively affected by the use enzymatic dissociation reagents like trypsin. Second, optimal timepoints at which to perform cell counts and GFP readings were determined, since it became clear that these factors can drastically alter the results of the assay. A subsidiary objective of this work was the optimisation and validation of methods to detect cells infected with our specific strains. We utilized the GHOST cell line to validate the KC57 anti-p24 antibody-based assay, as well as a PCR-based assay designed to target the LTR/*gag* and V3 loop regions of CM9 and SW7. Intracellular staining of p24 with the KC57 antibody showed good correlation with GFP positivity in GHOST cells infected with our selected isolates. The PCR assay was able to detect a minimum proportion of 1% infected cells for CM9 and 5% for SW7. In summary, we successfully developed the tool required for production, accurate quantification and detection of infected cells when using primary HIV-1-C isolates.

Chapter 4:

Optimization of cell culture conditions for increased susceptibility to HIV-1-C primary isolates in CD4$^+$ T lymphocytes and macrophages

1. Abstract

CD4$^+$ T lymphocytes and macrophages are key target cell types for HIV infection. In order to investigate the effects of infection at a transcriptomic level, optimal isolation and cell culture protocols had to be developed to maximize susceptibility. PBMNCs were isolated from peripheral blood and pure populations of CD4$^+$ T cells and monocytes were obtained using FACs. Monocytes were differentiated into MDM under the influence of either GM-CSF or M-CSF. Successful differentiation into functional macrophages was confirmed by analysis of classic macrophage markers using flow cytometry, and also by analysis of phagocytic capacity with the pHrodo™ assay. In order to determine whether GM-CSF-treated or M-CSF-treated macrophages would be more susceptible to infection, cell surface expression of CD4, CXCR4 and CCR5 was also assessed. M-CSF-treated cells were found to have higher levels of all these HIV receptor molecules; however, preliminary infection experiments revealed that both populations were in fact refractory to infection. For CD4$^+$ T cells, we evaluated various methods of *in vitro* activation as a means to enhance susceptibility, using flow cytometric cell proliferation and CD25 expression assays. We found that anti-CD3/anti-CD28 based stimulation was more effective than PHA-based activation. We also investigated the effects of activation on co-receptor expression and found that CXCR4 expression was markedly upregulated under the cell culture conditions used while CCR5 expression was significantly reduced, especially upon activation. Preliminary infection experiments were performed on activated CD4$^+$ T cells using CM9 and SW7 to determine the optimal infection conditions and the kinetics of infection. CM9 was found to infect optimally using an MOI of at least 2, and timepoints of 36h and 48h post-infection were selected for the final gene expression

experiments. SW7 was found to be massively cytotoxic to the activated cells and could not be used further.

2. Introduction

It is well established that the primary cellular hosts of HIV-1 are $CD4^+$ T lymphocytes and cells of the monocyte/macrophage lineage. It is thus a priority to understand the pathogenesis of HIV-1 within these cell subsets, as they have the greatest effect on the clinical outcome of the disease. In order to interrogate the transcriptome of these two cell types when exposed to HIV-1-C, which is the ultimate goal of this project, it was necessary to establish protocols for the isolation and culture of these respective cell populations. FACS was used to harvest pure cell populations of $CD4^+$ T lymphocytes and CD14+ monocytes from mixed PBMNCs. The monocytes were differentiated *in vitro* to obtain MDM, while the purified $CD4^+$ T cell population was used directly for experiments. Since infection efficiency has been reported to be lower in primary cells than in cell lines (115,197), it was anticipated that achieving successful infection in these primary cell cultures would be challenging. Therefore, optimisation of factors that might influence susceptibility to infection was required.

In the case of $CD4^+$ T lymphocytes, one of the most important factors influencing susceptibility to infection is activation (190–193). The activation of $CD4^+$ T cells *in vivo* is a complex process involving interaction with professional antigen-presenting cells, such as macrophages and dendritic cells, via the TCR (**Figure 4.1**). The TCR exists as a heterodimer of alpha and beta chains complexed with an array of CD3 proteins which are important for TCR signal transduction (198,199). The structure of the TCR complex is illustrated in **Figure 4.2**. An initial activation signal is provided by the binding of the TCR complex to its cognate antigen, which is presented by the antigen-presenting cell via the Major Histocompatibility Complex Class II (MHC II) protein (176). The CD4 molecule is closely associated with the TCR on the cell surface, and it stabilizes the interaction between the two complexes by binding to the MHC II protein (176). In order to induce an effective response, a second co-stimulatory signal is required. This signal is supplied by the binding of the CD28 receptor (expressed by T cells) to a suitable ligand on the antigen-presenting cell, such as CD80/CD86 (176). The combination of these two signals results in the cells entering an activated state, characterized by significant modulation of certain genes (200,201), the most important of which is the upregulation of

both IL-2 and the IL-2 receptor (IL-2R) (176). The upregulation of IL-2 and IL-2R leads to the induction of T cell proliferation and differentiation via autocrine signalling pathways. This results in a clonally expanded effector cell population which is able to respond to the activating antigen (176).

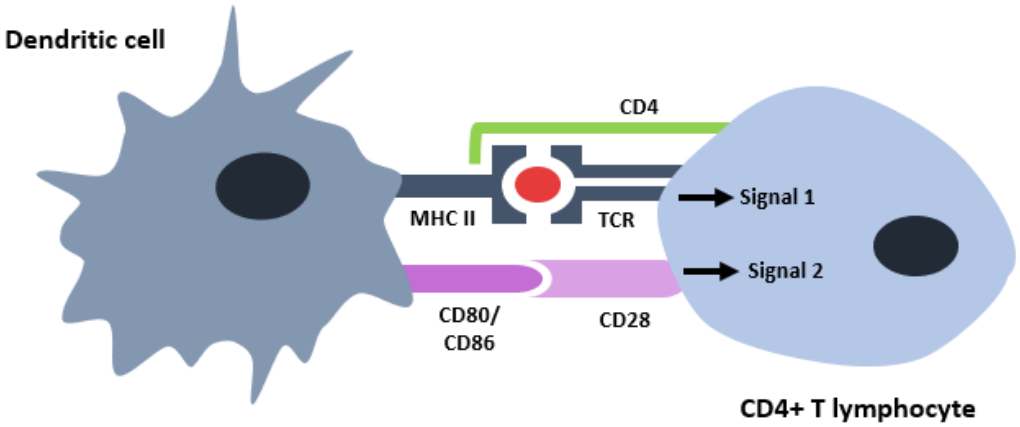

Figure 4.1: Illustration of cell receptor interactions required for CD4⁺ T lymphocyte activation. A dendritic cell is used as an example of an antigen-presenting cell. An antigenic peptide (indicated in red) complexed to the MHC II molecule is presented to a CD4⁺ T lymphocyte by the dendritic cell. The binding of MHC II to the TCR, facilitated by the co-receptor CD4, generates an initial activation signal (Signal 1). A second co-stimulatory signal (Signal 2) is received when the CD28 receptor on the T cell is bound by CD80/CD86 on the dendritic cell.

Activation of cultured CD4⁺ T cells *in vitro* requires these signals to be supplied in the absence of natural stimuli. Mitogens are often used to activate the cells through non-specific cross-linking of all cell surface glycoproteins, including the TCR (202). Common examples of mitogens used for T cell activation include phytohemagglutinin (PHA) or concanavalin A (202). Phorbol myristate acetate (PMA), which does not engage the TCR but promotes activation by acting on a downstream signalling pathway involving protein kinase C, is also commonly used (202). Another *in vitro* activation method involves the use of monoclonal antibodies which bind to CD3 and CD28, and in so doing provide artificial stimulatory signals to the TCR-CD3 complex and CD28 receptor respectively (202). The mitogen-associated and CD3/CD28 cross-linking methods are independent of antigen-binding, therefore T cells with many different antigen-specificities will be activated simultaneously, resulting in polyclonal expansion. An antigen-specific alternate method involves exposure of T cells to a particular antigen of interest in culture, in conjunction with suitable antigen-presenting cells that can mediate activation (203,204).

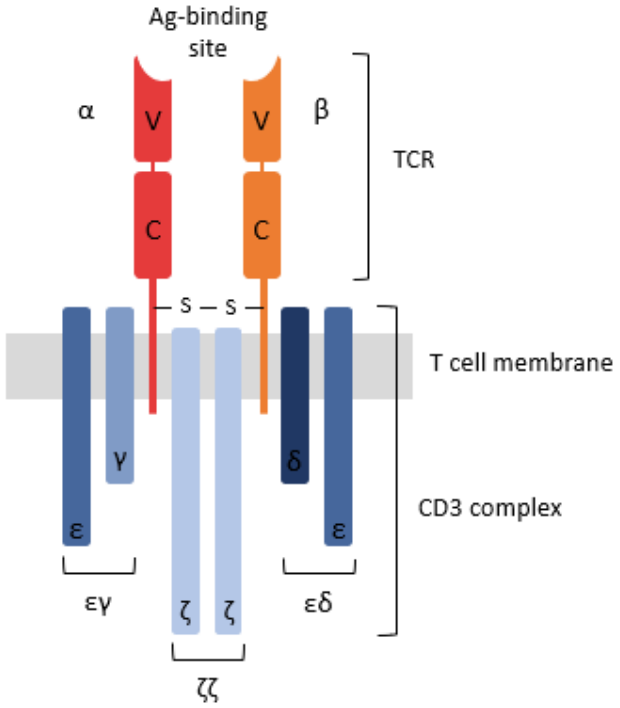

Figure 4.2: Structure of the T cell receptor complex. The TCR itself is a heterodimer comprising an α chain and a β chain linked by a disulphide bond. Each of these chains has a variable (V) and constant (C) region. The variable regions of both chains form a groove for antigen (Ag) binding. The TCR is non-covalently associated with the CD3 complex. The CD3 complex comprises three pairs of dimers: the CD3εγ and CD3εδ heterodimers as well as a CD3ζ homodimer.

Cells of the monocyte/macrophage lineage have very different responses to HIV infection compared to $CD4^+$ T lymphocytes, and the susceptibility of these cells to infection can be influenced by many factors. It has been well-established that differentiation of monocytes enhances susceptibility to CCR5-tropic strains of HIV (205–207), which is why macrophages were selected as the target for infection experiments in this study. However, the response to infection can also be profoundly altered by exposure to microbial gene products, such as lipopolysaccharides (LPS), or cytokines which induce differentiation down either pro-inflammatory or anti-inflammatory pathways which are designated as M1 and M2 respectively (138,139). M1 macrophages produce pro-inflammatory cytokines such as IL-1, IL-12, IL-23 and TNF-α, as well as reactive oxygen and nitrogen species (138,139). They are involved in supporting Th1 activities, tumour suppression and response to intracellular pathogens (138,139). M2 macrophages produce the anti-inflammatory cytokine IL-10 and are involved in Th2-type responses, elimination of extracellular parasites and promotion of tissue

repair (138,139). The addition of granulocyte-macrophage colony-stimulating factor (GM-CSF) to monocytes in culture promotes differentiation of macrophages with an M1-like phenotype, while M2-like macrophages can be induced by the addition of macrophage colony-stimulating factor (M-CSF) (137). In this study, we compared macrophages that were differentiated using these two cytokines in terms of their phagocytic capacity, cell surface protein expression and susceptibility to infection when exposed to HIV-1-C primary isolates.

Another key factor that can affect susceptibility in both cell types is the expression of the HIV-co-receptors CXCR4 and CCR5. Both form part of the chemokine receptor family: a group of seven-transmembrane-spanning G-coupled proteins (22,208) that respond to various chemokines. Chemokines are divided into the CC, CXC and CX3C families, characterized by the position of their cysteine residues (208). CCR5 is a receptor for members of the CC chemokine family (specifically RANTES, MIP-1α and MIP-1β) while the natural ligand of CXCR4 is SDF-1, a member of the CXC family (22). These co-receptors are normally involved in chemotaxis and mobilization of intracellular calcium (22). However, CCR5 and CXCR4 also essential for viral entry, since they facilitate the interaction between gp120 and CD4 that mediates fusion of the virus envelope with the host cell membrane (22). Analysis of CCR5 and CXCR4 expression was therefore included when phenotypic characterization of cultured $CD4^+$ T lymphocytes and macrophages was performed in this study.

3. Materials and Methods

3.1. Isolation of target cells from peripheral blood

3.1.1. PBMNC isolation and purification

Peripheral blood donors were recruited via advertisements within the University of Pretoria. The identity of the donors was kept strictly confidential. After donors had given their informed consent, approximately 250 mL blood was taken from each donor and processed for PBMNC isolation under University of Pretoria Faculty of Health Sciences Research Ethics Committee approval (Ethics Approval Number: 204/2016). The blood samples were layered on top of Histopaque®-1077 (Sigma-Aldrich; St. Louis, MO, USA) in 50 mL centrifuge tubes, using 15 mL of Histopaque®-1077 per 35 mL blood. The layered samples were subjected to density gradient centrifugation at 1700 rpm for 30 min at 4°C, without applying a brake. Under these

conditions, the PBMNCs formed a distinct layer which could be collected into 50 mL centrifuge tubes using a Pasteur pipette. Tubes containing approximately 20 mL of collected PBMNCs were filled with TP buffer (PBS, 1% Human Albumin [Sigma-Aldrich; St. Louis, MO, USA], 2 mM ethylenediaminetetraacetic acid [EDTA – Associated Chemical Enterprises; Johannesburg, South Africa]) to dilute any residual Histopaque®. The cells were centrifuged at 300 x *g* for 10 min at 4°C and the Histopaque®-containing supernatant was aspirated. The cell pellet was reconstituted in ammonium chloride lysis buffer (distilled water, 150 mM ammonium chloride [Labchem; Johannesburg, South Africa], 10 mM sodium bicarbonate [Sigma-Aldrich; St. Louis, MO, USA], 0.25 mM EDTA) and incubated at 4°C for 30 min in order to lyse any residual erythrocytes. The ammonium chloride was removed by centrifuging the cell suspension at 300 x *g* for 10 min and aspirating the supernatant. In order to minimize platelet contamination, a further two centrifugations at 100 x *g* for 10 min without applying a brake, followed by aspiration of supernatant, were performed. Although this step resulted in decreased PBMNC yields, it was important to remove the platelets as they are known to sequester HIV virions, thereby reducing the efficacy of viral culture. The final pellet containing the isolated PBMNCs was resuspended in 10 mL complete RPMI-1640 cell culture medium (RPMI-1640, 10% FBS, 2% penicillin/streptomycin). Following each isolation, the PBMNCs were enumerated and phenotyped for cell surface marker expression using flow cytometry.

3.1.2. PBMNC counting and immunophenotyping

3.1.2.1. Sample preparation

A 50 µL aliquot of PBMNC cell suspension was taken to determine the total PBMNC count as well as the relative proportions of $CD4^+$ T lymphocytes and monocytes present. The cell suspension was placed in a flow cytometry tube and CD45 Krome Orange (KO) and CD4 FITC anti-human monoclonal antibody conjugates were added, using 3 µL of each. CD45 is a general cell surface marker found on all leukocytes. CD4 is present on both $CD4^+$ T lymphocytes and monocytes, though it is only weakly expressed by the latter. An additional 3 µL of 7-AAD was added to assess sample viability. The cells were incubated for 10 min in the dark to allow antibody binding. Thereafter, 50 µL of Flow-Count™ fluorospheres was added for enumeration and the sample was supplemented with 500 µL PBS to increase the overall volume. The sample was subsequently analysed using the Gallios™ flow cytometer.

3.1.2.1.1. Flow cytometry setup, data acquisition and analysis

Flow-Count™ fluorospheres were detected in the FL3 channel [Excitation: 488 nm; Emission: 620/30 BP] on a FS Lin vs FL3 Log two-parameter plot in the "BEADS" region (**Figure 4.3a**). A FL3 Log vs Time plot gated on the "BEADS" region was used to exclude any fragmented or clumped fluorospheres (**Figure 4.3b**). PBMNCs were identified on the basis of size and cellular complexity using a FS Lin vs SS Log two-parameter plot. The Flow-Count™ fluorospheres were removed post-acquisition from the PBMNC profile using the Boolean gate "NOT BEADS" (**Figure 4.3c**). This was necessary as the fluorospheres overlapped with the PBMCs and were therefore present in the same region. Failure to remove the Flow-Count™ fluorospheres in the PBMNC region would therefore lead to an overestimation of the PBMNC cell count. The FS Lin vs SS Log plot also enabled the exclusion of unlysed erythrocytes, debris, and cell aggregates. A CD45 KO Log vs SS Log plot gated on "PBMNCs" (**Figure 4.3d**) was used to confirm that the PBMNCs were in fact positive for CD45 as they should be. CD45 KO was measured in the FL10 channel [Excitation: 405 nm; Emission: 550/40 BP]. A SS Log vs 7-AAD Log two-parameter plot, gated on "CD45", was used to determine the viable subset of the CD45 positive cells (**Figure 4.3e**), with 7-AAD being detected in the FL4 channel [Excitation: 488 nm; Emission: 695/30 BP]. The concentration of viable PBMNCs in the sample was obtained from this plot, using **Equation 4.1** to relate the proportion of cells in the "VIABLE" region to the number of Flow-Count™ fluorospheres in the "CAL" region in **Figure 4.3b**. The total cell number in the original PBMNC cell suspension was obtained using **Equation 4.2**. In order to distinguish $CD4^+$ T lymphocytes and monocytes, a SS Log vs CD4 FITC Log plot gated on viable, $CD45^+$ cells was used (**Figure 4.3f**), with CD4 FITC being measured in the FL1 channel [Excitation: 488 nm, Emission: 525/40]. $CD4^+$ T lymphocytes stain more brightly for CD4 than monocytes, which have intermediate CD4 expression. From this plot, the absolute numbers of $CD4^+$ T cells and monocytes present in the PBMNC suspension could also be calculated using **Equation 4.1** and **Equation 4.2**. The acquired data was analysed using Kaluza Flow Cytometry Analysis Software (Version 2.1).

Equation 4.1:

$$Cell\ concentration\ (cells/\mu L) = \frac{No.of\ events\ in\ region\ of\ interest\ (VIABLE)}{No.of\ events\ in\ CAL\ region} \times Cal\ factor$$

Equation 4.2:

$$Total\ cells = Cell\ concentration\ (cells/\mu L) \times Cell\ suspension\ volume\ (\mu L)$$

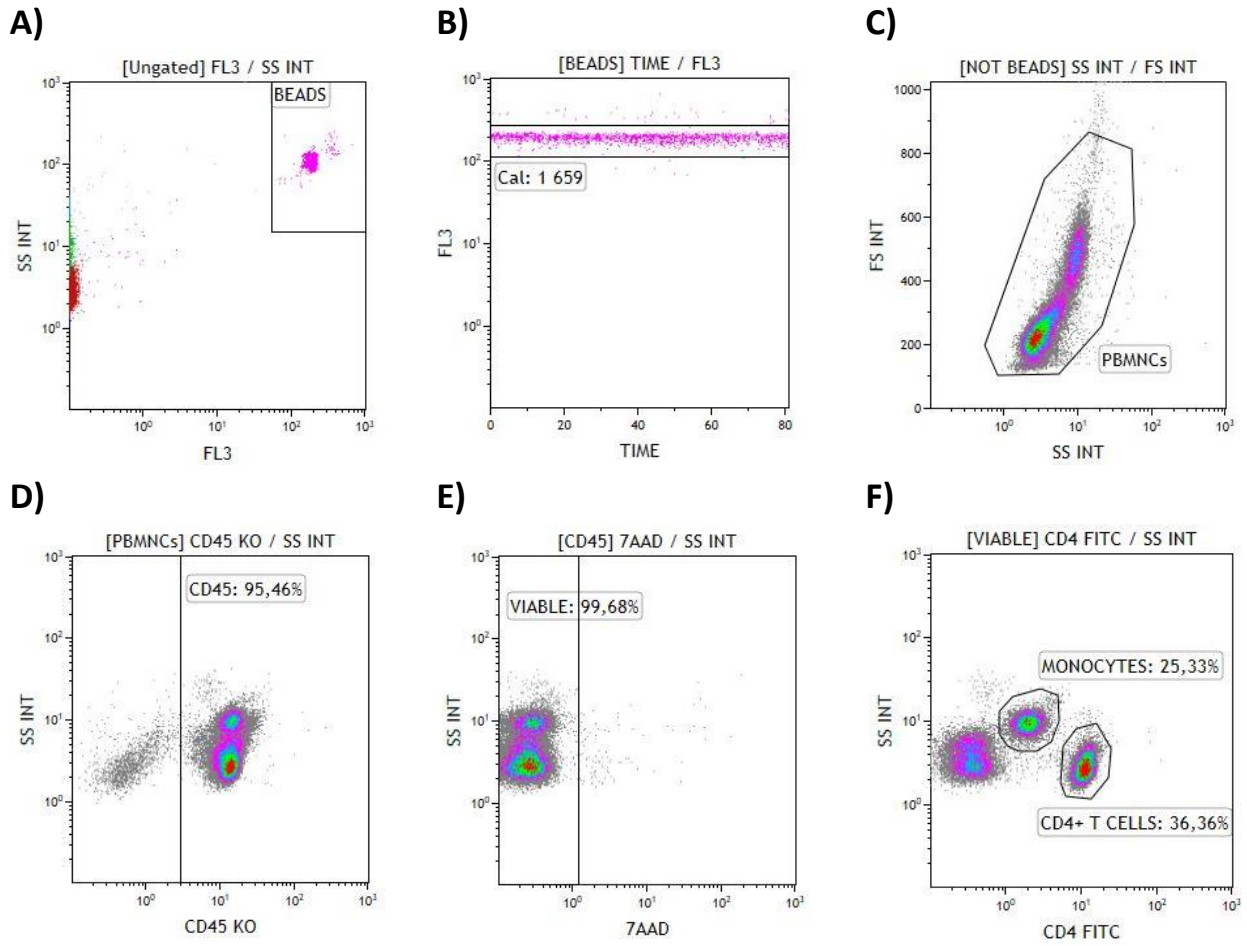

Figure 4.3: Flow cytometry setup for post-isolation analysis of PBMNCs. A) Flow-Count™ fluorospheres, indicated in the region "BEADS", were identified based on high fluorescence intensity in the FL3 channel. **B)** Single, intact fluorospheres were identified in a FL3 Log vs Time plot gated on "BEADS" in the region labelled "CAL". **C)** PBMNCs were identified based on their FS Lin vs SS Log prolife. The Boolean gate "NOT BEADS" allowed the exclusion of Flow-Count™ fluorospheres from this plot. **D)** The PBMNCs that were CD45 positive, and were therefore characterized as leukocytes, were indicated in the region "CD45" of a SS Log vs CD45 KO Log two-parameter plot. **E)** Viable, $CD45^+$ cells with intact membranes which were impermeable to 7-AAD were identified in the "VIABLE" region of a SS Log vs 7-AAD Log plot, gated on the "CD45" region. **F)** $CD4^+$ T lymphocytes and monocytes present in the PBMNC sample were differentiated based on their SS profiles and differential levels of CD4 expression in a SS Log vs CD4 FITC Log plot.

3.1.3. Storage of PBMNCs

Once the isolated PBMNCs had been enumerated and phenotyped, they were either used immediately for experiments or cryopreserved for long-term storage. Cells to be

cryopreserved were centrifuged at 300 x *g* for 10 min. The PBMNC pellet was resuspended in freezing medium (10% DMSO in FBS) at a concentration of 10^7 cells/mL. Working on ice, aliquots of 1 mL were transferred to cryovials and frozen at -80°C in Mr Frosty freezing containers (Thermo Fisher Scientific; Waltham, MA, USA). After at least 24 hours, the cells were transferred to a dewar for long-term storage in liquid nitrogen.

3.1.4. FACS-based isolation of CD4⁺ T lymphocytes and monocytes

3.1.4.1. Sample preparation

A sorting strategy was developed to simultaneously extract both $CD4^+$ T lymphocytes and monocytes from freshly isolated PBMNCs using the FACSAria™ Fusion cell sorter. An estimate of the number of monocytes and $CD4^+$ T cells present in the sample was obtained during the simultaneous phenotyping and count performed following isolation. From this information, it was determined what volume of the PBMNC cell suspension contained the desired number of cells to be sorted. Since the sorter has extremely stringent parameters, approximately half of the cells that pass through the instrument are discarded. Thus, the required number of input cells was doubled. In order to determine the optimal concentrations of monoclonal antibodies required to stain the cell surface markers used for sorting and immunophenotyping, titrations were carried out for each of the monoclonal antibody conjugates (**Appendix C**).

An aliquot of PBMNCs containing the appropriate number of cells was stained with the monoclonal antibody conjugates CD4 FITC and CD14 PE as well as the viability dye 7-AAD. The volume required was optimized to 0.6 µL of each per $1x10^6$ PBMNCs. Two additional 100 µL aliquots of PBMNCs were taken for a more comprehensive baseline immunophenotype, including analysis of HIV co-receptor expression. The first aliquot was stained with the monoclonal antibodies indicated in **Table 4.1.** In this panel, a CD45 Brilliant Violet™ 711 (BV711) conjugate was used instead of CD45 KO, to avoid spectral overlap with other fluorochromes. The second was stained with the same antibodies except for CCR5 PE-Cy7 and CXCR4 BV605, which were substituted for equal volumes of their corresponding isotypic controls. Staining was carried out for 20-30 min in the dark. The stained cells were washed with PBS, using 1 mL for the immunophenotype samples and one equivalent volume for the cells to be sorted. Both sets of cells were centrifuged at 300 x *g* for 10 min and the

supernatant was aspirated. This wash step was repeated once more to ensure removal of excess antibodies. The cells to be sorted were resuspended in approximately 1 mL complete RPMI-1640 per $1x10^7$ cells and passed through a filter to remove any clumps. The immunophenotype samples were resuspended in 500 µL PBS.

Table 4.1: Sample preparation for immunophenotyping of PBMNC isolates

TUBE 1:		**TUBE 2:**	
Monoclonal antibody	**Volume (µL)**	**Monoclonal antibody**	**Volume (µL)**
CD45 BV711	1.25	CD45 BV711	1.25
CD4 FITC	1.25	CD4 FITC	1.25
CD14 PE	2.5	CD14 PE	2.5
CCR5 PE-Cy7	2.5	PE-Cy7 Isotypic Control	2.5
CXCR4 BV605	5	BV605 Isotypic Control	5
Viability dye	**Volume (µL)**	**Viability dye**	**Volume (µL)**
7AAD	5	7AAD	5

3.1.4.2. Flow cytometry setup, sorting and data acquisition

Target cells were sorted using the purity sorting mode of the FACSAria™ Fusion cell sorter. The required number of target cells were sorted into 15 mL centrifuge tubes prepared with 2 mL complete RPMI-1640 using a serial gating strategy. In the sort protocol, illustrated in **Figure 4.4**, PBMNCs were first gated on a FS Lin vs SS Log two-parameter plot (**Figure 4.4a**). Viable cells were then detected using a SS Log vs 7-AAD Log two-parameter plot (**Figure 4.4b**). A CD4 Log vs CD14 Log two-parameter plot (**Figure 4.4c**) was used to distinguish monocytes ($CD4^{dim}$ CD14+) and $CD4^+$ T lymphocytes ($CD4^{bright}$ CD14-). The sorted cells were centrifuged at 300 x *g* for 10 min and the supernatant was discarded. The cells were resuspended in an appropriate volume of culture medium for further experiments. In order to ensure that sorting was successful, a post-sort purity check was carried out (**Figure 4.4d** & **Figure 4.4e**). Samples of sorted $CD4^+$ T lymphocytes and monocytes (approximately $2x10^4$ cells each) were analysed immediately after sorting using the same protocol. The percent of cells that fall into the original gate used for sorting indicates the purity of the sort. Data was acquired using BD FACSDiva™ (8.0.1) and analysed using Kaluza Flow Cytometry Analysis Software (Version 2.1).

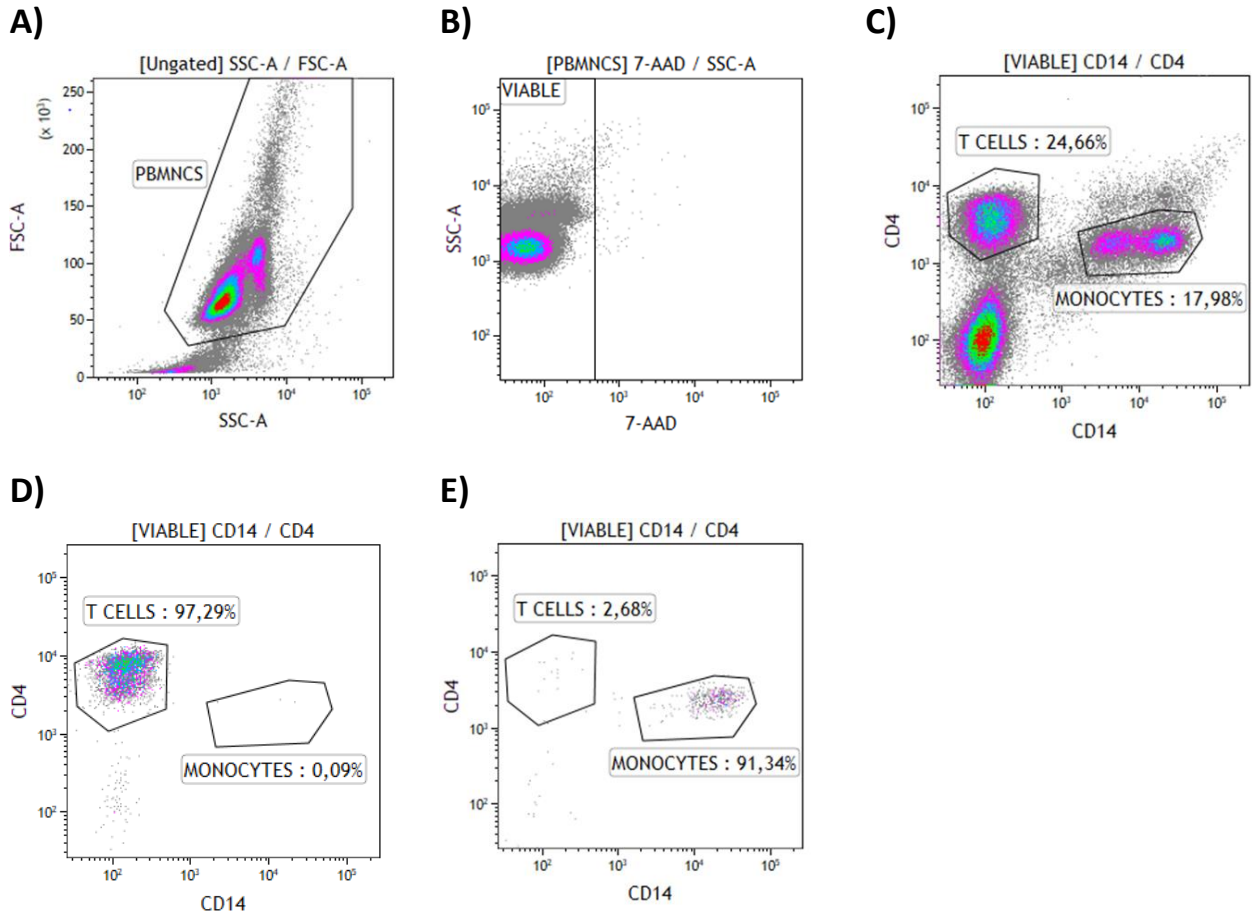

Figure 4.4: Flow cytometry setup for FACS-based isolation of CD4⁺ T lymphocytes and monocytes. A) The PBMNC population was defined based on FS Lin vs SS Log plot. **B)** Viable cells were identified as 7-AAD negative in a SS Log vs 7-AAD Log plot gated on the region "PBMNCs". **C)** A two-parameter plot of CD4 vs CD14, gated on the "VIABLE" region enabled differentiation of the two populations to be sorted. CD4⁺ T lymphocytes, indicated in the region "T CELLS" were highly CD4 positive while CD14 negative. Cells that were weakly CD4 positive and CD14 positive were identified in the region labelled "MONOCYTES". **D)** Representative image of post-sort purity check of sorted CD4⁺ T lymphocytes. **E)** Representative image of post-sort purity check of sorted monocytes.

For the immunophenotyping protocol, doublet discrimination was employed to exclude cell clumps from the analysis. The principles of this technique are described in **Chapter 3** (**Section 3.2.5.5.**). A FS-H Lin vs FS-A Lin two-parameter plot was used to identify single cells which have proportional FS-H to FS-A values (**Figure 4.5a**). A conventional FS Lin vs SS Log plot gated on the "SINGLE CELLS" region was used to identify the "PBMCS" population and exclude residual debris not gated out in the previous plot (**Figure 4.5b**). A SS Log vs 7-AAD Log plot was used to determine the viability of the cells (**Figure 4.5c**). The CD45⁺ leukocyte population was determined using a SS Log vs CD45 BV711 Log plot in the region labelled "LEUKOCYTES" (**Figure 4.5d**). In the subsequent CD4 FITC Log vs CD14 PE Log plot, also gated on

"LEUKOCYTES" (**Figure 4.5e**), the $CD4^+$ T lymphocyte and monocyte populations were identified using the same markers as for the sorting protocol, so that the HIV co-receptor expression of the sorted populations could be assessed by proxy. This was achieved using SS Log vs CXCR4 BV605 Log and SS Log vs CCR5 PE-Cy7 two-parameter plots, gated on the "CD4+ T CELLS" and "MONOCYTES" regions respectively (**Figure 4.5f-i**). The positions of the positive regions for these plots was set using the position of the negative population in the corresponding isotypic control samples. Data was acquired using BD FACSDiva™ (8.0.1) and analysed using Kaluza Flow Cytometry Analysis Software (Version 2.1).

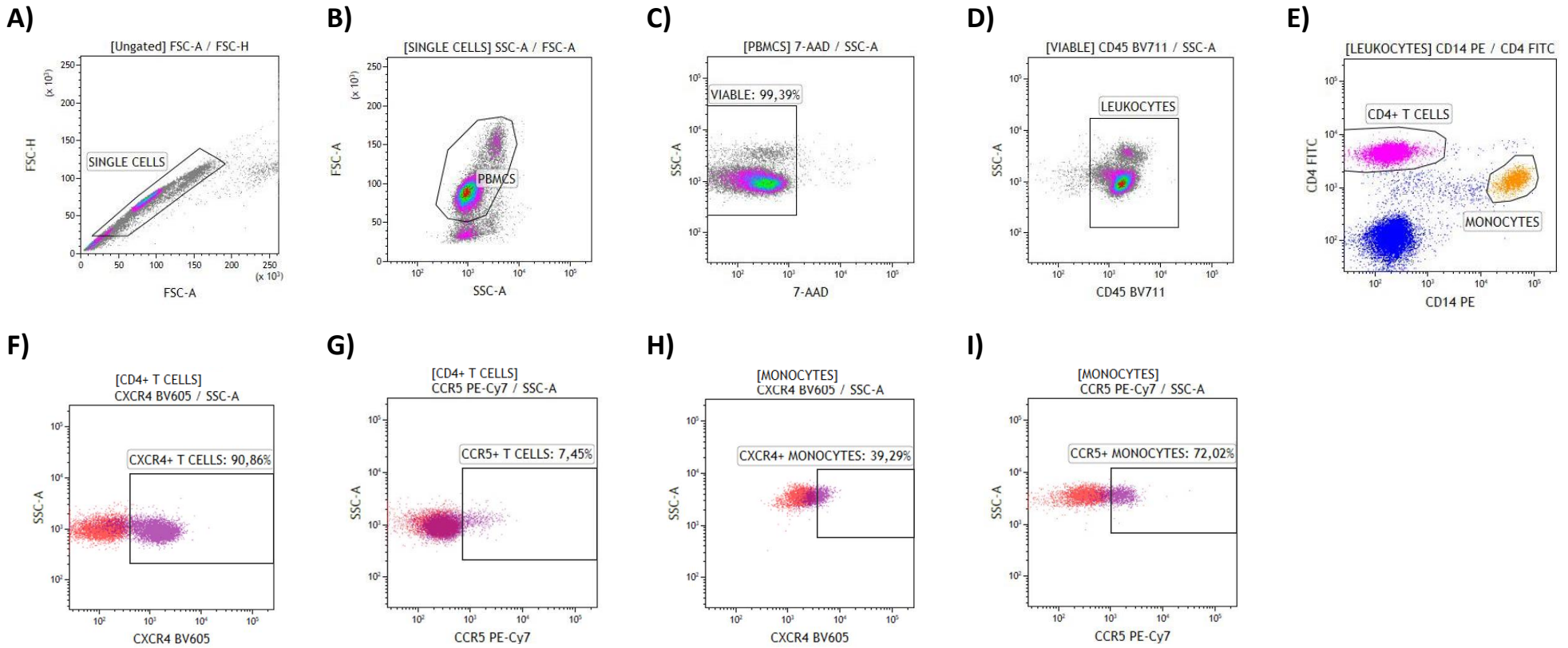

Figure 4.5: Flow cytometry setup for baseline immunophenotyping of PBMNCs. A) Single cells were identified on a FS-H Lin vs FS-A Lin plot. **B)** A FS Lin vs SS Log plot gated on "SINGLE CELLS" was used to exclude debris and define the "PBMCS" region. **C)** Live cells were identified in the "VIABLE" region using a SS Log vs 7-AAD Log plot gated on "PBMCS". **D)** The $CD45^+$ population was identified using a SS Log vs CD45 BV711 Log plot in the region "LEUKOCYTES". **E)** A CD4 FITC Log vs CD14 PE Log plot, also gated on "LEUKOCYTES", was used to define the $CD4^+$ T cell and monocyte populations. Co-receptor expression was determined using **F)** a SS Log vs CXCR4 BV605 Log plot and **G)** a SS Log vs CCR5 PE-Cy7 Log plot gated on the "CD4+ T CELLS" region. Overlay plots are used here to illustrate the setting of regions according to the isotypic control samples, indicated in red, while the stained samples are indicated in purple. Identical plots, gated on the "MONOCYTES" region, were used to analyse **H)** CXCR4 and **I)** CCR5 expression in the monocyte population.

3.2. Culture and activation of CD4$^+$ T Lymphocytes

3.2.1. Cell culture conditions

Sorted CD4$^+$ T lymphocytes were seeded at a concentration of 5x10^5 cells/mL in 600 µL of complete RPMI-1640 in 24-well cell culture plates. They were incubated at 37°C, 5% CO_2 for up to 24 hours, to allow recovery from sorting. After this resting period, the cells were treated to induce activation and proliferation followed by incubation at 37°C, 5% CO_2. The cells were used in downstream experiments after up to 7 days in culture depending on the experiment.

3.2.2. CD4$^+$ T lymphocyte activation

3.2.2.1. PHA-L-induced activation

In preliminary experiments, the potent mitogen Phytohemagglutinin-L (PHA-L) was investigated as a means to induce T cell activation. Sorted CD4$^+$ T lymphocytes were seeded in 12-well culture plates at 1.25x10^5 cells per well in 1.5 mL complete RPMI. PHA-L (Roche; Basel, Switzerland), was added to the cell culture medium at a range of concentrations in the presence of recombinant human IL-2 (Thermo Fisher Scientific; Waltham, MA, USA), also at a range of concentrations, as indicated in **Table 4.2**. The extent of cell proliferation was determined by flow cytometry and used as a measure of activation success (**Section 3.2.3**). Activation with PHA-L proved to be sub-optimal with respect to inducing proliferation and maintaining viability, therefore an alternative method was investigated following a series of troubleshooting experiments.

Table 4.2: Concentrations of IL-2 and PHA-L used in a checkerboard experiment to determine optimal T cell activation conditions

PHA-L concentration	**IL-2 concentration**			
	0 U/mL	**10 U/mL**	**20 U/mL**	**40 U/mL**
0 µg/mL	Non-induced	10 IL-2	20 IL-2	40 IL-2
1 µg/mL	1 PHA-L	10 IL-2 + 1 PHA-L	20 IL-2 + 1 PHA-L	40 IL-2 + 1 PHA-L
2 µg/mL	2 PHA-L	10 IL-2 + 2 PHA-L	20 IL-2 + 2 PHA-L	40 IL-2 + 2 PHA-L
4 µg/mL	4 PHA-L	10 IL-2 + 4 PHA-L	20 IL-2 + 4 PHA-L	40 IL-2 + 4 PHA-L

3.2.2.2. Antibody-mediated activation by co-stimulation with anti-CD3 and anti-CD28

A 1:100 dilution of Low-Endotoxin Azide-Free (LEAF™) anti-human CD3 antibody (Biolegend, San Diego, CA, USA) was prepared in PBS. This solution was added to a 24-well culture plate, using 300 µL per well at a concentration of 10 µg/mL. The plate was then sealed with parafilm and incubated at 4°C overnight to allow the antibodies to coat the surface of the plate. The antibody solution was removed, and the wells were washed with PBS. Sorted $CD4^+$ T cells that had been rested overnight were then transferred directly into the pre-coated wells of the 24-well plate. Recombinant human IL-2 and soluble LEAF™ anti-human CD28 antibody (Biolegend, San Diego, CA, USA) were added at final concentrations of 20 U/mL and 2 µg/mL respectively. The treated cells were then cultured at 37°C, 5% CO_2 for a further 4-6 days to allow activation and proliferation. The success of activation was determined by flow cytometry (See **Section 3.2.4**).

During optimization experiments, the addition of conditioned medium from autologous unsorted PBMNCs that had undergone activation using the same antibody-based method was tested as a possible means to enhance activation of the isolated $CD4^+$ T lymphocytes. After 2 days of activation, the culture medium was harvested from these PBMNCs by centrifugation of the cell suspension at 300 x *g* for 10 min followed by collection of the supernatant. Purified $CD4^+$ T lymphocytes that had been sorted and rested during the 2 days were then collected from their culture plate, centrifuged at 300 x *g* for 10 min and resuspended in the PBMNC-conditioned supernatant. They were then activated in an anti-CD3-coated plate as described above. This step was removed from the final protocol, based on the findings described in **Section 4.2.1.**

3.2.3. $CD4^+$ T lymphocyte proliferation assay

3.2.3.1. Sample preparation

Aliquots of 100 µL were taken directly from cell culture plates containing activated $CD4^+$ T lymphocytes. The cells were stained with 0.5 µL of the nuclear dye Vybrant® DyeCycle™ (VDC) Ruby (Thermo Fisher Scientific; Waltham, MA, USA). An equal volume (100 µL) of Flow-Count™ fluorospheres was added for enumeration of the cells and 500 µL of PBS was added for volume. Analysis was carried out on the Gallios™ flow cytometer.

3.2.3.2. Flow cytometry setup, data acquisition and analysis

The Flow Count™ beads were detected using a single-parameter histogram of events in the FL1 channel and are indicated in the region "BEADS" (**Figure 4.6a**). A FL1 Log vs Time two-parameter plot gated on "BEADS" was used to distinguish intact beads from fragments and small clumps (**Figure 4.6b**). The intact beads used for enumeration are indicated in the region "CAL". The nucleated cell population, which stained positively for VDC Ruby, was identified in a FS Lin vs VDC Ruby Log two-parameter plot (**Figure 4.6c**). VDC Ruby was detected in the FL7 channel [Excitation: 638 nm; Emission: 725/20 BP]. The number of Flow Count™ fluorospheres in the "CAL" region (**Figure 4.6b**) and the number of cells in the "Nucleated" region (**Figure 4.6c**), were used in **Equation 4.1** and **Equation 4.2** to obtain the total nucleated cell count. Data acquisition and analysis was performed using Kaluza Flow Cytometry Analysis Software (Version 2.1).

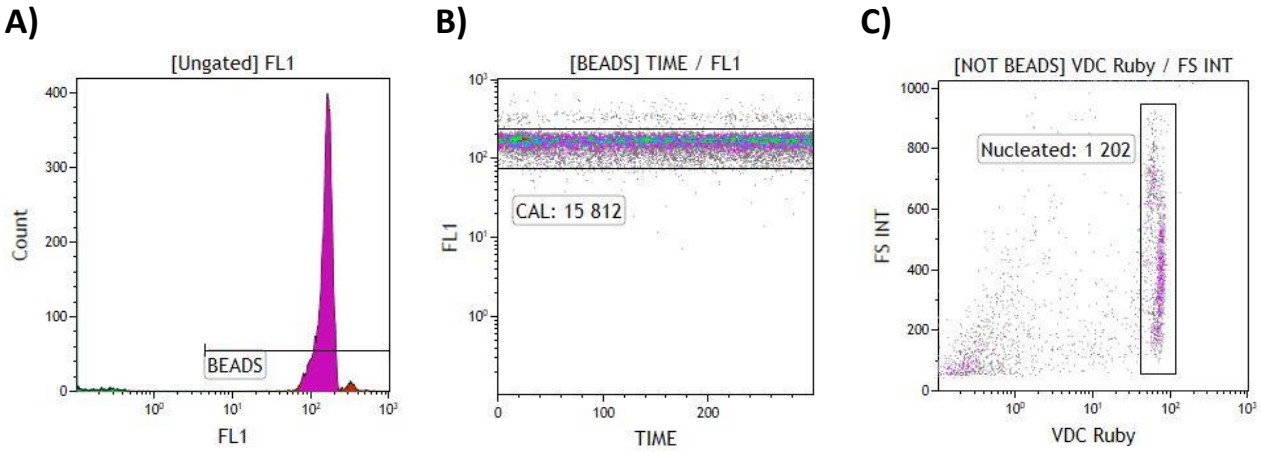

Figure 4.6: Flow cytometry setup for cell proliferation assay performed on activated CD4⁺ T lymphocytes. A) The Flow Count™ fluorospheres fluoresce brightly in the FL1 channel and were thus identified as a clear peak in a Count vs FL1 Log one-parameter plot in the "BEADS" region. **B)** A FL1 Log vs Time plot was used to identify intact Flow Count™ beads, indicated in the region "CAL". **C)** A FS Lin vs VDC Ruby Log two-parameter plot was used to detect the cells that stained positively for the nuclear dye VDC Ruby, indicated in the "Nucleated" region.

3.2.4. Analysis of CD25 expression and enumeration of activated CD4⁺ T lymphocytes

3.2.4.1. Sample preparation

$CD4^+$ T lymphocytes activated using the anti-CD3 and anti-CD28 co-stimulation method were analysed by flow cytometry to determine whether the cells had responded by upregulating

CD25, a classical T cell activation marker. A cell count was performed simultaneously to assess the degree to which they had undergone proliferation. A 50 µL aliquot of cell suspension was taken from each well to be tested. Each aliquot of cells was stained according to the table below (**Table 4.3**) for 10 min in the dark. Depending on antibody availability at the time of the experiment, either CD25 PE or CD25 FITC were used to assess activation state. To each sample, 50 µL of Flow-Count™ fluorospheres was added in order to perform a cell count, and 400 µL of PBS was added for volume. Data was acquired using the Gallios™ flow cytometer.

Table 4.3: Sample preparation for analysis of proliferation and activation of CD4⁺ T lymphocytes

Monoclonal antibody	**Volume (µL)**
CD45 KO	3
CD25 PE or CD25 FITC	3
Viability dye	**Volume (µL)**
7AAD	3

3.2.4.2. Flow cytometry setup, data acquisition and analysis

A single-parameter histogram of the FL1 channel was used to identify the Flow Count™ fluorospheres (**Figure 4.7a**) and a subsequent FL1 vs Time plot was used to select only the intact beads (**Figure 4.7b**). Leukocytes positive for CD45 expression were identified on a SS Log vs CD45 KO Log plot. The fluorospheres were excluded post-acquisition from the "LEUKOCYTES" region using the Boolean gate "NOT BEADS" (**Figure 4.7c**). CD45 KO expression was detected in the FL10 channel [Excitation: 405 nm; Emission: 550/40 BP]. Non-viable cells and cell debris were gated out of the leukocyte population using a SS Log vs 7-AAD Log plot (**Figure 4.7d**) and a FS Lin vs SS Log plot (**Figure 4.7e**), respectively. This viable, $CD45^+$ cell population was used to assess the extent of CD25 expression using either a SS Log vs CD25 PE Log plot (**Figure 4.7f**) or a SS Log vs CD25 FITC plot. CD25 PE was measured in the FL2 channel [Excitation: 488nm; Emission: 575/30 BP] while CD25 FITC was detected in the FL1 channel. The position of the gate for the CD25 positive region was set according to an unstained negative control and kept consistent throughout the analysis. The number of Flow Count™ fluorospheres, identified in the region "CAL" (**Figure 4.7b**) and the number of viable cells, identified in the region "PBMCS" (**Figure 4.7e**), were used in **Equation 4.1** and **Equation 4.2**

to obtain the total viable cell count. Data acquisition and analysis was performed using Kaluza Flow Cytometry Analysis Software (Version 2.1).

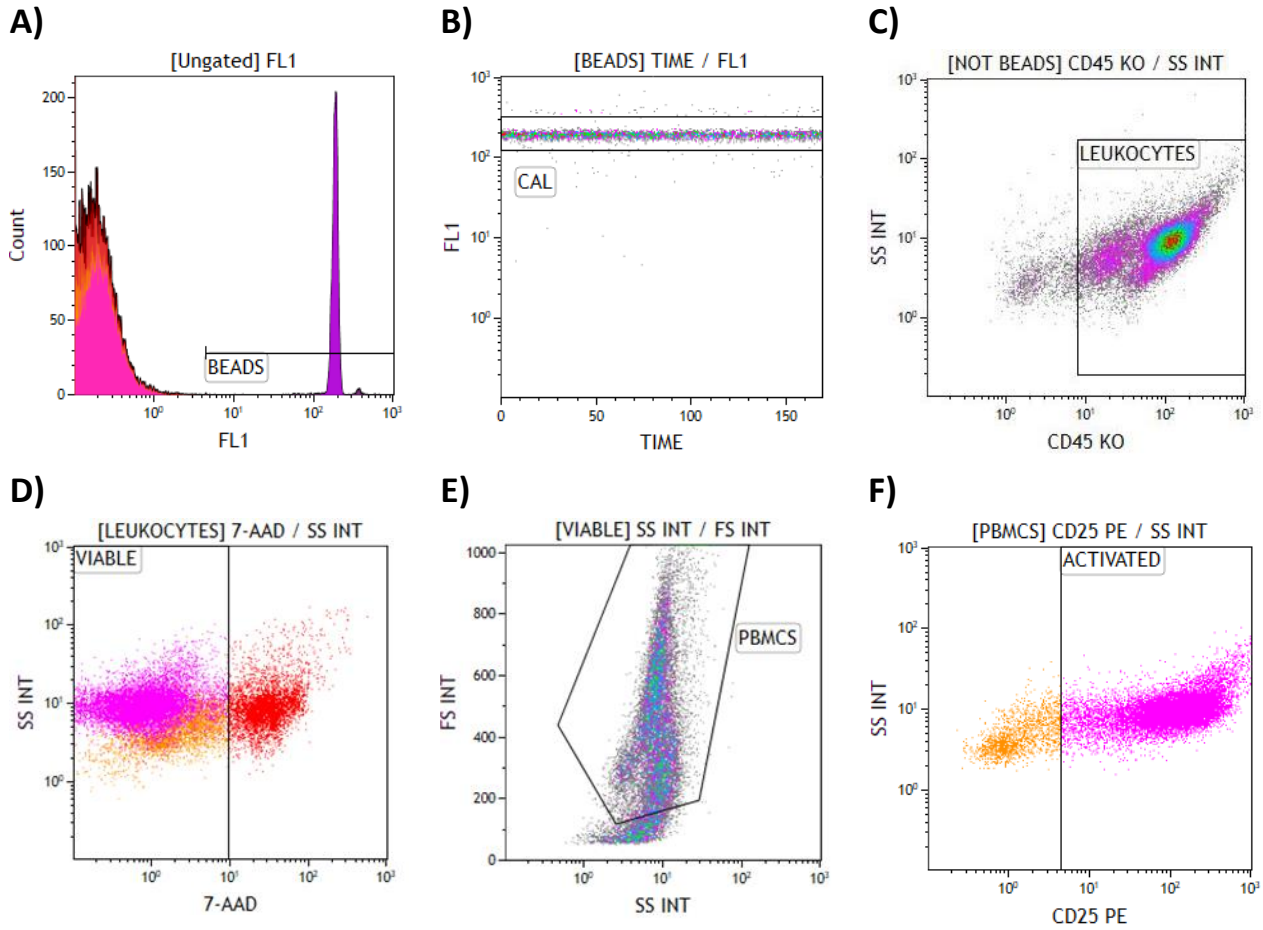

Figure 4.7: Flow cytometry setup for analysis of CD25 expression in activated CD4⁺ T lymphocytes. A) Flow Count™ fluorospheres were identified in the "BEADS" region using a FL1 Log vs Count one-parameter plot. **B)** Intact beads were identified in the region "CAL" using a FL1 Log vs Time plot, gated on "BEADS". **C)** A SS Log vs CD45 KO Log two-parameter plot enabled identification of the leukocyte population in the positive region, while a Boolean gate, "NOT BEADS", was used to exclude the Flow Count™ fluorospheres post-acquisition. **D)** A SS Log vs 7-AAD Log plot enabled identification of viable cells in the negative region. **E)** CD4⁺ T lymphocytes (only CD4⁺ T cells were sorted) were identified, labelled here as "PBMCS", and cell debris was excluded on a FS Lin vs SS Log two-parameter plot, gated on the "VIABLE" region. **F)** A SS Log vs CD25 Log plot gated on "PBMCS" was used to identify cells that are positive for CD25, indicating an activated phenotype. In this example, CD25 PE was used; however, CD25 FITC was also used as an alternative fluorochrome in some experiments.

3.2.5. Co-receptor expression analysis

3.2.5.1. Sample preparation

$CD4^+$ T lymphocytes that had been cultured and activated prior to co-receptor expression analysis had to be re-counted on the day of the assay to account for cell proliferation that may have occurred which would interfere with the ratio of cells to antibodies used. These cells were collected from their culture plates and 50 µL aliquots were taken for counting. The cells were stained with 3 µL of 7-AAD prior to the addition of 50 µL Flow Count™ fluorospheres and 400 µL of PBS for volume. The number of viable 7-AAD negative cells present in each sample was determined on the Gallios™ flow cytometer, and the concentration of cells in the original cell suspensions were calculated using **Equation 4.1**. Four aliquots containing $3x10^5$ cells each were taken from the enumerated cell suspensions, centrifuged at 300 x *g* for 10 min, resuspended in 100 µL of PBS and finally transferred into flow cytometry tubes. For the analysis of freshly sorted $CD4^+$ T lymphocytes, purified cells were first resuspended to a concentration of 500 000 cells/mL in complete RPMI-1640 as per the previously described culture protocol (**Section 3.2.1.**). Four 600 µL aliquots containing $3x10^5$cells each were then taken directly from this cell suspension.

For each sample set, the four tubes of cells to be analysed were stained as indicated in **Table 4.4** and incubated for 15 min in the dark. The first tube contained antibodies reactive against CD45 and CD4 for positive identification of the $CD4^+$ T lymphocytes, as well as the isotypic controls for the antibodies used for detection of the CCR5 and CXCR4 co-receptors. The second tube was a Fluorescence Minus One (FMO) control for the BV605 fluorochrome, containing all antibodies other than CXCR4 BV605, while the third tube was an FMO control for 7-AAD. These controls were included as it was observed that BV605 caused excessive spill-over into the 7-AAD channel even after compensation, confounding the correct placement of the positive regions. The final tube contains the full combination of antibodies used in the analysis. After staining, the cells were washed once with 1 mL of PBS to remove residual antibodies before being resuspended in a final volume of 500 µL of PBS for analysis on the FACSAria™ Fusion cell sorter.

Table 4.4: Sample preparation for analysis of co-receptor expression on $CD4^+$ T lymphocytes

	TUBE 1: ISOTYPIC CONTROLS	TUBE 2: BV605 FMO CONTROL	TUBE 3: 7-AAD FMO CONTROL	TUBE 4: AB COMBO
Monoclonal antibody	**Volume (µL)**	**Volume (µL)**	**Volume (µL)**	**Volume (µL)**
CD45 BV711	0.75	0.75	0.75	0.75
CD4 FITC	0.75	0.75	0.75	0.75
CCR5 PE-Cy7	-	1.5	1.5	1.5
CXCR4 BV605	-	-	3	3
PE-Cy7 Isotypic control	1.5	-	-	-
BV605 Isotypic Control	3	-	-	-
Viability dye	**Volume (µL)**	**Volume (µL)**	**Volume (µL)**	**Volume (µL)**
7AAD	3	3	-	3

3.2.5.2. Flow cytometry setup, data acquisition and analysis

During analysis, it was noticed that the activated and non-activated samples had very different expression profiles, particularly in CD45 (BV711) and CXCR4 (BV605), illustrated by **Figure 4.8**. Therefore, a unique compensation matrix was applied to the activated cells to account for these differences. The first part of the analysis involved the positive identification of the $CD4^+$ T cells to be assayed. The $CD45^+$ population was first identified using a SS Log vs CD45 BV711 Log plot in the region "LEUKOCYTES" (**Figure 4.9a**). A FS Lin vs SS Log plot was then used to exclude debris and identify intact cells in the region "T CELLS" (**Figure 4.9b**). The CD4 expression of this population was then checked in a subsequent plot of SS Log vs CD4 FITC Log gated on "T CELLS" (**Figure 4.9c**). The second part of the analysis involved the determination of viability and co-receptor expression, which was complicated by intense spill-over of BV605 signal into the 7-AAD channel, especially when the cells were activated. The full gating strategy, including the use of isotypic and FMO controls, is illustrated in **Figure 4.10.**

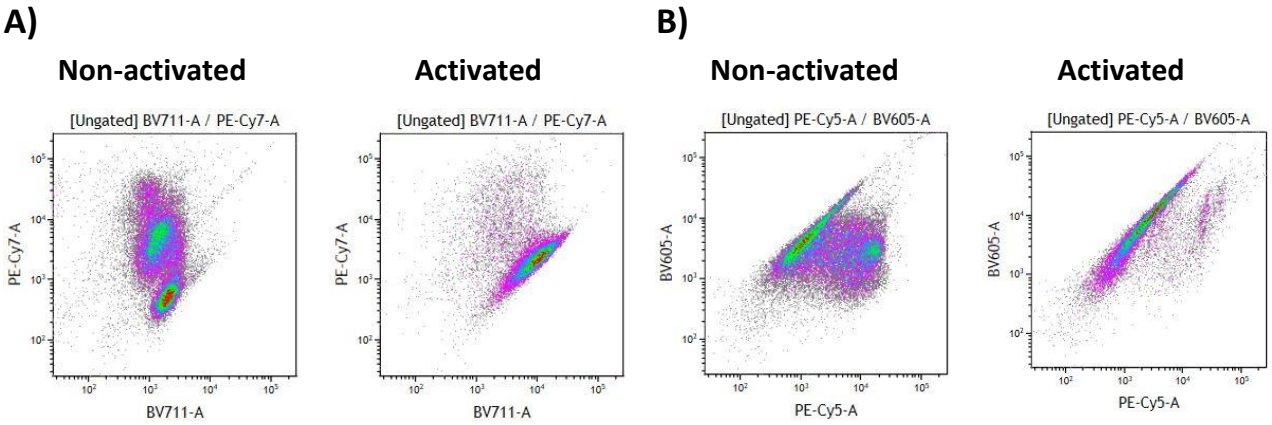

Figure 4.8: Uncompensated two-parameter plots of A) PE-Cy7 (CCR5) vs BV711 (CD45) and B) BV605 (CXCR4) vs PE-Cy5 (7-AAD) for non-activated and activated CD4⁺ T cells from the same donor after 7 days in culture. These plots illustrate the difference in spill-over due to BV711 (**A**) and BV605 (**B**) between these two conditions, requiring greater compensation to be applied to the activated cells than their non-activated counterparts.

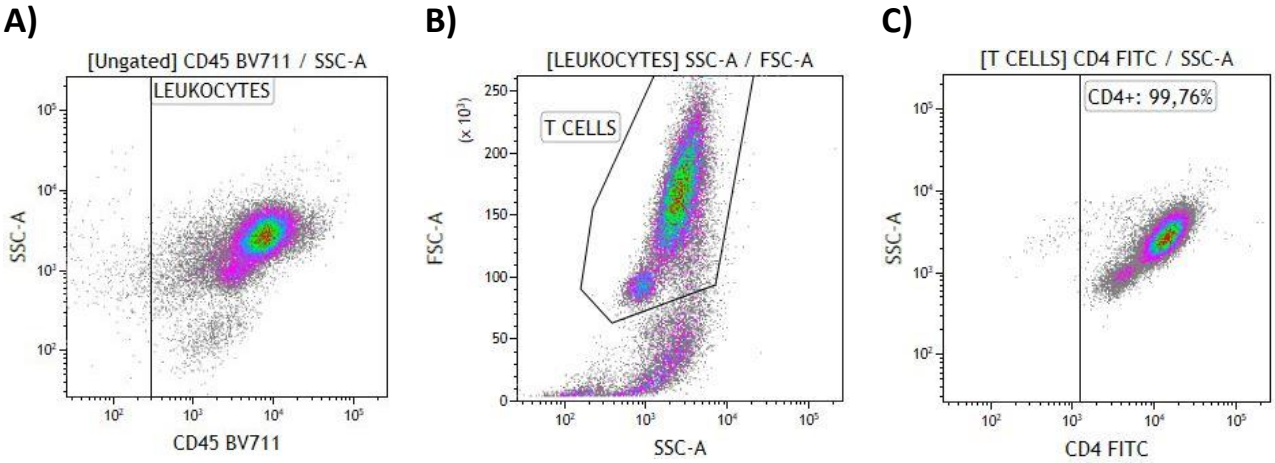

Figure 4.9: Flow cytometry setup for co-receptor analysis (Part 1 – identification of CD4⁺ T lymphocytes). A) The CD45⁺ cells were identified in the region "LEUKOCYTES" on a SS Log vs CD45 BV711 Log plot. **B)** The intact cells were identified in the "T CELLS" region using a FS Lin vs SS Log two-parameter plot, gated on "LEUKOCYTES". **C)** The CD4 expression of this population was assessed using a SS Log vs CD4 FITC Log plot, gated on the "T CELLS" region. Viability was assessed during the second part of the analysis along with co-receptor expression.

The isotypic control sample was used to determine the initial position of the viable population on a SS Log vs 7-AAD Log plot, gated on the "T CELLS" region identified in the first part of the analysis (**Figure 4.10a**). The isotypic control sample was also used to set the positions of the negative populations for CXCR4 and CCR5 using SS Log vs CXCR4 BV605 Log (**Figure 4.10b**) and SS Log vs CCR5 PE-Cy7 Log (**Figure 4.10c**) plots respectively, gated on the "VIABLE" region. The BV605 FMO control sample was then used to confirm the position of the 7-AAD negative

population in the absence of staining with BV605 (**Figure 4.10d**) and to check for any spill-over from 7-AAD into the BV605 channel by inspection of the SS Log vs CXCR4 BV605 Log plot (**Figure 4.10e**). No such spill-over was observed; however, there was a slight decrease in the fluorescence intensity of BV605 in the FMO compared to the isotypic control, indicating the occurrence of non-specific staining in the isotypic sample. The position of the "CXCR4+" region was thus kept as per the isotypic control to account for this. The 7-AAD FMO was likewise used to check for spill-over from BV605 into the 7-AAD channel. In this case, a very clear positive shift in the 7-AAD channel was observed (**Figure 4.10i**) due to the presence of a strong signal in the BV605 channel (**Figure 4.10j**). The boundary of the "VIABLE" region was thus shifted from its original position set using the isotypic samples (indicated by a dotted line) to a new position further to the right (indicated by a solid line), to account for this spill-over that could not be entirely compensated out. The final values for 7-AAD, CXCR4 and CCR5 expression were obtained from the "AB COMBO" sample set stained with the full panel of antibodies, using the regions defined in the controls (**Figure 4.10h-j**).

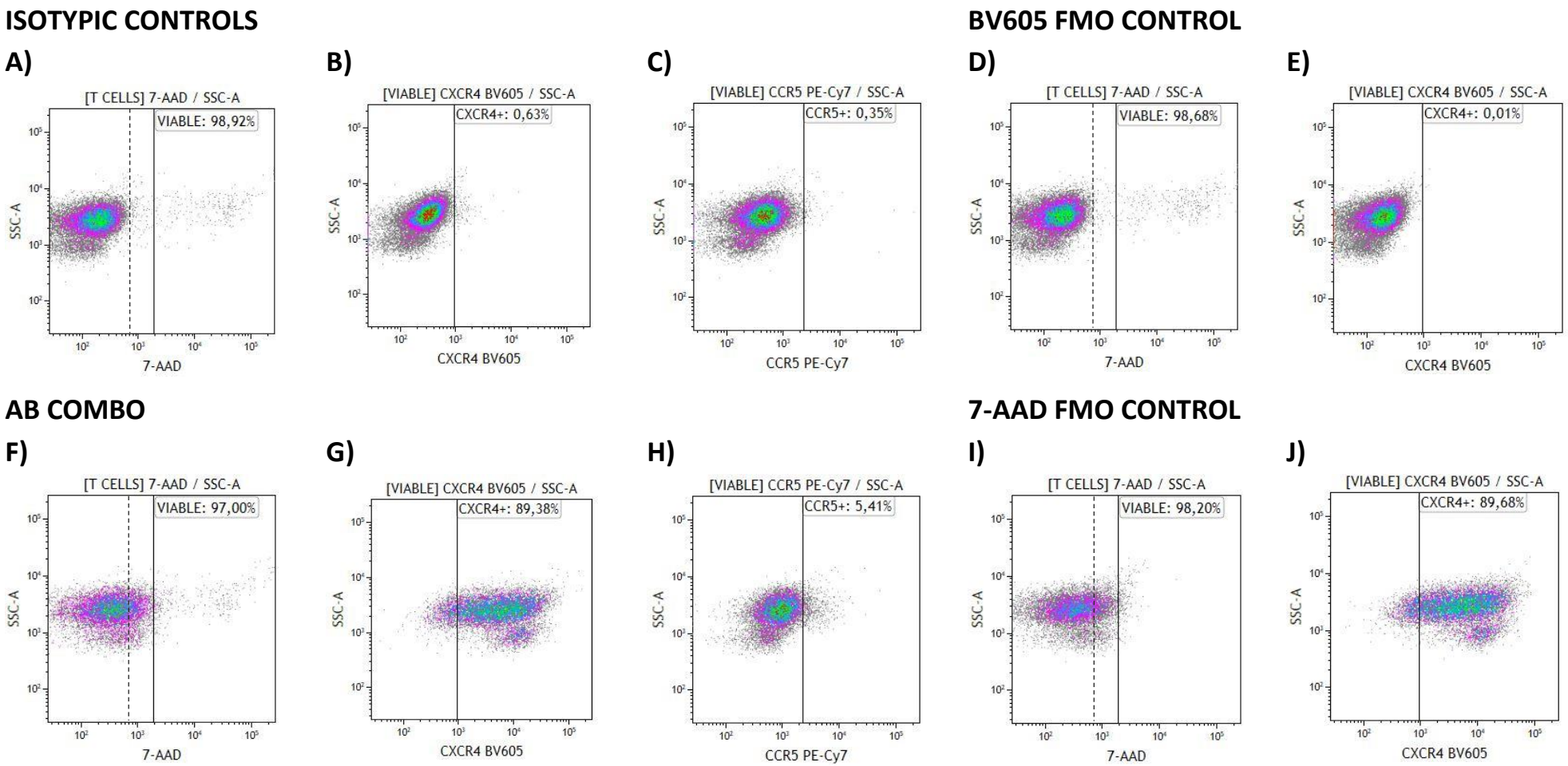

Figure 4.10: Flow cytometry setup for co-receptor analysis (Part 2 – viability and co-receptor expression). ISOTYPIC CONTROLS: A) The viable population was identified in the negative region on a SS Log vs 7-AAD Log plot. The positions of the $CXCR4^+$ and $CCR5^+$ regions were set using **B)** SS Log vs CXCR4 BV605 Log and **C)** SS Log vs CCR5 PE-Cy7 Log plots. **BV605 FMO:** the signal of the 7-AAD and BV605 channels were examined using **D)** SS Log vs 7-AAD Log and **E)** SS Log vs CXCR4 BV605 Log plots in the absence of staining with BV605**. 7-AAD FMO:** these same plots, **I)** SS Log vs 7-AAD Log and **J)** SS Log vs CXCR4 BV605 Log, were then examined in samples stained without 7-AAD. **AB COMBO:** The final analysis of viability, CXCR4 and CCR5 expression was carried out on samples stained with all antibodies, using **F)** SS Log vs 7-AAD Log **G)** SS Log vs CXCR4 BV605 Log and **H)** SS Log vs CCR5 PE-Cy7 Log plots respectively.

3.3. Culture and differentiation of monocyte-derived macrophages

3.3.1. Cell culture and cytokine induction

Isolated CD14 positive monocytes were plated into 6-well cell culture plates in 2 mL of complete RPMI-1640. The number of cells seeded was dependant on the yield from sorting, ranging from 200 000 – 250 000 monocytes per well. Plated cells were incubated at 37°C, 5% CO_2 for 48 hours to encourage adherence to the plastic surface. Non-adherent cells were then removed by aspirating the culture medium and rinsing each well gently with pre-warmed PBS or medium. Fresh medium was added to each well and the monocytes were treated with cytokines to promote differentiation. Stock solutions of M-CSF (Thermo Fisher Scientific; Waltham, MA, USA) and GM-CSF (Thermo Fisher Scientific; Waltham, MA, USA), with concentrations of 250 µg/mL M-CSF and 100 µg/mL GM-CSF respectively, were diluted 1:10 in RPMI-1640. In order to obtain final concentrations of 25 ng/mL M-CSF and 10 ng/mL GM-CSF in 2mL of cell culture medium, 2 µL of the dilutions were added to each well. After a further 7 days in culture at 37°C, 5% CO_2, the monocytes had differentiated into macrophages.

3.3.2. Functional phagocytosis assay

In order to confirm that the macrophages had retained their phagocytic potential following differentiation, a functional phagocytosis assay using pHrodo™ Red *S. aureus* and *E. coli* BioParticles® Conjugates (Life Technologies; Carlsbad, CA, USA) was performed. These microbe-derived particles are conjugated to the pH-reactive fluorescent dye pHrodo™ Red (Excitation: 560 nm; Emission: 585 nm). The intensity of the emitted fluorescence of pHrodo™ Red dye at its maximum emission wavelength increases dramatically in a low pH environment (**Figure 4.11**). Particles that are phagocytosed will be processed in intracellular vesicles called phagolysosomes, which are highly acidic and provide an ideal environment for pathogen degradation by hydrolytic enzymes (**Figure 4.12**). The pHrodo™ conjugate will therefore emit a strong signal when engulfed by phagocytic cells, such as macrophages, and can be easily captured using fluorescence microscopy.

To perform the assay, lyophilized BioParticles® were resuspended to a concentration of 1 mg/mL in complete RPMI-1640 medium. The culture medium was aspirated from the adherent macrophages and the cells were gently washed twice with pre-warmed medium.

BioParticles® were added to the macrophages using 100 µL per $1x10^5$ cells as per the manufacturer's instructions. The wells were topped up with complete RPMI medium to a final volume of 1 mL per well and the macrophages were incubated at 37°C for at least 2 hours. In order to visualize the nuclei, the macrophages were stained with either VDC Violet (Thermo Fisher Scientific; Waltham, MA, USA) or 4',6-diamidino-2-phenylindole (DAPI – Thermo Fisher Scientific; Waltham, MA, USA). If VDC Violet was used, 0.5 µL was added directly to the particle suspension and the cells were incubated for a further 10 min before visualization. If DAPI was used, the particles were removed and replaced with fresh medium, then incubated with 2 µL of dye solution with a concentration of 5 mg/mL overnight for optimal staining. Just before visualization, the cells were washed thoroughly with PBS to remove excess dye and/or particles. Microscopy was performed on a Zeiss AxioVert A1 microscope (Carl Zeiss AG; Oberkochen, Germany), using Zen 2.3 Lite software. Filter set 00 [Excitation: BP530-585, Beam splitter: FT600, Emission: LP615nm] was used to capture signal from pHrodo™ Red, while filter set 49 [Excitation: BP450-490, Beam splitter: FT395, Emission: BP445/50] was used to detect either DAPI or VDC Violet. The proportion of cells that had taken up pHrodo™ particles was determined by manual counting in five random fields (at 10x magnification) per condition.

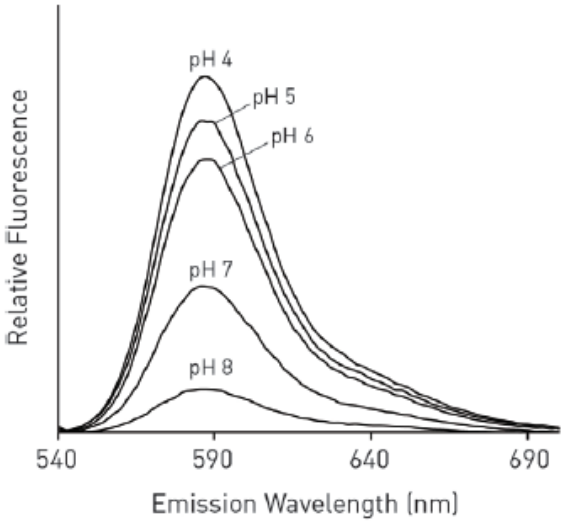

Figure 4.11: The fluorescence emission spectra of pHrodo™ Red under different pH conditions. As the pH decreases, the intensity of the fluorescence emitted increases dramatically. Taken from the pHrodo™ Red and Green BioParticles® Conjugates for Phagocytosis technical datasheet, available from: https://www.thermofisher.com/order/catalog/product/P35361

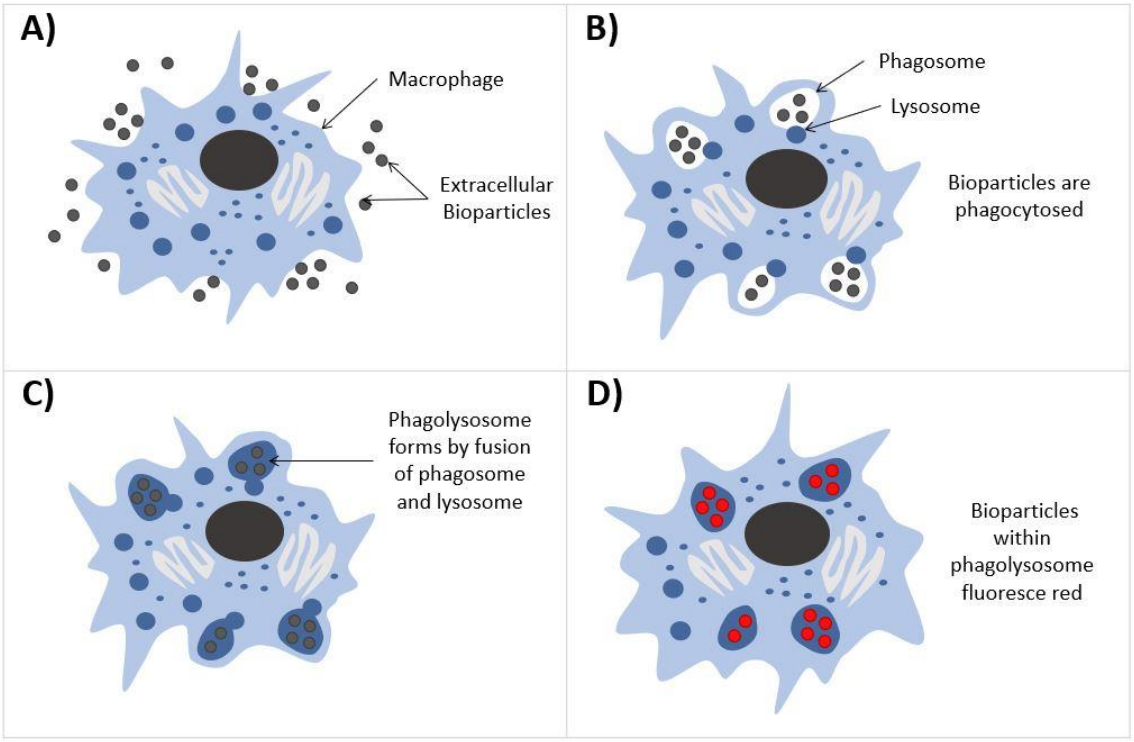

Figure 4.12: Principles of the pHrodo™ phagocytosis assay. A) Macrophages are exposed to pHrodo™ Red BioParticles™. **B)** The macrophages engulf the particles which become contained within intracellular vesicles called phagosomes during phagocytosis. Lysosomes are cell organelles specialized for degrading phagocytosed pathogens, containing hydrolytic enzymes within the acidic lumen of the structure. **C)** The phagosomes fuse with nearby lysosomes, forming structures called phagolysosomes in which the hydrolytic enzymes degrade the particles in an acidic environment. **D)** Due to the low pH within the phagolysosome, the pH-reactive dye conjugated to the particles fluoresces brightly at 590 nm (red).

3.3.3. Immunophenotyping of differentiated macrophages

3.3.3.1. Sample preparation

Differentiated macrophages were dissociated from their culture plates using 0.25% Trypsin-EDTA. The cell culture medium was removed, and the cells were washed with ice-cold PBS before adding 500 µL trypsin per well. The cells were incubated at 37°C and agitated by pipetting at 10-minute intervals. After 30 min total incubation time, the trypsin was neutralized by addition of 500 µL complete RPMI-1640 medium. The cells were collected, centrifuged at 300 x *g* for 10 min and resuspended in 250 µL PBS. Two aliquots of 100 µL were taken for each condition and stained for 15 min in the dark, as indicated in **Table 4.5.** The antibody panel included markers found on cells of the monocyte/macrophage lineage (CD14 PE, CD16 APC, CD64 Brilliant Violet™ 510 [BV510]), as well as the primary HIV receptor (CD4

FITC) and the most common co-receptors (CXCR4 BV605 and CCR5 PE-Cy7). The general leukocyte marker CD45 BV711 was also included.

Table 4.5: Sample preparation for immunophenotyping of differentiated macrophages

TUBE 1		TUBE 2	
Monoclonal antibody	**Volume (µL)**	**Monoclonal antibody**	**Volume (µL)**
CD45 BV711	1	CD45 BV711	1
CD4 FITC	1	CD4 FITC	1
CD14 PE	1	CD14 PE	1
CD16 APC	1	CD16 APC	1
CD64 BV510	1	CD64 BV510	1
CCR5 PE-Cy7	1	PE-Cy7 Isotypic Control	1
CXCR4 BV605	1	BV605 Isotypic Control	1
Viability dye	**Volume (µL)**	**Viability dye**	**Volume (µL)**
7AAD	1	7AAD	1

3.3.3.2. Flow cytometry setup, data acquisition and analysis

Viability was determined using a SS Log vs 7-AAD two-parameter plot. Viable, 7-AAD negative cells were identified in the "VIABLE" region (**Figure 4.13a**). A SS Log vs CD45 BV711 Log plot gated on viable cells was used to exclude any cells not expressing CD45, while the CD45-positive cells were identified in the region "LEUKOCYTES" (**Figure 4.13b**). A FS Lin vs SS Log plot gated on "LEUKOCYTES" was then used to exclude any residual debris. Viable, intact $CD45^+$ macrophages were selected in the "MACROPHAGES" region (**Figure 4.13c**). A series of subsequent plots were then used to assess expression of HIV receptors (CD4, CXCR4, CCR5) and macrophage markers (CD14, CD16, CD64), all gated on the "MACROPHAGES" region and plotted against SS Log (**Figure 4.13d-i**). The position of the positive regions for CXCR4 and CCR5 were set according to their corresponding isotypic controls, while the unstained control was used for the rest of the markers. A final set of plots gated on the "MACROPHAGES" region was used to assess co-expression of the HIV receptors (CD4, CCR5, CXCR4) (**Figure 4.13j-l**).

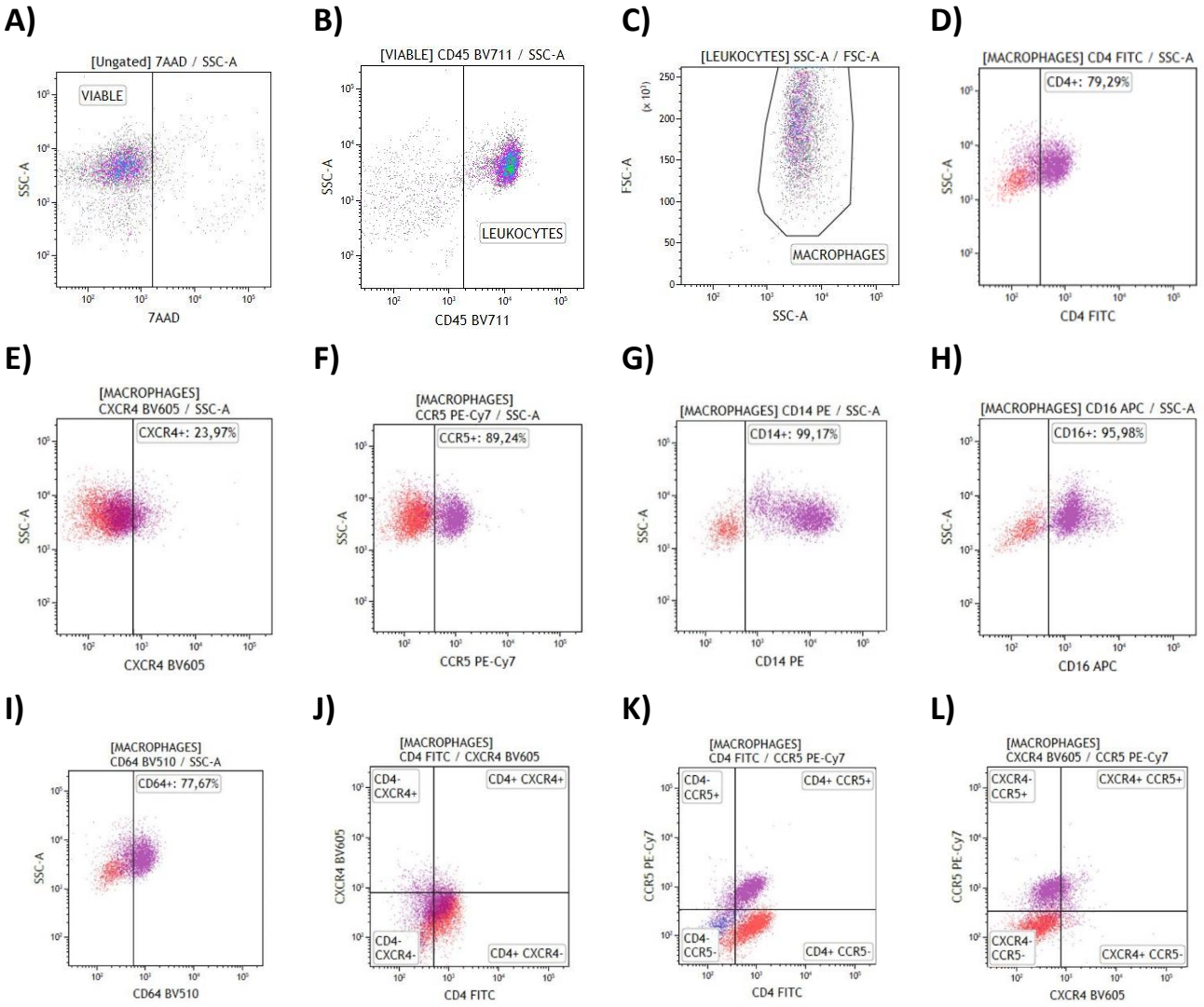

Figure 4.13: Flow cytometry setup for immunophenotyping of differentiated macrophages. A) Identification of the viable cells was carried out using a SS Log vs 7-AAD Log plot in the region labelled "VIABLE". **B)** $CD45^+$ cells were identified in the "LEUKOCYTES" region using a SS Log vs CD45 BV711 Log plot, gated on the "VIABLE" population. **C)** A FS Lin vs SS Log plot gated on "LEUKOCYTES" was used to remove any cell debris from the population of interest, defined by the region "MACROPHAGES". The expression of CD4, CCR5 and CXCR4 were assessed using a set of plots gated on the "MACROPHAGES" region: **D)** SS Log vs CD4 FITC Log, **E)** SS Log vs CXCR4 BV605 Log, **F)** SS Log vs CCR5 PE-Cy7 Log. The plots presented here are overlays which illustrate how the position of the regions was set according to the negative population in the control (either unstained or isotypic) shown in red, while a representative antibody-stained sample is shown in purple. The expression of a panel of macrophage markers was analysed on a similar set of plots, also gated on the "MACROPHAGES" region: **G)** SS Log vs CD14 PE Log, **H)** SS Log vs CD16 APC Log, **I)** SS Log vs CD64 BV510 Log. A final set of plots gated on "MACROPHAGES" was used to assess co-expression of CD4, CXCR4 and CCR5: **J)** CXCR4 BV605 Log vs CD4 FITC Log, **K)** CCR5 PE-Cy7 Log vs CD4 FITC Log, **L)** CCR5 PE-Cy7 Log vs CXCR4 BV605 Log. In **J)** and **K)** overlays are shown from both unstained (blue) and isotypic (red) controls in comparison to a stained sample (purple), since CD4 was set according to the unstained control, while CXCR4 and CCR5 were set according to their respective isotypic controls.

3.4. Infection of target cells with HIV-1

3.4.1. Infection protocols

3.4.1.1. $CD4^+$ T lymphocytes

Cells that had been sorted and activated by anti-CD3/anti-CD28 co-stimulation were used as the starting point for $CD4^+$ T lymphocyte infection experiments. The cultured cells were collected and viable cells were counted, as previously described (**Section 3.2.5.1.**). Aliquots of the cell suspension containing the required numbers of cells were transferred to microcentrifuge tubes and centrifuged at 300 x *g* for 10 min. The supernatant was aspirated, and the cells were resuspended in the required volume of cell-free HIV supernatant to yield the desired multiplicity of infection (MOI). The MOI describes the ratio of infectious virus particles to target cells present during the infection process. The volume of virus required can be calculated using **Equation 4.3**. The HIV-exposed cells were incubated in this volume for 2 hours at 37°C in a rotating incubator to maximise virus-to-cell contact. After this initial exposure period, the cells were topped up with serum-free RPMI-1640 to a final concentration of $5x10^5$ cells/mL. After overnight incubation at 37°C, 5% CO_2 for 16-18 hours, the HIV-exposed T lymphocytes were collected, centrifuged at 300 x *g* for 10 min and resuspended in complete RPMI-1640. The cells were then cultured at 37°C, 5% CO_2 until 48 hours post-infection, at which point the degree of productive infection achieved was assessed using the KC57 intracellular p24 assay.

3.4.1.2. Macrophages

Differentiated macrophages were infected using a similar method to the $CD4^+$ T lymphocytes, with some modifications made to account for their adherent nature. The culture medium of the cells to be infected was aspirated and the cells were rinsed with PBS to remove any residual FBS-containing medium. The appropriate volume of viral cell-free supernatant calculated using **Equation 4.3** was added directly to the wells. The cells were not counted, since this would require them to be lifted off the culture plate. The number of seeded monocytes prior to differentiation was thus used as an estimate for the number present at the time of infection. As for the T cells, the macrophages were incubated in the small volume of cell-free supernatant for 2 hours at 37°C to promote virus-to-cell contact and then topped

up with serum-free RPMI-1640 to a normal working well volume of 2 mL. After 16-18 hours, the medium was changed to HIV-free complete RPMI-1640 and the cells were cultured for a further 48 hours. The success of the infection was determined using the KC57 assay.

Equation 4.3:

$$Volume\ of\ virus = \frac{No.of\ target\ cells\ \times MOI}{IU/mL\ of\ viral\ stock}$$

3.4.2. Detection of HIV-infected target cells using the KC57 assay

3.4.2.1. Sample preparation

$CD4^+$ T lymphocytes to be assayed were collected from their culture plate in aliquots of $6x10^5$ cells per sample, using the number of cells counted at infection to estimate the concentration. The macrophage samples had to be trypsinised prior to flow cytometric analysis, which was performed as per the macrophage immunophenotyping protocol (**Section 3.3.3.**). Once again, enumeration was not possible for the macrophages since the input cell numbers were too low to waste any sample on a count. The target cells were processed according to the protocol for the KC57 assay presented in **Chapter 3** (**Section 3.3.1.1.**), with the inclusion of viability staining using Zombie Violet™ for both $CD4^+$ T lymphocytes and macrophages.

3.4.2.2. Flow cytometry setup, data acquisition and analysis

A similar protocol was used for the analysis of HIV positivity in both target cell types. The first step was the identification of either the $CD4^+$ T lymphocytes or the macrophages based on their profiles in FS Lin vs SS Log plots in the "T CELLS" (**Figure 4.14a**) and "MACROPHAGES" (**Figure 4.15**a) regions respectively. Next, viability was determined for each using a SS Log vs Zombie Violet Log plot, gated on the identified target cell population, and setting the "VIABLE" region on the negative population (**Figure 4.14b** & **Figure 4.15b**). Finally, the proportions of the HIV-infected cells were determined using SS Log vs KC57 PE Log two-parameter plots, gated on the "VIABLE" regions for each cell type (**Figure 4.14c** & **Figure 4.15c**). Data was acquired using BD FACSDiva™ software (Version 8.0.1) and analysed post-acquisition using Kaluza Flow Cytometry Analysis Software (Version 2.1).

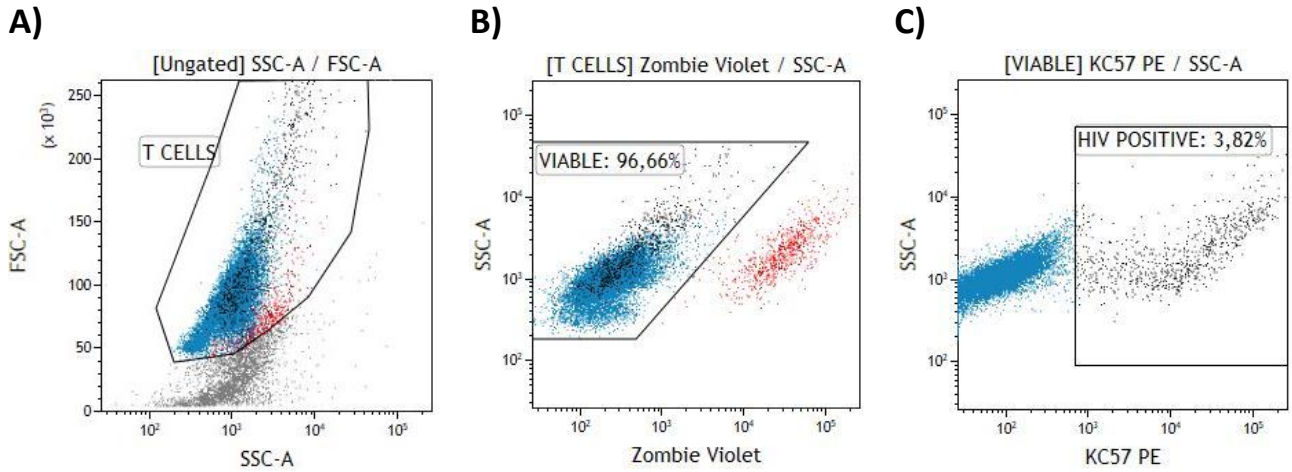

Figure 4.14: Flow cytometry setup for KC57 assay of HIV-exposed CD4⁺ T lymphocytes. A) A FS Lin vs SS Log plot was used to identify the CD4⁺ T cells in the region labelled "T CELLS". **B)** A SS Log vs Zombie Violet Log plot gated on "T CELLS" was used to set the "VIABLE" region. **C)** The HIV positive cells were detected using a SS Log vs KC57 PE Log two-parameter plot gated on the "VIABLE" population.

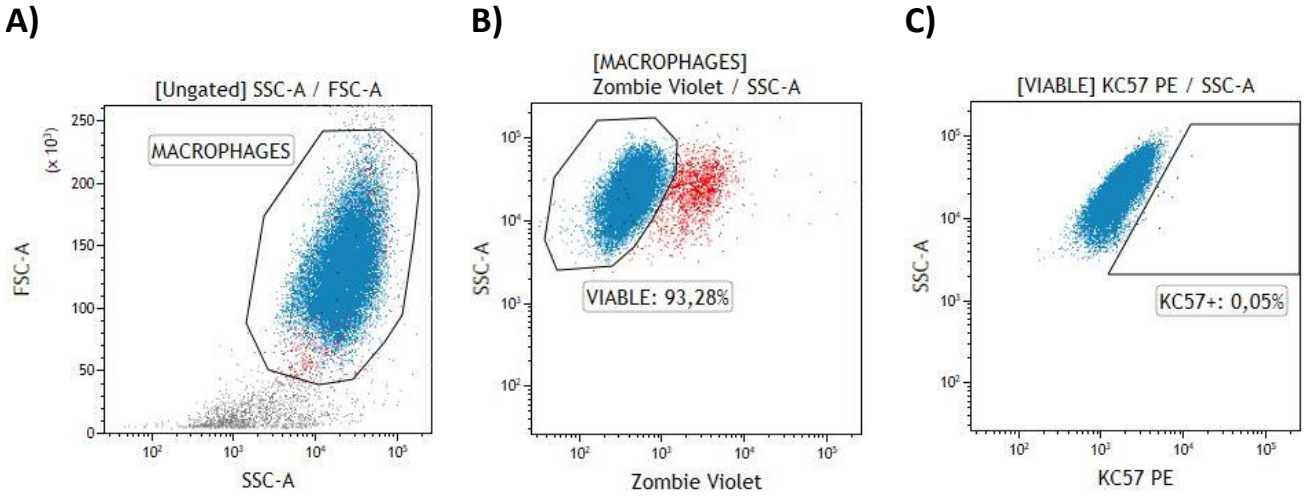

Figure 4.15: Flow cytometry setup for KC57 assay of HIV-exposed macrophages. A) A FS Lin vs SS Log plot was used to define the region labelled "MACROPHAGES" and exclude debris. **B)** Viability was determined using a SS Log vs Zombie Violet Log plot gated on "MACROPHAGES". **C)** HIV positivity was determined using a SS Log vs KC57 PE Log two-parameter plot, gated on the cells in the "VIABLE" region from the previous plot.

3.4.3. Determination of infection kinetics in CD4⁺ T lymphocytes

To determine the infection kinetics of the HIV primary isolates CM9 and SW7, an experiment was designed to assess the extent of infection observed in HIV-exposed CD4⁺ T lymphocytes using two independent detection methods at multiple time points. The cells were activated using anti-CD3/anti-CD28 co-stimulation (as per **Section 3.2.2**) and collected for infection 4 days post-induction. A 50 µL aliquot of this cell suspension was taken to perform a count and simultaneously determine the extent of activation through analysis of CD25 expression, as

previously described (**Section 3.2.4**). Aliquots containing the desired number of T cells to be infected were taken from the enumerated cell suspension and centrifuged at 300 x *g* for 10 min. The supernatants were removed, and the pellets were resuspended in the appropriate volume of viral cell-free supernatant (either CM9-020518 or SW7-110718) to yield an MOI of 2, as calculated using **Equation 4.3**. A negative control treated with serum-free RPMI-1640 instead of viral supernatant was also included. The cells were incubated for 2 hours at 37°C in a rotating incubator. Instead of an overnight incubation step in the viral supernatant, as was done previously, these cells were immediately centrifuged at 300 x *g* for 10 min and resuspended in complete RPMI-1640 to a concentration of 300 cells/µL. This modification to the infection protocol was instituted to improve cell viability by limiting the length of time the cells were kept in viral supernatant which has been depleted of nutrients by PBMNCs during viral culture. The cells were then plated in 24-well cell culture plates at $1.5x10^5$ cells per well and incubated at 37°C, 5% CO_2 until harvest.

The cells were harvested for analysis at 6-hour intervals over a 48-hour period. At each of the 8 time points, aliquots of cell suspension were collected firstly for p24 ELISA and secondly for PCR-based HIV detection. For the p24 ELISA, two aliquots of 200 µL were taken. One aliquot comprising both cells and the culture supernatant was frozen down at -20°C directly. The second aliquot was centrifuged at 300 x *g* for 10 min and the supernatant was transferred to a new tube prior to freezing, allowing the supernatant and the cell pellet to be analysed independently. For the PCR-based assay, an aliquot of 400 µL was collected and centrifuged at 300 x *g* for 10 min. The cell pellet was frozen at -20°C and stored until the end of the experiment when DNA extraction from the collected cell pellets was performed. The negative control was only collected at 48 hours to minimize the number of samples to be analysed. Once all samples had been collected, the HIV detection component of the experiment was performed. The p24 ELISA samples were thawed, using 200 µL of PBS to resuspend the cells-only sample, and then processed using the Lenti-X™ p24 Rapid Titer Kit as described in **Chapter 3** (**Section 3.2.1**). For the PCR samples, DNA was extracted from the cell pellets after thawing, using the QiaAmp® DNA Micro Kit as per the manufacturer's instructions. The PCR reaction was carried out using LTR/*gag* primer pairs specific to either CM9 or SW7, depending on which strain the cells were exposed to, as per the protocol in **Chapter 3** (**Section 3.3.2.3**).

3.5. Statistical analysis

Statistical analysis of quantitative results for which multiple technical and/or biological replicates were available was carried out in GraphPad Prism version 7.00 for Windows (GraphPad Software; La Jolla, CA, USA; Available from: www.graphpad.com). Since sample sizes were small in all experiments, only non-parametric statistical methods were used. Data from the T cell proliferation assay described in **Section 3.2.3** were analysed using the Kruskal-Wallis test for statistical significance, followed by correction for multiple comparisons using Dunn's test. The same tests were used to check for significant differences among all conditions tested in the combined assay to determine CD25 expression in conjunction with T cell proliferation (**Section 3.2.4**). In addition, Mann-Whitney tests were used to determine significance in the difference between the control and each treatment condition separately, to give the analysis greater power. The data from analysis of co-receptor expression (**Section 3.2.5**) were also analysed using a Kruskal-Wallis test with Dunn's test to correct for multiple comparisons. The results from the pHrodo assay (**Section 3.3.2**) and from immunophenotyping of macrophages (**Section 3.3.3**) were analysed using the Mann-Whitney test to compare cells treated with either M-CSF or GM-CSF. Statistical analysis of the data obtained from the KC57 assay to determine infection efficiency in T cells and macrophages (**Section 3.4.2**) was handled differently for each of the two cell types. For the T cells, three different MOIs were being tested, therefore a Kruskal-Wallis with Dunn's test to correct for multiple comparisons was used. For the macrophages, the MOI was kept constant while the effects of treatment with either M-CSF or GM-CSF were being examined. Therefore, the Mann-Whitney test was used to determine statistical significance. In all tests, a p-value < 0.05 was considered significant.

4. Results

4.1. Isolation of target cells from peripheral blood

4.1.1. Quantification and characterization of isolated PBMNCs

Flow cytometric evaluation of the freshly isolated PBMNCs was performed to ensure that the quantity and quality of the isolated cells was acceptable for use in downstream experiments. The first step was to obtain a total cell count directly after isolation and determine what

proportion of the PBMCs expressed CD4. This allowed for estimation of the numbers of monocytes and $CD4^+$ T cells present in the sample prior to sorting. A summary of this information is presented for all donors in **Appendix D** (**Table D.1**). The second step was a more comprehensive baseline immunophenotype, performed on the FACSAria™ Fusion cell sorter. The purpose of this experiment was primarily to determine the expression levels of the HIV co-receptors CXCR4 and CCR5 on the $CD4^+$ T-cells and monocytes, since any deficiencies in these receptors would impact on the suitability of using these cells for viral culture or HIV infection experiments. The results are summarised in **Figure 4.16.** For the individual results of each donor phenotyped, see **Appendix D** (**Table D.2**). CXCR4 positivity was high in $CD4^+$ T lymphocytes (75.81% ± 11.47%) and low in monocytes (37.54% ± 24.99%), while CCR5 expression was relatively high in monocytes (52.67% ± 23.44) but very low in $CD4^+$ T lymphocytes (10.34% ± 3.81%) (**Figure 4.16**). Beyond this general trend, the results were highly variable across donors.

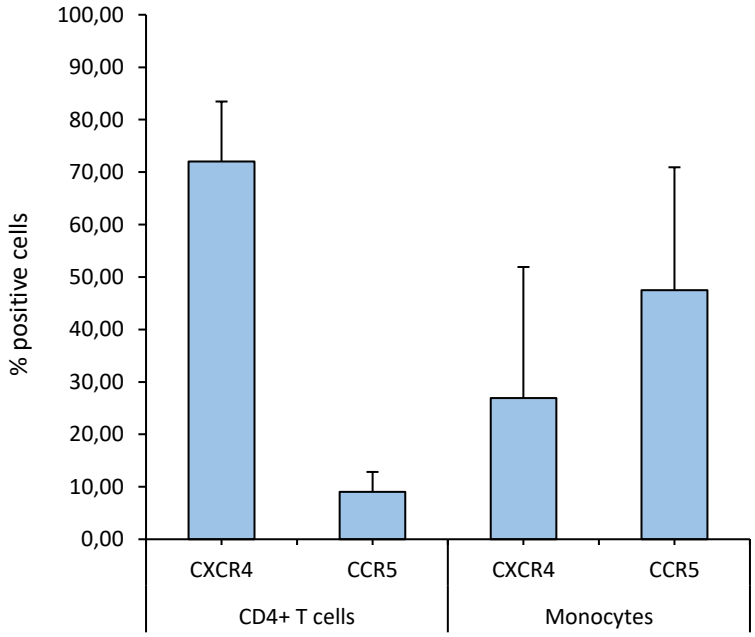

Figure 4.16: Results of immunophenotypic analysis of co-receptor expression in PBMNCs. Expression levels of the CXCR4 and CCR5 co-receptors are presented as a percentage of positive cells in the $CD4^+$ T cell and monocyte populations. Results are expressed as the mean percent expression ± SD (n = 11).

4.2. $CD4^+$ T lymphocyte culture and activation

4.2.1. Optimization of activation conditions

During cell culture optimization, the use of PHA-L was initially investigated as a means to induce T cell activation with the ultimate aim of enhancing susceptibility to HIV. The effect of adding the cytokine IL-2 was investigated in parallel, using a checkerboard experiment where pure populations of isolated $CD4^+$ T cells were cultured at four different concentrations of PHA-L (0 µg/mL, 1 µg/mL, 2 µg/mL, 40 µg/mL) in combination with four different concentrations of IL-2 (0 U/mL, 10 U/mL 20 U/mL, 40 U/mL) over a period of either 4 or 6 days. The extent of cell proliferation was used as a measure of activation success and was determined by performing duplicate cell counts on a flow cytometer, as per the protocol described in **Section 3.2.3.** The mean cell count for each condition was used to calculate the fold change compared to the non-induced control (no PHA-L, no IL-2). The results of this preliminary experiment, in which only one biological replicate (PB15) was used, are presented in **Figure 4.17**. Unfortunately, no major increases in cell count were observed for any of the culture conditions, indicating that the PHA-L failed to significantly induce T cell population proliferation, even in the presence of the activation signalling cytokine IL-2. In fact, by day 6 the cell counts from the induced samples were in fact lower than the non-induced control, except for the conditions where 40 U/mL of IL-2 was used.

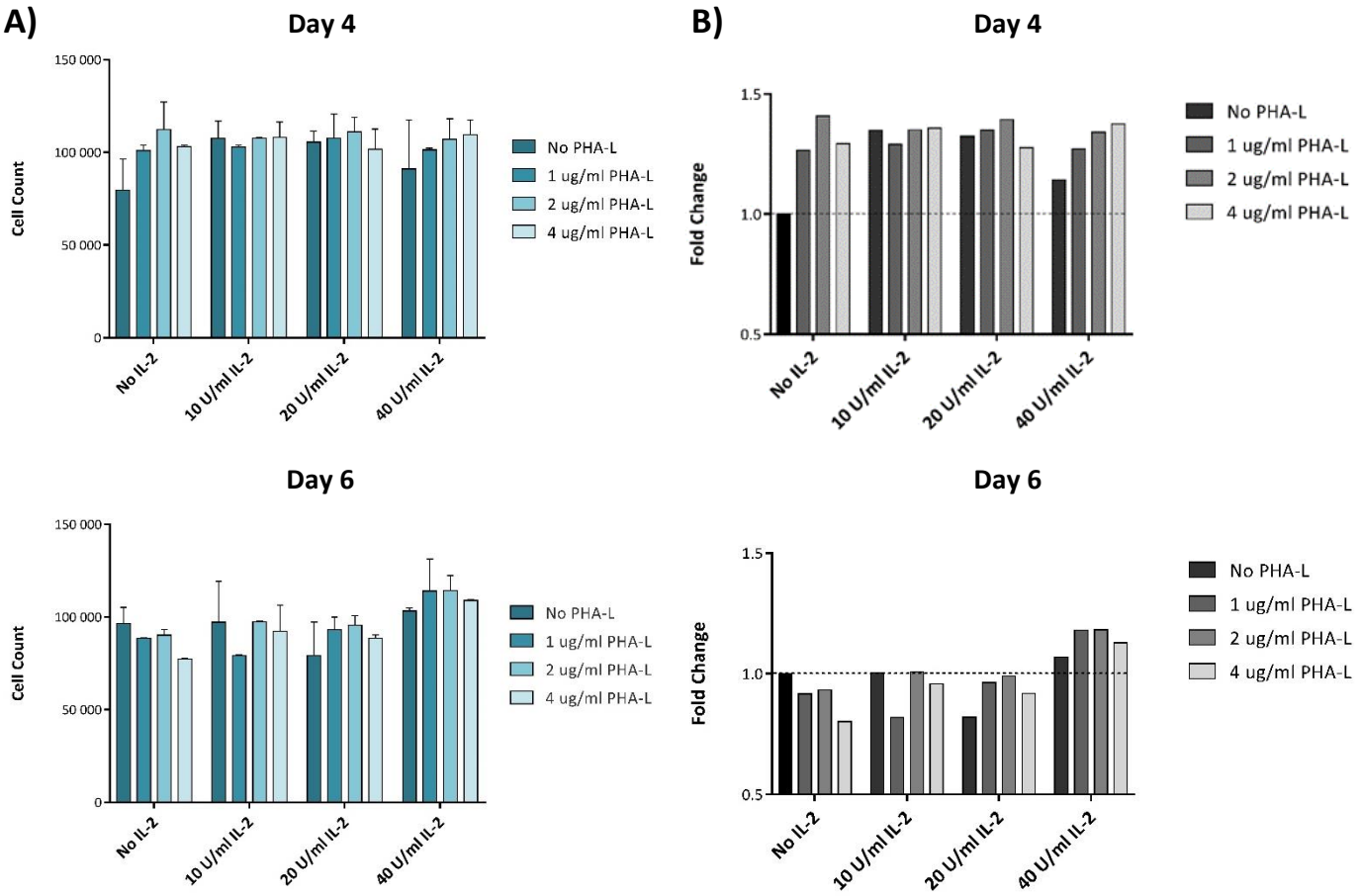

Figure 4.17: Results of cell proliferation assay performed using CD4⁺ T lymphocytes stimulated with varying concentrations of both PHA-L and IL-2. The assay was performed at both Day 4 and Day 6 following treatment with PHA-L and/or IL-2. A) The raw cell counts are reported as the mean ± SD from two technical replicates for each condition. **B)** The relative fold change of the mean cell counts compared to the non-induced control (No PHA-L, No IL-2) is presented for each condition. The dotted line indicates a fold change of 1, i.e. no change relative to the control. Data is representative of one biological repeat.

Several follow-up experiments were performed to troubleshoot the failure of PHA-L to activate the cultured T cells. Two possibilities were investigated. Firstly, it was suspected that the frozen PHA-L stocks may have been stored too long or been through too many freeze-thaw cycles. The cell proliferation assay was thus repeated using both the original frozen stocks and a freshly made PHA-L solution, both of which were added at 2 µg/mL. As a positive control, PHA-P was used at the same concentration since it had been clearly shown to activate PBMNCs during viral culture. PHA-L and PHA-P are both preparations containing mitogenic lectins isolated from the red kidney bean, *Phaseolus vulgaris*. However, PHA-P is a crude extract containing a mixture of isolectins which are able to induce agglutination of both

erythrocytes (erythroagglutinating) and leukocytes (leukoagglutinating), while PHA-L is a purified extract containing only leukoagglutinating isolectins (209).

The other possibility considered was that residual anti-CD3 Allophycocyanin-Cyanine 7 (APC-Cy7) conjugated antibody, bound to the cells during sorting of the pure $CD4^+$ T cell population, may be interfering with the mitogenic potential of the PHA-L by preventing CD3 cross-linking and the resultant TCR stimulation. In order to test for this potential interference, a final condition was included in the cell proliferation experiment in which the anti-CD3 antibody was added to cells treated with the fresh PHA-L solution. In all the above conditions, IL-2 was added at a concentration of 20 U/mL. The results of the proliferation assay after 6 days in culture are illustrated in **Figure 4.18.** The frozen PHA-L stocks demonstrated a clear failure to induce proliferation (cell count = $6.11x10^4 \pm 3.38x10^3$) compared to both the fresh PHA-L ($1.60x10^5 \pm 2.69x10^4$) and the PHA-P ($2x10^5 \pm 3.90x10^4$), indicating that this was indeed a problem. Interestingly, it was apparent that addition of the anti-CD3 antibody greatly stimulated proliferation, resulting in the highest absolute cell counts observed ($4.06x10^5 \pm 8.09x10^4$). This increase was statistically significant compared to the use of the original frozen PHA-L stocks (p-value = 0.0102).

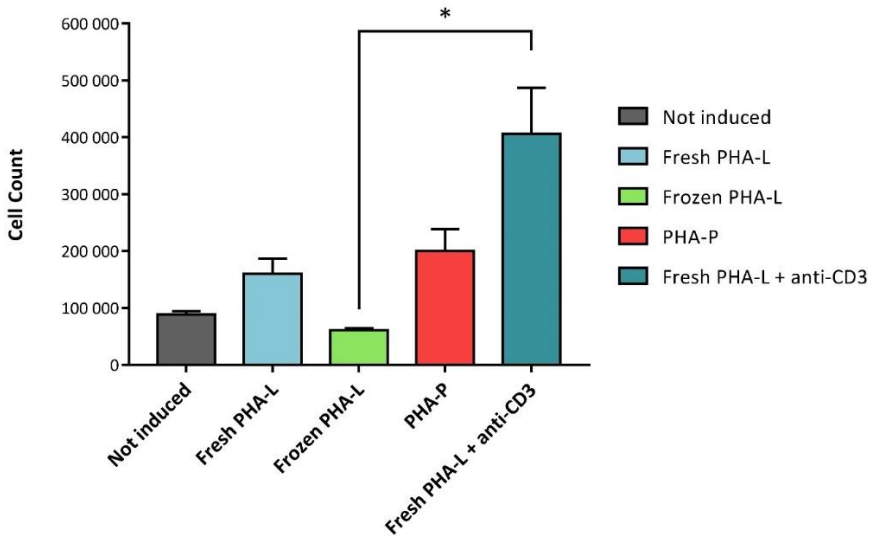

Figure 4.18: Results of cell proliferation assays performed during troubleshooting of PHA-mediated $CD4^+$ T cell activation. The same frozen PHA-L stocks used in the previous activation experiment were tested, as well as several alternative options. These included the use of fresh PHA-L, PHA-P and PHA-L in combination with an anti-CD3 antibody. A non-induced control was included for comparison with the different conditions. The cell counts for each of the conditions were obtained 6 days after activation. The mean ± SD of the cell counts for three technical replicates are presented on the graph. Data is representative of one biological repeat. * $p < 0.05$

Since the addition of the anti-CD3 antibody appeared to have such a strong impact on cell proliferation, further investigation was carried out to see if it could be used to supplement PHA-mediated activation. The proliferation assay was repeated once more, using PHA-L and PHA-P (at 2 µg/mL each) either alone or in combination with 0.5 µL anti-CD3 antibody (200 µg/mL). Use of the anti-CD3 antibody alone was also tested. The resulting cell counts are presented in **Figure 4.19**. These results seem to indicate, firstly, that PHA-P was slightly more effective than PHA-L ($9.46x10^5 \pm 1.16x10^4$ vs $7.26x10^5 \pm 2.79x10^5$) and secondly that addition of anti-CD3 antibody to either PHA-L ($1.04x10^6 \pm 1.94x10^5$) or PHA-P ($1.08x10^6 \pm 2.12x10^5$) improves proliferation slightly. However, use of anti-CD3 antibody alone was clearly the most effective ($1.33x10^6 \pm 2.19x10^5$), showing a significant increase in cell count compared to the non-induced control (p value = 0.0198). Based on the results of these two experiments, it was decided that antibody-mediated T cell activation was a more promising method than the use of PHA. The anti-CD3 antibody used in previous experiments, which was conjugated to an APC-Cy7 fluorochrome, was replaced with a LEAF™ unconjugated substitute which is more appropriate for cell culture applications. In addition, use of an antibody directed against the CD28 co-stimulatory molecule was included in the protocol based on recommendations in existing literature (202,210,211).

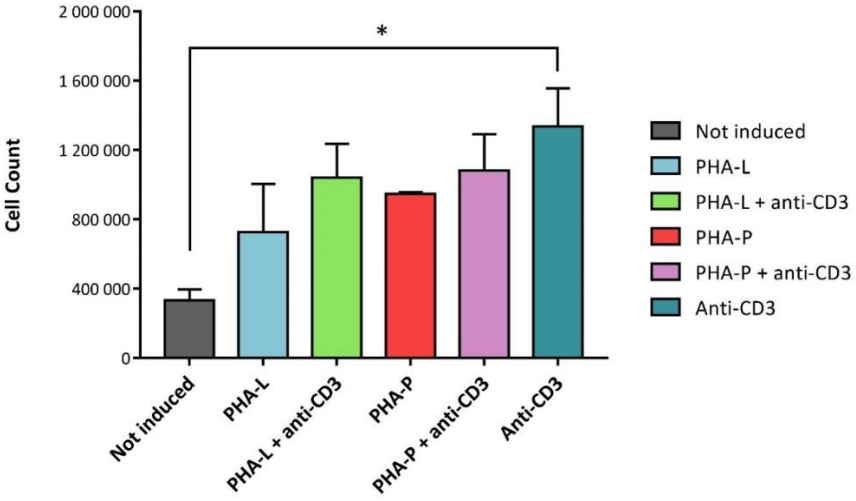

Figure 4.19: Results of cell proliferation assay performed to compare the activation efficiency of PHA-L and PHA-P with and without the addition of an anti-CD3 antibody. The conditions tested were as follows: non-induced, induced with PHA-L alone, induced with PHA-L in combination with the CD3 antibody, induced with PHA-P alone, induced with PHA-P in combination with the CD3 antibody and finally induced with the CD3 antibody alone. Cell counts were obtained 6 days after activation. Data is representative of one biological repeat and cell counts are reported as the mean ± SD of three technical replicates. *$p < 0.05$

In order to validate and optimize the new antibody-based activation method, a final set of experiments was performed. In addition to assessing cell proliferation, expression levels of the classical T cell activation marker CD25 were also investigated using flow cytometry. The possibility was considered that the isolated CD4 T cell population may need the influence of paracrine signals from other cell types present in the PBMNC pool to undergo effective activation. Therefore, the degree of activation in antibody treated $CD4^+$ T cells was compared with and without the addition of conditioned medium harvested from activated PBMNCs. Both these conditions were compared to non-activated control cells. All conditions were tested using three technical replicates per experiment and were repeated using three different donors (PB18, PB21 and PB22).

The results of the T cell activation experiment are illustrated in **Figure 4.20**. It appears that the anti-CD3/anti-CD28 antibody treatment does result in increased cell counts compared to the respective controls at both Day 4 (Control: $1.33x10^5 \pm 3.77x10^4$ vs AB only: $3.85x10^5 \pm 2.65x10^5$) and Day 6 (Control: $1.02x10^5 \pm 7.57x10^4$ vs AB only: $4.13x10^5 \pm 2.4x10^5$), although this difference is statistically non-significant due to the large inter-donor variability (**Figure 4.20a**). The addition of conditioned medium seems to increase the cell count marginally at Day 4 ($4.40x10^5 \pm 6.66x10^4$) and at Day 6 ($5.21x10^5 \pm 1.29x10^5$), but once again is not significantly different from either the controls or from antibody treatment alone. The variability in cell counts is much greater in the antibody-only samples than in the antibody treatment with conditioned medium. CD25 expression appears to increase dramatically for both the antibody-only (Day 4: 79.22% ± 13.19%, Day 6: 85.62% ± 3.85%) and combination treated cells (Day 4: 83.81% ± 3.86%, Day 6: 88.10% ± 2.79) when compared to the control (Day 4: 7.79% ± 3.46%, Day 6: 7.88% ± 6.53%), but the increase was not statistically significant (**Figure 4.20b**).

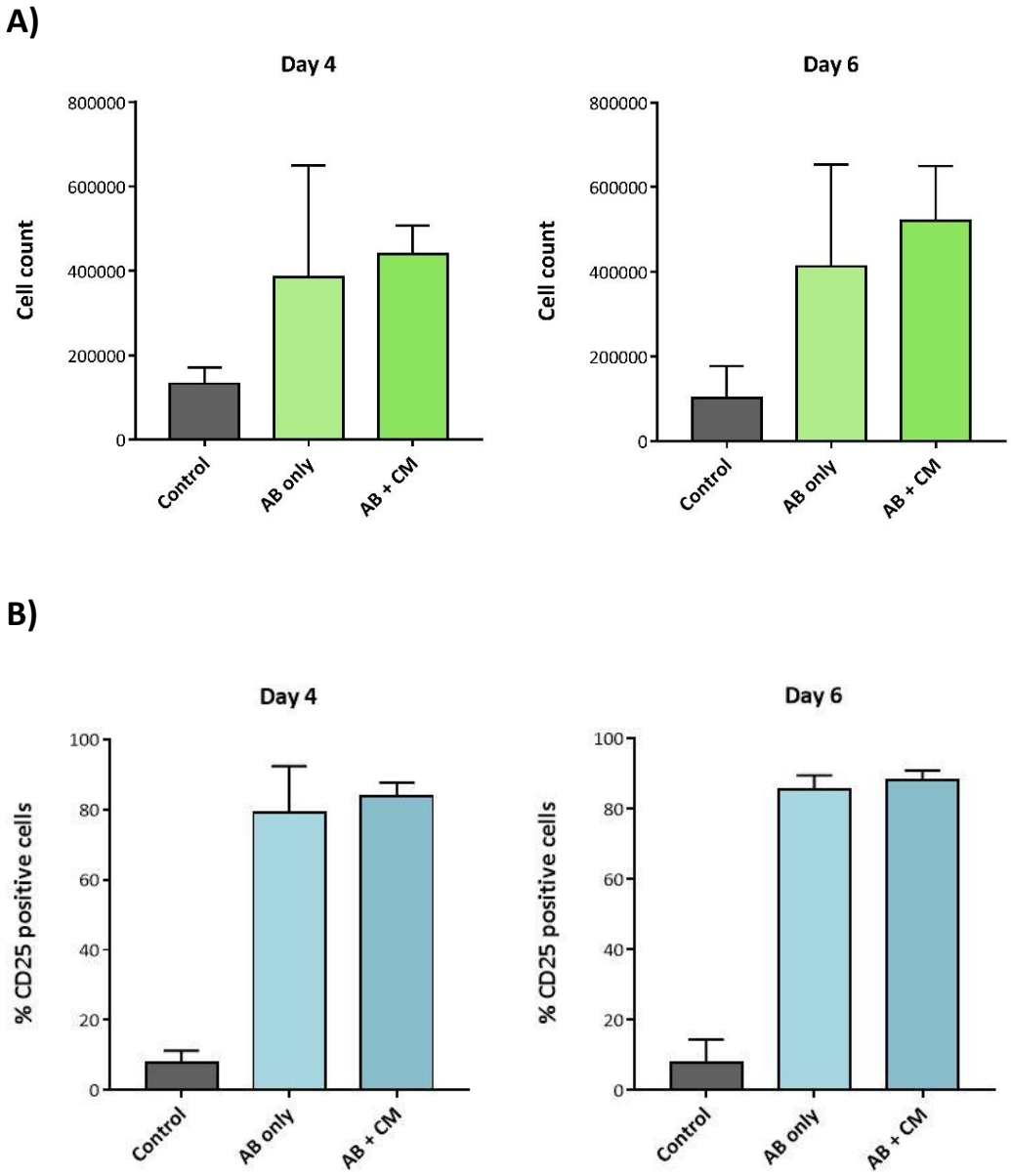

Figure 4.20: Results of T cell activation experiments, using anti-CD3 and anti-CD28 co-stimulation. The effects of using the anti-CD3/anti-CD28 antibody treatment alone (AB only) or in combination with conditioned medium treatment (AB + CM) were compared against a non-activated control. The assays were carried out 4 days and 6 days post-treatment. **A)** The results of the cell proliferation assay are presented as the mean cell count ± SD of three biological replicates. **B)** The results of CD25 expression analysis indicate the proportion of total T cells that were positive for CD25, expressed as the mean ± SD of three biological replicates.

4.2.2. CCR5 and CXCR4 co-receptor expression analysis

A flow cytometric analysis was carried out to determine what the effect of antibody-mediated activation was on the expression of the essential HIV co-receptors, CXCR4 and CCR5. The assay was performed at different time points during the culturing process to give a complete picture of the changes induced by activation. Firstly, the cells were analysed directly after isolation

and sorting, to establish baseline expression levels. After a 24 resting period and prior to activation, they were assayed once more to check for any changes induced by cell culture conditions. Finally, they were analysed after 7 days in culture, both with and without antibody-mediated activation. The results of this experiment are expressed as the mean ± SD of three biological replicates (PB32, PB33, PB34) (**Figure 4.21**).

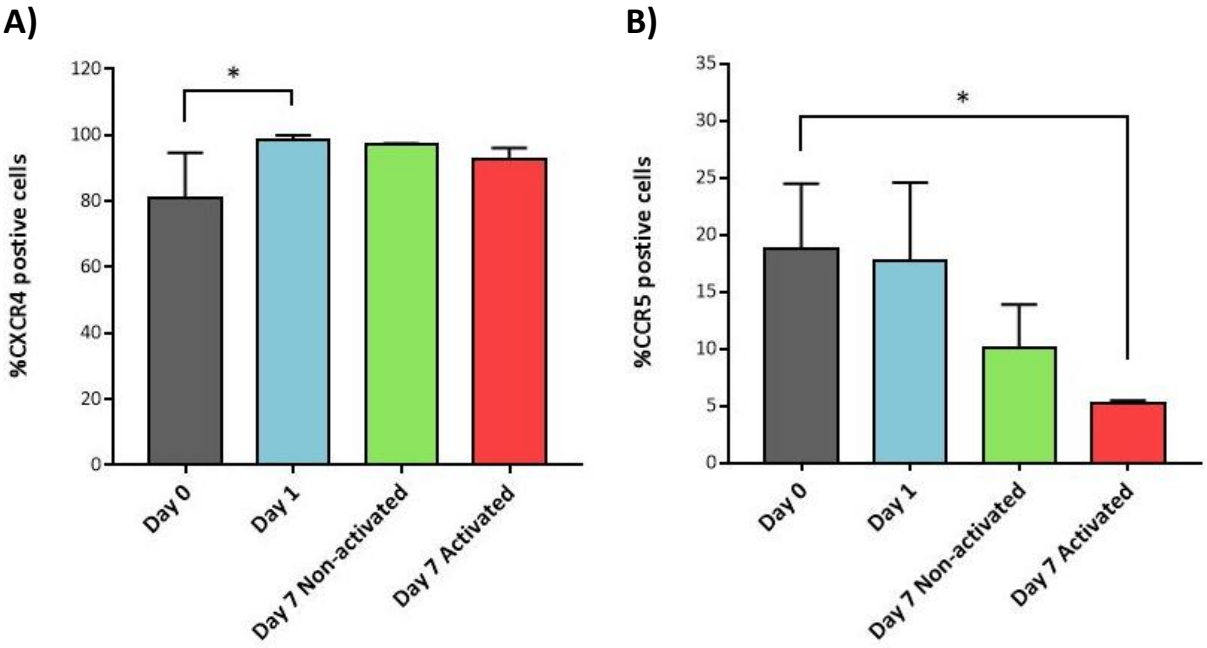

Figure 4.21: Analysis of expression levels of the HIV co-receptors CXCR4 and CCR5 on CD4$^+$ T lymphocytes at various time points during culture. A) The proportion of CXCR4$^+$ cells as determined by flow cytometry is indicated at three time points: Day 0 (directly after isolation; grey bars), Day 1 (pre-activation; blue bars) and Day 7 (post-activation; red bars). A Day 7 non-activated control is also included (green bars). **B)** The proportion of cells in the CCR5+ population was simultaneously determined under the same conditions. * p <0.05

The expression of CXCR4 was consistently high, even in the baseline Day 0 samples (80% ± 13.85%). There was a statistically significant increase (p-value = 0.0197) in expression from baseline to Day 1 prior to activation (98.62% ± 1.25%), indicating that the cell culture conditions appear to enhance CXCR4 expression. Both the activated (92.66% ± 3.40%) and non-activated Day 7 (97.14% ± 0.36%) samples show the same trend, although these increases were not statistically significant. The similarity in the Day 7 samples supports the hypothesis that the increase from baseline is independent of activation. The average CCR5 expression profile, on the other hand, started out much lower at 18.8% ± 5.69%. The proportion of cells expressing CCR5 decreased even further during culture. At Day 1, 17.74% ± 5.69% of activated T-cells expressed CCR5, which decreased to 10.09% ± 3.8% and 5.23% ± 0.24% (p = 0.0276) at

Day 7 for non-activated and activated T-cells respectively. The significant decrease observed in the Day 7 activated samples compared to Day 0 indicates that the activation method used inhibits CCR5 expression, independently of the cell culture conditions.

4.3. Differentiation and culture of monocyte-derived macrophages

4.3.1. Morphological examination of differentiated macrophages

The first indication that the macrophages had undergone differentiation successfully was though examination under a light microscope to check for any changes in their morphological features. As can be seen in **Figure 4.22**, the macrophages comprised a mixture of cells with round "fried egg" shapes as well as elongated spindle-shaped cells. This showed a clear change from the typical monocyte morphology observed immediately after plating, in which the cells were entirely rounded with no protrusions. There was little difference observed between cells treated with the two different cytokines.

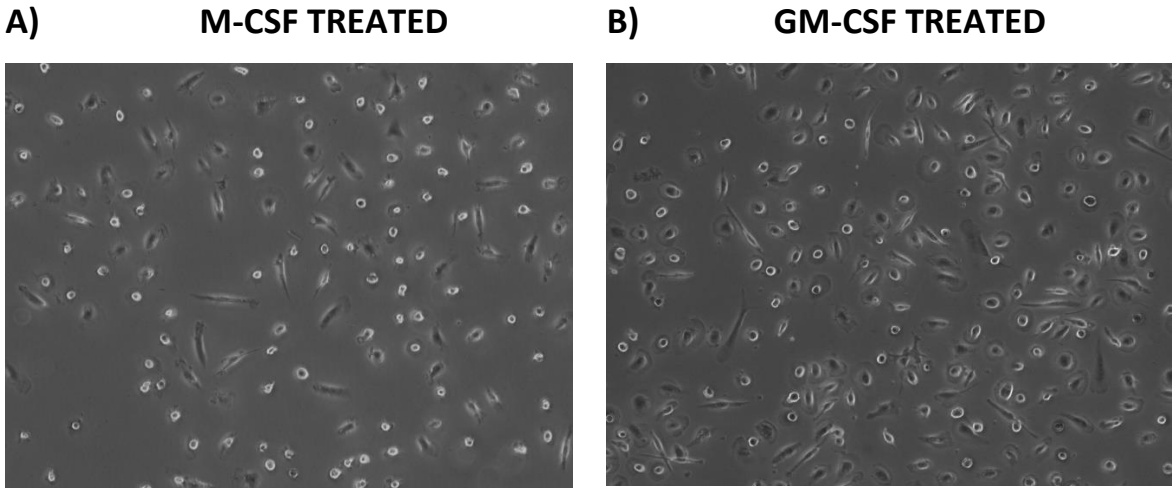

Figure 4.22: Light micrographs (5x magnification) of morphological changes observed in differentiated macrophages treated with A) M-CSF and B) GM-CSF.

4.3.2. Analysis of phagocytic potential of differentiated macrophages

The pHrodo™ assay was used as another indicator that the monocytes had successfully differentiated into functional macrophages. The phagocytic potential of monocytes differentiated under the influence of either GM-CSF or M-CSF were also compared. These two cytokines promote different macrophage activation pathways with specialized functions; therefore, it is possible that they may have different phagocytic capacities. Since HIV has been

reported to infect macrophages via phagocytosis (212), the efficiency with which they phagocytose may impact their susceptibility to infection. Differentiated macrophages were obtained from three different donors (PB28, PB31 and PB32), exposed to the pHrodo™ BioParticles™ and examined under a fluorescence microscope. In order to roughly determine the proportion of cells that took up the particles, five micrographs were taken of random fields for each condition at 10x objective magnification. The mean proportion of positively stained cells for each donor was determined for each by manual counting and averaging the results across the five replicates. The percent positivity was generally high, averaging 58.13 ± 36.90% for GM-CSF and 73.54% ± 20.21% for M-CSF treated cells across all donors (**Table 4.6**). Although the M-CSF treated cells seemed to respond better overall, there is no statistically significant difference due to the large sample-to-sample variation. A second set of micrographs was taken at 20x objective magnification for the purpose of illustration (**Figure 4.23**).

Table 4.6: Proportions of macrophages differentiated with either GM-CSF or M-CSF that stained positively for pHrodo™ BioParticles™

	GM-CSF TREATED		M-CSF TREATED	
Donor ID	**Mean % positive**	**SD**	**Mean % positive**	**SD**
PB28	17.04	9.14	50.38	19.14
PB31	88.43	12.25	82.64	6.25
PB32	68.91	19.43	87.59	7.66
AVERAGE	58.13	36.90	73.54	20.21

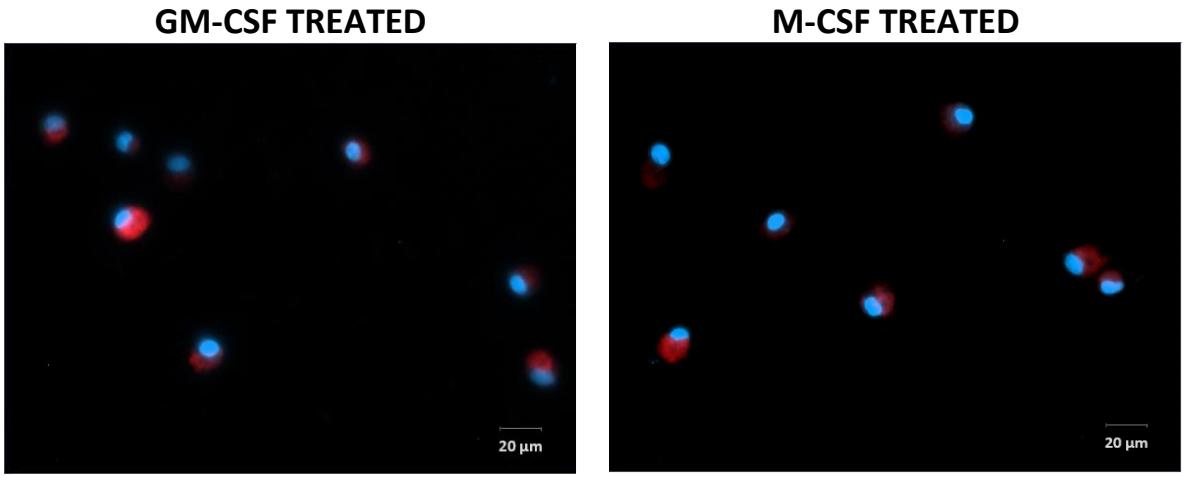

Figure 4.23: Representative fluorescence micrographs (20x magnification) from the pHrodo™ functional phagocytosis assay. Micrographs were taken of macrophages differentiated under the influence of either GM-CSF or M-CSF and then exposed to pHrodo™ BioParticles™. The nuclei were stained with either DAPI/VDC Violet, and thus appeared blue under the fluorescence microscope, while the BioParticles™ that have been phagocytosed appeared red. Areas of co-localization of red and blue staining thus represent macrophages that were capable of phagocytosis.

4.3.3. Immunophenotyping of differentiated macrophages

The reasons for performing characterization of surface marker expression on macrophages differentiated with either M-CSF or GM-CSF treatment were two-fold. Firstly, it was intended as a check to ensure that the cells were in fact expressing classic macrophage markers (CD14, CD16, CD64), and secondly it enabled comparison of HIV receptor (CD4, CXCR4, CCR5) expression levels between the two groups. It was reasoned that cells with increased receptor expression would be more susceptible to HIV infection and would thus be preferable for use in this study. The results of this experiment are illustrated in **Figure 4.24**. Although expression was not statistically significantly different between GM-CSF- and M-CSF-treated cells for any of the markers analysed, a few trends were observed. In terms of macrophage marker expression, it was found, as expected, that both CD14 and CD16 were extremely highly expressed in both groups of cells. CD64 expression was moderate, averaging 50.28% and 71.13% for GM-CSF- and M-CSF-treated cells respectively. While the levels were quite variable, both groups of macrophages expressed appreciable levels of these classical macrophage markers, indicating that the majority of the cells were behaving as expected following differentiation.

A high level of variability was also observed for the expression of HIV receptor molecules across the donors. However, the same trend of slightly higher levels in the M-CSF-treated cells compared to the GM-CSF-treated cells was observed. CD4 expression was variable but generally low in both groups, averaging 33.14% for the M-CSF-treated and 46.16% for the GM-CSF-treated cells. CXCR4 expression was low but not entirely absent, indicating a slight possibility that X4-tropic HIV strains might be able to infect these cells. As expected, CCR5 expression was much higher than CXCR4, reaching 88.4% in the M-CSF-treated cells. A brief analysis of the degree of co-expression of CD4, CCR5 and CXCR4 was carried out (**Table 4.7**). However, no clear patterns of reproducible co-expression emerged from this analysis. Overall, it would seem that the macrophages differentiated using M-CSF would have the greatest susceptibility to HIV-infection, particularly with an R5-tropic strain, although it is acknowledged that co-receptor expression is not the sole deciding factor for viral entry.

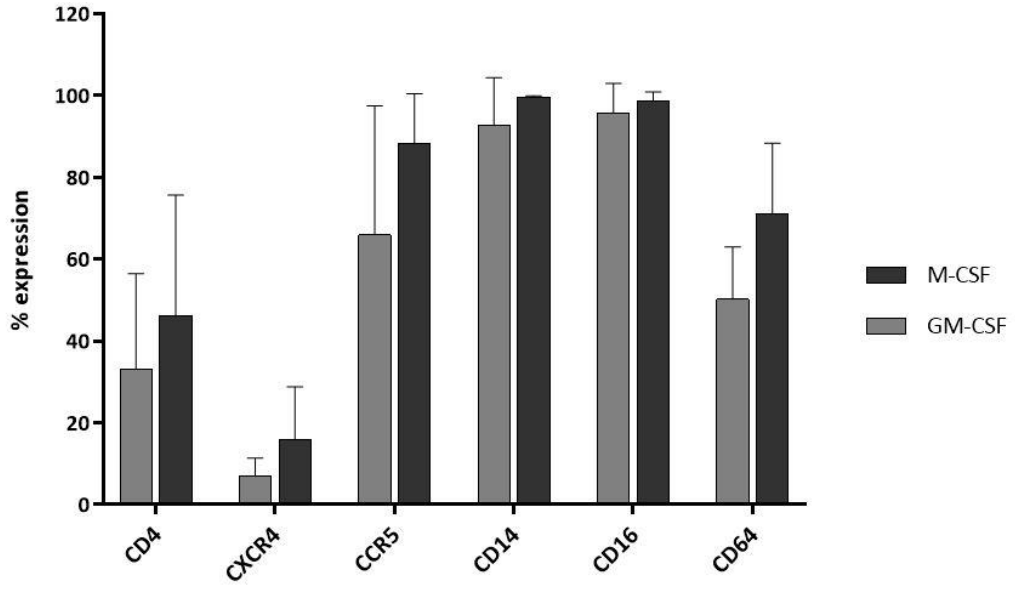

Figure 4.24: Results of immunophenotyping to determine of expression of surface markers on differentiated macrophages treated with either M-CSF or GM-CSF. Expression levels are indicated as the mean ± SD percentage of viable, $CD45^+$ macrophage that express the respective markers. Results are representative of 3 biological repeats.

Table 4.7: Co-expression of CD4, CXCR4 and CCR5 in macrophages differentiated with either GM-CSF or M-CSF

	GM-CSF TREATED			M-CSF TREATED		
Donor ID	**% $CD4^+$ $CCR5^+$**	**% $CD4^+$ $CXCR4^+$**	**% $CXCR4^+$ $CCR5^+$**	**% $CD4^+$ $CCR5^+$**	**% $CD4^+$ $CXCR4^+$**	**% $CXCR4^+$ $CCR5^+$**
PB32	31.16	12.95	92.7	36.99	15.92	95.05
PB33	20.78	5.45	18.1	5.1	0.63	3.21
PB34	61.45	4.27	6.94	78.78	9.67	15.99
MEAN	37.80	7.56	39.25	40.29	8.74	38.08
SD	21.13	4.71	46.63	36.95	7.69	49.75

4.4. Infection of target cells with HIV-1

4.4.1. Optimization of MOI for infection of $CD4^+$ T lymphocytes

A critical parameter to optimize for infection studies is how much virus to add to the target cells, since too much virus will result in cell death, while too little will result in sub-optimal infection. In order to determine the ideal MOI (i.e. the ratio of infectious virus particles to target cells), activated $CD4^+$ T lymphocytes from four different donors (PB28, PB35, PB36 and PB37) were infected with varying amounts of CM9 viral stock (MOI = 1, MOI = 2, MOI = 4). The proportion of HIV positive cells was measured using the KC57 intracellular p24 flow cytometric assay at 48 h post-infection. The response to infection is expected to be highly donor-dependant; therefore, the percent HIV positive values were not only reported as an averaged percentage across donors, but also as the individual results obtained for the three donors, as is illustrated in **Figure 4.25**. The percent HIV+ was very low across all donors. This is not entirely unexpected since the experiment was performed with primary cells and using viral stocks with a relatively low concentration of infectious virus particles. In each donor, there is a definite trend towards increasing percent HIV positivity with increasing MOI, although in some donors this difference is almost negligible, and it was not statistically significant. The first donor, which appears to have a greater susceptibility to infection than the others, illustrates this trend best with a maximum of 3.82% HIV+ cells when using an MOI of 4. Although this data suggests that an MOI of 4 gives the highest percent infection, it was noted during data acquisition that cells treated with higher MOI tended to have greatly

decreased viability. It was thus decided that an MOI of 2 should give sufficiently high levels of infection without causing excessive cell death.

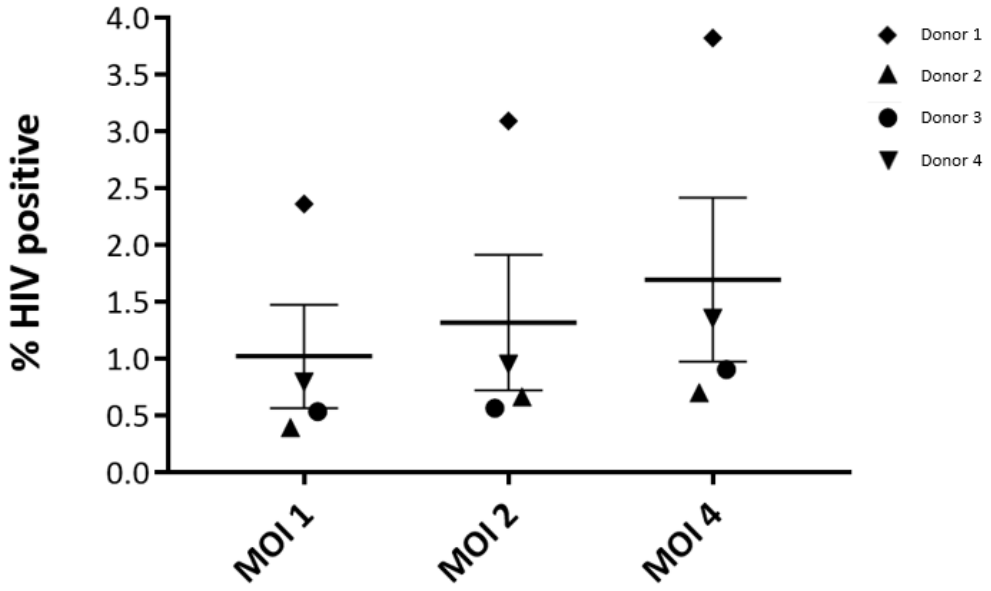

Figure 4.25: Results of KC57 intracellular p24 assay to determine optimal MOI for infection of activated CD4$^+$ T lymphocytes. The percent HIV positive cells detected 48 hours after exposure to HIV at three different MOIs is reported as the mean ± standard error of the mean (SEM) of 4 biological replicates (horizontal bars). The values for each donor are represented by individual symbols with different shapes for each donor.

4.4.2. Analysis of infection kinetics of CM9 and SW7 in CD4$^+$ T lymphocytes

Once the optimal MOI was determined, the next step was to decide on optimal time points at which to collect RNA samples for gene expression analysis. The ideal time point would fall within a window period in which the target cells are viable, with detectable HIV that is intracellular and integrated into the host cell. To assist in this decision, an experiment was designed to assess the infection kinetics of the two HIV isolates to be used: CM9 and SW7. Activated CD4 T lymphocytes were exposed to HIV using an MOI of 2 and assayed for the presence of HIV at 6 h intervals over a 48 h period. Both p24 ELISA and PCR were used for HIV detection. For the p24 ELISA, two aliquots were assayed at each time point: an aliquot containing both cells and supernatant, and a second aliquot in which the cells and supernatant were separated by centrifugation. The resulting three samples were then assayed separately, which allowed discrimination between p24 still in the host cell and p24 which had been released into the cell culture medium. An additional aliquot of infected cells

was collected for DNA extraction and subsequent PCR analysis. The assay was performed in duplicate for CM9 but could not be replicated in SW7 due to extensive syncytium formation and rapid cell death. An illustration of the syncytia observed during the second replicate of the experiment is presented in **Figure 4.26.**

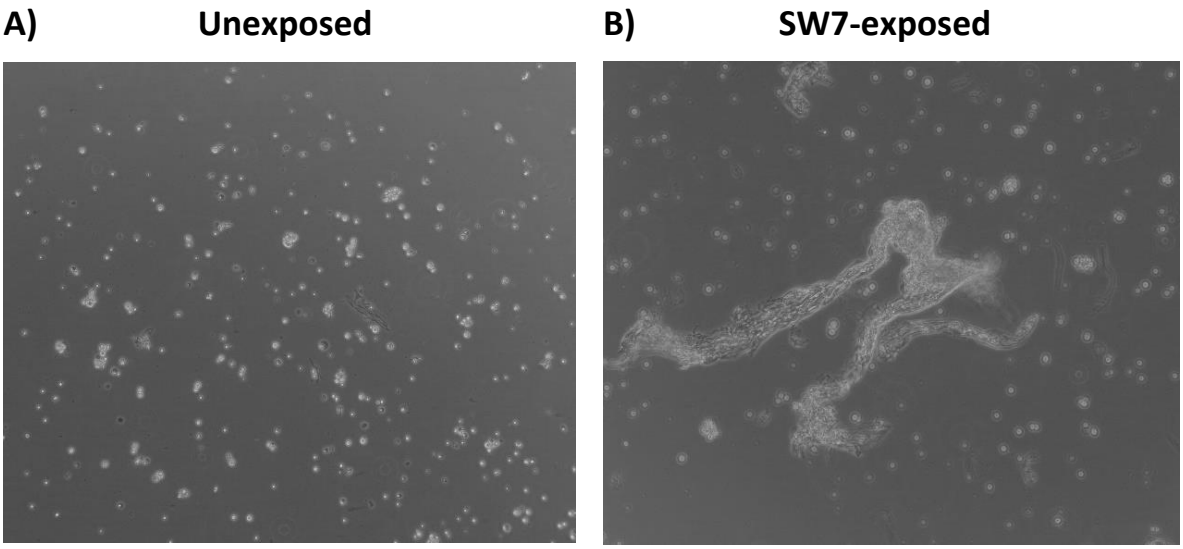

Figure 4.26: Light micrographs (20x magnification) illustrating syncytium formation in activated $CD4^+$ T lymphocytes following exposure to the HIV isolate SW7. A) Control cells that were not exposed to SW7 demonstrate a scattered pattern of mainly single cells with a few small cell clumps. **B)** Cells exposed to SW7 formed long twisted structures comprising large numbers of cells fused together (syncytia).

The results of the p24 ELISA component of the experiment are presented in **Figure 4.27**. For CM9, the two replicates appear to have responded in a similar fashion, although the first replicate appears to have been more successful in terms of p24 production. As expected, the majority of p24 signal appears to come from the supernatant in both cases, although some intracellular p24 is detectable. Both seem to indicate a progressive increase in p24 over time, although in the first replicate there are dips at 18 h, 24 h and 42 h post-infection. Given that the same dips are not observed in the second replicate, it seems that they are artefactual, most likely due to the fact that there were two groups of samples which were infected at staggered start times in the first replicate, for ease of sample collection (Group 1 time points: 6 h, 12 h, 30 h, 36 h, 48 h; Group 2 time points: 18 h, 24 h and 42 h). The overall signal intensity is lower in the second replicate, perhaps indicating a more resistant donor. Taking both replicates into consideration, it seems that p24 signal starts to increase from around 24 h onwards and peaks at 48 h. The p24 signal for the SW7 experiment is more erratic and difficult to interpret. However, it does seem that there is a peak of intracellular p24 at 24 h followed

by a peak in the supernatant at 30 h, which might be indicative of infected cells completing a lytic cycle at this time point.

The results of the PCR component of the infection kinetics experiment are presented in **Figure 4.28**. In the first replicate for isolate CM9, HIV was detected with extremely faint bands appearing at 24 h to 42 h and a clearer band observed at 48 h. This correlates well with the p24 ELISA data, indicating a gradual increase peaking at 48 h (**Figure 4.28**). For both the second CM9 replicate and SW7, the PCR is clearly negative at all time points, indicating that infection was below the detection limit for the PCR despite the apparent positivity in the p24 ELISA assay. It appears that the p24 ELISA was slightly more sensitive than the PCR, perhaps because the input number of cells used for DNA extraction was too low. Based on these results, the time points decided on for analysis of CM9-infected cells were 36 h and 48 h post-infection. SW7 was problematic, since no clear PCR detection was achieved and the p24 profile was not definitive. Additional replicates could not be performed, because this strain is extremely cytotoxic. Within a few hours of exposure, it caused the formation of massive syncytia which lysed very rapidly, making further analysis impossible.

A)

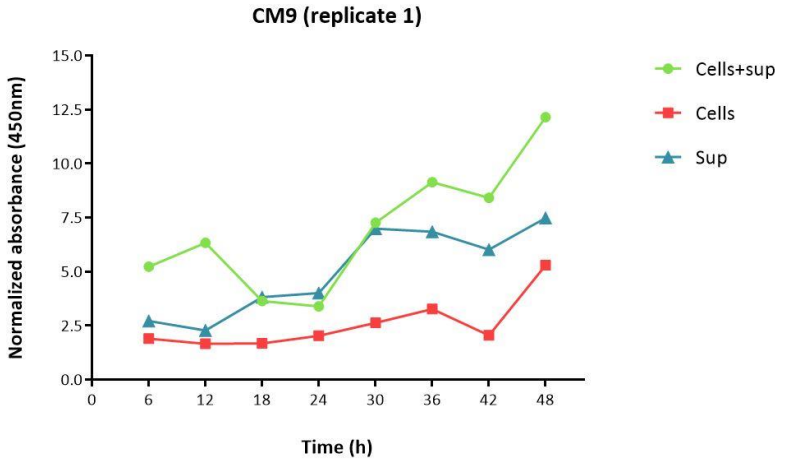

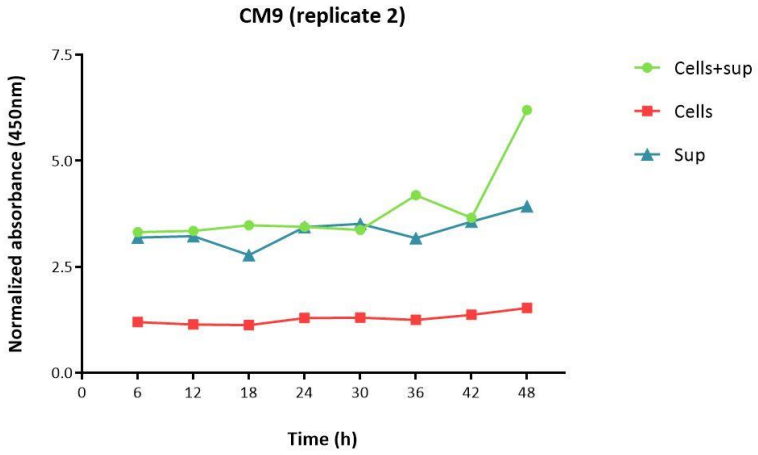

B)

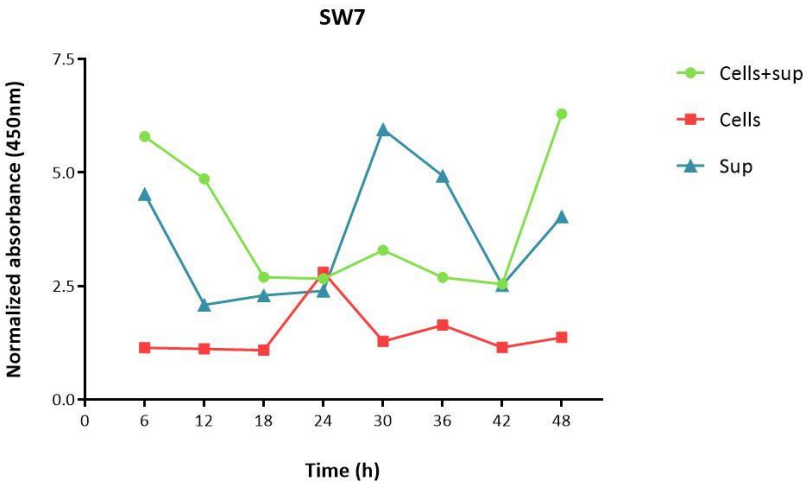

Figure 4.27: Results of the p24 ELISA for HIV detection to determine the infection kinetics of A) CM9 and B) SW7. Three different samples types were assayed at each time point: combined cells and supernatant (cells+sup), cells only (cells) and supernatant only (sup). The p24 signal is reported as the absorbance measured at 450 nm, normalized to an HIV negative control collected at 48 h post-infection. Note: the scale of the axes for CM9 (replicate 1) is different to the other graphs since the p24 signal was generally much higher.

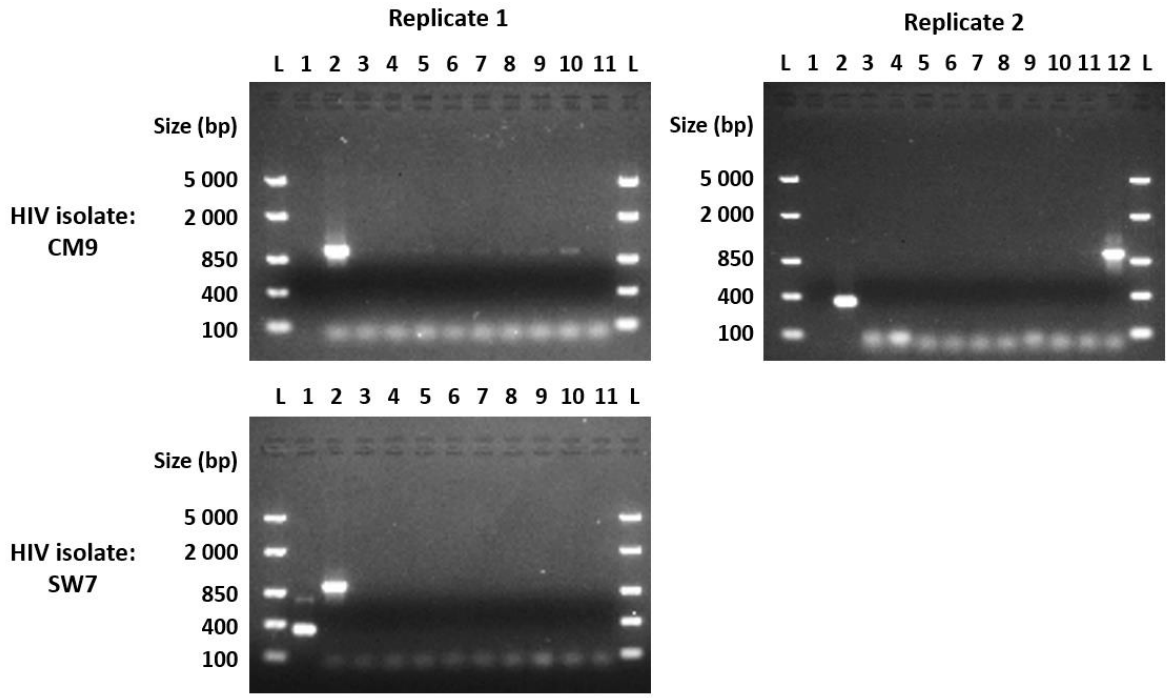

Figure 4.28: Results of PCR-based detection for the determination of the infection kinetics of CM9 and SW7. In replicate one, both strains were analysed on a single gel, while in replicate two only CM9 was used. **Replicate 1 CM9:** L = ladder, 1 = No template negative PCR control, 2 = CM9 HIV+ GHOST cell control, 3-10 = CM9 HIV+ T cells (6h, 12h, 18h, 24h, 30h, 36h, 42h, 48h), 11 = CM9 HIV- T cell control. **Replicate 1 SW7:** L = ladder, 1 = L32 positive PCR control, 2 = SW7 HIV+ GHOST cell control, 3-10 = SW7 HIV+ T cells (6h, 12h, 18h, 24h, 30h, 36h, 42h, 48h), 11 = CM9 HIV- T cell control. **Replicate 2 CM9:** L = ladder, 1 = No template negative PCR control, 2 = L32 positive PCR control, 3-10 = CM9 HIV+ T cells (6h, 12h, 18h, 24h, 30h, 36h, 42h, 48h), 11 = CM9 HIV- T cell control, 12 = CM9 HIV+ GHOST cell control.

4.4.3. Susceptibility of macrophages to infection

Once it had been established that the MDM were expressing the correct cell surface molecules and were indeed capable of phagocytic activity, their susceptibility to HIV challenge was investigated. Macrophages from four independent donors (PB34, PB35, PB36, and PB37) were differentiated under the influence of either GM-CSF or M-CSF and were subsequently exposed to the HIV isolate CM9 at an MOI of 4. After 48 hours, the proportion of HIV-infected cells was determined using the KC57 intracellular p24 assay (**Figure 4.29** & **Figure 4.30**). The percent positivity was extremely low in all donors even at this relatively high MOI, indicating that the efficiency of infection was extremely poor. Only one of the M-CSF-treated samples (Donor PB36) showed definitive evidence of infection, in which the infected cells appear as a distinct population comprising 1.11% of the viable macrophages. However, even in this

sample, the absolute number of infected cells was extremely low. Since the infection efficiency was so low using the dual-tropic isolate CM9 and no R5-tropic primary isolates were available to use instead, no further infection experiments were carried out using macrophages.

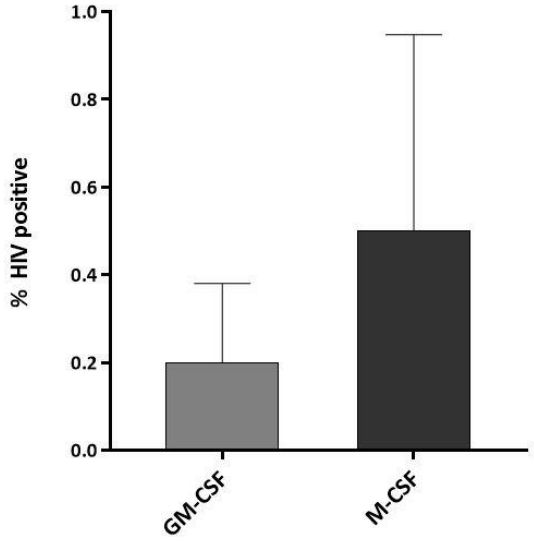

Figure 4.29 : Results of KC57 intracellular p24 assay to determine infection efficiency in macrophages differentiated using either GM-CSF or M-CSF. The percentage of viable macrophages identified as HIV positive is reported as the mean ± SD for four biological replicates.

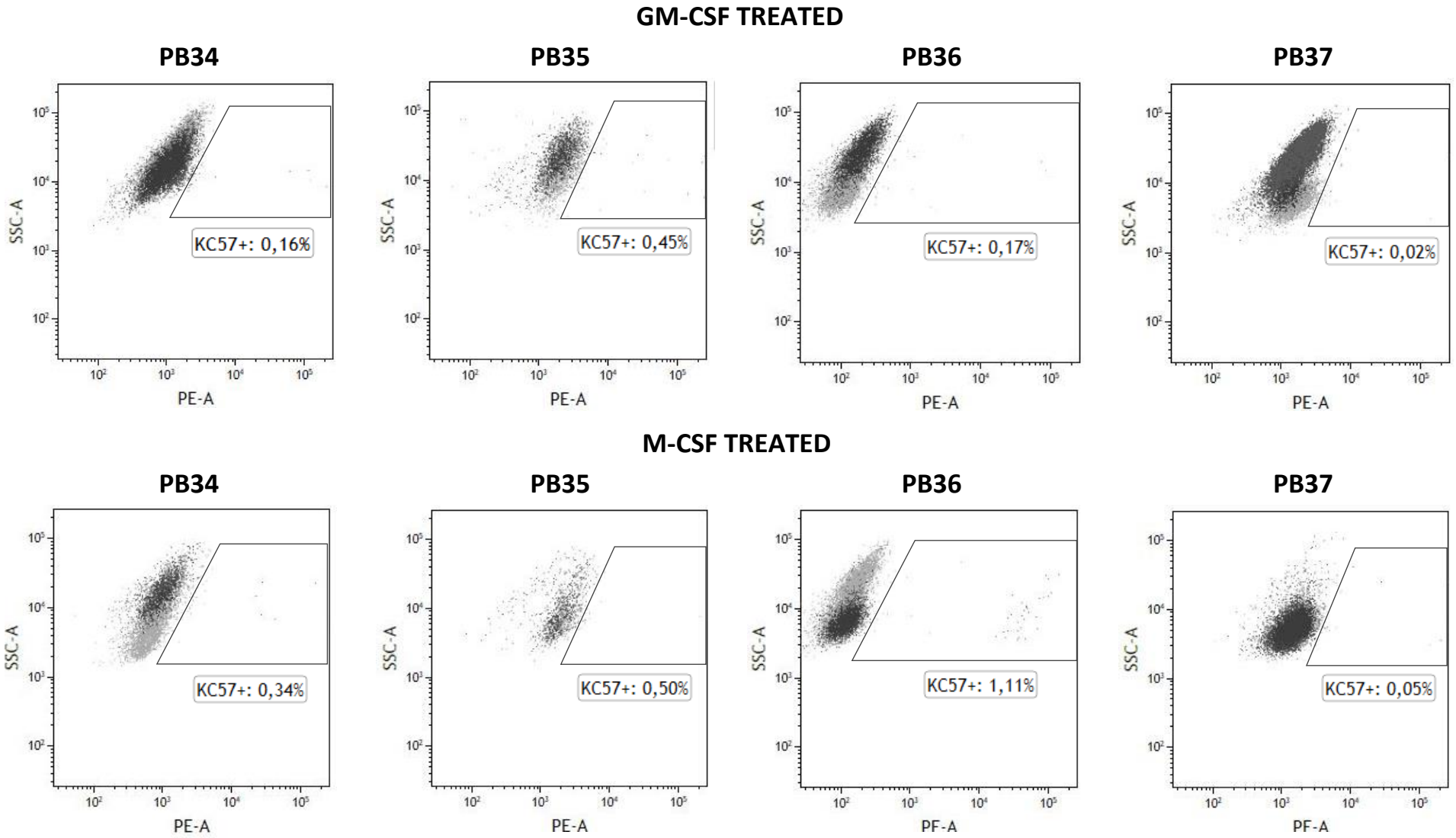

Figure 4.30: Results of KC57 assays to determine the extent of infection in MDMs from 4 donors (PB34, PB35, PB36, PB37) treated with either GM-CSF or M-CSF during differentiation. Overlay two-parameter plots of SS Log vs PE Log (KC57) are used to compare KC57 positivity of the uninfected control (light grey) to that of the sample exposed to HIV at an MOI of 4 (dark grey) for each condition. The percent positive cells observed in the exposed sample is indicated below the "KC57+" region.

5. Discussion and Conclusions

The first component of this chapter was the optimization of the PBMNC isolation protocol and a FACS-based strategy to separate populations of $CD4^+$ T lymphocytes and monocytes. The sorting strategy used took advantage of the fact that the combination of the two markers CD4 and CD14 is sufficient to distinguish between the two populations of interest. Immunophenotyping of the PBMNCs revealed that CXCR4 and CCR5 were present in both the $CD4^+$ T lymphocyte and monocyte populations, though CXCR4 was much greater in T cells than monocytes, while the reverse was true of CCR5. In both cases, however, the expression levels were highly variable across different donors. The rest of the chapter focussed on optimizing cell culture conditions to ensure maximum susceptibility of the target cells to HIV. Two common $CD4^+$ T cell activation methods were investigated, since activation is predicted to enhance HIV infection. In addition, though the differentiation of the monocytes into MDM was performed using well-established protocols, we decided to perform additional characterization of the differentiated cells to determine the effects of differentiation and whether they might impact HIV infection.

Several different approaches can be used to activate $CD4^+$ T lymphocytes, as outlined in the beginning of this chapter. However, as showed in our experiments, mitogens like PHA do not always work well in a pure $CD4^+$ T cell populations due to the lack of accessory cells that assist activation by providing co-stimulatory signals (202,204). There is also some evidence that PHA-mediated activation can result in functional impairment of the $CD4^+$ T cells in their ability to respond to further antigenic stimulation (211), which is not ideal for infection studies aimed at investigating the response to viral exposure. Since PHA-mediated activation yielded suboptimal results in our preliminary experiments, activation with anti-CD3/anti-CD28 antibodies was investigated as an alternative. This method is believed to be a more physiologically relevant model than mitogenic activation (202,211), since it provides specific stimulation to the TCR-CD3 complex in addition to co-stimulation via binding to the CD28 molecule, as occurs during activation mediated by an antigen-presenting cell *in vivo*. This method was highly effective and was able to induce both cell proliferation and upregulation of the activation marker CD25 (**Figure 4.20**). Although no significant increase in activation was

observed when the antibody-treatment was supplemented with conditioned medium, it did reduce variability in the cell proliferation assay.

Once the activation protocol was fully optimized, changes in co-receptor expression of $CD4^+$ T lymphocytes in response to activation were investigated since this has important implications for susceptibility to infection. The effect of activation on the expression of CXCR4 and CCR5 as reported in literature appears to be largely dependent on the type of activation stimulus used. Studies in which stimulation was achieved using the mitogen PHA supplemented with IL-2 demonstrated robust upregulation of CXCR4 cell surface expression (213–215). PHA appears to have no effect on CCR5 expression in isolation (213), but in the presence of IL-2, an increase in cell surface expression was observed (213–215). The reported effects of stimulation with anti-CD3/anti-CD28 coated beads on CXCR4 are contradictory. Carroll and colleagues (1997) observed increased CXCR4 transcript expression during CD3/CD28 antibody-mediated activation(216), while Riley and colleagues (1998) reported decreased cell surface expression of the CXCR4 protein (214). These results may indicate that there are levels of post-transcriptional regulation affecting cell surface expression. In contrast to PHA-activated cells, CCR5 expression in cells activated with anti-CD3/anti-CD28 coated beads was downregulated on the cell surface (214), and undetectable on the transcript level (216). The use of anti-CD3 and anti-CD28 antibodies immobilized on a cell culture plate yields similarly contradictory findings. One study found that there was downregulation of CXCR4 when both antibodies were used simultaneously (217), while a second group reported upregulation (218). CCR5 expression was reported to be unchanged compared to unstimulated cells using the combined immobilized antibody approach (217).

Schweighardt and colleagues (2004) performed a study using plate-bound anti-CD3 in combination with soluble anti-CD28 (215), as was used in this chapter. This study demonstrated that CXCR4 expression was constitutively high and approached 100% expression upon stimulation (215). CCR5 expression was shown to be much lower than CXCR4, but also increased slightly when the cells were activated (215). We also found that CXCR4 expression was high in freshly isolated cells and increased further at later time points. However, our data seems to suggest that this increase is an artefact of the *in vitro* culture conditions rather than as a result of activation, since it was observed in both the unstimulated Day 1 and Day 7 controls as well as in the stimulated cells (**Figure 4.21**). In addition, our results

for CCR5 expression seem to contradict the findings of the Schweighardt study (215), since a statistically significant decrease in expression was observed between the freshly isolated cells and the Day 7 activated cells. This is more consistent with the results observed in the previously discussed studies that used anti-CD3/anti-CD28 beads or used immobilized anti-CD3 in combination with immobilized anti-CD28, in which CCR5 expression was generally unchanged or lowered upon activation (214,216–218).

Clearly there are many factors influencing CXCR4 and CCR5 expression in response to activation, leading to a lack of agreement among *in vitro* studies, even when the same activation stimulus is used. Some authors have proposed alternate approaches to obtain a more clinically relevant picture using models approximating the *in vivo* response better. Maier *et al.* (203), for instance, used a system in which T cells were activated by exposure to Staphylococcal enterotoxin b (SEB) in the presence of autologous monocytes which serve as antigen-presenting cells. They determined that the expression of both CXCR4 and CCR5 are upregulated using this system. Ebert and colleagues (2002) also observed increases in CCR5 expression, using an allogeneic mixed lymphocyte reaction (MLR)-based system to induce activation (219). If these findings are indeed a true reflection of the *in vivo* response, it would be consistent with the long-standing hypothesis that activation promotes HIV susceptibility and provides a mechanism by which $CD4^+$ T lymphocytes can be readily infected with R5-tropic strains. It does however raise concerns that the lowered CCR5 expression observed in our experiments could be an artefact of the activation strategy used and thus not a physiologically relevant phenomenon.

In this study, two approaches were used to confirm the success of the differentiation of cultured monocytes to macrophages: a functional phagocytosis assay and immunophenotyping by flow cytometry. The pHrodo™ assay used for the determination of phagocytic ability following differentiation clearly demonstrated that both the M-CSF-treated and GM-CSF-treated MDMs retained their ability to phagocytose pHrodo™ BioParticles™. We did not observe any statistically significant difference in the proportion of cells that took up particles when comparing M-CSF- to GM-CSF-treated cells, although the average was slightly higher for the M-CSF-treated cells. Previous studies seem to indicate that M2-like macrophages induced with M-CSF have greater phagocytic abilities (220,221), which correlates with the trend observed in our results.

In hindsight, the panel of macrophage markers used for immunophenotyping, while somewhat useful for confirming that the cells were of the monocyte/macrophage lineage, could have been improved to give more informative results. The main problem with this panel is that it does not provide definitive evidence of differentiation since CD14, CD16 and CD64 can all be expressed by both macrophages and various subsets of monocytes (137,222,223). Monocyte subsets are defined based on CD14 and CD16 expression and are as follows: classical (CD14+CD16-), non-classical ($CD14^{low}$ CD16+) and intermediate (CD14+CD16+) (137,222). The classical subset is the most common, comprising approximately 80-90% of peripheral blood monocytes, while the non-classical comprises the larger portion of the remainder (137,222). Since the non-classical monocytes do not strongly express CD14, they would have been excluded during sorting for experiments, leaving behind only a very small proportion of CD16+ intermediate monocytes. The fact that our results indicated CD16 expression in over 90% of both the M-CSF-treated and GM-CSF-treated cells therefore provides indirect evidence that the cells have differentiated into CD16+ macrophages from a predominantly CD14+CD16- classical monocyte population. However, use of macrophage-specific differentiation markers which are not expressed on monocytes would have been preferable for use in this panel and should be considered in future studies.

Another challenge was that the selected panel was not optimal for differentiation between different macrophage subsets. CD14 is not known to be differentially expressed by macrophages polarized with M-CSF compared to GM-CSF. Indeed, our results showed that the expression profiles were uniformly high across both groups. CD16 has been reported to be more highly expressed on M-CSF-treated cells compared to GM-CSF-treated cells (224), which was contrary to our observations in which it was highly expressed on both. CD64 on the other hand, has been proposed as a potential marker for M-CSF polarized macrophages in which it is generally highly upregulated (221,224,225). Our results for CD64 expression appeared to be consistent with these findings, since only 50% of the GM-CSF-treated cells were positive, compared to 71% of the M-CSF-treated cells. In future, other markers could be included in the panel to increase its power to resolve the two groups, such as CD206 (upregulated in GM-CSF-polarized cells) and CD163 (upregulated in M-CSF-polarized cells) (224).

During optimization of the macrophage culture protocol, monocytes induced to differentiate using either M-CSF or GM-CSF were compared for any differences that might have influenced their response to infection by investigating the relative expression profiles of CD4, CXCR4 and CCR5. We found that expression of CD4 was relatively low for both M-CSF- and GM-CSF-treated cells, which is unsurprising since monocytes have been shown to undergo reduction in cell surface expression of CD4 during differentiation into macrophages (205,226,227). MDM that are differentiated without any additional growth factors are reported to downregulate CXCR4, while upregulating CCR5 (205,207,228). According to literature, the expression levels of both CXCR4 (145) and CCR5 (145,206) are expected to increase under the influence of M-CSF. On the other hand, GM-CSF has been reported to lower CXCR4 expression (145) and increase CCR5 expression, although the effect is not as pronounced as for M-CSF (145,206). Our results indicated that CXCR4 expression was generally noticeably lower than CCR5 expression, with the M-CSF-treated cells displaying consistently higher levels of both co-receptors than the GM-CSF-treated cells. The lower levels of CXCR4 in GM-CSF- compared to M-CSF-treated cells and the higher levels of CCR5 in M-CSF- compared to GM-CSF-treated cells are therefore in agreement with what was reported in other studies.

The next step was the optimization of the infection protocol to be used when exposing the respective target cell types to HIV. $CD4^+$ T lymphocytes are well known as the primary target host cell of HIV *in vivo* and are therefore expected to be highly susceptible to infection. However, the frequency of productive infection in primary $CD4^+$ T cells is much lower than in cell lines (**Table 4.8**). Our results at 48 h were most comparable with those of Imbeault and colleagues (2012), who achieved infection levels of only 5.8% at the same time point, using a modified X4-tropic laboratory strain (44). The infection efficiency was further decreased in our study due to the use of primary viral isolates with low infectivity. During optimization experiments, the highest observed percent KC57 positive $CD4^+$ T lymphocytes was only 3.82%. While this is not entirely surprising given the circumstances, it did raise concerns about whether a microarray analysis performed using bulk RNA from these cells would be able to detect changes in gene expression from such a small population of infected cells. In the study by Imbeault and colleagues (2012) this problem was overcome through use of a reporter virus strain that enabled enrichment the sample for HIV-infected cells (44). This was unfortunately not possible in the present study, since our primary isolates carry no such reporter, and there

are currently no cell surface markers available to enable FACS-based sorting of infected cells without prior fixation and permeabilization, as for the KC57 assay.

Table 4.8: Previously reported infection efficiencies in CD4⁺ T lymphocytes using various HIV-1 strains/HIV-1-based constructs

Ref	HIV strain	CD4⁺ T cell source	Time P.I.	Infection efficiency
(115)	NL4-3-based vector (VSV-G)	Primary	36 h	23-32%
(229)	HIV-1-BAL (VSV-G)	Primary	72 h	50-60%
(229)	HIV-BAL	Primary	72 h	10-20%
(44)	NL4-3 BAL-IRES-HSA	Primary	24 h	1.1%
			48 h	5.8%
			72 h	6.6%
(105)	NL4-3-based vector (VSV-G)	Cell line (SupT1)	36 h	93%
(115)	NL4-3-based vector (VSV-G)	Cell line (SupT1)	36 h	93%
(103)	HIV-1-LAI	Cell line (CEM-CCRF)	48 h	80%
(106)	HIV-1- NL4-3	Cell line (Jurkat)	48 h	70%
(104)	HIV-1-LAI	Cell line (CEM-GFP)	24 h	29%
			48 h	86%
			72 h	92%
(136)	HIV-1-SF33	Cell line (HUT78)	48 h	85.3%
			72 h	96.2%

P.I. = post-infection. (VSV-G) = VSV-G pseudotyped strain.

The infection kinetics experiment was critical for the selection of time points at which to perform gene expression experiments. As demonstrated in the previous chapter, different viral strains do have very different replication dynamics and effects on cell viability. Therefore, it was necessary to determine how our target cells responded to CM9 exposure over time. For the purposes of the downstream microarray experiments, the sample needs to contain a sufficient number of viable cells after infection in order to allow for the extraction of RNA. The optimisation experiment therefore assisted in the identification of the earliest point at which observable infection can be expected, without overly compromising sample viability. The detection of infection at 24 h to 42 h using PCR was not wholly convincing and was only clearly demonstrated at 48 h post infection. In the p24 ELISA, infection was observable from 24 h onwards. Taking the results from both methods into account, time points of 36 h and 48

h were selected. At 48 h, infection is definitively observed with both methods, but cell viability might be reduced. At 36 h there is a good chance of picking up infection (since the p24 ELISA is positive) and viability should be improved, but there is a risk that it may not be clearly PCR-positive.

One of the challenges encountered when working with the X4-tropic isolate SW7 was the formation of massive syncytia in the target $CD4^+$ T cells. Syncytium induction is a well-documented phenomenon, in which exposure to HIV particles results in fusion of $CD4^+$ T cells into a large multinucleated structure (230,231). It is postulated that this is most likely the result of interactions between CD4 and the fusogenic gp120 envelope glycoprotein of virus particles coating the target cell surface (231,232). When large quantities of both these molecules are present, interactions occur between adjacent cells causing fusion of their cell membranes. We believe that syncytium formation was greatly exacerbated when using this particular virus stock since it is a primary isolate with a large number of non-infectious virus particles present. These particles, while not enumerated during titration and therefore not accounted for in the MOI calculation, are still present and possess gp120 molecules that may still be fusogenic. The target cells comprise a pure population of T lymphocytes with plentiful CD4 on their cell surfaces. Furthermore, they have been activated and will therefore form closely packed clusters of cells during expansion. The combination of these factors leads to the creation of an environment that promotes extensive syncytium formation, which renders the cells extremely fragile and prone to cell lysis (230). As a result, we could not recover enough viable cells following exposure to SW7 to perform further experiments.

The factors affecting the susceptibility of macrophages to infection are not fully understood, but a few key points have emerged. Firstly, macrophages have been shown to be more susceptible to infection than undifferentiated monocytes. It has been clearly established that as monocytes differentiate, CCR5 is upregulated, causing a concurrent increase in the susceptibility of these cells to infection with CCR5-tropic strains (205–207). It has also been demonstrated that differentiation into macrophages is correlated with decreased expression of host restriction factors such as APOBEC3G and APOBEC3A (147), as well as reduced expression of anti-HIV microRNAs (146). Secondly, polarization of macrophages can lead to both enhancement or inhibition of susceptibility, depending on the type of stimulation and the state of the macrophages upon infection (139). It should be noted that stimulation with

GM-CSF or M-CSF alone does not lead to full polarization in the absence of additional stimuli, but rather initiates differentiation towards M1-like and M2-like phenotypes respectively. These stimuli include IFN-γ, TNF-α and LPS for M1 macrophages, and IL-4/IL-13 for M2 macrophages (139). Some studies have found that unpolarized and M-CSF or GM-CSF-stimulated macrophages were highly susceptible to infection (233), while stimuli that promote full polarization to M1 or M2 types (such as IFN-γ and IL-4 respectively) seem to impose blocks to viral replication (138,233).

Despite our best efforts to improve the susceptibility of the macrophages used in this study, we were unable to achieve reproducible infection with CM9. Since there is no clear reason for the cells to not be susceptible, we suspect that it may be due to the virus itself. Our immunophenotyping experiments indicated extremely low CXCR4 expression in the differentiated macrophages, which would be problematic if our dual-tropic HIV isolate has a much greater preference for CXCR4 than CCR5 or has undergone a complete tropism switch. To confirm whether this is the case, we would have to sequence or re-screen the virus to determine co-receptor usage. Unfortunately, this would have been too time-consuming, and we did not have any stocks of CCR5 virus to use instead, forcing us to abandon further work in this cell type for the time being. This is, however, an important consideration for future studies and it is recommended that the tropism of primary viral isolates should be verified at regular intervals.

The purpose of this chapter was to develop cell culture protocols for $CD4^+$ T lymphocytes and macrophages, and to optimize their susceptibility to infection. Unfortunately, since the macrophages proved resistant to infection with the dual-tropic isolate CM9 despite our efforts to improve susceptibility, we could not complete this component of the project. We did, however, succeed in characterizing the effects of differentiation on phagocytic ability, as well as on the expression levels of a panel of cell surface proteins including macrophage markers and HIV receptors. Our work with $CD4^+$ T lymphocytes was largely successful, resulting in the optimization of an antibody-mediated activation protocol that markedly increased cell proliferation and expression of the activation marker CD25. Our investigation of the effects of activation on co-receptor expression revealed that the cell culture conditions resulted in massive upregulation of CXCR4, while activation was shown to attenuate CCR5 expression. Activated $CD4^+$ T cells demonstrated permissiveness to infection, albeit at

relatively low levels, and the MOI used to infect the cells was optimized. The infection kinetics of isolate CM9 were also determined in activated T cells, to assist in the selection of optimal time points for gene expression analysis. In conclusion, all the necessary groundwork has been completed for gene expression experiments using both primary $CD4^+$ T cells and a primary dual-tropic HIV-1-C isolate.

6. Key Findings

In this chapter, we aimed to optimize $CD4^+$ T cell and macrophage culture protocols to maximize susceptibility to HIV infection for later gene expression experiments. For $CD4^+$ T cells, we investigated the use of PHA as well as anti-CD3/anti-CD28 monoclonal antibodies to stimulate TCR-mediated activation, since activation is predicted to enhance HIV infection. Antibody-mediated activation was found to be more effective than PHA and was able to induce both cell proliferation and upregulation of CD25. We next looked at co-receptor expression in the activated cells, since this could impact susceptibility. We found that CXCR4 was highly expressed, increasing further in cultured cells, seemingly independently of activation. CCR5 expression, on the other hand, was much lower in freshly isolated cells and was significantly decreased upon activation. We managed to achieve productive infection in preliminary infection experiments, although the highest observed percentage of HIV positive cells was only 3.82%. The low infection efficiency was likely due to the combined use of primary $CD4^+$ T cells, which have been shown to be more resistant to infection than most cell lines, as well as primary viral strains with naturally low infectivity. In order to select optimal time points for analysis of gene expression, we investigated the kinetics of infection of both CM9 and SW7. SW7 proved to be highly cytotoxic and we could not recover enough viable cells to complete experiments using this isolate.

In terms of macrophage culture, we were primarily interested in comparing the effects of differentiation under the influence of M-CSF and GM-CSF, since polarization with these growth factors has been reported to alter susceptibility to HIV. The pHrodo™ assay demonstrated that both the M-CSF-treated and GM-CSF-treated cells retained their phagocytic abilities. Flow cytometric analysis showed that the differentiated cells expressed high levels of classic macrophage markers (CD14, CD16 and CD64), with little difference between M-CSF- and GM-CSF-treated populations. Analysis of HIV receptor cell surface

expression revealed that CD4 expression was relatively low but still present in both, as expected for differentiated MDM. CXCR4 expression was much lower than CCR5 expression in both populations. The M-CSF-treated cells had higher levels of both co-receptors than the GM-CSF-treated cells, although this difference was non-significant. Unfortunately, our macrophage cultures proved to be completely resistant to infection with the dual-tropic CM9 strain, despite their apparent expression of the requisite receptors.

Chapter 5:

Transcriptomic analysis of activated CD4$^+$ T lymphocytes exposed to a dual-tropic HIV-1-C isolate

1. Abstract

The development of future treatment and potential cure strategies for HIV hinges on our ability to understand how the host cell responds to HIV infection. Changes in the host cell at the gene-expression level could provide insight into mechanisms by which the virus manipulates the host for its benefit or could reveal important host defence mechanisms. Therefore, the aim of this chapter was to perform microarray-based gene expression analysis on primary CD4$^+$ T lymphocytes, activated using anti-CD3/anti-CD28 antibodies and subsequently exposed to a dual-tropic HIV-1-C isolate (CM9). RNA was extracted from both HIV-exposed and unexposed cells collected at 36h and 48h post-infection. The samples were processed and analysed using the Affymetrix GeneChip™ platform. Differential gene expression analysis comparing HIV-exposed and unexposed cells revealed 284 differentially expressed genes at 36h and 229 at 48h. Many of the differentially expressed genes had functional annotations relating to apoptosis, TCR-mediated activation, and immune system function, which have all been previously implicated in HIV infection. However, we also observed modulation of non-coding transcripts (miRNAs, snoRNAs, and lncRNAs), pseudogenes, and a diverse array of other genes with no clear link to HIV responses previously reported in literature. Interestingly, we noticed upregulation of a group of deubiquitinating enzymes belonging to a single family (USP17L). Gene ontology analysis using the PANTHER tool identified apoptotic processes and deubiquitination as being statistically overrepresented biological processes, highlighting their importance in HIV infection. Unfortunately, the lack of additional biological replicates makes it difficult to state with certainty whether these findings represent true responses to infection with HIV-1-C.

2. Introduction

Despite the extensive research which has been conducted on HIV, much is still unknown about the intricate mechanisms of its pathogenesis and precisely how target host cells respond to infection. Understanding how HIV interacts with its cellular targets is essential in the development of novel therapeutic strategies, potentially leading to a functional cure. A key step in unravelling this problem is examining the effect of infection on the transcriptional networks of the host cell, which can reveal changes in cell regulation, signalling and metabolic activities. Although several studies have attempted to study these effects using HIV-1-B strains, none to date have investigated the effects of infection with HIV-1-C strains. This is a troubling oversight, since HIV-1-C has become the most prevalent HIV subtype and accounts for the bulk of new infections in this continued epidemic. The overarching goal of this project was therefore to determine the host cell response to infection with HIV-1-C isolates at the transcriptome level. The obstacles encountered in the previous chapters led to the narrowing of the focus in this chapter to the investigation of the effects of exposure to the dual-tropic clade C isolate CM9 on $CD4^+$ T lymphocytes activated by co-stimulation with anti-CD3/anti-CD28 antibodies. In order to confirm that infection of the target cells was successful, the HIV detection methods developed in the previous chapters were employed prior to gene expression analysis.

There are many methods available to assess changes in gene expression, though several of the older methods, such as Northern blotting, have generally been rendered obsolete. Currently, the most commonly used techniques include RT-PCR, RNA sequencing (RNA-Seq) and microarray-based analysis (234). RT-PCR utilizes RNA which has been reverse-transcribed to cDNA as the template for a PCR reaction with primers designed to amplify the transcript of interest (234,235). The problem with this method is that it is complicated and labour intensive, using conventional equipment, and is not able to analyse more than a few genes at a time. Another disadvantage is that it is a targeted approach and is thus biased towards a few selected genes. Therefore, for examination of gene expression across the whole transcriptome, higher throughput methods such as microarrays or RNA-Seq are required. Microarray-based gene expression analysis makes use of numerous oligonucleotide probes bound to a single chip to enable simultaneous evaluation of hundreds to thousands of genes

(234). It is a robust, reliable method that has been honed into a streamlined, quick and straightforward procedure by commercial providers. RNA-Seq is a more current method that utilizes next-generation sequencing technology to analyse the sequences of RNA transcripts that have been converted into a cDNA library (234,236). The sequenced reads are then mapped to a reference genome to identify and quantify each transcript present (234,236). RNA-Seq is widely regarded as being superior to microarray-based methods, since it is more easily quantifiable, less prone to background noise and is not limited by a pre-defined set of probes (234,236). However, since RNA-Seq is also very costly and technically challenging in terms of data analysis, for this study we elected to use microarray technology to investigate the transcriptome of HIV-exposed $CD4^+$ T lymphocytes.

The response of $CD4^+$ T lymphocytes to infection with HIV-1-B strains in terms of gene expression has been extensively studied, both *in vitro* and *ex vivo*, using a wide range of techniques and experimental conditions. These studies have reported modulation of gene expression across a plethora of cellular processes, including immune functions, cell cycle regulation, apoptosis, DNA repair processes, transcriptional regulation, and cellular metabolism (44,103,237,104–106,109,115,124,125,136), as per the detailed discussion presented in **Chapter 2**. These widespread effects can be attributed to the general subversion of the host cell's transcriptional machinery for the purposes of viral replication, evidenced by the increased production of viral transcripts relative to cellular transcripts (104,109). Furthermore, viral accessory proteins such as Nef have been shown to directly mediate additional effects on transcriptional regulation and host cell processes (22,131). What is not clear is how these responses may differ when using primary viral strains with a very different genetic background, such as the HIV-1-C isolate CM9.

3. Materials and Methods

3.1. Infection of $CD4^+$ T lymphocytes and collection of RNA samples

Gene expression analysis requires the collection of RNA in order to quantify the mRNA transcripts expressed in the target cells. An infection experiment was set up for the purpose of RNA sample collection (**Figure 5.1**). $CD4^+$ T lymphocytes that had been isolated from PBMNCs and purified by FACS (**Chapter 4, Section 3.1.)** from two separate donors (PB57 and

PB58) were activated by anti-CD3/anti-CD28 co-stimulation, as described in **Chapter 4** (**Section 3.2.2.2.**). The cultured cells were collected for use in the infection experiment 4 days after stimulation. Prior to infection, the cells were counted and immunophenotyped for CD25 expression (in addition to CD45 and 7-AAD) by flow cytometry, as previously described (**Chapter 4, Section 3.2.4.**). This was done to confirm that the cells had been activated properly and would therefore be sensitive to infection.

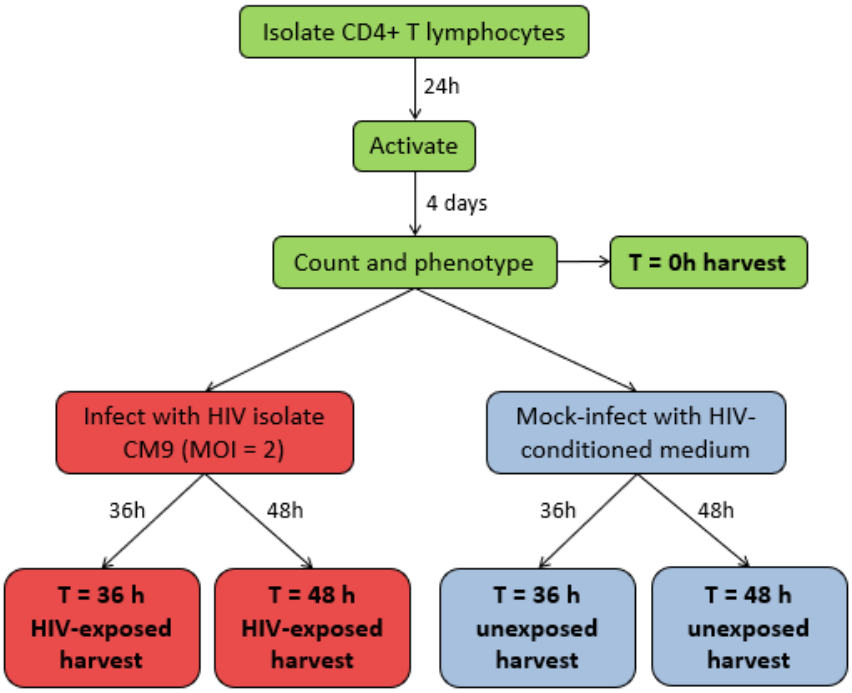

Figure 5.1: Flow diagram of the infection experiment setup. The $CD4^+$ T lymphocyte population was purified by FACS and rested for 24 hours prior to activation. After 4 days in culture, the cells were collected, counted and phenotyped by flow cytometry to confirm activation marker expression. An aliquot of these cells was collected for RNA extraction (T = 0 h harvest). The rest of the cells were either exposed to the HIV isolate CM9 (using an MOI of 2), or to an HIV negative conditioned medium control. Cells were harvested from both groups at 36 h and 48 h post-exposure, for RNA and DNA extraction.

In order to perform differential gene expression analysis, RNA samples from both infected and uninfected control cells at the same time points were required. It is important to note that the virus stock used for infection was harvested directly from a PBMNC-HIV co-culture, and therefore contains large quantities of cytokines and other cell signalling molecules secreted by the activated PBMNCs during the production. In order to account for this effect, the uninfected cells were treated with a conditioned medium control. The conditioned

medium was produced by running a mock-viral production, carried out in the exact same manner without the addition of viral inoculum. To assess the baseline gene expression profiles of the $CD4^+$ cells without conditioned medium, an additional sample of cells was harvested just prior to virus exposure (T = 0 h) for RNA extraction.

The rest of the samples for RNA extraction were harvested at two different time points (36 h and 48 h post-exposure). These time points were selected based on the optimisation experiments performed in **Chapter 4** (**Section 4.3.5**), which demonstrated that the target cells were detectably infected by 36 h using both PCR and p24 ELISA, without excessive cell death. However, the HIV positive signal for both assays was much greater at 48 h. Aliquots of cell suspension containing the required numbers of cells, previously determined in optimization experiments, were collected and centrifuged at 300 x *g* for 10 min. The supernatant was aspirated, and the cells were resuspended in either CM9-020518 cell-free supernatant or HIV negative conditioned medium. The numbers of cells used for each biological replicate and the volume of virus used for infection (MOI = 2), calculated according to **Equation 4.3**, are indicated in **Table 5.1**. The cells were incubated for 2 hours at 37°C in a rotating incubator, after which the cells were centrifuged at 300 x *g* for 10 min. The viral supernatant or conditioned medium was aspirated, and the cells were resuspended in complete RPMI-1640 to a concentration of 500 cells/µL. The cells were plated in 24-well cell culture plates at $3x10^5$ cells per well and incubated at 37°C, 5% CO2 until harvest.

Table 5.1: CD4+ T lymphocyte infection conditions

Donor	Treatment	IU/mL of viral stock	Number of cells	Volume added (mL)
PB57	CM9-020518 viral stock, MOI =2	$1.05x10^6$	$3x10^6$	5.714
	Conditioned medium	-	$3x10^6$	5.714
PB58	CM9-020518 viral stock, MOI =2	$1.05x10^6$	$3.6x10^6$	6.857
	Conditioned medium	-	$3.6x10^6$	6.857

At each harvest, aliquots of cell suspension containing $2.5x10^5$ cells were collected for RNA extraction. For the second donor (PB58), duplicate samples were harvested, and each was processed separately. The cells were centrifuged at 300 x *g* for 10 min and the cell culture

medium was removed. RNA was extracted from the cell pellets using the Qiagen RNeasy® Micro Kit (Qiagen; Hilden, Germany) as per the manufacturers' instructions. β-mercaptoethanol (Sigma-Aldrich; St. Louis, MO, USA), which inhibits RNase activity, was added to the RLT lysis buffer at 1% of the total volume to improve the RNA yield. The final elution step was performed using 14 µL RNase-free water. The purity and concentration of the RNA samples were assessed using a NanoDrop™ spectrophotometer, after which the RNA samples were stored at -80°C. Additional aliquots of cells were harvested at 36 h and 48 h for detection of HIV infection. These samples were centrifuged at 300 x *g* for 10 min and the supernatants were collected. Both the supernatant and cell pellet samples were frozen at -20°C and stored until the end of the experiment.

3.2. Confirmation of HIV infection in target cells

3.2.1. PCR-based detection of HIV infection

In order to assess whether the HIV-exposed $CD4^+$ T lymphocytes had been successfully infected, a PCR to detect viral DNA was performed. The frozen cell pellet samples collected during the infection experiment were thawed in 50 µL PBS. DNA was extracted using the Qiagen QiaAmp® DNA Micro Kit, as per the manufacturer's instructions supplied in the product handbook (using the protocol: Isolation of Genomic DNA from Small Volumes of Blood). The concentration of the resulting DNA samples was determined using a NanoDrop™ spectrophotometer. PCR reactions were carried out as previously described in **Chapter 3** (**Section 3.3.2.3.**), using the CM9 LTR/gag primer pair. The following controls using the L32 primer pair were included: a positive PCR control using T cell template DNA (from the PB57 HIV- 36 h sample) and a negative no-template control.

3.2.2. p24-ELISA for detection of HIV infection

While viral DNA may be present in both latently and productively infected cells, the p24 capsid protein is only produced during productive infection. A p24-ELISA was therefore also performed to confirm that productive infection had been achieved in the HIV-exposed $CD4^+$ T lymphocytes. The frozen supernatant samples collected during the infection experiment were thawed, and 200 µL aliquots from each sample were processed using the Lenti-X™ p24

Rapid Titer Kit as described in **Chapter 3** (**Section 3.2.1.**). A standard curve was generated simultaneously to enable estimation of the concentration of p24 protein in each sample.

3.3. Microarray-based analysis of gene expression in HIV-exposed $CD4^+$ T lymphocytes

Microarray-based gene expression analysis is a technique used to simultaneously analyse the expression profiles of thousands of genes using chips with DNA oligonucleotides printed in defined positions (234). These DNA probes are complementary to target sequences of interest and can therefore be used to detect the presence of the target sequences when they are bound to the gene chip (234). However, the probes on the chip require the RNA transcripts to be converted to single-stranded DNA in order to hybridise (234). In addition, when small input quantities of RNA are used it is difficult to detect binding to the probe (234). Therefore, commercially available microarrays like the Affymetrix GeneChip™, which was used for this study, are supplied with a reagent kit that is used to convert the transcripts to cDNA with an incorporated amplification step prior to hybridisation. The procedure for RNA processing can be split into several stages **Figure 5.2**.

First, the mRNA transcripts present in a bulk RNA sample are converted to cDNA by reverse transcription, with each strand being synthesised in a separate reaction (first cycle cDNA synthesis). The first strand cDNA synthesis is primed using poly-T primers linked to a T7 promoter sequence, which bind to the poly-A tails of the mRNAs. A reverse transcriptase enzyme uses the RNA sequence as a template, producing a strand of cDNA with the T7 promoter sequence incorporated at the 5' end. The next reaction is carried out using a combination of RNase H, to degrade the RNA template, and DNA polymerase to synthesise the second strand of cDNA, using the first strand as the template. The product of first cycle cDNA synthesis is thus a set of double-stranded cDNA (ds-cDNA) molecules, containing the sequences of all the mRNA transcripts present in the sample, to which a T7 promoter has been attached. The next step involves amplification of the sample through an *in vitro* transcription (IVT) reaction which creates multiple copies of complementary RNA (cRNA) from the ds-cDNA template. The reaction is catalysed by a T7 RNA polymerase, which initiates RNA synthesis from the T7 promoter sequence in the cDNA templates. The number of copies of the original target transcripts is thus amplified exponentially, but the relative proportions remain constant.

A second cycle of cDNA synthesis is then carried out to convert the cRNA back to sense-strand cDNA using reverse transcriptase. In contrast to the first cycle cDNA synthesis, both deoxyuridine triphosphate (dUTP) and deoxythymidine triphosphate (dTTP) are provided, which allows dUTP residues to be incorporated sporadically into the new cDNA strand. The RNA template attached to the resulting single-stranded cDNA (ss-cDNA) is degraded using RNase H. The product is then treated with the enzymes uracil-DNA glycosylase (UDG) and apurinic/apyrimidinic endonuclease 1 (APE 1) which cleave the ss-cDNA at incorporated dUTP residues. Once fragmented, the ss-cDNA is labelled with a proprietary biotinylated Labelling Reagent which can be used to detect the fragments on the chip. The labelled ss-cDNA fragments are added to the gene chip and the target sequences hybridise to their corresponding probes on the array. A scanner is used to detect the bound fragments and compute the signal intensity at the location of each probe. The measured signal intensity is proportional to the number of transcripts present in the original sample.

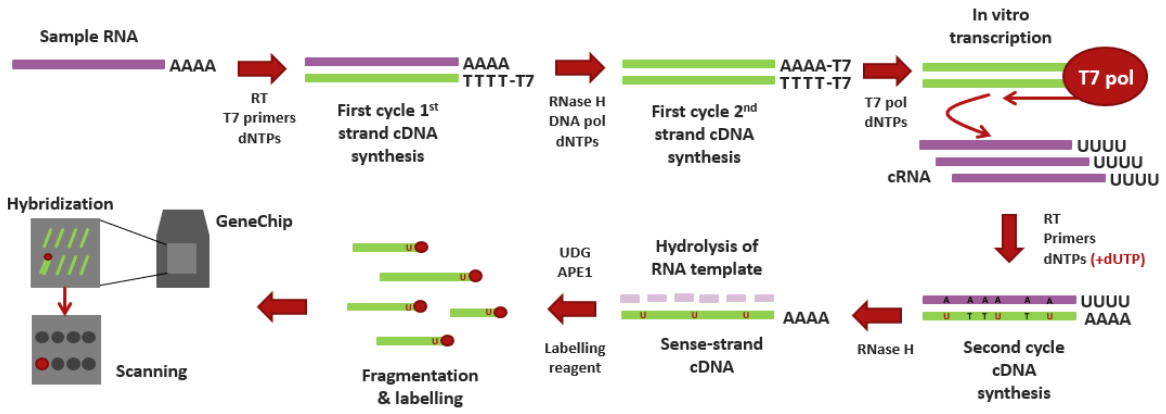

Figure 5.2: Summary of sample processing for microarray-based gene expression analysis using the Affymetrix GeneChip™ platform. The mRNA transcripts in the sample are converted to cDNA using reverse transcriptase (RT) and poly-T/T7 primers for the first strand synthesis reaction, and RNase H combined with DNA polymerase for the second strand synthesis reaction. A T7 polymerase is used to catalyse in vitro transcription which yields multiple copies of cRNA. A second cycle of cDNA synthesis is catalysed by reverse transcriptase. dUTP residues are incorporated into the cDNA at random (indicated with red U's). The RNA template is hydrolysed by RNase H treatment, followed by fragmentation at the dUTP residues with the UDG and APE 1 enzymes, and labelling of the resulting fragments. The labelled ss-cDNA fragments are hybridised to the GeneChip™ array and detected by scanning.

3.3.1. RNA sample preparation and quality control

Preliminary analysis using the NanoDrop™ revealed that the RNA concentration of some samples was too low for microarray analysis. After thawing, these samples were concentrated by first dehydrating them in a Savant™ SpeedVac® SVC 100 vacuum concentrator (Thermo Fisher Scientific; Waltham, MA, USA), then resuspending the RNA pellets in 5 µL RNase-free water. Where duplicate RNA samples were available (PB58), the two samples were pooled prior to concentrating. The concentration and integrity of the processed RNA samples was assessed using the TapeStation™ 2200 (Agilent Technologies; Santa Clara, CA, USA). Aliquots of the RNA samples (1 µL each) were added to Sample Buffer (Agilent Technologies; Santa Clara, CA, USA), using 5 µL buffer per sample. The mixtures were vortexed for 1 min and then heated to 72˚C for 3 min in a thermocycler (GeneAmp™ PCR System 9700). The samples were incubated on ice for 2 min then loaded into the TapeStation™ for analysis on an RNA ScreenTape™ (Agilent Technologies; Santa Clara, CA, USA). Once it was established that the samples had high enough concentration and RNA integrity number equivalent (RIN^e) values, they were used for microarray analysis on the Affymetrix GeneChip™ platform.

3.3.2. Processing of samples for microarray analysis

The preparation of samples for the microarray analysis was performed using the Affymetrix GeneChip™ WT Plus Reagent kit (Affymetrix; Santa Clara, CA, USA). Unless otherwise stated, all processing of samples and mixing of reagents was carried out on ice. An overage of 5% was factored into the volumes used for all master mixes. Mixing of samples was carried out by gentle pulse vortexing, then centrifuging the tubes briefly to collect the contents at the bottom. Samples were also centrifuged briefly after all thermocycling reactions to collect any condensed liquid at the top of the tube.

3.3.2.1. Preparation of RNA dilutions

The concentration of the RNA samples to be analysed needed to be normalized so that all samples had the same amount of input RNA. This ensures that the relative proportions of the transcripts are comparable across the different conditions. The input amount of RNA selected for this study was 50 ng, the minimum quantity that gives sufficient cRNA yields according to the Affymetrix handbook. Although increased input RNA would improve the yield of the

reaction, the RNA concentrations of our samples were simply too low to consider this. Sample dilutions were made up in nuclease-free water such that 50 ng of RNA was present in a total final volume of 3 µL, as indicated in **Table 5.2**. If the original RNA concentration was greater than 50 ng/µL, the sample was pre-diluted to keep the volume required above 1 µL for accurate pipetting. Only samples from PB58 were prepared for microarray analysis, since some of the RNA concentration values for PB57 were too low, even after concentrating.

Table 5.2: Preparation of RNA sample dilutions

Sample	[RNA] (ng/µL)	Dilution	[RNA] after dilution (ng/µL)	Volume containing 50 ng RNA (µL)	Volume of nuclease-free water (µL)	Total volume (µL)
PB58 0 h unexposed	50.30	2X	25.15	2.0	1.0	3.0
PB58 36 h unexposed	29.10	None	29.10	1.7	1.3	3.0
PB58 36 h HIV-exposed	25.70	None	25.70	1.9	1.1	3.0
PB58 48 h unexposed	29.60	None	29.60	1.7	1.3	3.0
PB58 48 h HIV-exposed	33.50	None	33.50	1.5	1.5	3.0

During this initial sample preparation phase, a Poly-A RNA Labelling Control mixture was spiked into the RNA samples. This control mixture contains a set of unlabelled, polyadenylated bacterial RNAs derived from several *Bacillus subtilis* genes (dap, thr, phe and lys), which are used to determine the overall success of the target sample preparation steps. Unlike the rest of the internal Affymetrix controls, they are labelled along with the target samples, and can thus be used to confirm the success of the labelling procedure. The Poly-A RNA control mixture was prepared using a set of four serial dilutions made up in Poly-A Control Buffer, as indicated in **Table 5.3.** The 4th dilution of the Poly-A control was added to all the RNA sample dilutions, using 2 µL each.

Table 5.3: Preparation of the Poly-A control solution by serial dilution

Dilution	Dilution ratio	Volume of Poly-A control solution (µL)	Volume transferred from previous dilution (µL)	Volume of buffer (µL)
1st dilution	1:20	2	-	38
2nd dilution	1:50	-	2	98
3rd dilution	1:50	-	2	98
4th dilution	1:20	-	2	38

3.3.2.2. Synthesis of cDNA from mRNA transcripts

The synthesis of cDNA from RNA transcripts present in the sample was carried out by reverse transcription. The first strand cDNA synthesis reaction was initiated using poly-T primers linked to a T7 promoter, resulting in the production of ss-cDNA with the T7 promoter sequence incorporated at the 5' end. A reaction master mix, comprising 4 µL First-Strand Buffer and 1 µL First-Strand Enzyme per reaction was prepared. The master mix was added to the RNA samples, using 5 µL each. The resulting 10 µL mixtures were incubated in the GeneAmp™ PCR System 9700 for 1 h at 25°C, a further 1 h at 42°C, and finally for 2 min at 4°C.

The second strand cDNA synthesis reaction made use of RNase H and DNA polymerase to simultaneously degrade the RNA template from the first-strand reaction and synthesize the second strand of the cDNA, using the first strand as template. The reaction master mix consisted of 18 µL Second-strand Buffer and 2 µL Second-strand Enzyme per reaction. The master mix was added to the first-strand synthesis reaction product, using 20 µL per sample to give a final reaction volume of 30 µL. The reaction mixes were incubated in the thermocycler for 1 h at 16°C, then 10 min at 65°C and finally at 4°C for 2 min.

3.3.2.3. Synthesis of cRNA by in vitro transcription

In this step, the ds-cDNA template was used as the template for an IVT reaction to produce many copies of cRNA using a T7 RNA polymerase. This enzyme initiates RNA synthesis from the T7 promoter sequence incorporated into the cDNA template. The preparation for this reaction was carried out at room temperature. The IVT master mix was prepared by adding 24 µL IVT Buffer to 6 µL IVT Enzyme. The master mix was added to the cDNA synthesis product,

using 30 µL per sample. The IVT reaction was carried out in the thermocycler for 16 h at 40°C, after which the samples were kept on hold at 4°C.

Purification of the cRNA samples to remove residual enzymes, nucleotides and salts was carried out using magnetic Purification Beads. These beads were added to the cRNA, using 100 µL per sample. The samples were transferred to wells of a U-bottom plate and mixed well by pipetting. The mixtures were incubated for 10 min at room temperature to allow the cRNA to bind to the beads. The plate was placed on a magnetic stand which captures the beads towards the bottom of the wells. The supernatant was removed carefully without disturbing the beads. The beads were then washed 3 times with 200 µL of 80% ethanol, which was kept on the beads for 30 seconds before being aspirated. The beads were allowed to air-dry on the stand before the cRNA was eluted. This was achieved by removing the plate from the stand and incubating the beads in 25 µL of pre-warmed nuclease-free water (65°C) for 1 min. After mixing well by pipetting, the plate was placed back on the magnetic stand to recapture the beads, now separated from the eluted cRNA in suspension. The supernatant containing the cRNA was carefully harvested. The cRNA yield was determined using the NanoDrop™.

3.3.2.4. Synthesis of second-cycle cDNA and hydrolysis with RNase H

In the second-cycle cDNA synthesis, the cRNA was used as a template by a reverse transcriptase enzyme to generate sense-strand cDNA. Both dUTP and dTTP were supplied in equal quantities, such that dUTP residues are incorporated throughout the cDNA instead of dTTP at about half the available sites in the template. The reaction requires an input of 15 µg of cRNA, in a final volume of 24 µL. The concentration of the cRNA samples was therefore normalized to 625 ng/µL (15 000 ng/ 24 µL) using nuclease-free water. The primers for the second-cycle reaction were added to the normalized samples, using 4 µL each. Primer annealing was carried out in the GeneAmp™ PCR System 9700 by incubating the samples at 70°C for 5 min, then 25°C for 5 min and finally at 4°C for 2 min. The second-cycle ss-cDNA synthesis master mix was prepared by combining 8 µL of 2nd-Cycle ss-cDNA Buffer with 4 µL 2nd-Cycle ss-cDNA Enzyme. Aliquots of master mix (12 µL) were added to the cRNA/2nd-Cycle Primer mixture, yielding a final reaction volume of 40 µL. The reaction was carried out in the thermocycler as follows: 10 min at 25°C, 90 min at 42°C, 10 min at 70°C, and finally 2 min at 4°C.

In order to degrade the RNA templates still attached to the ss-cDNA, the samples were treated with RNase H, leaving only the ss-cDNA behind. The RNase H was added directly to the second-cycle ss-cDNA synthesis products, using 4 µL each. The mixtures were incubated in the thermocycler for 45 min at 37°C, then 5 min at 95°C, and finally for 2 min at 4°C. The hydrolysed ss-cDNA samples were supplemented with 11 µL nuclease-free water and then purified with the magnetic Purification Beads using a protocol similar to that used for the cRNA purification**.** The ss-cDNA was bound to the beads by adding 100 µL of beads and 150 µL of absolute ethanol to each sample, mixing well and incubating at room temperature for 20 min. The rest of the purification procedure was performed as previously described (**Section 3.3.2.3**) but using 30 µL nuclease-free water for elution. The final ss-cDNA product was analysed on the NanoDrop™ to determine the yield.

3.3.2.5. Fragmentation and labelling of ss-cDNA

In this step, the sense ss-cDNA was fragmented with UDG and APE 1, which cleave the target ss-cDNA at the dUTP residues incorporated during the second-cycle ss-cDNA synthesis reaction. The fragmented strands were then labelled with the Affymetrix DNA Labelling Reagent, catalysed by the enzyme terminal deoxynucleotidyl transferase (TdT). The input ss-cDNA required was 5.5 µg in a volume of 31.2 µL, therefore the samples were normalized to a concentration of 176 ng/µL (5 500 ng/ 31.2 µL) with nuclease-free water. The fragmentation master mix was produced by adding 4.8 µL 10x cDNA Fragmentation Buffer, 1 µL UDG (10 U/mL) and 1 µL APE 1 (1 000 U/µL) to 10 µL nuclease-free water per reaction. The master mix was added to the ss-cDNA samples, using 16.8 µL each. The fragmentation reaction was carried out in the thermocycler as follows: 60 min at 37°C, 2 min at 93°C, 2 min at 4°C. Immediately after fragmentation, 45 µL aliquots of the samples were labelled with 15 µL of labelling master mix, comprising 12 µL 5x TdT Buffer, 1 µL 5 mM DNA Labelling Reagent and 2 µL TdT enzyme (30 U/mL) per reaction. The final reaction volume was 60 µL. The labelling reaction was carried out as follows: 60 min at 37°C, 10 min at 70°C, 2 min at 4°C.

3.3.2.6. Hybridisation of samples to the GeneChip® arrays

In this procedure, the labelled sense stand cDNA fragments were hybridised to the probes on the microarray. In this study, we used GeneChip® Human Gene 2.0 ST Arrays (Affymetrix; Santa Clara, CA, USA). The reagents used were supplied in the GeneChip® Hybridisation, Wash

and Stain Kit. The 20x Eukaryotic Hybridisation Controls were heated at 65°C for 5 min in the thermocycler after thawing at room temperature. This control mix contains pre-labelled, non-eukaryotic DNA fragments derived from three *E. coli* genes (bioB, bioC, and bioD) and the recombinase gene from P1 bacteriophage virus (cre). Since these bacterial/viral-derived controls are not expected to hybridise with the eukaryotic DNA present in the sample, they can be used to accurately assess the efficiency of hybridisation to the chip. The Control Oligonucleotide B2 solution was also thawed at room temperature prior to starting. Control Oligonucleotide B2 is a pre-labelled DNA spike-in control that hybridizes to corresponding control probes on the array which are used for grid alignment by the scanner software, as well as to assess signal intensity. The hybridisation master mix was made up using 2.5 µL Control Oligonucleotide B2 (3 nM), 7.5 µL 20x Eukaryotic Hybridisation Controls, 75 µL 2x Hybridisation Mix, 10.5 µL DMSO and 13.5 µL nuclease-free water per reaction. The hybridisation cocktails for each sample were produced by adding 109 µL of the hybridisation master mix to 41 µL aliquots of the fragmented and labelled ss-cDNA (3.5 µg) samples. The hybridisation cocktails were incubated in the thermocycler at 99°C for 5 min and then at 45°C for another 5 min. After incubation, 130 µL of each hybridisation cocktail was injected into an array cartridge. The arrays were then placed in the Affymetrix Hybridisation Oven 645 (Affymetrix; Santa Clara, CA, USA), pre-warmed to 45°C, with the rotation set to 60 rpm. The arrays were incubated in the hybridisation oven for 16 h.

3.3.2.7. Washing and staining of the GeneChip® arrays

Following hybridisation of the samples, the arrays were removed from the oven and the hybridisation cocktails were extracted from the arrays. The arrays were filled with Wash Buffer A and allowed to equilibrate to room temperature. The washing and staining protocol was then carried out on the Affymetrix GeneChip™ Fluidics Station 450Dx (Affymetrix; Santa Clara, CA, USA), using 600 µL Stain Cocktail 1, 600 µL Stain Cocktail 2, and 800 µL Array Holding Buffer per run. The procedure was performed using the FS450_0002 fluidics protocol.

3.3.3. Data acquisition and analysis

The processed microarrays were scanned using the GeneChip™ Scanner 3000 7G (Affymetrix; Santa Clara, CA, USA) and Affymetrix® Molecular Diagnostic Software (Version 1.1.1). The location of the probes was determined by alignment to a grid, using controls arranged on the

array border. The signal intensities at each location was then computed and the raw data were extracted in the form of CEL files. These files were analysed using Transcriptome Analysis Console (TAC) Version 4.0 (Affymetrix; Santa Clara, CA, USA). The raw data were summarised and normalized using the Robust Multi-array Average (RMA) algorithm, which outputs CHP files. Differential gene expression analysis was performed on these files using the gene level protocol in TAC. Comparisons were performed between the HIV-exposed samples and the unexposed controls at each time point (HIV- 36 h vs HIV+ 36 h; HIV- 48 h vs HIV+ 48 h), as well as between the T = 0 h baseline control and each of the other samples (HIV- 36 h, HIV- 48 h, HIV+ 36 h, HIV+ 48 h). The fold change of the expression data was used to determine differential gene expression, using a cut-off fold change value of 2. The statistical significance of the data could not be determined since only one biological replicate was used.

Basic functional annotations for the differentially modulated genes identified were obtained from the GeneCards human gene database (https://www.genecards.org/), which combines information from multiple databases such as UniProtKB, Entrez and Ensembl. Further analysis to detect enriched functional groups of genes was carried out using the online PANTHER Functional Classification and Statistical Overrepresentation Test tool, available from http://pantherdb.org/. Fisher's exact test was used for determination of statistical significance, corrected for multiple comparisons by calculation of the False Discovery Rate and corresponding adjustment of the p-value. PANTHER GO-Slim annotation datasets (Biological Process, Molecular Function, and Cellular Component) were used for this analysis. These datasets are based on the Gene Ontology (GO) classification system but have been curated to limit redundancy in the output.

4. Results

4.1. Infection of $CD4^+$ T lymphocytes and isolation of RNA samples

4.1.1. Quality control of isolated RNA samples

The RNA samples from the various harvests were analysed immediately after isolation using the NanoDrop™, which provides an indication of the concentration of RNA in the sample as well the purity. This instrument is a specialized spectrophotometer that detects the optical density of the sample at different wavelengths. Nucleic acids have absorbance maxima at 260

nm. Therefore, the instrument measures the optical density at this wavelength and relates it to the concentration of RNA, as per the Beer-Lambert Law. Proteins absorb primarily at 280 nm, while common contaminants like salts tend to absorb primarily at 230 nm. The ratio of the absorbance measured at 260 nm to 280 nm (260/280) or to 230 nm (260/230) therefore gives an indication of the extent of protein and salt contamination respectively. The 260/280 and 260/230 ratios of a pure RNA sample should be close to 2.

The results of NanoDrop™ analysis for the RNA samples obtained during the infection experiment are presented in **Table 5.4.** The concentration of the samples was generally quite low, which is not unexpected since small input cell numbers were used and spin-column kits tend to suffer from losses in RNA yield. Microarray analysis requires a minimum of 50 ng RNA in a maximum volume of 3 µL, making the minimum acceptable concentration 16.67 ng/µL. Several samples were below, or very close to this threshold, therefore it was decided that these samples needed to be concentrated further. The 260/280 ratios were generally acceptable in the samples with higher concentrations, however, they become quite poor in the low concentration samples. The 260/230 ratios were very low for all samples. It has been noted by the manufacturers of the RNeasy® Micro kit that the buffers used tend to cause decreased 260/230 ratios, but that this does not affect the success of downstream applications like microarray analysis. The 260/280 ratio was therefore considered more relevant in deciding whether the quality of the RNA was acceptable. It should also be noted that the accuracy of the NanoDrop™ decreases at such low RNA concentrations, and that RNA integrity is the most important measure of RNA quality for gene expression analysis. Therefore, the final quality control and quantification of the samples prior to using the samples for microarray analysis was performed on the TapeStation™.

Table 5.4: Concentration and purity of RNA samples post-isolation as determined by NanoDrop™ analysis

Donor	Time point	Condition	Concentration (ng/ul)	260/280 ratio	260/230 ratio
PB57	**0 h**	Baseline (Unexposed)	16.71	2.57	0.08
	36 h	Unexposed	9.39	1.70	0.31
		HIV-exposed	17.95	1.78	0.10
	48 h	Unexposed	7.07	1.48	0.42
		HIV-exposed	23.28	1.56	0.23
PB58	**0 h**	HIV-exposed	32.60	1.93	0.25
	36 h	Unexposed R1	9.56	1.90	0.32
		Unexposed R2	24.08	1.70	0.36
		HIV-exposed R1	25.47	1.63	0.45
		HIV-exposed R2	21.56	1.56	0.43
	48 h	Unexposed R1	9.77	1.43	0.55
		Unexposed R2	7.31	2.07	003
		HIV-exposed R1	10.01	1.90	0.06
		HIV-exposed R2	34.90	1.51	0.52

4.2. Confirmation of productive HIV infection in target cells

Two independent methods were used to confirm the presence of HIV in the CM9-exposed target $CD4^+$ T lymphocytes: LTR/*gag* PCR and p24 ELISA. This enabled the positive identification of HIV-infected samples based on the presence of viral DNA as well as through the active expression of the viral p24 gene product. The intracellular KC57 assay was not included, since it requires large input cell numbers for accurate detection of rare events, such as HIV positivity. The results of the PCR-based assay are presented in **Figure 5.3**. All the HIV-exposed samples demonstrate the presence of a distinct band, which corresponds to the size of the expected amplicon (983 bp), while no PCR products were observed in any of the unexposed controls. The p24 ELISA results (**Table 5.5** & **Figure 5.4**) corroborate these findings, with all HIV-exposed samples yielding positive results. No significant differences were observed in the amount of p24 detected between either the different donors or the different time points, although the readings for PB58 were slightly higher than for PB57.

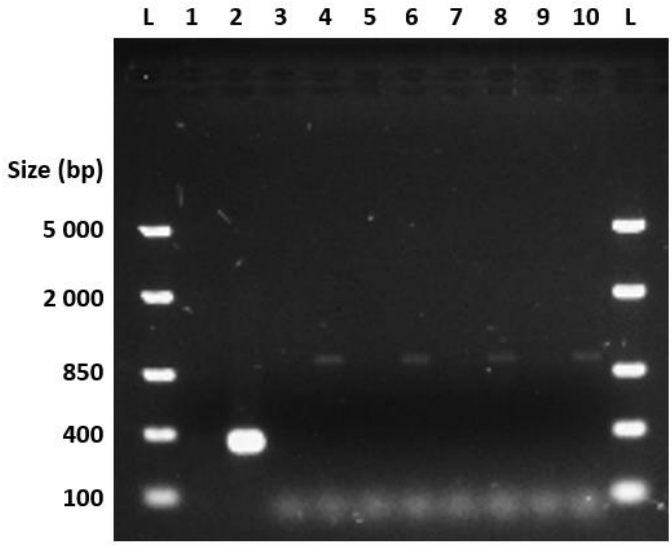

Figure 5.3: Gel electropherogram of products generated during PCR of the LTR/gag region of CM9 in HIV-exposed and unexposed CD4⁺ T lymphocytes. L = ladder, 1 = No template negative PCR control, 2 = L32 positive PCR control, 3 = PB57 HIV- 36h, 4 = PB57 HIV+ 36h, 5 = PB57 HIV- 48h, 6 = PB57 HIV+ 48h, 7 = PB58 HIV- 36h, 8 = PB58 HIV+ 36h, 9 = PB58 HIV- 48h, 10 = PB58 HIV+ 48h.

Table 5.5: Results of the p24 ELISA assay performed on HIV-exposed and unexposed CD4⁺ T lymphocytes from different donors (PB57, PB58) at different time points

Sample description	Raw absorbance (450 nm)	Normalized absorbance (450 nm)	p24 concentration (pg/mL)
Blank	0.155	1.000	-
PB57 36 h unexposed	0.132	0.852	-
PB57 36 h HIV-exposed	0.690	4.452	49.52
PB57 48 h unexposed	0.139	0.897	-
PB57 48 h HIV-exposed	0.547	3.529	35.24
PB58 36 h unexposed	0.165	1.065	-
PB58 36 h HIV-exposed	0.758	4.890	56.31
PB58 48 h unexposed	0.155	1.000	-
PB58 48 h HIV-exposed	0.882	5.690	68.70

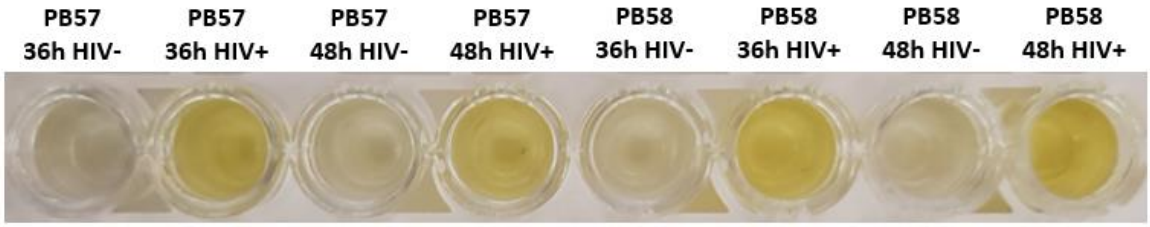

Figure 5.4: A representative image of the colorimetric changes observed in the various wells of a p24 ELISA 8-well strip used to assay cell culture supernatant from CM9-exposed (HIV+) and unexposed (HIV-) $CD4^+$ T lymphocytes. For each of the two donors (PB57 and PB58), HIV+ and HIV- samples were analysed at each time point (36 h and 48 h).

4.3. Microarray-based analysis of gene expression in HIV-exposed $CD4^+$ T lymphocytes

4.3.1. Quality control of RNA samples prepared for microarray analysis

Prior to microarray analysis, RNA samples with low yields were concentrated (after pooling, if duplicate samples were available), and the final processed samples were analysed on the TapeStation™. This instrument performs gel electrophoresis in an automated microcapillary format and uses the output to calculate the RNA concentration and integrity. Many of the samples that initially appeared to have sufficiently high RNA content using the NanoDrop™ which were therefore not concentrated prior to running, were revealed to have much lower concentrations than expected on the TapeStation™. Therefore, these samples were concentrated (after pooling if possible) and re-analysed. The final values obtained for the processed RNA samples are indicated in **Table 5.6.**

For PB57, the final concentrations of two of the samples (36 h HIV-exposed, 48 h unexposed) were still below the usable threshold even after processing. Furthermore, the RIN^e value of the 36-h unexposed sample was below 8, indicating that the RNA integrity was likely insufficient for the microarray analysis. For differential gene expression analysis, an unexposed/HIV-exposed sample pair is required at each time point, so that the relative intensity of expression can be compared. This donor was therefore excluded from the final experiment, since the HIV-exposed sample from the 36-h time point and the unexposed control sample from the 48-h time point were both unsuitable. In contrast, the concentration and RNA integrity parameters for all the PB58 samples were well above the threshold values

required for gene expression analysis (RNA concentration ≥ 16.67 ng/µL; RIN^e ≥ 8) and were therefore deemed suitable for use. Unfortunately, further infection experiments on additional donors to replace the PB57 samples could not be performed, since the viral stocks were depleted and could not be produced within the project timeframe.

Table 5.6: Concentration and integrity of processed RNA samples as determined by analysis on the TapeStation™

Donor	Time point	Condition	Processing of sample	ng/ul	RIN^e
PB57	**0 h**	Baseline (Unexposed)	Concentrated	129.00	9.5
	36 h	Unexposed	Concentrated	16.70	7.8*
		HIV-exposed	Concentrated	15.10*	8.30
	48 h	Unexposed	Concentrated	7.97*	8.40
		HIV-exposed	None	36.20	10.0
PB58	**0 h**	Baseline (Unexposed)	Concentrated	50.30	9.0
	36 h	Unexposed	Pooled + concentrated	29.10	9.3
		HIV-exposed	Pooled + concentrated	25.70	9.2
	48 h	Unexposed	Pooled + concentrated	29.60	8.3
		HIV-exposed	Pooled + concentrated	33.50	9.1

*Parameter falls below the quality requirements for gene expression analysis

4.3.2. Quality controls performed during sample processing for microarray analysis

During the processing of samples for microarray analysis, quality controls were performed at various stages to ensure that the reagents and equipment used were working correctly. In order to confirm that the first-strand cDNA synthesis and subsequent *in vitro* transcription steps were successful, the yield of cRNA obtained was assessed using the NanoDrop™ (**Table 5.7**). The expected yield of cRNA from an input of 50 ng RNA can range between 15 to 40 µg, depending on the cell type, with 15 µg being the minimum requirement to continue to the next stage. The yields for all samples were well above this threshold and were therefore deemed suitable for use in the second-cycle cDNA synthesis step. Following the second-cycle cDNA synthesis reaction and hydrolysis with RNase H, the samples were quantified once more to determine the yield of the ss-cDNA products (**Table 5.8**), which should fall within the range of 5.5 to 15 µg. Since the total yields were all well above the minimum requirement of 5.5 µg,

it can be concluded that this step of the process was successful. Each of the five samples were subsequently fragmented, labelled and hybridized to the GeneChip arrays.

Table 5.7: cRNA yields obtained following IVT as determined by NanoDrop™ analysis

Sample	Concentration (ng/µL)	260/280 ratio	260/230 ratio	Total Yield (µg)
PB58 0 h unexposed	1328.70	2.14	2.42	33.21
PB58 36 h unexposed	1554.66	2.13	2.40	38.87
PB58 36 h HIV-exposed	1142.54	2.12	2.42	28.56
PB58 48 h unexposed	1294.82	2.17	2.43	32.37
PB58 48 h HIV-exposed	1865.06	2.14	2.41	46.63

Table 5.8: Second-cycle ss-cDNA yields determined by NanoDrop™ analysis

Sample	Concentration (ng/µL)	260/280 ratio	260/230 ratio	Total Yield (µg)
PB58 0 h unexposed	196.17	2.02	2.26	5.89
PB58 36 h unexposed	194.71	2.04	2.27	5.84
PB58 36 h HIV-exposed	189.75	2.03	2.25	5.69
PB58 48 h unexposed	197.73	2.01	2.26	5.93
PB58 48 h HIV-exposed	202.41	2.01	2.29	6.07

Signal intensity data was obtained from each array during scanning and was processed in TAC. Prior to differential gene expression analysis, several quality control analyses were performed using the processed data. Firstly, the distribution of signal intensities in each array was assessed using a series of box plots to compare inter-array variability. Most genes in the array are expected to be equally expressed or not expresssed at all, while only a minority will be altered between conditions. Therefore, the signal distribution is expected to be fairly uniform across different arrays, especially following normalization which should correct for shifts in signal intensity due to technical artefacts. The signal intensity distributions for the analysed arrays (**Figure 5.5**) were almost identical, indicating that the array signal intensities were comparable and did not demonstrate any array-specific biases.

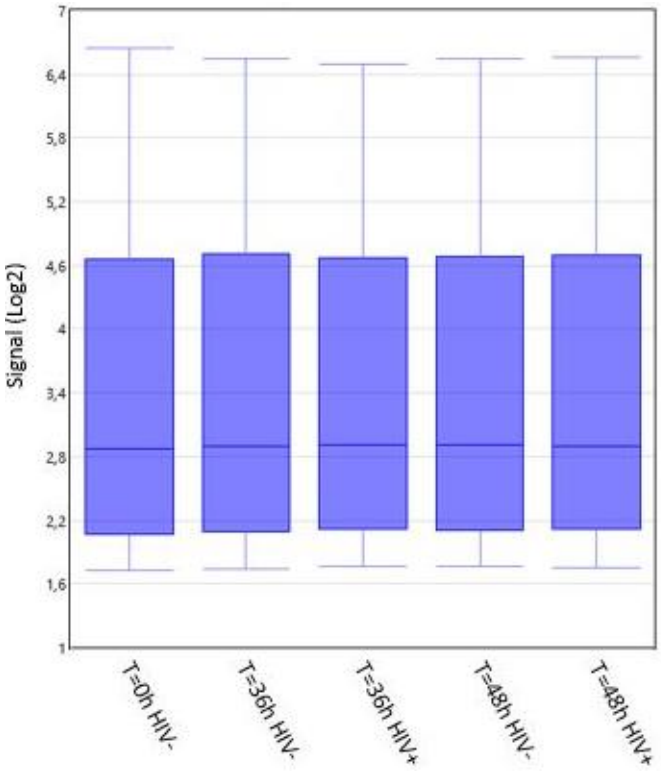

Figure 5.5: Box-whisker plots indicating signal intensity distribution. The minimum, maximum, median and inter-quartile values for the normalized Log2-transformed signal intensities (y-axis) are presented for each of the five arrays indicated on the x-axis (T=0h, T=36h HIV-, T=36h HIV+, T=48h HIV-, T=48h HIV+).

The overall signal quality was then assessed using the positive vs negative area under the curve (AUC) metric. This value is obtained from a receiver operating characteristic (ROC) plot which compares signal values from negative and positive control probe sets derived from either intronic or exonic regions of housekeeping genes respectively. The area under the ROC curve gives an indication of how well the signal intensities of the negative controls seperate from those of the positive controls. Better seperation decreases the risk of misidentifying a negative signal as a false positive. An AUC of 1 would indicate perfect seperation while a value of 0.5 indicates no seperation. In practise, values ranging between 0.8 and 0.9 are typical and indicate good signal quality. The AUC values from the analysed arrays all fall within this range (**Figure 5.6**). This metric is the most important indicator of overall signal quality across all aspects of the experiment, including target preparation, chip quality, hybridisation, scanning and grid alignment.

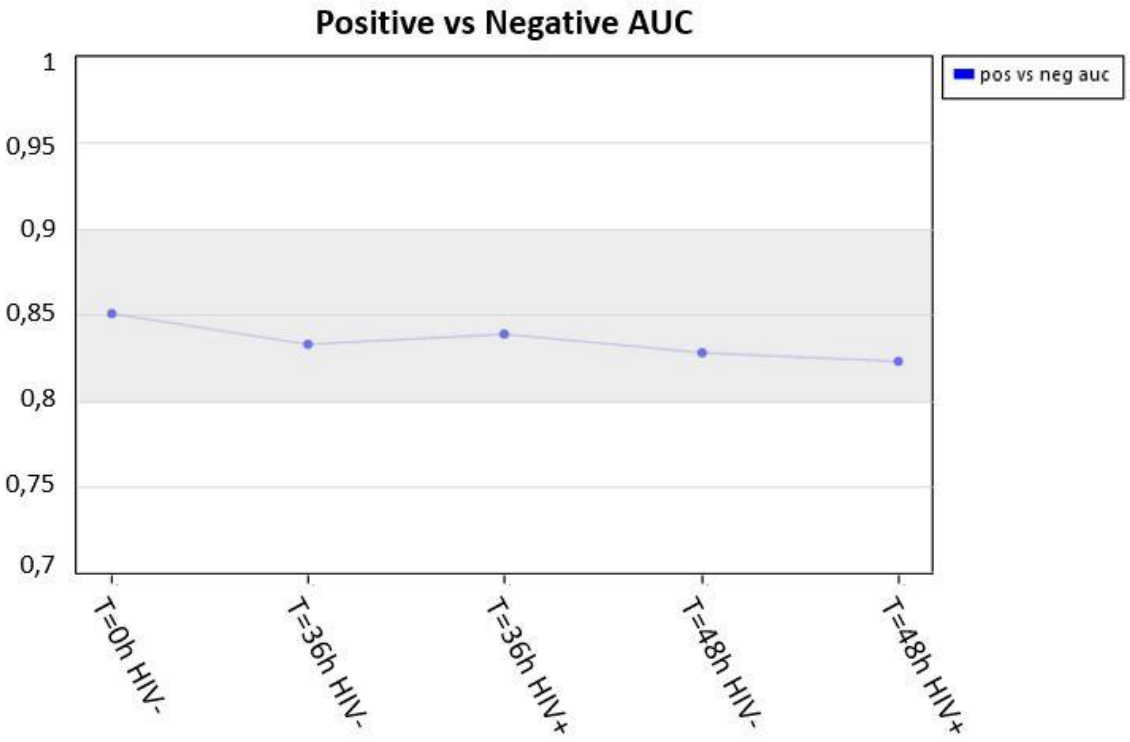

Figure 5.6: Graph of positive vs negative AUC values. The AUC values (y-axis) are plotted for each of the five arrays (indicated on the x-axis). The grey shaded region demarcates the typical range of AUC values which indicate good signal quality.

As an additional quality control step, the signal intensities of the hybridisation control probe sets were analysed. The hybridisation and labelling controls are usually only important to assess when an array does not meet the AUC quality criteria described and are used to identify where in the process the problem occurred. However, since the arrays used for this project were beyond their expiry date, it was decided that it would be important to confirm that the hybridisation procedure was successful. The hybridisation controls comprise probe sets for the non-eukaryotic genes bioB, bioC, bioD and cre, which were added at fixed concentrations to the hybridisation cocktail such that cre > bioD > bioC > bioB. The relative proportions of the signal intensities for these probe sets were determined using line graphs generated in TAC (**Figure 5.7**). These results confirm that the correct order was maintained in all the arrays analysed, thereby indicating that hybridisation was successful. Since all arrays demonstrated uniform signal distributions, conformed to the expected hybridisation control profiles and, most importantly, had AUC values within the normal range, it was decided that they were of sufficient quality for use in differential gene expression analysis.

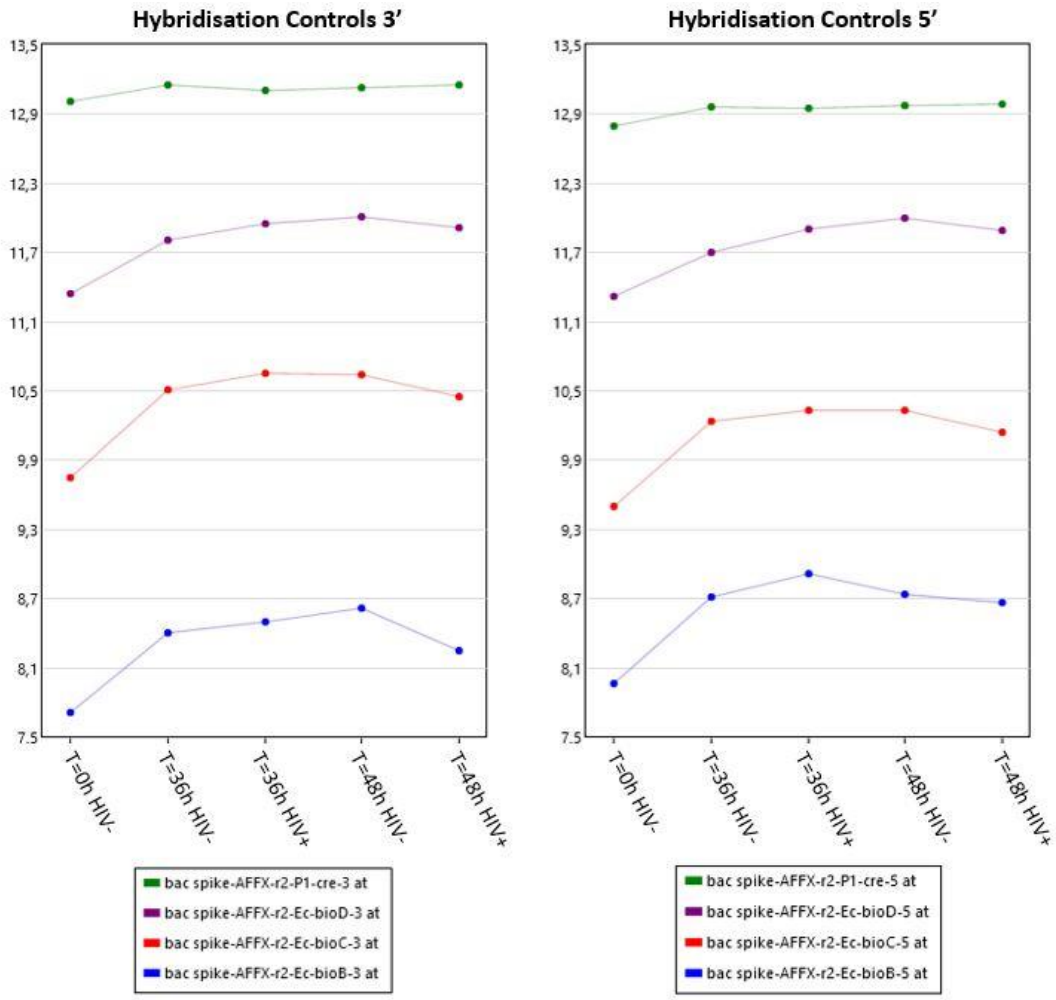

Figure 5.7: Line graphs indicating signal intensities for the 3' and 5' hybridisation control probe sets observed in each array. The signal intensity is indicated on the y-axis, while the array names are indicated on the x-axis. The key below each graph indicates the expected order of the four different controls (cre > bioD > bioC > bioB).

The final quality control step involved the analysis of correlation between arrays, to determine whether the gene expression signals observed in the arrays displayed expected patterns of clustering. This was achieved using principal component analysis in TAC. This analysis projects the data along several axes, known as components, where the distance between points indicates the extent of correlation. Therefore, clustering indicates groups of samples with similarity in their expression signals. The components are ordered by decreasing significance in terms of their ability to explain the variance observed between samples. The three components with the greatest significance, which therefore explain most of the variations in expression signals observed, were used to plot a 3-dimensional graph (**Figure 5.8**). Principal component 1 (PCA1) appears to separate the T = 0 h baseline sample from the rest, indicating clustering according to either exposure to conditioned medium or increased

time in culture (or a combination of these two factors). This component explains 56.3% of the differences observed. The rest of the samples appear to cluster according to their time point, with the 36 h and 48 h pairs appearing separated along PCA2 (21.6%). The samples do not appear to cluster according to whether or not they were exposed to HIV, although the HIV-exposed samples do not closely associate with the unexposed controls at their respective time points either. Since very few arrays were analysed, it is difficult to say whether these loose clusters indicate true, strong correlations. However, they do seem to indicate that the arrays generally correlate to each other in ways that can be explained by the experimental design.

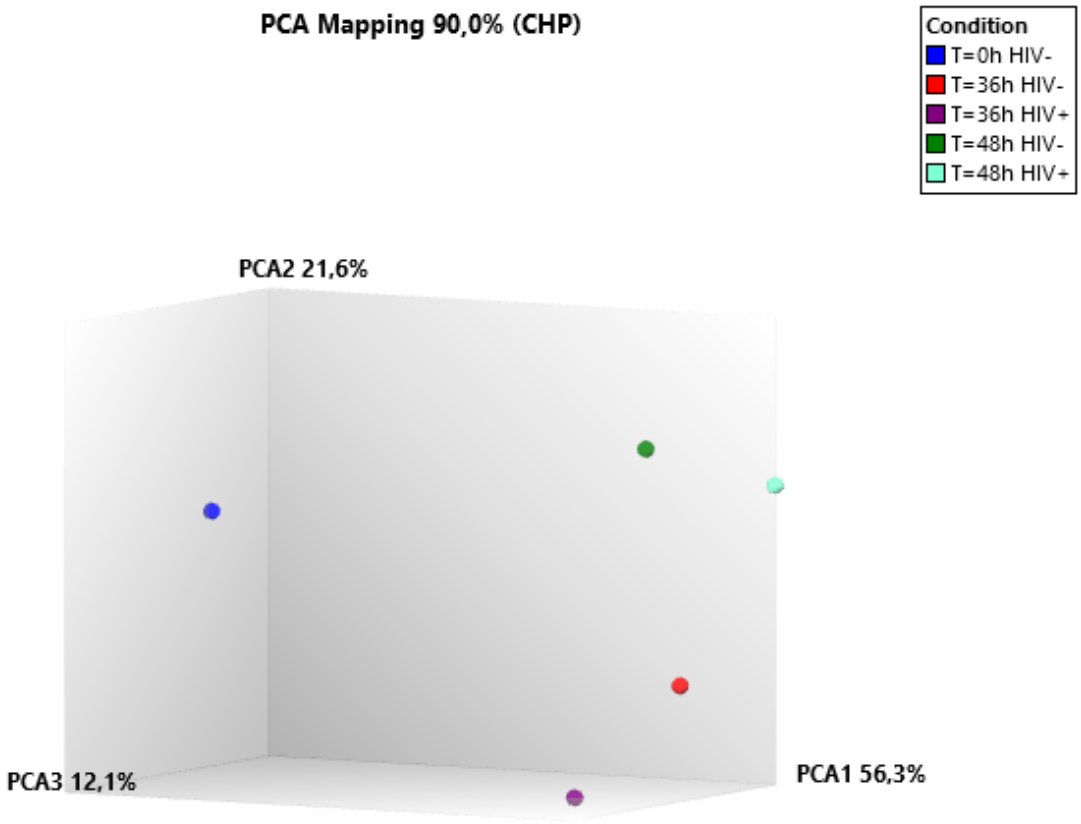

Figure 5.8: Principal component analysis indicating correlation in gene expression patterns among the different arrays. The three most significant Principal Components (PCA1, PCA2, PCA3) were used as the axes in a 3-dimensional graph, with the significance indicated as a percentage of the total variance explained by each. The five arrays were plotted along these axes, with the extent of correlation in gene expression between them indicated by their distance to each other. The arrays are indicated as follows: T=0h control (blue), 36h HIV unexposed control (red), 36h HIV positive sample (purple), 48h HIV unexposed control (green), 48h HIV positive sample (turquoise).

4.3.3. Differential gene expression analysis

During differential gene expression analysis, two groups of comparisons were performed. The first set of comparisons was straightforward, involving comparison of the HIV-exposed (HIV+) samples to their corresponding unexposed (HIV-) controls at the two different time points. The purpose of these comparisons was to determine the effects of HIV exposure and whether the response changes over time. The second group of comparisons was intended to assess the effect of cytokines and other molecules secreted by activated PBMNCs during culture. The array from the T = 0 h baseline control sample, which was not exposed to any form of conditioned medium, would indicate baseline gene expression levels, allowing the identification of genes modulated due to cytokines secreted in the culture medium in the absence and presence of HIV. Since the conditioned medium and viral cell-free supernatant were not produced under identical culture conditions, it was important to check whether they caused comparable effects. This was achieved by comparing the T = 0 h sample with each of the other four samples. The results of differential gene expression analysis performed using these comparisons is summarised in **Figure 5.9**. The greatest numbers of differentially expressed genes (DEGs) were observed in the comparisons with the T = 0 h baseline control, indicating that exposure to conditioned medium has a substantial effect on gene expression. The number of DEGs is greater in the 0 h vs 48 h comparisons than in the 0 h vs 36 h comparisons, indicating that this effect became more pronounced over time. The direct comparisons between HIV+ and HIV- samples revealed a much smaller, but still substantial number of DEGs at both time points. An interesting observation is that at 36 h, the majority of DEGs are upregulated, while at 48 h this trend is reversed.

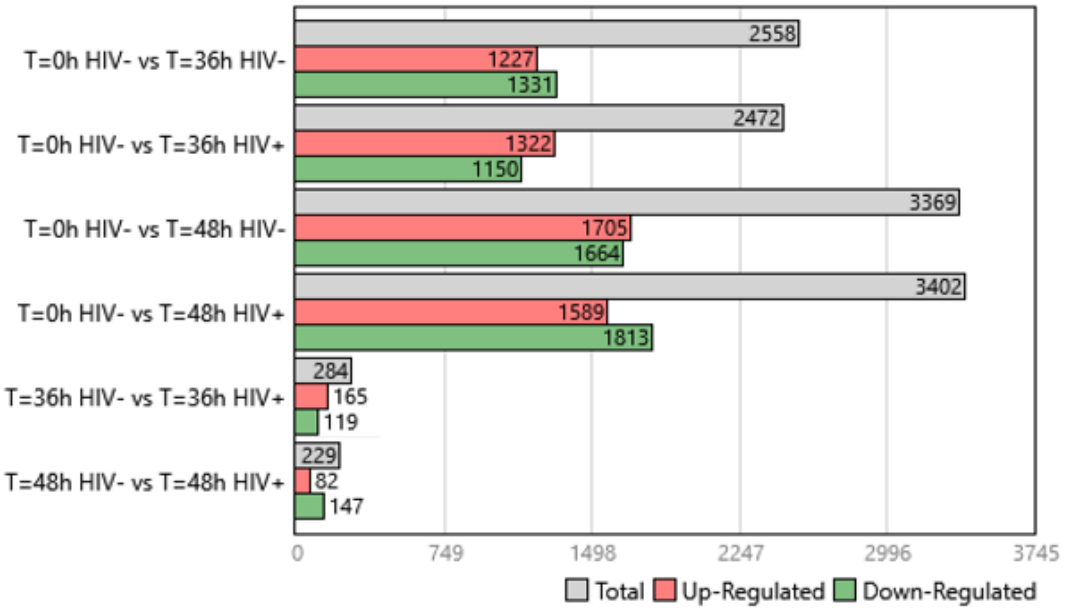

Figure 5.9: Summary of the numbers of differentially expressed genes observed when comparing different pairs of arrays. The number of DEGS observed is indicated on the x-axis of the bar graph, while the pairs of arrays compared are listed on the y-axis. The total number of DEGs is indicated in grey, while the upregulated and downregulated genes are shown in red and green respectively.

In order to detect overlap in the sets of DEGs observed across different comparisons, a series of Venn diagrams was created in TAC (**Figure 5.10**). The first Venn diagram (**Figure 5.10a**) looks at the overlap in the list of DEGs observed in the HIV-exposed vs unexposed comparisons at the two different time points. Only 21 of the identified DEGs (4.27%) are shared across both time points, indicating that the patterns of differential gene expression are very different with increased time post-exposure. The DEGs observed in comparisons made between the T = 0 h baseline control and the HIV negative conditioned medium treated samples at either 36 h or 48 h post-exposure appear to overlap significantly, with 46.13% of the genes being shared (**Figure 5.10b**). The marked overlap in these two sets of comparisons seems to indicate that there are effects induced by the conditioned medium that are common to both time points. The comparisons made between the T = 0 h baseline control and the HIV-exposed samples yielded similar results with a 43.27% overlap (**Figure 5.10c**), once again indicating a large set of DEGs that are modified in response to treatment with viral supernatant that are shared across both time points. A final Venn diagram (**Figure 5.10d**) was made to determine the extent of overlap between the subset of DEGs shared across time

points in the T = 0 h vs HIV- comparisons and the subset of DEGs shared across time points in the T = 0 h vs HIV+ comparisons (indicated as “0h vs HIV- combined” and “0h vs HIV+ combined” in **Figure 5.10b** and **Figure 5.10c** respectively). This yielded a population of 1423 DEGs common to both subsets (64.04%) which are modulated in response to exposure to conditioned medium, irrespective of time since exposure and whether or not the medium contains HIV particles (**Figure 5.10d**). This overlap suggests that both the HIV negative conditioned medium and HIV positive viral supernatant affect expression of similar groups of genes.

The complete lists of DEGs obtained following differential gene expression analysis between the HIV-exposed samples and unexposed controls are presented in **Table 5.9** and **Table 5.10**. In some cases, the identified DEGs corresponded to probe sets for which no annotation was available to indicate the nature of the target sequence. These probe sets are presumably intended for the investigation of gene expression in poorly characterized genomic regions. For the purposes of this study, however, these probe sets were excluded from further analysis. It is clear that differential gene expression between the HIV-exposed and unexposed controls varies greatly between the two time points, reiterating the findings illustrated in **Figure 5.10a**. Of the 21 DEGs shared across both time points, only 4 correspond to annotated transcripts, which are highlighted in red in **Table 5.9** and **Table 5.10**. Although these DEGs were common to both time points, they appear to have different patterns of expression at each time point. The genes that are upregulated at 36 h (MIR1200, MIR1269B, LOC100131541) are downregulated at 48 h and MAP kinase kinase kinase 8 (MAP3K8), which is downregulated at 36 h, is upregulated at 48 h.

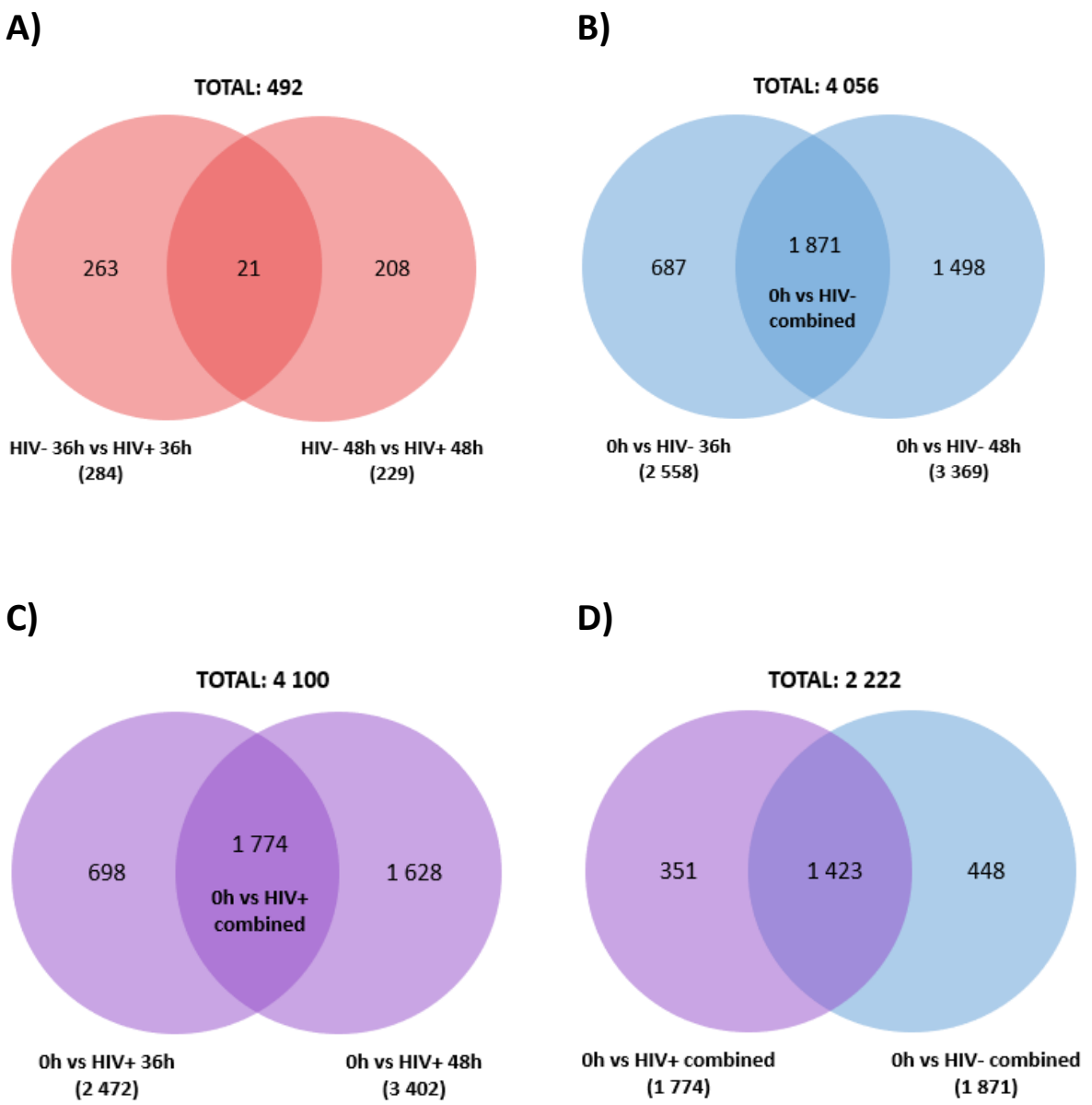

Figure 5.10: Numbers of differentially expressed genes shared across various comparisons, illustrated by Venn diagrams. A) Overlap in DEGs identified between the HIV- 36h vs HIV+ 36h and HIV- 48h vs HIV+ 48h comparisons. **B)** Overlap in DEGs identified between the 0h vs HIV- 36h and 0h vs HIV- 48h comparisons. The shared population of DEGs was designated as "0h vs HIV- combined". **C)** Overlap in DEGs identified between the 0h vs HIV+ 36h and 0h vs HIV+ 48h comparisons. The shared population of DEGs was designated as "0h vs HIV+ combined". **D)** Overlap in the "0h vs HIV- combined" and "0h vs HIV+ combined" DEG subsets.

1 ***Table 5.9: Results of differential gene expression analysis between HIV-exposed and unexposed CD4⁺ T lymphocytes at 36 h***

UPREGULATED				DOWNREGULATED			
ID	**Fold↑**	**Gene Symbol**	**Description**	**ID**	**Fold↓**	**Gene Symbol**	**Description**
16927684	4.81	MIR130B	microRNA 130b	16850428	-4	ROCK1P1	Rho-associated, coiled-coil containing protein kinase 1 pseudogene 1
16715997	3.55	NUTM2B-AS1	NUTM2B antisense RNA 1	17099703	-3.81	MIR3689E	microRNA 3689e
16753543	3.31	MIR548C	microRNA 548c	16735253	-3.66	LOC100506258	uncharacterized LOC100506258
16852371	3.14	SMAD4	SMAD family member 4	16865530	-3.01	KIR3DL2; KIR3DL1	killer cell immunoglobulin-like receptor, three domains, long cytoplasmic tail, 2; killer cell immunoglobulin-like receptor, three domains, long cytoplasmic tail, 1
16699862	3.09	MIR4742	microRNA 4742	16816018	-2.96	MIR365A	microRNA 365a
16761514	2.94	TAS2R19	taste receptor, type 2, member 19	16698784	-2.57	MIR29B2; C1orf132	microRNA 29b-2; chromosome 1 open reading frame 132
16722321	2.88	PDE3B	phosphodiesterase 3B, cGMP-inhibited	16743215	-2.42	TRIM53AP	tripartite motif containing 53A, pseudogene
17117932	2.87	LOC105372990; LOC646513	uncharacterized LOC105372990; VLGN1945	16738375	-2.38	OR5R1	olfactory receptor, family 5, subfamily R, member 1 (gene/pseudogene)
16825446	2.81	LOC101928188	uncharacterized LOC101928188	17118058	-2.38	LOC728093; LOC643784	putative POM121-like protein 1-like; NLR family, apoptosis inhibitory protein pseudogene
16942681	2.75	EBLN2	endogenous Bornavirus-like nucleoprotein 2	17118066	-2.38	LOC441081	POM121 membrane glycoprotein (rat) pseudogene
16927821	2.72	IGLV2-11	immunoglobulin lambda variable 2-11	17118127	-2.38	LOC102724994; LOC102724995; LOC101929599; LOC105369229; LOC101929812	putative POM121-like protein 1-like
17077818	2.72	LOC102724687	uncharacterized LOC102724687	16985748	-2.37	LOC728093; LOC643784; LOC102725182	putative POM121-like protein 1-like; NLR family, apoptosis inhibitory protein pseudogene
16991760	2.61	MIR3142	microRNA 3142	16981168	-2.35	GK3P	glycerol kinase 3 pseudogene
17117545	2.6	LOC100131541	uncharacterized LOC100131541	16783308	-2.33	IGBP1P1	immunoglobulin (CD79A) binding protein 1 pseudogene 1
16699507	2.58	SNORA36B; MIR664A	small nucleolar RNA, H/ACA box 36B; microRNA 664a	16806435	-2.33	GOLGA6L7P	golgin A6 family-like 7, pseudogene

17017353	2.55	MIR4646	microRNA 4646	16805995	-2.32	NIPA1	non imprinted in Prader-Willi/Angelman syndrome 1
17044793	2.52	MIR550A1	microRNA 550a-1	16965002	-2.31	USP17L12	ubiquitin specific peptidase 17-like family member 12
16777624	2.51	LINC00412	long intergenic non-protein coding RNA 412	16965015	-2.31	USP17L21	ubiquitin specific peptidase 17-like family member 21
16937882	2.48	LINC00620	long intergenic non-protein coding RNA 620	16974824	-2.3	ERVH-1	endogenous retrovirus group H, member 1
16863566	2.44	MIR3190	microRNA 3190	17094667	-2.29	PGM5-AS1	PGM5 antisense RNA 1
17118039	2.44	LOC100507209	uncharacterized LOC100507209	17008529	-2.27	PRICKLE4; TOMM6	prickle homolog 4; translocase of outer mitochondrial membrane 6 homolog (yeast)
17017924	2.43	MIR3135B	microRNA 3135b	17049466	-2.26	EPO	erythropoietin
16919223	2.41	SNORA71B; SNHG17	small nucleolar RNA, H/ACA box 71B; small nucleolar RNA host gene 17	16703659	-2.23	MAP3K8	mitogen-activated protein kinase kinase kinase 8
16865050	2.38	MIR518B	microRNA 518b	16963113	-2.19	APOD	apolipoprotein D
16924101	2.35	TEKT4P2	tektin 4 pseudogene 2	16721771	-2.18	KRT8P41	keratin 8 pseudogene 41
16756222	2.34	IGANRP	uncharacterized LOC100652933	16924788	-2.16	LINC00307	long intergenic non-protein coding RNA 307
16777766	2.29	RNU6-53P	RNA, U6 small nuclear 53, pseudogene	16965009	-2.15	USP17L18; USP17L11	ubiquitin specific peptidase 17-like family member 18; ubiquitin specific peptidase 17-like family member 11
17056785	2.28	MIR1200	microRNA 1200	17076481	-2.15	RNF5P1	ring finger protein 5, E3 ubiquitin protein ligase pseudogene 1
16666977	2.25	LRRC8C	leucine rich repeat containing 8 family, member C	16805942	-2.12	GOLGA8DP	golgin A8 family, member D, pseudogene
16841481	2.22	MIR1269B	microRNA 1269b	16884903	-2.11	DDX18	DEAD (Asp-Glu-Ala-Asp) box polypeptide 18
16671692	2.2	MIR92B	microRNA 92b	16965000	-2.11	USP17L11; USP17L9P; USP17L20	ubiquitin specific peptidase 17-like family member 11; ubiquitin specific peptidase 17-like family member 9, pseudogene; ubiquitin specific peptidase 17-like family member 20
16996969	2.2	GUSBP3	glucuronidase, beta pseudogene 3	17085459	-2.11	LOC101928608; LOC105369249	uncharacterized LOC101928608; uncharacterized LOC105369249
16998042	2.19	LOC729040	uncharacterized LOC729040	17107983	-2.1	ZFP92	ZFP92 zinc finger protein
16738628	2.17	OR5B21	olfactory receptor, family 5, subfamily B, member 21	16782010	-2.09	TRAJ59	T cell receptor alpha joining 59 (non-functional)
16860183	2.17	ZNF493	zinc finger protein 493	16965013	-2.09	USP17L20; USP17L9P	ubiquitin specific peptidase 17-like family member 20; ubiquitin specific peptidase 17-like family member 9, pseudogene

16846173	2.16	MIR152	microRNA 152
17118384	2.16	C9orf3	chromosome 9 open reading frame 3
16881098	2.15	GMCL1	germ cell-less, spermatogenesis associated 1
17049700	2.15	MIR4653	microRNA 4653
17063975	2.13	CTAGE6	CTAGE family, member 6
16874182	2.12	LHB	luteinizing hormone beta polypeptide
16677221	2.11	MIR3122	microRNA 3122
16862375	2.11	CYP2B7P	cytochrome P450, family 2, subfamily B, polypeptide 7, pseudogene
16767599	2.1	MRS2P2	MRS2 pseudogene 2
16707047	2.09	PTEN	phosphatase and tensin homolog
16974898	2.08	MIR573	microRNA 573
17070307	2.08	FABP5	fatty acid binding protein 5 (psoriasis-associated)
17008025	2.07	RAB44	RAB44, member RAS oncogene family
17046482	2.05	ZNF138	zinc finger protein 138
16797152	2.04	MIR4710	microRNA 4710
16670364	2.03	LOC100996721	protein FAM231D
16766341	2.03	RDH16	retinol dehydrogenase 16 (all-trans)
16925398	2.03	RUNX1-IT1	RUNX1 intronic transcript 1
16726515	2.01	MIR1237	microRNA 1237
16744770	2.01	SIK3-IT1	SIK3 intronic transcript 1
16965017	-2.09	USP17L22; USP17L9P	ubiquitin specific peptidase 17-like family member 22; ubiquitin specific peptidase 17-like family member 9, pseudogene
16840210	-2.07	SLC52A1	solute carrier family 52 (riboflavin transporter), member 1
16776418	-2.05	LOC105370360	uncharacterized LOC105370360
17023638	-2.05	OR2A4	olfactory receptor, family 2, subfamily A, member 4
16775229	-2.04	OR7E156P	olfactory receptor, family 7, subfamily E, member 156 pseudogene
16965004	-2.04	USP17L15	ubiquitin specific peptidase 17-like family member 15
16715223	-2.03	C10orf105	chromosome 10 open reading frame 105
16711404	2.72	LOC105376380	uncharacterized LOC105376380

1

2

3

4

1 ***Table 5.10: Results of differential gene expression analysis between HIV-exposed and unexposed CD4⁺ T lymphocytes at 48 h***

UPREGULATED				DOWNREGULATED			
ID	**Fold↑**	**Gene Symbol**	**Description**	**ID**	**Fold↓**	**Gene Symbol**	**Description**
16851586	3.67	CABYR	calcium binding tyrosine-(Y)-phosphorylation regulated	16682691	-2.7	AKR7A2	aldo-keto reductase family 7, member A2
17005862	3.31	HIST1H3H	histone cluster 1, H3h	16959320	-2.21	BFSP2-AS1	BFSP2 antisense RNA 1
16927850	2.85	IGLJ2	immunoglobulin lambda joining 2	17005685	-2.09	BTN3A3	butyrophilin, subfamily 3, member A3
16782032	2.81	TRAJ46	T cell receptor alpha joining 46	17069577	-2.08	C8orf46	chromosome 8 open reading frame 46
17025294	2.59	SOD2	superoxide dismutase 2, mitochondrial	16659612	-2.68	CTRC	chymotrypsin C (caldecrin)
16826273	2.53	ITFG1	integrin alpha FG-GAP repeat containing 1	16804141	-2.02	EFTUD1P1	elongation factor Tu GTP binding domain containing 1 pseudogene 1
16846246	2.44	HOXB4	homeobox B4	16682278	-2.33	ESPNP	espin pseudogene
16963053	2.44	MIR3137	microRNA 3137	17011939	-2.03	FAM26F	family with sequence similarity 26, member F
16894422	2.43	SNORA80B	small nucleolar RNA, H/ACA box 80B	17117815	-2.21	FLJ21369	uncharacterized protein FLJ21369
16927869	2.39	IGLC7	immunoglobulin lambda constant 7	17058758	-2.03	GATSL2	GATS protein-like 2
17069873	2.35	SDCBPP2	syndecan binding protein (syntenin) pseudogene 2	17006605	-3. 17	HCP5	HLA complex P5 (non-protein coding)
16869684	2.34	ADGRE2	adhesion G protein-coupled receptor E2	17016490	-2.48	HIST1H2AJ	histone cluster 1, H2aj
16873389	2.34	MIR642B	microRNA 642b	16728153	-2.32	IGHMBP2	immunoglobulin mu binding protein 2
17118436	2.26	LOC651337	uncharacterized LOC651337	16821621	-2.13	IRF8	interferon regulatory factor 8
16772811	2.21	ZNF605	zinc finger protein 605	16726416	-2.01	KCNK4	potassium channel, two pore domain subfamily K, member 4
16929193	2.2	PIK3IP1-AS1	PIK3IP1 antisense RNA 1 (head to head)	16876297	-2.2	KIR3DL2	killer cell immunoglobulin-like receptor, three domains, long cytoplasmic tail, 2
16873168	2.17	ZNF285	zinc finger protein 285	17117545	-2.14	LOC100131541	uncharacterized LOC100131541
16950655	2.16	CIDECP; CIDEC	cell death-inducing DFFA-like effector c pseudogene; cell death-inducing DFFA-like effector c	17056644	-2.06	LOC101928421	uncharacterized LOC101928421
16982006	2.16	LVCAT8	liver cancer-associated transcript 8	16781168	-2.01	LOC102725228; LOC440149	uncharacterized LOC102725228; uncharacterized LOC440149
16850278	2.11	RAB40B	RAB40B, member RAS oncogene family	16713838	-2.31	LOC102725241	putative neutral ceramidase C
16667733	2.09	SLC30A7	solute carrier family 30 (zinc transporter), member 7	16678899	-2.07	LOC105373206	uncharacterized LOC105373206

16703659	2.05	MAP3K8	mitogen-activated protein kinase kinase kinase 8
16900605	2.04	LOC100506036	uncharacterized LOC100506036
16863342	2.03	MIR642A	microRNA 642a
16985964	2.02	MIR4803	microRNA 4803
17065851	2.01	FAM66D	family with sequence similarity 66, member D
16826043	2.01	HERC2P4	hect domain and RLD 2 pseudogene 4
16670291	201	LOC105369140	putative neuroblastoma breakpoint family member 6-like protein

17015130	-2,.09	LOC105374888	uncharacterized LOC105374888
17094671	-2.06	LOC105376070	uncharacterized LOC105376070
16777992	-2.44	MINOS1P1	mitochondrial inner membrane organizing system 1 pseudogene 1
17056785	-2.06	MIR1200	microRNA 1200
17072721	-2.08	MIR1205	microRNA 1205
16841481	-2.48	MIR1269B	microRNA 1269b
17102650	-2.69	MIR1587	microRNA 1587
17098533	-3.23	MIR3911	microRNA 3911
16756224	-2.1	MIR3922	microRNA 3922
16965079	-2.23	MIR572	microRNA 572
16679791	-2.42	OR2M3	olfactory receptor, family 2, subfamily M, member 3
16883477	-2.75	PDCL3	phosducin like 3
16847863	-2.33	PLEKHM1P	pleckstrin homology domain containing, family M (with RUN domain) member 1 pseudogene
16678281	-2.13	PRSS38	protease, serine 38
16660891	-2.01	RHD	Rh blood group, D antigen
16774043	-2.87	RNU6-71P	RNA, U6 small nuclear 71, pseudogene
16773581	-2.1	RNU6-82P	RNA, U6 small nuclear 82, pseudogene
16843074	-2.05	RNY4P13	RNA, Ro-associated Y4 pseudogene 13
17117567	-2.08	SCN8A	sodium channel, voltage gated, type VIII alpha subunit
16763968	-2	SNORA2B	small nucleolar RNA, H/ACA box 2B
16761526	-2.38	TAS2R30	taste receptor, type 2, member 30
17063773	-2.79	TRBV7-7	T cell receptor beta variable 7-7
17115160	-2.27	TREX2	three prime repair exonuclease 2
16841662	-2.16	TRIM16	tripartite motif containing 16
16865935	-2.03	ZNF470	zinc finger protein 470
16861481	-2.23	ZNF568	zinc finger protein 568

1

Functional annotation of the differentially expressed genes using GeneCards revealed several genes that could be biologically relevant to HIV infection. A relatively large number of the DEGs were identified as transcription factors (SMAD4, PTEN, MAP3K8, HOXB4, GATSL2, IGHMBP2) or DNA-binding zinc finger (ZNF) proteins with possible transcription factor activity (ZNF493, ZNF138, ZFP92, ZNF605, ZNF285, ZNF470, ZNF568). A subset of DEGs appeared to relate to immune system signalling, such as the immunoglobulin components (IGLV2-11, IGLJ2, IGLC7), killer immunoglobulin-like receptors (KIR3DL1, KIR3DL2) and T cell receptor components (TRAJ59, TRAJ46, TRBV7-7). BTN3A3, ITFG1 and IRF-8 were also identified as immunomodulatory molecules that were affected. A large set of deubiquitinating enzymes called ubiquitin specific peptidases (USPs) was identified as downregulated at 36 h, while two other genes with possible ubiquitin ligase activity (RAB40B, TRIM16) were identified at 48 h. A few genes relating to induction of apoptotic pathways (TRIM16, CIDEC, PDCL3, SOD2) and DNA repair (TREX2) were also identified.

Many other genes for which the link to HIV infection is unclear were identified, such as histone proteins (HIST1H3H, HIST1H2AJ), solute carriers (SLC52A1, SLC30A7, NIPA1), lipid carriers (FABP5, APOD) and membrane ion channel components (LRRC8C, FAM26F, KCNK4, SCN8A). Most of the remaining coding DEGs were identified as enzymes with specific catalytic abilities such as oxidoreductases (RDH16, AKR7A2), proteases (C9orf3, CTRC) and a cyclic nucleotide phosphodiesterase (PDE3B). Oddly, several genes relating to sensory perception such as taste (TAS2R19, TAS2R30) and olfaction (OR5B21, OR2A4, OR2M3) were also detected. Many of the differentially expressed transcripts observed at both time points corresponded to non-coding RNAs (ncRNAs). This includes microRNAs (miRNAs), small nucleolar RNAs (snoRNAs), intronic and intergenic long non-coding RNAs (lncRNAs) and other uncategorized RNA genes. The microRNAs comprised a significant fraction of the total differentially expressed transcripts at both time points (16.67% for 36 h; 14.67% for 48 h), which are primarily upregulated at 36 h and downregulated at 48 h. Interestingly, large numbers of transcripts derived from pseudogenes were also identified at both time points (20.83% for 36 h and 12% for 48 h).

4.3.4. Analysis of over-represented functional groups of differentially expressed genes

Analysis of functional groups of DEGs was carried out using a Gene Ontology (GO) based method to detect Biological Process, Molecular Function and Cellular Component terms that were statistically over-represented in the output gene lists. The statistically significant results of the GO analysis for the HIV+ vs HIV- comparison at 36 h are presented in **Table 5.11**. Unfortunately, no GO terms in any of the three categories were identified as being significantly over-represented in the HIV+ vs HIV- comparison from the 48-h time point. The terms are listed to reflect the hierarchical structure of the GO classification system, with the most specific terms listed first without indentation, followed by parent terms indented below. The terms are ordered by decreasing fold enrichment. The results reveal that the major biological processes affected by exposure to HIV mainly relate to apoptosis (regulation of apoptotic processes, apoptotic signalling pathway, bleb assembly, execution phase of apoptosis). A population of terms involving protein deubiquitination, which relates to protein degradation pathways, were also identified as highly enriched. In terms of Molecular Function annotation, only two groups of terms were identified, the first relating to thiol-dependent ubiquitin-specific protease activity and the second relating to cysteine-type endopeptidase activity. These molecular functions are both aligned to the previous identification of biological processes relating to deubiquitination. No Cellular Component terms were statistically over-represented.

Table 5.11: Results of PANTHER statistical over-representation test for comparison of HIV+ vs HIV- samples at 36 h post-exposure

GO term (Biological Process)	Fold enrichment	q-value*
regulation of apoptotic process	46.66	4.54×10^{-7}
→ regulation of programmed cell death	46.66	2.27×10^{-7}
→ regulation of cell death	16.35	7.55×10^{-5}
protein deubiquitination	45.45	1.80×10^{-7}
→ protein modification by small protein removal	41.17	2.58×10^{-7}
→ protein modification by small protein conjugation or removal	12.03	3.06×10^{-4}
→ cellular protein modification process	5.32	4.01×10^{-2}
→ protein modification process	5.30	3.82×10^{-2}
apoptotic signaling pathway	16.90	7.28×10^{-5}
→ signal transduction	3.24	1.36×10^{-2}
bleb assembly	14.64	1.33×10^{-4}
→ plasma membrane bounded cell projection assembly	12.77	2.53×10^{-4}
→ cell projection organization	9.89	9.90×10^{-4}
→ cell projection assembly	12.11	3.21×10^{-4}
execution phase of apoptosis	14.64	1.17×10^{-4}
GO term (Molecular Function)	**Fold enrichment**	**q-value***
thiol-dependent ubiquitin-specific protease activity	44.86	1.68×10^{-7}
→ thiol-dependent ubiquitinyl hydrolase activity	44.86	8.40×10^{-8}
→ ubiquitinyl hydrolase activity	44.86	5.60×10^{-8}
→ catalytic activity, acting on a protein	3.82	1.34×10^{-2}
→ peptidase activity, acting on L-amino acid peptides	12.16	2.50×10^{-5}
→ peptidase activity	10.99	4.52×10^{-5}
cysteine-type endopeptidase activity	36.45	1.64×10^{-7}
→ endopeptidase activity	18.81	1.03×10^{-5}
GO term (Cellular Component)	**Fold enrichment**	**q-value***
No statistically significant results	-	-

*q-value = p-value adjusted according to the calculated FDR

Differential gene expression analysis performed between the T = 0 h baseline control and the rest of the samples collected at later time points revealed modulation in thousands of genes. Since the gene expression profiles were altered so drastically, it was important to confirm that the conditioned medium control was exerting comparable effects to the cell-free viral supernatant at a functional level. Therefore, a GO analysis was carried out on the lists of DEGs obtained from these four comparisons (0 h vs HIV- 36 h; 0 h vs HIV+ 36 h; 0 h vs HIV- 48 h; 0 h vs HIV+ 48 h) using the Biological Process annotation database (**Table 5.12**). While some

terms are over-represented uniquely in only one of the conditions, there is generally a large overlap in the terms identified, both across time points and across conditions. The results of the previous GO analysis, performed on DEGs identified in the HIV- vs HIV+ comparison at 36 h, were reiterated in the 0 h vs HIV+ 36 h condition of this analysis, in which “protein deubiquitination” and “regulation of apoptotic process” recurred as uniquely over-represented processes.

1 ***Table 5.12: Results of PANTHER statistical over-representation test for comparisons with T=0 h baseline control***

0 h vs HIV- 36 h		
GO term (Biological Process)	**Fold enrichment**	**q-value**
ribosomal large subunit export from nucleus	9.67	3.27×10^{-2}
→ ribosomal subunit export from nucleus	7.90	1.07×10^{-2}
→ cellular component organization or biogenesis	1.26	4.73×10^{-2}
→ establishment of protein localization	3.87	1.37×10^{-2}
→ ribosome localization	7.90	1.11×10^{-2}
DNA strand elongation involved in DNA replication	8.46	4.59×10^{-2}
→ DNA metabolic process	1.82	2.06×10^{-2}
→ nucleic acid metabolic process	2.01	4.34×10^{-5}
→ nucleobase-containing compound metabolic process	1.86	4.86×10^{-5}
→ cellular metabolic process	1.35	2.30×10^{-2}
→ cellular aromatic compound metabolic process	1.81	1.16×10^{-4}
→ cellular macromolecule metabolic process	1.70	4.56×10^{-2}
DNA replication initiation	8.33	4.68×10^{-3}
maturation of LSU-rRNA	5.92	2.81×10^{-2}
→ rRNA processing	4.43	3.82×10^{-8}
→ rRNA metabolic process	4.13	3.48×10^{-8}
→ ncRNA metabolic process	3.90	7.20×10^{-11}
→ RNA metabolic process	2.07	3.47×10^{-5}
G2/M transition of mitotic cell cycle	5.41	2.19×10^{-2}
→ cell cycle G2/M phase transition	5.41	2.25×10^{-2}
→ cell cycle phase transition	4.31	3.21×10^{-3}
G1/S transition of mitotic cell cycle	5.41	2.13×10^{-2}
→ cell cycle G1/S phase transition	4.92	3.05×10^{-2}
protein transmembrane import into intracellular organelle	5.30	1.28×10^{-2}
→ establishment of protein localization to organelle	3.96	1.21×10^{-2}
regulation of G2/M transition of mitotic cell cycle	5.26	4.46×10^{-2}
→ regulation of cell cycle	2.34	7.85×10^{-3}
→ regulation of mitotic cell cycle phase transition	4.78	4.62×10^{-3}
→ regulation of mitotic cell cycle	4.71	4.59×10^{-4}
DNA biosynthetic process	4.51	2.24×10^{-4}

0 h vs HIV+ 36 h		
GO term (Biological Process)	**Fold enrichment**	**q-value**
ribosomal large subunit export from nucleus	9.70	2.53×10^{-2}
→ ribosomal subunit export from nucleus	7.92	8.95×10^{-3}
→ ribonucleoprotein complex biogenesis	3.48	4.58×10^{-2}
→ cellular component organization or biogenesis	1.35	1.86×10^{-3}
→ establishment of protein localization	4.53	1.70×10^{-3}
→ nucleocytoplasmic transport	3.04	3.05×10^{-2}
→ ribosome localization	7.92	9.22×10^{-3}
DNA replication initiation	7.31	1.07×10^{-2}
→ DNA metabolic process	1.91	6.39×10^{-3}
→ nucleic acid metabolic process	2.09	5.76×10^{-6}
→ nucleobase-containing compound metabolic process	1.82	1.31×10^{-4}
→ cellular metabolic process	1.39	6.15×10^{-3}
→ cellular aromatic compound metabolic process	1.80	1.63×10^{-4}
→ cellular macromolecule metabolic process	1.74	2.51×10^{-2}
pyrimidine nucleotide metabolic process	6.27	3.83×10^{-2}
protein import into mitochondrial matrix	6.04	1.10×10^{-2}
→ cellular component organization	1.31	9.99×10^{-3}
→ establishment of protein localization to organelle	4.64	1.52×10^{-3}
→ protein transmembrane import into intracellular organelle	6.50	1.12×10^{-3}
maturation of LSU-rRNA	5.94	2.23×10^{-2}
→ rRNA processing	4.57	9.38×10^{-9}
→ rRNA metabolic process	4.26	8.97×10^{-9}
→ ncRNA metabolic process	4.07	5.43×10^{-12}
→ RNA metabolic process	2.16	2.83×10^{-6}
G2/M transition of mitotic cell cycle	5.43	1.72×10^{-2}
→ cell cycle G2/M phase transition	5.43	1.76×10^{-2}
→ cell cycle phase transition	4.01	5.98×10^{-3}
regulation of G2/M transition of mitotic cell cycle	5.28	3.48×10^{-2}
→ regulation of cell cycle	2.18	1.83×10^{-2}
→ regulation of mitotic cell cycle phase transition	4.79	3.51×10^{-3}

tRNA metabolic process	3.84	1.90×10^{-3}
mitotic nuclear division	2.62	1.98×10^{-3}
→ nuclear division	2.33	6.54×10^{-3}
→ organelle fission	2.31	1.02×10^{-2}
cytokine-mediated signaling pathway	2.53	2.32×10^{-2}
regulation of hydrolase activity	2.22	4.63×10^{-2}
formation of translation initiation ternary complex	2.11	1.05×10^{-2}
→ ribonucleoprotein complex assembly	2.21	2.96×10^{-4}
→ ribonucleoprotein complex subunit organization	2.19	4.51×10^{-4}
→ protein-containing complex subunit organization	1.82	4.96×10^{-3}
translational termination	2.11	1.01×10^{-2}
→ cellular protein complex disassembly	2.08	1.03×10^{-2}
→ protein-containing complex disassembly	1.98	1.75×10^{-2}
translational elongation	2.11	9.75×10^{-3}
detection of chemical stimulus involved in sensory perception	0.20	2.24×10^{-2}
→ detection of stimulus involved in sensory perception	0.20	2.18×10^{-2}
→ detection of stimulus	0.17	7.37×10^{-3}
anatomical structure development	0.17	5.60×10^{-5}

→ regulation of mitotic cell cycle	4.13	3.40×10^{-3}
maturation of SSU-rRNA from tricistronic rRNA transcript	4.68	1.04×10^{-2}
→ maturation of SSU-rRNA	3.88	2.53×10^{-2}
tRNA metabolic process	4.30	1.88×10^{-4}
DNA biosynthetic process	4.28	5.32×10^{-4}
protein deubiquitination	3.70	3.10×10^{-4}
→ protein modification by small protein removal	3.83	7.14×10^{-5}
→ protein modification by small protein conjugation or removal	1.87	2.14×10^{-2}
protein import into nucleus	3.21	2.23×10^{-2}
→ import into nucleus	3.21	2.27×10^{-2}
regulation of apoptotic process	2.90	1.82×10^{-2}
→ regulation of programmed cell death	2.90	1.78×10^{-2}
cytokine-mediated signaling pathway	2.67	9.11×10^{-3}
mitotic nuclear division	2.54	2.98×10^{-3}
→ nuclear division	2.26	9.84×10^{-3}
→ organelle fission	2.24	1.04×10^{-2}
cellular response to stress	2.43	2.54×10^{-2}
formation of translation initiation ternary complex	2.18	5.71×10^{-3}
→ ribonucleoprotein complex assembly	2.22	2.56×10^{-4}
→ ribonucleoprotein complex subunit organization	2.20	2.83×10^{-4}
→ protein-containing complex subunit organization	1.89	1.49×10^{-3}
translational termination	2.18	5.48×10^{-3}
→ cellular protein complex disassembly	2.15	5.34×10^{-3}
→ protein-containing complex disassembly	2.04	9.78×10^{-3}
translational elongation	2.18	5.27×10^{-3}
anatomical structure development	0.21	1.76×10^{-4}
→ developmental process	0.46	6.90×10^{-5}
detection of chemical stimulus involved in sensory perception	0.20	1.88×10^{-2}
→ multicellular organismal process	0.57	3.82×10^{-2}
→ detection of stimulus involved in sensory perception	0.20	1.84×10^{-2}
→ detection of stimulus	0.17	5.46×10^{-3}

0 h vs HIV- 48 h		
GO term (Biological Process)	**Fold enrichment**	**q-value**
nuclear DNA replication	6.66	3.89×10^{-2}
→ DNA metabolic process	1.86	1.53×10^{-3}
→ nucleic acid metabolic process	1.88	1.57×10^{-5}
→ metabolic process	1.19	1.07×10^{-3}
→ nucleobase-containing compound metabolic process	1.75	1.61×10^{-5}
→ cellular metabolic process	1.37	1.59×10^{-3}
→ cellular aromatic compound metabolic process	1.71	4.86×10^{-5}
→ cellular macromolecule metabolic process	1.69	1.02×10^{-2}
→ biosynthetic process	1.26	4.39×10^{-2}
→ cell cycle process	2.18	1.29×10^{-3}
→ cell cycle	1.68	1.69×10^{-2}
purine nucleobase biosynthetic process	5.99	5.02×10^{-2}
maturation of LSU-rRNA	4.99	2.98×10^{-2}
→ ribonucleoprotein complex biogenesis	3.84	3.24×10^{-3}
→ cellular component biogenesis	3.26	7.71×10^{-3}
→ cellular component organization or biogenesis	1.42	2.90×10^{-6}
→ rRNA processing	3.46	3.11×10^{-6}
→ rRNA metabolic process	3.22	3.44×10^{-6}
→ ncRNA metabolic process	3.27	2.26×10^{-9}
→ RNA metabolic process	1.95	7.41×10^{-6}
protein transmembrane import into intracellular organelle	4.78	5.97×10^{-3}
→ establishment of protein localization	3.57	5.72×10^{-3}
→ establishment of protein localization to organelle	3.65	4.84×10^{-3}
G1/S transition of mitotic cell cycle	4.49	2.79×10^{-2}
→ cell cycle G1/S phase transition	4.09	4.03×10^{-2}
→ cell cycle phase transition	3.63	3.31×10^{-3}
regulation of mitotic cell cycle phase transition	4.11	3.32×10^{-3}
→ regulation of mitotic cell cycle	3.69	1.77×10^{-3}
→ regulation of cell cycle	2.68	1.48×10^{-5}
nucleosome assembly	3.88	4.73×10^{-3}
→ chromatin organization	2.09	3.98×10^{-2}
→ cellular component organization	1.39	1.33×10^{-5}

0 h vs HIV+ 48 h		
GO term (Biological Process)	**Fold enrichment**	**q-value**
DNA replication initiation	6.17	1.55×10^{-2}
→ DNA metabolic process	1.99	2.29×10^{-4}
→ nucleic acid metabolic process	2.12	1.94×10^{-8}
→ metabolic process	1.20	2.92×10^{-4}
→ nucleobase-containing compound metabolic process	1.97	1.59×10^{-8}
→ cellular metabolic process	1.45	5.10×10^{-5}
→ cellular aromatic compound metabolic process	1.94	2.55×10^{-8}
→ cellular macromolecule metabolic process	1.80	2.79×10^{-3}
→ DNA replication	2.20	4.29×10^{-2}
→ cellular macromolecule biosynthetic process	1.27	4.21×10^{-2}
→ biosynthetic process	1.27	3.39×10^{-2}
→ macromolecule biosynthetic process	1.26	4.19×10^{-2}
→ organic substance biosynthetic process	1.26	4.24×10^{-2}
purine nucleobase biosynthetic process	6.01	4.75×10^{-2}
ribosomal subunit export from nucleus	5.85	3.13×10^{-2}
→ ribonucleoprotein complex biogenesis	3.08	4.17×10^{-2}
→ cellular component biogenesis	2.86	3.94×10^{-2}
→ cellular component organization or biogenesis	1.29	3.94×10^{-3}
→ establishment of protein localization	3.58	9.21×10^{-3}
→ ribosome localization	5.85	3.19×10^{-2}
inner mitochondrial membrane organization	5.01	4.49×10^{-2}
→ mitochondrial membrane organization	5.01	1.94×10^{-2}
→ cellular component organization	1.26	1.58×10^{-2}
protein transmembrane import into intracellular organelle	4.79	9.16×10^{-3}
→ establishment of protein localization to organelle	3.67	8.07×10^{-3}
DNA biosynthetic process	4.27	3.65×10^{-5}
maturation of SSU-rRNA from tricistronic rRNA transcript	4.15	1.17×10^{-2}
→ maturation of SSU-rRNA	3.72	1.37×10^{-2}
→ rRNA processing	3.66	1.85×10^{-7}
→ rRNA metabolic process	3.57	5.39×10^{-8}
→ ncRNA metabolic process	3.62	3.26×10^{-12}
→ RNA metabolic process	2.21	6.66×10^{-9}

→ chromosome organization	2.30	4.82×10^{-2}
→ protein-DNA complex subunit organization	2.50	1.04×10^{-2}
→ protein-containing complex subunit organization	2.20	1.52×10^{-7}
→ protein-DNA complex assembly	2.52	9.69×10^{-3}
maturation of SSU-rRNA from tricistronic rRNA transcript	3.79	2.47×10^{-2}
→ maturation of SSU-rRNA	3.42	2.79×10^{-2}
DNA biosynthetic process	3.51	1.38×10^{-3}
tRNA metabolic process	3.50	7.15×10^{-4}
negative regulation of cell cycle	2.80	4.19×10^{-2}
mitotic nuclear division	2.80	1.38×10^{-5}
→ nuclear division	2.53	7.10×10^{-5}
→ organelle fission	2.50	7.53×10^{-5}
protein import into nucleus	2.72	3.91×10^{-2}
→ import into nucleus	2.72	3.97×10^{-2}
→ nucleocytoplasmic transport	2.93	1.30×10^{-2}
→ nuclear transport	2.40	4.62×10^{-2}
formation of translation initiation ternary complex	2.11	1.53×10^{-3}
→ ribonucleoprotein complex assembly	2.30	2.76×10^{-6}
→ ribonucleoprotein complex subunit organization	2.27	2.92×10^{-6}
translational termination	2.11	1.47×10^{-3}
→ cellular protein complex disassembly	2.05	1.56×10^{-3}
→ protein-containing complex disassembly	1.95	4.13×10^{-3}
translational elongation	2.11	1.41×10^{-3}
cellular amino acid metabolic process	1.96	3.00×10^{-2}
phosphorus metabolic process	1.63	4.17×10^{-2}
vesicle organization	0.47	2.81×10^{-2}
anatomical structure morphogenesis	0.30	4.96×10^{-2}
→ anatomical structure development	0.31	1.70×10^{-4}
→ developmental process	0.54	8.57×10^{-5}
detection of chemical stimulus involved in sensory perception	0.19	1.84×10^{-3}
→ sensory perception	0.17	3.99×10^{-2}
→ nervous system process	0.48	2.58×10^{-2}
→ system process	0.55	3.50×10^{-2}
→ multicellular organismal process	0.52	1.61×10^{-3}
→ detection of stimulus involved in sensory perception	0.19	1.78×10^{-3}

nucleosome assembly	3.90	7.76×10^{-3}
→ chromatin organization	2.26	1.55×10^{-2}
→ protein-DNA complex subunit organization	2.29	4.00×10^{-2}
→ protein-containing complex subunit organization	1.92	5.80×10^{-5}
→ protein-DNA complex assembly	2.31	3.94×10^{-2}
tRNA metabolic process	3.84	1.11×10^{-4}
regulation of mitotic cell cycle phase transition	3.54	2.44×10^{-2}
→ regulation of mitotic cell cycle	3.05	2.85×10^{-2}
→ regulation of cell cycle	2.09	1.20×10^{-2}
cell cycle phase transition	2.96	4.09×10^{-2}
→ cell cycle process	1.93	1.89×10^{-2}
mitotic nuclear division	2.20	8.84×10^{-3}
→ nuclear division	2.07	1.34×10^{-2}
→ organelle fission	2.05	1.41×10^{-2}
formation of translation initiation ternary complex	1.88	1.90×10^{-2}
→ ribonucleoprotein complex assembly	1.97	7.39×10^{-4}
→ ribonucleoprotein complex subunit organization	1.95	1.12×10^{-3}
translational termination	1.88	1.85×10^{-2}
→ cellular protein complex disassembly	1.84	1.89×10^{-2}
→ protein-containing complex disassembly	1.75	3.93×10^{-2}
translational elongation	1.88	1.81×10^{-2}
cell differentiation	0.43	1.93×10^{-2}
→ developmental process	0.52	4.40×10^{-5}
vesicle budding from membrane	0.36	4.19×10^{-2}
→ vesicle organization	0.36	3.34×10^{-3}
membrane invagination	0.34	4.13×10^{-2}
adaptive immune response	0.22	4.24×10^{-2}
regulation of transport	0.21	9.11×10^{-3}
→ regulation of localization	0.32	2.46×10^{-2}
sensory perception	0.17	3.94×10^{-2}
→ nervous system process	0.46	1.88×10^{-2}
→ system process	0.49	1.17×10^{-2}
→ multicellular organismal process	0.46	1.86×10^{-4}
vesicle fusion to plasma membrane	0.17	3.88×10^{-2}
→ vesicle fusion	0.21	3.69×10^{-2}

→ detection of stimulus	0.17	2.48×10^{-4}
→ response to stimulus	0.74	4.15×10^{-2}
defense response to bacterium	0.16	3.06×10^{-2}
→ defense response to other organism	0.16	2.95×10^{-2}
regulation of membrane potential	0.16	3.01×10^{-2}
regulation of MAPK cascade	0.11	5.08×10^{-2}
→ regulation of protein phosphorylation	0.11	4.98×10^{-2}

defense response to bacterium	0.16	3.36×10^{-2}
→ defense response to other organism	0.16	3.23×10^{-2}
regulation of membrane potential	0.16	3.29×10^{-2}
immune effector process	0.15	1.51×10^{-2}
B cell activation	0.11	4.78×10^{-2}
embryo development	0.10	3.14×10^{-2}
→ multicellular organism development	0.16	3.92×10^{-2}
→ anatomical structure development	0.18	6.14×10^{-7}
humoral immune response	0.09	2.59×10^{-2}

1

KEY:

GO term name	Term found in HIV negative samples at both time points
GO term name	Term found in HIV positive samples at both time points
GO term name	Term found in both HIV negative and HIV positive samples at 36 h
GO term name	Term found in both HIV negative and HIV positive samples at 48 h

2

3

4

5

6

7

8

9

5. Discussion and Conclusions

The results of the Affymetrix microarray-based gene expression analysis yielded an appreciable number of genes for which expression was modulated as a result of exposure to the dual-tropic HIV-1-C isolate, CM9. The HIV detection methods used after harvesting the target cells provided solid evidence of productive HIV infection, both in terms of detection of viral DNA in the PCR and detection of p24 capsid protein. Although the proportion of infected cells present was not determined, based the KC57 assay results of the previous chapter it is likely that the majority of cells were not directly infected. Therefore, the changes in gene expression observed are likely more representative of a bystander effect, rather than direct infection. However, the bystander effect is an important part of the host response to infection and is likely to play an important role *in vivo*. An unfortunate shortcoming of the study was that gene expression analysis could only be performed on cells from a single donor which prevented statistical analysis of significance. The findings should therefore not be regarded as definitive, since the effects observed on gene expression could be due to stochastic or donor-specific responses to HIV infection.

An important question to consider prior to analysis of the results of this experiment, is whether the conditioned medium was in fact an appropriate negative control. The comparisons between the T=0 h baseline control, which was not exposed to conditioned medium, revealed significant changes in gene expression. Since many of the modulated genes were shared across both the HIV negative and HIV positive conditions, we believe that most differences observed were due to the cytokines and other products secreted by activated PBMNCs found in both the conditioned medium and viral supernatant, as well as due to the ongoing effects of anti-CD3/anti-CD28-mediated activation. These findings were echoed in the GO analysis, in which substantial overlap in the identified GO terms was observed both across time points within conditions, and across the HIV negative and HIV positive comparisons within the same time point. Recurring themes identified include processes related to ribosome biogenesis and trafficking, DNA replication, cell cycle regulation, mitotic cell division, and regulation of translation. These terms indicate a state of ongoing cellular proliferation and active protein production under these conditions.

The similarities in affected pathways confirms that exposure to HIV negative conditioned medium serves as a relatively good control for the changes induced by the secreted factors present in the viral supernatant. However, it is not a perfectly matched control for two reasons. Firstly, although the numbers of input cells in the virus and mock productions were the same, the infected cells undergo more extensive cell death, making the cell numbers higher in the mock-infected production and possibly increasing the concentration of secreted products. Secondly, the PBMNCs used in the productions were from a different group of source donors, which may have had some impact on the secreted products. This means that there is a slight possibility that the differences observed in the HIV-exposed samples may not truly be due to the virus itself, since the composition or quantity of secreted products in the medium may also differ from the negative control.

Keeping these factors in mind, we proceeded to examine the results of differential gene expression analysis performed between HIV-exposed and unexposed $CD4^+$ T lymphocytes. Our findings illustrated that the response to HIV exposure was drastically altered at 48 h in comparison to 36 h post-exposure, and that very little overlap was observed in the lists of DEGs obtained at each time point. Only four transcripts were common to both (MAP3K, MIR1200, MIR1269B, LOC100131541) and even these genes differed in their patterns of up- and downregulation, which were reversed for all these transcripts at 48 h compared to 36 h. This indicates that the effects exerted on these genes are not a consistent feature of infection but are a result of time-dependant processes. This is perhaps to be expected, since other studies investigating the transcriptome of $CD4^+$ T cells infected with HIV-1-B have found that the transcriptional regime is highly variable over time (44,104,115), and that these variations can be linked to events in the virus life cycle (115). Unfortunately, in this study we had no way to directly assess the progression of viral life cycle events, since we could not detect viral transcripts, so it is difficult to interpret the biological relevance of these findings.

The GO analysis component of this study highlighted apoptotic processes and deubiquitination as statistically over-represented functional groups in the HIV-exposed cells. The finding that apoptotic pathways are modulated by HIV exposure is not surprising, since HIV is well known to be highly cytotoxic to $CD4^+$ T cells (37,58) and previous gene expression studies performed in $CD4^+$ T cell lines and primary $CD4^+$ T cells infected with HIV-1-B *in vitro* have also identified apoptosis as a major recurring biological theme (44,104,105,238).

However, closer examination revealed that the genes used to identify both these biological processes were in fact the same 7 ubiquitin specific peptidases (USPs) which all belong to the same USP17 like (USP17L) family. USPs are involved in catalysing the cleavage of ubiquitin from various target proteins, which can greatly alter their fate in the cell (239,240). USP17L family members have been shown to induce apoptosis when over-expressed in cancer cell lines (239), which explains their GO annotations. However, the precise mechanism of their involvement is not known. The fact that a large group of these deubiquitinating enzymes was downregulated in $CD4^+$ T lymphocytes at 36 h post-exposure to HIV could represent an interesting avenue for further research.

In addition to the 7 USP genes identified as being related to apoptosis in the GO analysis, we also found other DEGs that have potential involvement in apoptotic processes. For instance, GMCL1 was upregulated in the HIV exposed cells at 36 h post-infection. The mouse homolog of this gene has been implicated in the degradation of mouse double minute 2 homolog (MDM2), which causes increased p53 levels and subsequent induction of apoptosis (241). In contrast, PDCL3 which is a modulator of caspase activation (242) was downregulated at 48 h, indicating a possible reduction in apoptotic processes. This may also potentially be indicative of a population resistant to apoptosis emerging at the later time point, possibly leading towards the establishment of latent infection. It is widely believed that the activation of apoptotic pathways in HIV infection is due to DNA damage initiated by integration of the virus into the host genome (44), which may also be linked to the altered expression of DNA damage response and repair genes observed in HIV-infected cells in previous studies (105,107). Our findings indicated the downregulation of TREX2, an exonuclease with DNA repair functionality at 48 h, as well as concurrent upregulation of SOD2, a catalyst for the degradation of reactive oxygen species (ROS). The generation of ROS is associated with DNA damage and the induction of apoptosis, so the upregulation of SOD2 may also indicate an emerging anti-apoptotic response.

A consistent finding in many gene expression studies of HIV infection in $CD4^+$ T lymphocytes is that the virus has dramatic effects on transcription factors and other transcriptional regulators, though which a diverse array of cellular processes may be affected. A network of inter-related pathways relating to T cell activation as well as apoptosis were identified as being modulated by HIV infection in these studies (44,55,113,243). Many DEGS detected in

our study seem to be involved in these same pathways, although the identities of the specific transcription factors involved are not the same as those previously described. One such pathway of particular relevance to HIV infection is the NF-κB pathway (55), which is induced by TCR-mediated signalling and promotes expression of genes involved in T cell activation and proliferation (244). The LTR element of the viral genome contains binding sites for NF-κB, therefore the release of NF-κB from its inhibitory interaction partner (IκB) in the cytosol enables it to translocate to the nucleus and initiate transcription from the viral promoter (245). In our study, we detected modulation of MAP3K which forms part of the MAP kinase pathway that leads to NF-κB activation (246–248).

Another transcription factor usually involved in lymphocyte proliferation and differentiation for which binding sites are found in the viral LTR is AP-1, which is composed of Fos and Jun subunits (249). Previous studies have identified genes related to AP-1 formation as being highly upregulated in HIV-infected cells (44,113,243). This is echoed by our findings in which SMAD4, which functions as a component of Fos-Jun complexes (250), was one of the most highly upregulated DEGs identified in our study. SMAD4 also operates within the TGF-β pathway as a mediator of signal transduction from the cell surface to the nucleus, and therefore plays an role in this pro-apoptotic pathway (250,251). A previous study has also implicated the AKT/PKB pathway as an important determinant of the non-progressor phenotype in HIV-infected patients (113). Our findings demonstrated upregulation of the transcription factor PTEN, a well-known tumour suppressor gene that which forms part of the AKT/PKB signalling pathway and is involved in inhibition of cell proliferation and induction of apoptosis (252–254). This gene has also been shown to be modulated by the HIV Tat protein, which associates with the PTEN promoter and stimulates its transcription (255). In addition to these well characterized transcription factors, many differentially expressed zinc finger proteins with DNA-binding capacity and putative functions as transcription factors were identified, indicating that there are likely other uncharacterized transcriptional pathways being affected.

Another group of HIV-modulated genes frequently encountered in literature are those involved in the immune response and regulation of immune system cells (44,103,107,125,238), which is in accordance with observations of HIV-mediated dysregulation of immune system functions at multiple levels. Most notably, HIV is associated

with an overall state of inflammation (256), with dysregulation of cytokine production (257) and activation of $CD4^+$ T cells (191). Upregulation of TCR components has been observed in previous transcriptomic studies (103,113,136), and is generally indicative of increased T cell activation. Our findings demonstrated mixed modulation of T cell receptor components (downregulation of TRAJ59 at 36 h; upregulation of TRAJ46 and downregulation of TRBV7-7 at 48 h). Genes that exert immunomodulatory effects on T cell function were also identified. We observed downregulation of BTN3A3 and IRF8, with concurrent upregulation of ITFG1 at 48 h, none of which have been previously reported in gene expression studies. BTN3A3 is an MHC-associated protein that is linked to TCR stimulation of the unconventional γδ T cell population, which are involved in innate immune responses (258). IRF8 is a member of the interferon regulatory factor family which is expressed in Treg and Th1 subsets (259). ITFG1 (also known as T cell immunomodulatory protein) has been demonstrated to induce secretion of both pro-inflammatory (IFN-γ, TNF-α) and anti-inflammatory (IL-10) cytokines from T cells (260).

In addition to these T cell-related genes, we also observed upregulation of immunoglobulin components (IGLV2-11, IGLJ2, IGLC7) and downregulation of killer immunoglobulin-like receptors (KIR3DL1, KIR3DL2). The involvement of immunoglobulin components and KIR genes, while linked to HIV responses in other cell types, has not been previously reported in $CD4^+$ T cells. Immunoglobulins are generally expressed on the surfaces of B lymphocytes, where they function as antigenic receptors, and are secreted from plasma cells in response to activation by a $CD4^+$ T cell with corresponding antigen-specificity. Abnormal polyclonal B cell activation and dysregulation of immunoglobulin production, specifically increased secretion of IgG, IgM, IgD (261) and IgA (262), is a ubiquitous feature of HIV-infected patients. The KIR genes are highly polymorphic and encode for surface receptors, generally found on natural killer (NK) cells and some subsets of T cells, which are used to mediate destruction of cells lacking MHC Class I as a result of viral infection or cancerous transformation (263). Certain KIR genotypes have been associated with susceptibility to HIV infection and disease outcomes (264). KIRs have also been linked to modulation of $CD8^+$ T cell functions both directly, by promoting cell survival, and through the actions of NK cells (265), which may affect the overall host response to HIV infection.

Interestingly, a large proportion of the DEGs identified at both time points corresponded to ncRNA transcripts. The majority of the ncRNAs observed were miRNAs, a class of small RNAs that are involved in targeting complementary mRNA molecules for degradation (266). Previous studies have identified modulation of cellular miRNAs in the context of HIV infection (115,123,266), and it would be interesting to perform a detailed analysis of the role of miRNAs in HIV-1-C infection. A few of the ncRNAs corresponded to snoRNAs, which are involved in chemical modification of other RNAs, while the rest comprised lncRNAs and uncharacterized RNA genes. Although it has recently been established that many lncRNAs can exert regulatory effects on gene expression (267), their precise functions are poorly understood and it is not clear what their biological significance in the context of HIV infection may be. In addition, the presence of large number of modulated pseudogenes was observed, which is puzzling since these genes no longer encode functional protein products. This phenomenon has also been observed as a result of HIV exposure in another study (268). Gupta and colleagues (2015) suggested that cross-regulation of pseudogenes may arise from mechanisms normally involved in regulation of their parent genes, or from off-target effects from unrelated genes (268).

The ultimate goal of the project was successfully achieved, with the analysis of gene expression in HIV-exposed $CD4^+$ T lymphocytes enabling us to obtain a transcriptome-wide view of the host cell response, with the caveat that it is representative of a single donor. We observed modulation of a small but diverse group of genes involved in apoptosis, deubiquitination, transcriptional regulation and immune system regulation. In addition, a large group of ncRNAs was identified that may play a further role in transcriptomic regulation of HIV-exposed cells. While this study has highlighted the involvement of several genes that warrant further investigation, it was difficult to determine with certainty whether any of the effects observed were unique to HIV-1-C. Although many of the DEGs observed in our study have not specifically been reported in previous studies using HIV-1-B, they do tend to belong to similar pathways. In order to gain a better understanding of how the transcriptional response differs between HIV-1-B and HIV-1-C, more replicates are required and the DEGs identified need to individually validated by quantitative RT-PCR to provide conclusive evidence of the effects of HIV-1-C exposure.

6. Key Findings

In this chapter, microarray-based gene expression analysis was performed on primary $CD4^+$ T lymphocytes activated using anti-CD3/anti-CD28 antibodies to investigate the response to infection with a dual-tropic HIV-1-C isolate (CM9). Comparisons were performed between HIV-exposed and unexposed cells at 36h and 48h post-infection to determine differential gene expression. Our findings indicated drastically altered patterns of gene expression at 48 h in comparison to 36 h post-exposure, with very little overlap in the genes identified. The GO analysis component of this study highlighted apoptotic processes and deubiquitination as statistically over-represented functional groups in the HIV-exposed cells at 36h. Closer examination revealed that the genes used to identify both these biological processes were in fact the same 7 genes from the USP17L family, indicating that this family may play an important role in HIV infection. Among the differentially expressed genes identified, many had functional annotations relating to apoptosis, TCR-mediated activation, and immune system function, all of which correspond to findings reported in previous studies performed using HIV-1-B. Interestingly, a large proportion of the DEGs identified at both time points corresponded to ncRNA transcripts, pseudogenes, and other unusual genes not reported in previous transcriptomic studies. Unfortunately, since only a single biological replicate was used, it is impossible to say whether these represent novel responses unique to HIV-1-C or are due to stochasticity in gene expression. It is also important to note that since infection efficiency in primary $CD4^+$ T cells is so low (as shown in **Chapter 4**), the responses observed are likely to be as a result of bystander effects rather than from direct infection with HIV.

Chapter 6:

Concluding discussion and future perspectives

The original aim of this study was to investigate the effects of exposure to primary HIV-1-C isolates of varying tropisms on the transcriptomic profiles of canonical target cell types, namely $CD4^+$ T lymphocytes and macrophages. In order to achieve this aim, several essential experimental components were required. First, stocks of primary HIV-1-C isolates with a sufficiently high titre which could be used to infect target cells in our cell culture system were needed. Second, the target cells themselves had to be isolated and the culture conditions optimized to enable successful infection upon viral challenge. This included the *in vitro* activation of $CD4^+$ T cells and the differentiation of macrophages under the influence of either M-CSF or GM-CSF. Finally, a detection system capable of identifying target cells infected with the specific HIV-1-C strains used in this study was required, in order to prove that infection in our model system was successful. Many challenges were encountered while working towards these goals, which in some cases required compromises to be made. Despite these obstacles, the overall aim of the project was achieved with respect to $CD4^+$ T lymphocytes, leading to the generation of a valuable dataset that highlights important features of infection with the dual-tropic HIV-1-C isolate CM9.

The production of primary HIV-1-C cultures was by no means a simple procedure. We based our production strategy on a previously published method from the Montefiori laboratory but discovered that the protocol had to be tailored to fit the unique replication dynamics of each primary isolate produced. These modifications enabled the successful production of two of the isolates: CM9 (dual-tropic) and SW7 (X4-tropic), although the infectivity was relatively low. The R5-tropic cultures suffered particularly severe losses of infectivity from which they could not be rescued, despite our best efforts. We believe these difficulties were largely due to the due to the highly mutable nature of the virus and the inherent stochasticity of viral replication, leading to some strains losing their ability to replicate effectively in culture. These issues could be circumvented in future studies through the use of molecular clones or HIV-

based lentiviral vectors, as is commonly done in the field. However, there is a risk that infection with these strains is not an accurate representation of physiological infection conditions, limiting the clinical utility of the results obtained. The titre of the produced strains was measured using the GHOST cell assay. The optimisation of the GHOST assay for quantification of primary isolates with low infectivity was a critical prerequisite for the downstream HIV-related experiments of this project. As part of the optimisation process, the expression of CD4 and the HIV co-receptors in our GHOST cell stocks was investigated. An important point arising from these experiments was that CD4 expression in the GHOST cell line can be quite variable and may be affected by use of enzymatic dissociation reagents like trypsin. The GHOST cell line also proved useful for the optimisation of two methods used to confirm infection of the target cells with the HIV-1-C primary isolates, namely the KC57 flow cytometric assay and a PCR based assay targeting the LTR/*gag* regions of CM9 and SW7.

In **Chapter 4**, cell culture protocols for $CD4^+$ T lymphocytes and macrophages were developed and optimized to enhance susceptibility to infection. Optimisation of the culture conditions for macrophages was largely based on determining the effects of treatment with GM-CSF or M-CSF, since literature indicates that polarization using these growth factors into M1-like and M2-like macrophages respectively can affect their susceptibility to infection. The first step was to determine whether the monocytes had in fact differentiated into functional macrophages in culture. This was determined though flow cytometric examination of macrophage cell surface marker expression, as well as determination of phagocytic ability using the pHrodo™ assay and examination of morphological changes. Our results indicated successful differentiation using both M-CSF and GM-CSF. In order to ascertain whether GM-CSF-treated or M-CSF-treated macrophages would be more susceptible to infection, we also investigated expression of CD4, CXCR4 and CCR5 in both populations by flow cytometry. We found that expression of all HIV receptor molecules was elevated in the M-CSF-treated cells. However, when we performed preliminary infection experiments with the CM9 primary isolate it became apparent that neither macrophage population was susceptible to infection. Since we could not achieve successful infection, further work on this cell type was not pursued.

In the case of $CD4^+$ T lymphocytes, it was established from literature that activation is one of the most important determinants of susceptibility to infection. As such, we aimed to optimize

the cell culture conditions for maximum activation while preserving cell viability, as measured by cell proliferation and CD25 expression assays. After testing PHA-based activation and finding that it was not very effective in our pure $CD4^+$ T cell populations, we elected to use anti-CD3/anti-CD28 antibodies to induce TCR stimulation. This method was found to increase proliferation and CD25 expression, although the extent of the response was quite variable across different donors. We also investigated the effects of activation on the expression of the CXCR4 and CCR5 co-receptors, since this could impact on susceptibility to infection. Our results showed that CXCR4 expression was markedly upregulated under cell culture conditions used, indicating that the cell cultures should be highly susceptible to our X4- and dual-tropic isolates. CCR5 expression, on the other hand, was significantly reduced. Finally, the protocol used for infection of these cells was optimized and the infection kinetics of the HIV-1-C strains were investigated in order to select timepoints for gene expression analysis at which the cells were detectably infected. It became apparent during these experiments that the X4-tropic strain, SW7, had devasting effects on the viability of the activated $CD4^+$ T cell population due to the formation of massive syncytia. As a result, this strain was not used for gene expression analysis, since the lack of viable cells would have made collection of high-quality RNA impossible.

The final gene expression experiments were performed using primary $CD4^+$ T lymphocyte cultures activated using anti-CD3/anti-CD28 antibodies and subsequently exposed to the dual-tropic HIV-1-C isolate, CM9. Due to the limited viral stocks available, only two biological replicates could be performed and unfortunately one of these did not yield sufficient quantities of RNA for microarray analysis. Therefore, the results presented in **Chapter 5** are representative of only a single donor, making it difficult to draw generalized conclusions. However, this snapshot of the transcriptomic profile of CM9-infected cells has yielded some promising findings. Among the differentially expressed genes identified, many had functional annotations relating to apoptosis, TCR-mediated activation, and immune system function, all of which correspond to findings reported in previous studies performed using HIV-1-B. The link between activation and HIV-1 infection is a well-documented phenomenon, so it is not surprising that activation pathways involving classical activation-associated transcription factors NF-κB and AP-1 were modulated in response to infection. The induction of apoptotic pathways as result of the multiple stresses imposed on the cell by viral replication is another

typical response of $CD4^+$ T cells to infection. In addition to genes directly involved in regulating apoptosis, we observed modulation of genes involved in DNA repair and ROS degradation, possibly as a reaction to genotoxic and metabolic stress. It has also been reported previously that HIV-1 causes severe dysregulation of the immune functions of $CD4^+$ T cells. Modulated genes pertaining to immune function identified in our study included T cell receptor components, immunomodulatory transcription factors, immunoglobulin components and killer immunoglobulin-like receptors.

Beyond these largely expected responses, we also observed modulation of a diverse array of other genes. A large proportion of these comprised non-coding transcripts such as RNA genes (encoding miRNAs, snoRNAs, and lncRNAs) and defunct pseudogenes. These transcripts do not encode functional proteins; however, they can be involved in regulation of gene expression and might therefore play an important role in infection. The functional characterisation of these non-coding regions and the effects they have on cell functioning was beyond the scope of this project, but it does present an interesting direction for future research. Another interesting observation that warrants further investigation was the marked upregulation of a group of genes belonging to the USP17L family of deubiquitinating enzymes. Since no deubiquitinating enzymes from any other families were altered, this seems to be a very specific interaction which may play a functionally important role in infection. An unfortunate consequence of the lack of additional biological replicates is that it makes it difficult to state with certainty that these unreported interactions are truly novel responses to infection with HIV-1-C. As mentioned previously, these findings need to be rigorously verified, firstly through the generation of additional microarray datasets and secondly through validation of individual target genes through quantitative RT-PCR. Ideally, we would also perform similar studies using strains of varying tropisms in multiple cell types, as was initially envisioned, and perhaps include a study in which HIV-1-B and HIV-1-C strains are compared directly.

Although this project was performed using bulk RNA for microarray analysis, further work in this field is undoubtedly moving towards single cell transcriptome analysis. This is a novel application of RNA-Seq and microfluidics technologies which allows RNA-Seq sample preparation and analysis of hundreds of single cells to be performed simultaneously (269). The single cell resolution of this technique enables researchers to gain a complete picture of

gene expression without confounding factors from other cells. In our study, for instance, we might have been able to examine the effects of HIV in directly infected cells, identified through a panel of gene expression-based biomarkers, rather than taking an average measure of expression across a population mostly comprised of bystander cells. It can also be used for the analysis of heterogeneity in the cell population of interest, perhaps allowing us to identify $CD4^+$ T lymphocyte subpopulations with different responses to infection. Studies using this technology for the identification of HIV permissiveness factors in $CD4^+$ T lymphocytes (190) and investigation of the heterogeneity of transcriptional signatures of latently infected cells (270) have already been published. Although bulk RNA-based methods like microarrays have taken us far in this field, we believe that the intricacies of the host response to HIV infection may truly begin to be unravelled with the application of single cell transcriptome technology in the future.

Appendix A:

Instrument configurations and index of antibodies used for flow cytometry

1. Configuration of the Gallios™ flow cytometer

The Gallios™ flow cytometer is a ten-colour instrument with three lasers: 488 nm (Blue), 638 nm (Red) and 405 nm (Violet). The filter configurations for each of its ten channels are indicated in **Table A.1** ***Table 3.3:***, as well as common fluorochromes that can be detected in these channels. The instrument makes use of both bandpass (BP) and longpass (LP) optical filters. Bandpass filters transmit a particular band of wavelengths while blocking the rest. The range of the band is indicated in the filter designation, with the first number corresponding to the median wavelength that can be transmitted, and the second number indicating the size of the range above and below the median. A longpass filter attenuates lower wavelengths while transmitting higher ones. The filter designation states the cut-on wavelength, which is the lower bound beyond which it will be able transmit. When a fluorochrome, excited by one of the flow cytometer's lasers causes emission of light at a particular wavelength, it must fall within the range of at least one of the instrument's filters to be detected. This limits which fluorochromes can be used for a particular instrument.

Table A.1: Configuration of filters installed on the Gallios Flow Cytometer

Laser	Channel	Filter	Fluorochromes / Dyes
488 nm, 22 mW	FL1	525/40 BP	FITC
	FL2	575/30 BP	PE
	FL3	620/30 BP	ECD, Propidium Iodide
	FL4	695/30 BP	7-AAD, PE-Cy5
	FL5	775 LP	PE-Cy7
638 nm, 25 mW	FL6	660/20 BP	APC, Alexa Fluor 647
	FL7	725/20 BP	APC-Alexa Fluor 700
	FL8	755 LP	APC-Alexa Fluor 750, APC-Cy7
405 nm, 40 mW	FL9	450/40 BP	Pacific Blue, Zombie Violet
	FL10	550/40 BP	Pacific Orange, Krome Orange

2. Configuration of the FACSAria Fusion™ cell sorter

The FACAria Fusion™ is a more complex instrument than the Gallios™, with multiple laser and filter configurations possible. Five lasers with the following wavelengths are available: 375 nm (UV), 407 nm (Violet), 488 nm (Blue), 561 nm (Yellow-Green), 633 nm (Red). The instrument can be set up to accommodate 20 detectors, allowing simultaneous measurement of a maximum of 18 colours as well as forward scatter and side scatter. The collection optics are arranged in a series of detectors with either octagonal or quadrangular configurations. The first detector collects light of the highest wavelength, while the subsequent detectors capture light of successively decreasing wavelengths. This is achieved through the use of filters coupled to each detector, which allow light of the correct wavelength for that detector to pass through, and mirrors which reflect light of lower wavelengths on to the next detector in the series. In this study, a standard configuration utilizing the 407 nm, 488 nm, 561 nm and 633 nm lasers and the 70 µ nozzle was used for all immunophenotyping and sorting experiments. The configuration of the filters used for each laser is indicated in **Figure A.1.**

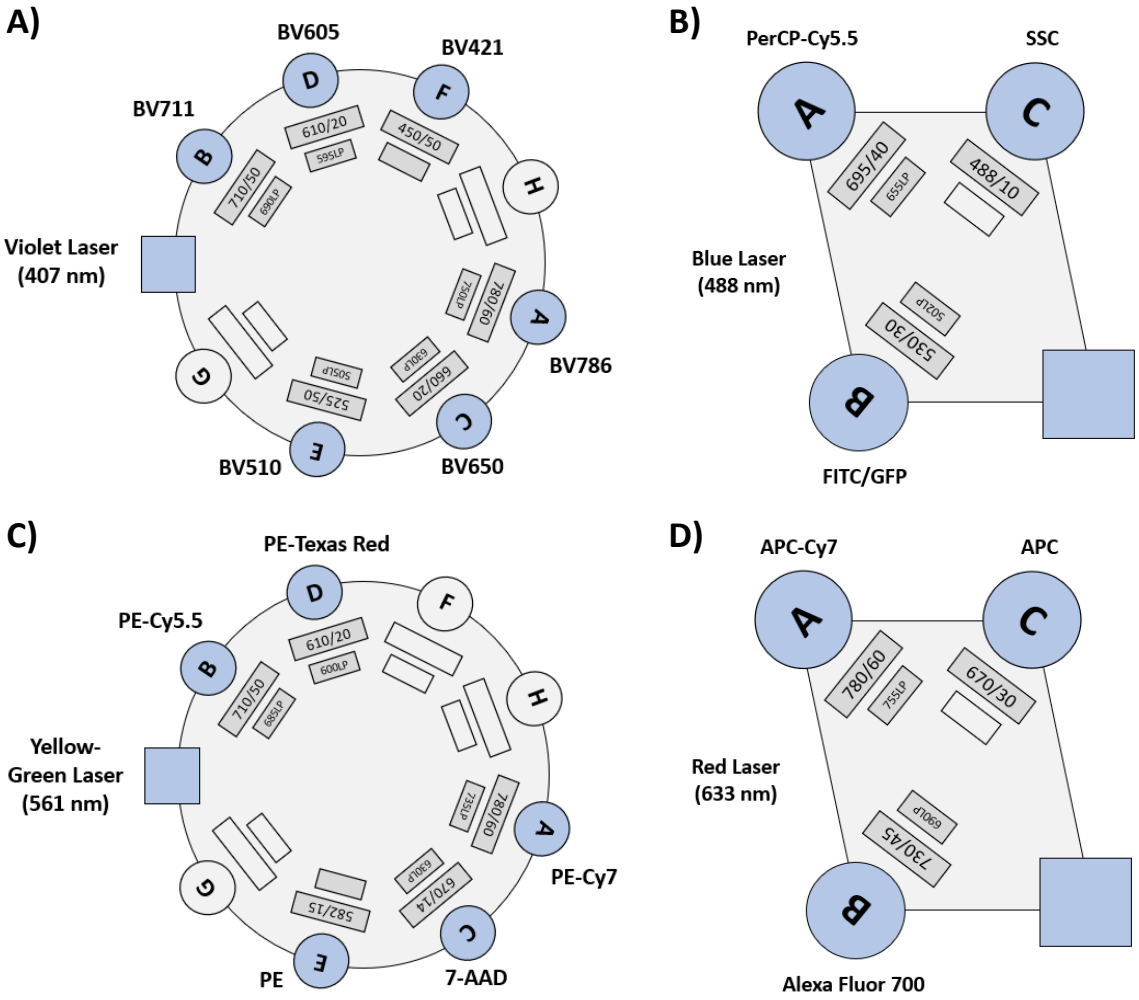

Figure A.1: Filter configurations for the FACAria Fusion™ cell sorter used in this study. Configurations are indicated for the **A)** violet, **B)** blue, **C)** yellow-green and **D)** red laser arrays. The detectors are illustrated with circles, the specifications of the filters in front of each detector are indicated in the larger boxes directly below the circles and the specifications of the mirrors that reflect light to the next detector are indicated in the smaller boxes. Each detector is also labelled with the fluorochrome/s it could be used to detect.

3. Antibody index

The antibodies selected for use in this study were all reactive against human antigens, since all our sample cells were of human origin. They were sourced from either BioLegend (San Diego, CA, USA) or Beckman Coulter (Miami, FL, USA). The technical details for each antibody are supplied in **Table A.2**, listed in the order they are mentioned in the main body of the dissertation. Unfortunately, the concentrations of antibodies are lot-specific, so in some instances when the lot number was not recorded, the concentration of the antibody could not be determined.

Table A.2: Index of all monoclonal antibody conjugates and other fluorescent dyes used for flow cytometry in this study

Antibody	Clone	Isotype	Concentration (μg/mL)	Supplier
CCR5 PE-Cy7	J418F1	Rat IgG2b κ	200	Biolegend
PE-Cy7 isotype control	RTK4530	Rat IgG2b κ	200	Biolegend
CXCR4 BV605	12G5	Mouse IgG2a κ	100	Biolegend
BV605 isotype control	MOPC-173	Mouse IgG2a κ	-	Biolegend
CD4 APC	13B8.2	Mouse IgG1	-	Beckman Coulter
APC isotype control	679.1Mc7	Mouse IgG1	-	Beckman Coulter
KC57 PE	FH190-1-1	Mouse IgG1 κ	-	Beckman Coulter
KC57 PE isotype control	2T8-2F5	Mouse IgG1 κ	-	Beckman Coulter
CD45 KO	J33	Mouse IgG1	-	Beckman Coulter
CD4 FITC	A161A1	Rat IgG2b κ	50	Biolegend
CD14 PE	63D3	Mouse IgG1 κ	200	Biolegend
CD45 BV711	HI30	Mouse IgG1 κ	50	Biolegend
CD25 PE	BC96	Mouse IgG1 κ	50	Biolegend
CD16 APC	3G8	Mouse IgG1 κ	-	Biolegend
CD64 BV510	10.1	Mouse IgG1 κ	80	Biolegend
CD3 APC-Cy7	UCTH1	Mouse IgG1 κ	200	Biolegend

Appendix B:

Optimisation of PCR primer pairs

1. PCR Primer details

During the course of this study, PCR was used for two purposes. Firstly, for the detection of the CD4 mRNA during optimization of the GHOST cell assay, and secondly, for the detection of viral DNA in exposed host cells to confirm successful infection. Sequences for an RT-qPCR primer pair targeting a region of the CD4 mRNA were sourced from a study by Kolte and colleagues (2009) (185). Primers for the detection of HIV-1-C LTR/*gag* and V3-loop regions were designed *de novo,* as described in **Chapter 3** (**Section 3.3.2**). For all PCR reactions, a positive PCR control reaction was included. This reaction was performed using a set of well-validated primers targeting the *Homo sapiens* ribosomal protein L32 pseudogene published by the Lentiviral Vectors Lab at the University of Geneva, originally designed as part of an assay for detection of mycoplasma contamination in cell cultures (271). The sequences and relevant physical properties for each primer used in this study are presented in **Table B.2**, while the details of the primer pairs used for amplification of each target sequence are indicated in **Table B.1**.

Table B.1: Primer pairs used for various PCR reactions and the predicted size of the resulting amplicons

Primer pair target	Forward primer	Reverse primer	Expected amplicon size
Human L32 pseudogene	L32F	L32R	350 bp
Human CD4	CD4F	CD4R	67 bp
HIV CM9 LTR/*gag*	LTR fwd6	ts5'Gag(R) CM9	983 bp
HIV SW7 LTR/*gag*	LTR fwd6	ts5'Gag(R)	978 bp
HIV CM9 V3-loop	V3 fwd6	V3 rvs1.2	406 bp
HIV SW7 V3-loop	V3 fwd3	V3 rvs2	551 bp

Table B.2: Sequences and selected physical properties of the PCR primers used in this study

Primer name	Sequence (5' to 3')	Tm (°C)	%GC	ΔG (Kcal/mol)
L32F	GTG AAG CCC AAG ATC GTC AA	52.38	50	25.9
L32R	TTG GTG ACT CTG ATG GCC AG	53.68	55	26.2
CD4F	GTC CCT TTT AGG CAC TTG CTT CT	55.97	48	29.7
CD4R	TCT TTC CCT GAG TGG CTG CT	55.56	55	26.9
LTR fwd6	CCC TCA GAT GCT GCA TAT AAG CAG CTG C	65.59	54	38.6
ts5'Gag(R) CM9	TCC TTT AAC ATT TGC ATG GCT GCT TG	59.11	42	33.7
ts5'Gag(R)	TCT TTT AAC ATT TGC ATG GCT GCT TG	58.05	38	32.8
V3 fwd3	GGA CCA TGC CAT AAT GTC AGC	53.10	52	26.7
V3 fwd6	GGA CCA TGC AAT AAT GTC AGC	51.73	48	25.8
V3 rvs1.2	GTG TTG TAA TTT CTA GGT CCC C	49.93	45	26.3
V3 rvs2	CCT ACC CCC TGC CAC ATG	51.88	67	24.5

2. Optimisation of CD4 primer pair annealing temperature

Although the primer pair for amplification of the CD4 mRNA was sourced from literature, and had therefore been previously validated, it was designed for RT-qPCR applications. Since our protocol was slightly different, with reverse transcription and PCR amplification performed in discrete steps, it was decided it would be prudent to perform some basic optimisation of the reaction before it was used for experiments. The annealing temperature of a PCR reaction is an important parameter that determines the specificity of primer binding. A high annealing temperature prevents a primer from binding strongly to the DNA template, thereby inhibiting non-specific binding of a primer to a sequence with which it has imperfect complementarity. However, if the temperature is too high, the primer will not be able to bind its target sequence either and the reaction will fail to amplify. The annealing temperature of the PCR reaction for CD4 was optimized using a series of PCR reactions carried out using a temperature gradient.

The PCR reactions were set up as indicated in **Table B.3** using the KAPA Taq ReadyMix (Kapa Biosystems; Wilmington, MA, USA). The template cDNA used was derived from TZM-bl cells, which have high CD4 expression, and was generated as described in **Chapter 3** (**Section 3.2.4**). A positive control reaction using the L32 primer pair was included to confirm that the reagents were functioning correctly, as well as a negative control reaction using the CD4 primers but

no template DNA. The reactions were carried out in the CFX96 Touch Real-Time PCR Detection System (Bio-Rad Laboratories; Hercules, CA, USA) using a temperature gradient ranging between 58°C and 68°C, spread across 8 wells. The thermocycling conditions that were used are indicated in **Table B.4.** The control reactions were performed separately in the GeneAmp™ PCR System 9700, using a set annealing temperature of 55°C. The resulting products were visualized by gel electrophoresis which was run for 1 hour at 90 V in a 1% agarose gel made in TAE buffer. Band sizes were determined using the Low Range FastRuler™ DNA Ladder. The results show that amplification occurred at all temperatures tested (**Figure B.1**). An annealing temperature of 65°C was selected for further experiments.

Table B.3: Reaction setup for optimisation of CD4 PCR annealing temperature

Component	**Volume per reaction**
2X Kapa Taq ReadyMix™	12.5 µL
Forward primer (10 µM)	0.75 µL
Reverse primer (10 µM)	0.75 µL
TZM-bl template cDNA	1 µL
Nuclease-free water	10 µL
	Total reaction volume: 25 µL

Table B.4: Thermocycling conditions for optimisation of CD4 PCR annealing temperature

Step	**Temperature**	**Duration**	**Number of cycles**
Initial denaturation	94°C	2 min	1
Denaturation	94°C	10 sec	30
Annealing	58 - 68°C gradient	10 sec	
Extension	72°C	1 min	
Final extension	72°C	10 min	1
Hold	4°C	∞	-

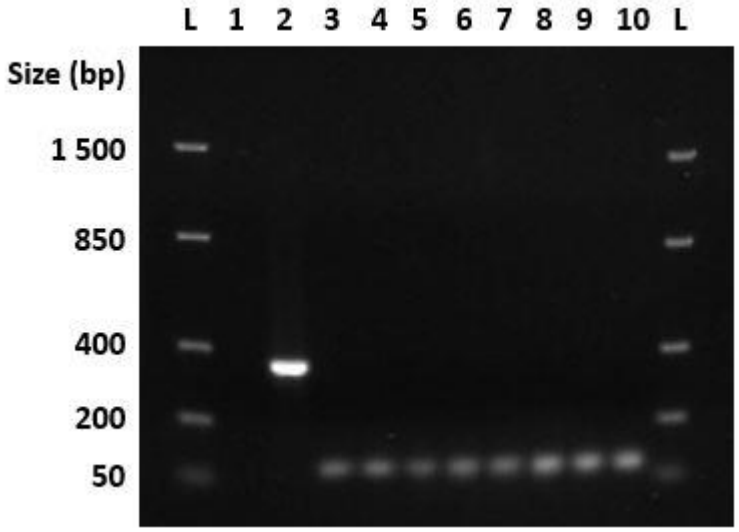

Figure B.1: Gel electropherogram of CD4 PCR products generated using different annealing temperatures. L = ladder, 1 = No template negative PCR control, 2 = L32 positive PCR control, 3 = 68°C, 4 = 67.5°C, 5 = 66.4°C, 6 = 64.4°C, 7 = 62°C, 8 = 60°C, 9 = 58.7°C, 10 = 58°C.

3. Optimisation of HIV primer pair annealing temperature

As for the CD4 PCR assay, the annealing temperature of the PCR reactions to be used for detection of CM9 and SW7 strains of HIV-1-C required optimisation prior to use. PCR reactions were set up as per **Table B.5**, using template DNA extracted from either uninfected, CM9-infected or SW7-infected GHOST cells. The protocol used for infection and isolation of DNA from these cells is described in **Chapter 3** (**Section 3.3.2.2.**). Reactions were carried out using the thermocycling conditions indicated in **Table B.6** in the GeneAmp™ PCR System 9700, using separate runs for each temperature tested. The resulting PCR products were visualized by gel electrophoresis. Electrophoresis conditions were as follows: 40 min to 1 hour at 90 V in a 1% agarose TAE gel. Band sizes were determined using the Low Range FastRuler™ DNA Ladder. The gel electropherogram obtained (**Figure B.2**) was used to determine the optimal annealing temperatures. For the LTR/*gag* PCR reactions, all temperatures tested yielded good amplification. The V3-loop reactions using SW7 were likewise successful at all temperatures; however, for CM9 the reactions were clearly more successful at lower annealing temperatures. The bands were brightest at 54°C to 57°C, slighter fainter bands were observed from 58.5°C to 61.5°C, while at 63°C and 64.5°C, no amplification was observed. An annealing

temperature of 58.5°C was thus selected for further experiments, since amplification for both gene regions in both strains was achieved at this temperature and the risk of non-specific binding is minimized.

Table B.5: Reaction setup for optimisation of LTR/gag and V3-loop region PCR annealing temperature

Component	**Volume per reaction**
2X Kapa Taq ReadyMix™	12.5 µL
Forward primer (10 µM)	0.75 µL
Reverse primer (10 µM)	0.75 µL
DNA template	1 µL
Nuclease-free water	10 µL
	Total reaction volume: 25 µL

Table B.6: Thermocycling conditions for optimisation of LTR/gag and V3-loop region PCR annealing temperature

Step	**Temperature**	**Duration**	**Number of cycles**
Initial denaturation	94°C	2 min	1
Denaturation	94°C	10 sec	
Annealing	54°C - 64.5°C (1.5°C intervals)	10 sec	30
Extension	72°C	1 min	
Final extension	72°C	10 min	1
Hold	4°C	∞	-

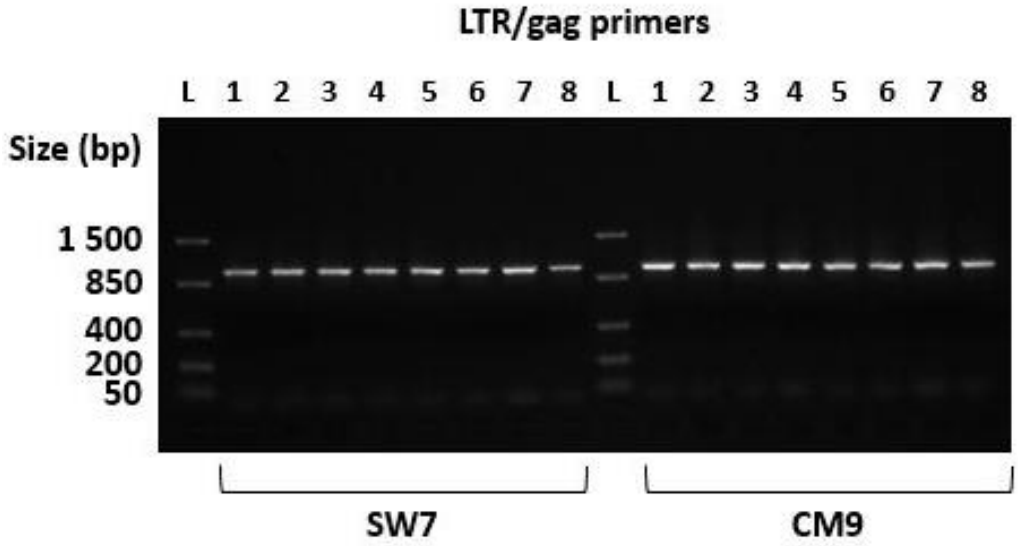

1

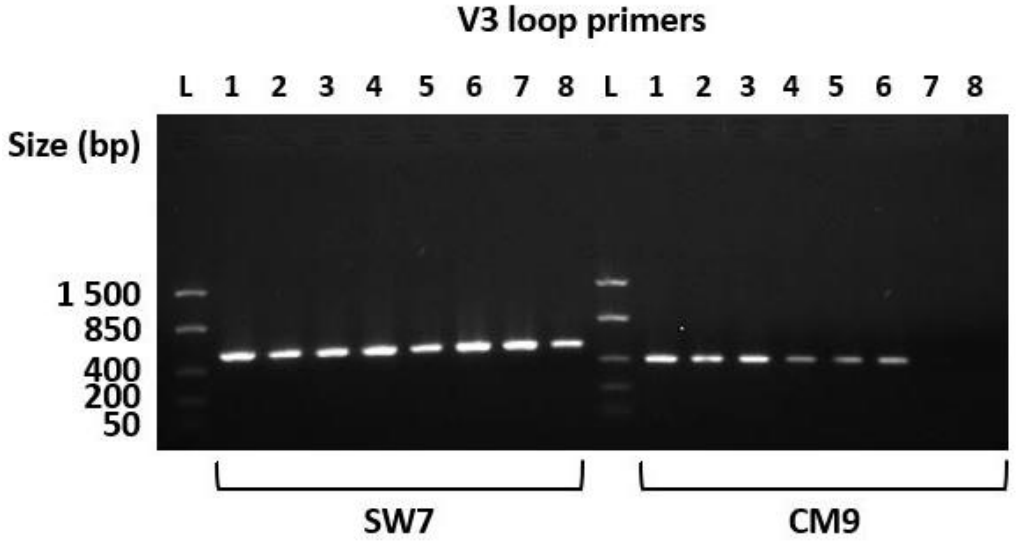

2

3 **Figure B.2: Gel electropherograms of PCR reactions targeting the LTR/*gag* and V3-loop regions of HIV-1 strains**
4 **CM9 and SW1, generated using various annealing temperatures.** L = ladder, 1 = 54°C, 2 = 55.5°C, 3 = 57°C, 4 =
5 58.5°C, 5 = 60°C, 6 = 61.5°C, 7 = 63°C, 8 = 64.5°C.

6

Appendix C:

Titration of antibodies used for flow cytometry

1. Principles of antibody titration

The titration of monoclonal antibodies used in flow cytometry experiments is an important but often overlooked step which ensures optimal staining for the cell type being used. The use of too little antibody results in diminished positive signal, since too few antibodies are available to bind their respective epitopes on the target cells. However, too much antibody can increase the incidence of non-specific binding, resulting in negative cells having artificially increased signal. In an ideal situation, the antibody should provide a clear distinction between positive stained cells and negative cells. To perform an antibody titration, a series of samples is stained with varying quantities of the antibody in question and the resulting signal is analysed. The extent of the separation between positive signal and noise from negative cells can be quantified using the staining index. The staining index (SI) is defined as the difference between the Median Fluorescence Intensity (MFI) of the positively stained population (signal) and the MFI of the negative population (noise), divided by two times the standard deviation of the negative population, as per **Equation C.1**. The higher the staining index value, the greater the resolution between the two populations; therefore, the quantity of antibody yielding the highest staining index is generally considered optimal for flow cytometry experiments. The expected relationship between antibody concentration and the staining index in a typical titration experiment is illustrated in **Figure C.1**.

Equation C.1:

$$Staining\ index\ (SI) = \frac{MFI\ of\ signal - MFI\ of\ noise}{2(SD\ of\ noise)}$$

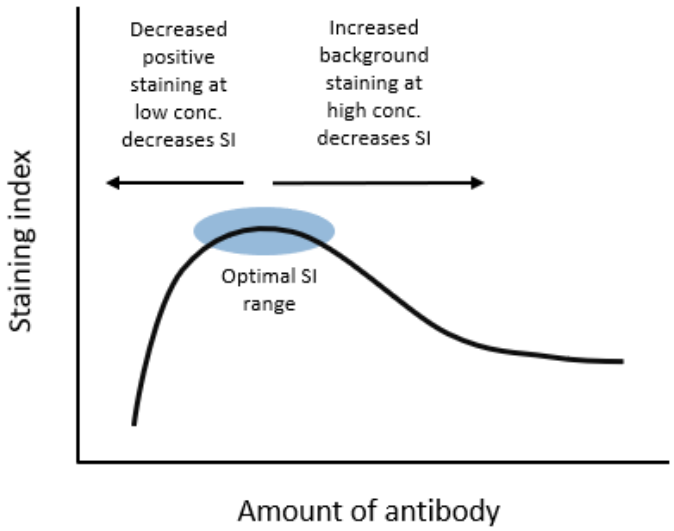

Figure C.1: Illustration of the relationship between the amount of antibody used and the resulting staining index values. The optimal range where the positive and negative populations are distinct, and the staining index is highest is indicated in the blue. circle The SI is reduced at lower antibody concentrations due to a lack of positive staining, while at higher concentrations the SI is decreased by increased background noise due to non-specific staining.

2. Antibody titration experiment setup

The optimal volumes of several antibodies used in this study for immunophenotyping of PBMNCs, $CD4^+$ T cells and macrophages were determined in a simple titration experiment. The following antibodies were included: CD4 FITC, CD45 BV711, CD3 APC-Cy7, CD16 APC, CD64 BV510, and CXCR4 BV605. CCR5 BV785 was also included, but since it was later replaced with CCR5 PE-Cy7, the results are not shown. CD14 PE and CCR5 PE-Cy7 were not titrated, since they were added to the antibody panels at a later stage and were determined to work well at the supplier's recommended concentrations. The CXCR4 BV605 antibody displayed poor resolution in the first experiment, necessitating several repeat experiments using multiple donors, in which an isotypic control was included to facilitate identification of the position of the negative population.

Aliquots of freshly isolated PBMNCs containing $1x10^6$ cells each were added to flow cytometry tubes. The PBMNC samples were stained using varying volumes of the antibodies being tested, as per **Table C.1**, for 15 min in the dark. For CXCR4 BV605, additional samples were stained with the corresponding isotypic control antibody, using the same volumes as for the antibody-stained samples. The cells were washed twice with PBS, prior to resuspending the

final cell pellets in 100 µL PBS. An additional 700 µL PBS was added for volume before analysing the samples using the FACAria Fusion™ cell sorter. The flow cytometry setup for the experiment is illustrated using CD64 BV510 as an example (**Figure C.2**). For all analyses, the PBMNC population was identified using a FS Lin vs SS Log two-parameter plot (**Figure C.2a**). The fluorescence intensities in each sample were assessed using two-parameter plots gated on the region "PBMNCS" for each fluorochrome, plotted against FS Lin (e.g. FS Lin vs CD64 BV510 Log, **Figure C.2b-f**). The positive "SIGNAL" and negative "NOISE" regions were identified on these plots, using either an unstained or isotypic control sample to confirm the position of the negative population if necessary (**Figure C.2f**). The staining index of each sample was calculated using **Equation C.1** and the results were assessed to determine the optimal volume of antibody used for staining.

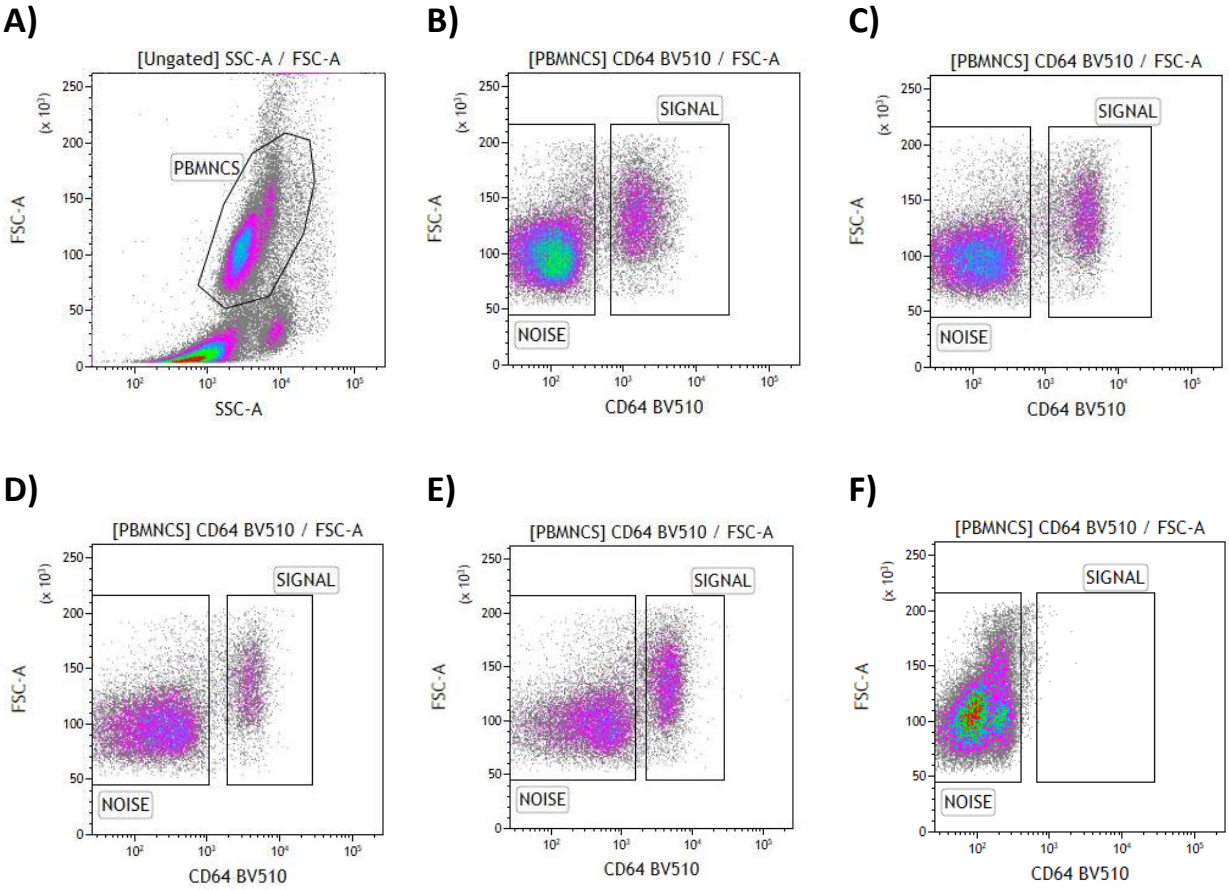

Figure C.2: Flow cytometry setup for analysis of signal obtained after staining PBMNCs with various volumes of antibody, using CD64 BV510 as an example. A) The PBMNC population was identified on a FS Lin vs SS Log plot, in the region marked "PBMNCS". A series of FS Lin vs CD64 BV510 Log plots gated on "PBMNCS" were used to assess signal intensity in the BV510 channel for each volume of antibody tested: **B)** 1.25 µL. **C)** 2.5 µL., **D)** 5 µL, **E)** 10 µL. **F)** An unstained control was used to confirm the position of the negative population.

Table C.1: Volumes of monoclonal antibodies tested during titration experiments

Antibody	Donor ID	Volume of antibody tested (µL)				
		Vol 1	Vol 2	Vol 3	Vol 4	Vol 5
CD4 FITC	PB-03	1.25	2.5	5	10	-
CD45 BV711	PB-03	1.25	2.5	5	10	-
CD3 APC-Cy7	PB-03	1.25	2.5	5	10	-
CD16 APC	PB-03	1.25	2.5	5	10	-
CD64 BV510	PB-03	1.25	2.5	5	10	-
CXCR4 BV605	PB-11	0.3	0.6	1.5	-	-
	PB-12	-	0.6	1.5	2.5	5
	PB-13	-	-	1.5	2.5	5

3. Results of antibody titration experiment

The responses to staining with different concentrations of antibody were largely as expected, exemplified by the results obtained for CD64 BV510 (**Figure C.2**). Lower resolution was generally observed at the smallest volumes due to insufficient staining and at the highest volumes due to increased non-specific staining. This was echoed in the staining index values obtained **Figure C.3**). CD4 FITC, CD45 BV711, CD3 APC-Cy7 and CD64 BV510 demonstrated typical staining index profiles, with peaks occurring at 2.5 µL. The results for CD16 APC were slightly different in that the staining index was optimal at the lowest volume tested (1.25 µL), indicating that it could be titrated even further using lower volumes. However, since the resolution observed at this volume was sufficiently high (SI = 21.93), it was decided that there was no real need to decrease the volume and increase the risk of pipetting error. In contrast, the CXCR4 BV605 antibody showed little difference in staining index across the different concentrations tested, although it did increase slightly at higher concentrations. It is possible that this is due to a genuine lack of distinct positive and negative populations of cells, rather than a failure of the antibody to resolve them. CXCR4 expression is known to be quite variable, possibly resulting in the cells being spread out across a spectrum of different expression levels. It was decided that 5 µL should be used, since this volume gave the highest staining index and correlates with the quantity recommended for use by the supplier.

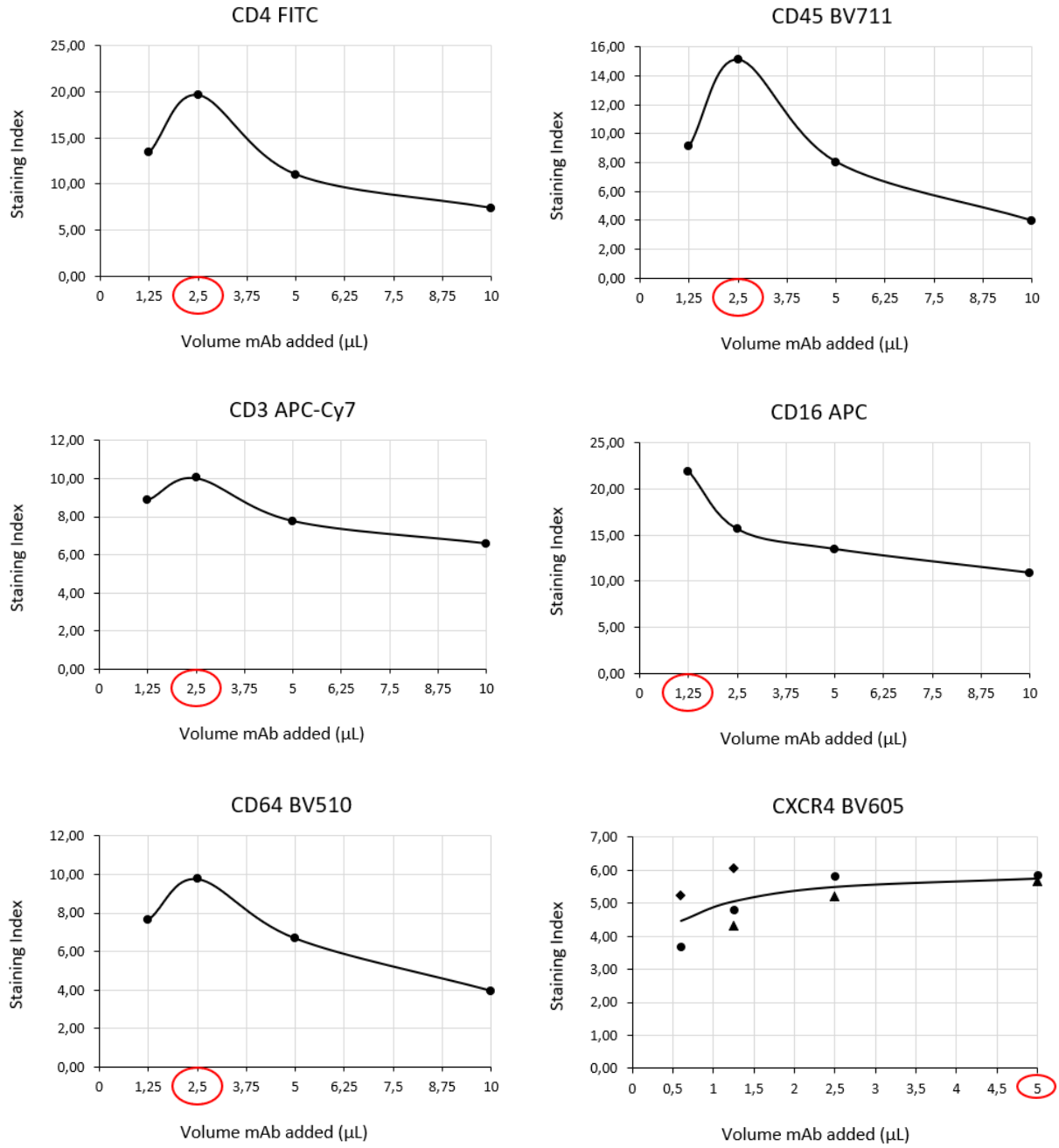

Figure C.3: Line graphs indicating the staining index values obtained for each antibody tested in the titration experiment. The volumes of antibody used are indicated on the x-axis, while the staining index values are indicated on the y-axis. The data for CD4 FITC, CD45 BV711, CD3 APC-Cy7, CD16 APC, CD64 BV510 are representative of one biological replicate, while for CXCR4 the data is representative of the mean two (0.6 µL, 2.5 µL, 5 µL) or three (1.25 µL) biological repeats, depending on the volumes tested for each donor (**Table C.1**). The final volumes selected for use in further experiments are circled in red.

Appendix D:

Additional data from quantification and characterization of PBMNCs and CD4$^+$ T lymphocyte/monocyte populations

1. Quantification of PBMNCs and CD4$^+$ T lymphocyte/monocyte populations

The quantification of PBMNCs was carried out immediately after isolation by flow cytometric analysis, as described in **Chapter 4** (**Section 3.1.2.** & **Section 4.1.1**). This was a critical step, since it enabled the use of specific numbers of cells for downstream experiments and the freezing of PBMNC stocks with known cell numbers. In later isolations, the relative proportions of CD4$^+$ T cells and monocytes were determined concurrently. Since donors have varying quantities of these two cell types depending on their immune activation state and other intrinsic factors, this information was critical for calculation of the required numbers of input cells when sorting pure populations. The results of these analyses for every donor used in this study are indicated in **Table D.1**.

Table D.1: Results of PBMNC quantification and identification of CD4$^+$ T lymphocyte and monocyte subsets based on CD4 expression

Donor ID	% Viable	% CD4$^+$ T cells	% Monocytes	Cells/µL	Total cell count
PB3	66.00	-	-	$9.27x10^3$	$9.27x10^7$
PB5	97.87	-	-	$4.01x10^4$	$4.01x10^8$
PB6	83.65	-	-	$8.91x10^3$	$8.91x10^7$
PB7	93.06	-	-	$8.50x10^3$	$8.50x10^7$
PB8	90.35	-	-	$5.16x10^3$	$5.16x10^7$
PB9	95.59	-	-	$1.80x10^4$	$1.80x10^8$
PB10	97.44	-	-	$9.85x10^3$	$9.85x10^7$
PB11	94.81	-	-	$1.25x10^4$	$1.25x10^8$
PB12	95.66	-	-	$9.45x10^3$	$9.45x10^7$

PB13	96.11	28.78	27.75	$2.32x10^4$	$2.32x10^8$
PB14	99.28	28.79	34.57	$8.73x10^3$	$8.73x10^7$
PB15	89.74	38.87	24.81	$1,90x10^4$	$1,90x10^8$
PB16	98.06	37.54	27.41	$1.43x10^4$	$1.43x10^8$
PB17	99.50	25.38	32.80	$1.42x10^4$	$1.42x10^8$
PB18	99.58	35.27	27.99	$1.42x10^4$	$1.42x10^8$
PB20	99.06	36.50	21.47	$1.76x10^4$	$1.76x10^8$
PB21	99.43	33.03	26.8	$2.59x10^4$	$2.59x10^8$
PB22	99.29	29.50	24.62	$1.22x10^4$	$1.22x10^8$
PB24	98.42	28.47	18.79	$1.38x10^4$	$1.38x10^8$
PB25	98.01	31.36	23.18	$1.88x10^4$	$1.88x10^8$
PB26	99.44	34.86	28.01	$1.21x10^4$	$1.21x10^8$
PB28	97.03	29.90	26.65	$1.90x10^4$	$1.90x10^8$
PB29	94.86	15.12	33.76	$1.16x10^4$	$1.16x10^8$
PB31	92.17	34.48	26.32	$1.29x10^4$	$1.29x10^8$
PB32	99.72	38.86	21.34	$1.33x10^4$	$1.33x10^8$
PB34	99.63	19.88	40.40	$2.18x10^4$	$2.18x10^8$
PB35	99.65	30.40	28.19	$2.60x10^4$	$2.60x10^8$
PB36	93.33	39.28	26.88	$1.15x10^4$	$1.15x10^8$
PB37	99.65	24.63	32.90	$1,66x10^4$	$1,66x10^8$
PB38	99.33	33.92	25.57	$2,04x10^4$	$2,04x10^8$
PB39	98.34	28.42	27.33	$1,18x10^4$	$1,18x10^8$
PB41	95.88	26.55	28.46	$8.12x10^3$	$8.12x10^7$
PB42	99.68	36.36	25.33	$1.81x10^4$	$1.81x10^8$
PB44	99.15	12.57	38.78	$1.45x10^4$	$1.45x10^8$
PB45	99.58	31.46	12.17	$2.97x10^4$	$2.97x10^8$
PB47	99.75	26.20	24.67	$1.09x10^4$	$1.09x10^8$
PB49	99.01	44.25	17.13	$8.99x10^3$	$8.99x10^7$
PB50	98.89	43.9	20.03	$1.01x10^4$	$1.01x10^8$
PB51	95.78	35.97	25.18	$1.16x10^4$	$1.16x10^8$
PB52	95.83	37.95	14.46	$9.57x10^3$	$9.57x10^7$
PB57	99.51	26.58	25.07	$1.49x10^4$	$1.49x10^8$
PB58	99.13	26.11	27.41	$1.88x10^4$	$1.88x10^8$

1

2. Characterisation of co-receptor expression in CD4$^+$ T lymphocyte/monocyte populations

Part of the protocol for immunophenotyping of isolated PBMNCs was the flow cytometric analysis of CCR5 and CXCR4 expression, as described in **Chapter 4** (**Section 3.1.4.** & **Section 4.1.1**). **Table D.2** presents the full results of this analysis for each donor that was assayed. It is important to note that some donors made more than one donation (**Table D.3**). This had important implications for the selection of unique donors for viral culture, as well as for selection of biological replicates to be used for the various experiments carried out in this study. In the case of co-receptor characterisation, many of the PBMNC isolates were not directly immunophenotyped. However, an idea of their co-receptor expression profiles could be obtained from other isolations performed on the same donor that had been analysed. Samples for which co-receptor expression was directly determined are highlighted in red in **Table D.3**.

Table D.2: Co-receptor expression in the CD4$^+$ T lymphocyte and monocyte populations of immunophenotyped PBMNCs

	CD4$^+$ T Lymphocytes		**Monocytes**	
Donor ID	**CXCR4$^+$**	**CCR5$^+$**	**CXCR4$^+$**	**CCR5$^+$**
PB17	76.16	9.43	37.30	92.88
PB22	86.18	8.91	83.26	38.04
PB25	69.44	7.18	75.71	59.34
PB29	56.56	18.85	34.11	14.66
PB31	56.86	11.32	29.72	70.74
PB32	76.78	4.95	1.07	60.59
PB33	82.35	10.29	49.76	22.27
PB34	86.07	9.11	6.58	59.90
PB35	70.81	11.61	26.85	32.24
PB36	90.86	7.45	39.29	72.02
PB37	81.83	14.65	29.30	56.74

Table D.3: List of peripheral blood donors indicating those from which multiple donations were taken

Donor	Additional sample IDs corresponding to same donor
PB3	-
PB4	PB18
PB5	PB12, PB17, PB25, PB28, PB33, PB41, PB44, PB52
PB6	PB11, PB19, PB39
PB7	-
PB8	-
PB9	-
PB10	-
PB13	PB16, PB21, PB35
PB14	PB20, PB32, PB38, PB42, PB51
PB15	PB26, PB49
PB22	PB31, PB57
PB24	-
PB29	-
PB34	-
PB36	PB50
PB37	PB47, PB58
PB45	-

Appendix E: Ethics Approval Certificate

The Research Ethics Committee, Faculty Health Sciences, University of Pretoria complies with ICH-GCP guidelines and has US Federal wide Assurance.
- FWA 00002567, Approved dd 22 May 2002 and Expires 20 Oct 2016.
- IRB 0000 2235 IORG0001762 Approved dd 22/04/2014 and Expires 22/04/2017.

UNIVERSITEIT VAN PRETORIA
UNIVERSITY OF PRETORIA
YUNIBESITHI YA PRETORIA

Faculty of Health Sciences Research Ethics Committee

28/07/2016

Approval Certificate
New Application

Ethics Reference No.: 204/2016

Title: Transcriptional analysis of the host response to HIV-1 infection in CD4+ T lymphocytes and macrophages

Dear Catherine Heather Wickham

The **New Application** as supported by documents specified in your cover letter dated 20/07/2016 for your research received on the 20/07/2016, was approved by the Faculty of Health Sciences Research Ethics Committee on its quorate meeting of 27/07/2016.

Please note the following about your ethics approval:
- Ethics Approval is valid for 3 years
- Please remember to use your protocol number (**204/2016**) on any documents or correspondence with the Research Ethics Committee regarding your research.
- Please note that the Research Ethics Committee may ask further questions, seek additional information, require further modification, or monitor the conduct of your research.

Ethics approval is subject to the following:
- The ethics approval is conditional on the receipt of **6 monthly written Progress Reports**, and
- The ethics approval is conditional on the research being conducted as stipulated by the details of all documents submitted to the Committee. In the event that a further need arises to change who the investigators are, the methods or any other aspect, such changes must be submitted as an Amendment for approval by the Committee.

We wish you the best with your research.

Yours sincerely

Dr R Sommers; MBChB; MMed (Int); MPharMed,PhD
Deputy Chairperson of the Faculty of Health Sciences Research Ethics Committee, University of Pretoria

The Faculty of Health Sciences Research Ethics Committee complies with the SA National Act 61 of 2003 as it pertains to health research and the United States Code of Federal Regulations Title 45 and 46. This committee abides by the ethical norms and principles for research, established by the Declaration of Helsinki, the South African Medical Research Council Guidelines as well as the Guidelines for Ethical Research: Principles Structures and Processes 2004 (Department of Health).

☎ 012 356 3084 fhsethics@up.ac.za http://www.up.ac.za/healthethics
✉ Private Bag X323, Arcadia, 0007 - Tswelopele Building, Level 4, Room 60, Gezina, Pretoria

References

1. Levy JA, Hoffman AD, Kramer SM, Landis JA, Shimabukuro JM, Oshiro LS. Isolation of lymphocytopathic retroviruses from San Francisco patients with AIDS. Science. 1984 Aug 24;225(4664):840–2.

2. Barré-Sinoussi F, Chermann JC, Rey F, Nugeyre MT, Chamaret S, Gruest J, et al. Isolation of a T-lymphotropic retrovirus from a patient at risk for acquired immune deficiency syndrome (AIDS). Science. 1983 May 20;220(4599):868–71.

3. Gallo RC, Salahuddin SZ, Popovic M, Shearer GM, Kaplan M, Haynes BF, et al. Frequent detection and isolation of cytopathic retroviruses (HTLV-III) from patients with AIDS and at risk for AIDS. Science. 1984 May 4;224(4648):500–3.

4. Kilmarx PH. Global epidemiology of HIV. Curr Opin HIV AIDS. 2009 Jul;4(4):240–6.

5. McCutchan FE. Global epidemiology of HIV. J Med Virol. 2006;78(S1):S7–12.

6. Statistics South Africa. Mid-year population estimates 2018 [Internet]. Mid-year population estimates. 2018. Available from: http://www.statssa.gov.za/?page_id=1854&PPN=P0302&SCH=7362

7. The Antiretroviral Therapy Cohort Collaboration. Life expectancy of individuals on combination antiretroviral therapy in high-income countries: a collaborative analysis of 14 cohort studies. Lancet. 2008 Jul 26;372(9635):293–9.

8. Johnson LF, Mossong J, Dorrington RE, Schomaker M, Hoffmann CJ, Keiser O, et al. Life expectancies of South African adults starting antiretroviral treatment: Collaborative analysis of cohort studies. Celentano DD, editor. PLoS Med. 2013 Apr 9;10(4):e1001418.

9. Shibuyama S, Gevorkyan A, Yoo U, Tim S, Dzhangiryan K, Scott J. Understanding and avoiding antiretroviral adverse events. Curr Pharm Des. 2006 Mar 1;12(9):1075–90.

10. Ho Y-C, Shan L, Hosmane NN, Wang J, Laskey SB, Rosenbloom DIS, et al. Replication-competent noninduced proviruses in the latent reservoir increase barrier to HIV-1 cure. Cell. 2013 Oct 24;155(3):540–51.

11. Chun TW, Stuyver L, Mizell SB, Ehler LA, Mican JA, Baseler M, et al. Presence of an inducible

HIV-1 latent reservoir during highly active antiretroviral therapy. Proc Natl Acad Sci U S A. 1997 Nov 25;94(24):13193–7.

12. Bulteel N, Bansi-Matharu L, Churchill D, Dunn D, Bibby D, Hill T, et al. The emergence of drug resistant HIV variants at virological failure of HAART combinations containing efavirenz, tenofovir and lamivudine or emtricitabine within the UK Collaborative HIV Cohort. J Infect. 2014;68(1):77–84.

13. Santos AF, Soares MA. HIV genetic diversity and drug resistance. Viruses. 2010 Feb;2(2):503–31.

14. Burton DR, Ahmed R, Barouch DH, Butera ST, Crotty S, Godzik A, et al. A blueprint for HIV vaccine discovery. Cell Host Microbe. 2012 Oct 18;12(4):396–407.

15. Lynch RM, Shen T, Gnanakaran S, Derdeyn CA. Appreciating HIV type 1 diversity: subtype differences in Env. AIDS Res Hum Retroviruses. 2009;25(3):237–48.

16. Taylor BS, Sobieszczyk ME, McCutchan FE, Hammer SM. The challenge of HIV-1 subtype diversity. N Engl J Med. 2008 Apr 10;358(15):1590–602.

17. Coiras M, López-Huertas MR, Pérez-Olmeda M, Alcamí J. Understanding HIV-1 latency provides clues for the eradication of long-term reservoirs. Nat Rev Microbiol. 2009 Nov 1;7(11):798–812.

18. Xu W, Li H, Wang Q, Hua C, Zhang H, Li W, et al. Advancements in developing strategies for sterilizing and functional HIV cures. Biomed Res Int. 2017 Apr 26;2017:1–12.

19. Kuhlmann A-S, Peterson CW, Kiem H-P. Chimeric antigen receptor T-cell approaches to HIV cure. Curr Opin HIV AIDS. 2018 Jun;13(5):1.

20. Luciw PA. Human immunodeficiency viruses and their replication. In: Fields BN, Knipe DM, Howley PM, editors. Fields Virology. 3rd ed. Philadelphia: Lippincott-Raven Publishers; 1996. p. 1881–1952.

21. Ganser-Pornillos BK, Yeager M, Sundquist WI. The structural biology of HIV assembly. Curr Opin Struct Biol. 2008;18(2):203–17.

22. Frankel AD, Young JAT. HIV-1: Fifteen proteins and an RNA. Annu Rev Biochem. 1998;67:1–25.

23. Watts JM, Dang KK, Gorelick RJ, Leonard CW, Bess Jr JW, Swanstrom R, et al. Architecture and secondary structure of an entire HIV-1 RNA genome. Nature. 2009 Aug 6;460(7256):711–6.

24. Gentile M, Adrian T, Scheidler A, Ewald M, Dianzani F, Pauli G, et al. Determination of the size of HIV using adenovirus type 2 as an internal length marker. J Virol Methods. 1994 Jun;48(1):43–52.

25. Castro-Nallar E, Pérez-Losada M, Burton GF, Crandall KA. The evolution of HIV: Inferences using phylogenetics. Mol Phylogenet Evol. 2012 Feb;62(2):777–92.

26. Qu X, Wang P, Ding D, Wang X, Zhang G, Zhou X, et al. Zinc finger nuclease: a new approach for excising HIV-1 proviral DNA from infected human T cells. Mol Biol Rep. 2014 Sep 29;41(9):5819–27.

27. Zhou H, Xu M, Huang Q, Gates AT, Zhang XD, Castle JC, et al. Genome-scale RNAi screen for host factors required for HIV replication. Cell Host Microbe. 2008 Nov 13;4(5):495–504.

28. Li G, Piampongsant S, Faria NR, Voet A, Pineda-Peña A-C, Khouri R, et al. An integrated map of HIV genome-wide variation from a population perspective. Retrovirology. 2015;12(1):18.

29. Freed EO. HIV-1 Replication. Somat Cell Mol Genet. 2001;26(1/6):13–33.

30. Ayinde D, Maudet C, Transy C, Margottin-Goguet F. Limelight on two HIV/SIV accessory proteins in macrophage infection: is Vpx overshadowing Vpr? Retrovirology. 2010;7:35.

31. Schulze T, Nawrath M, Moelling K. Cleavage of the HIV-1 p66 reverse transcriptase/RNase H by the p9 protease in vitro generates active p15 RNase H. Arch Virol. 1991 Sep;118(3–4):179–88.

32. Hill M, Tachedjian G, Mak J. The packaging and maturation of the HIV-1 Pol proteins. Curr HIV Res. 2005 Jan 1;3(1):73–85.

33. Stoltzfus CM. Chapter 1: Regulation of HIV-1 alternative RNA splicing and its role in virus replication. In: Advances in virus research. 2009. p. 1–40.

34. Karn J, Stoltzfus CM. Transcriptional and posttranscriptional regulation of HIV-1 gene expression. Cold Spring Harb Perspect Med. 2012 Feb;2(2):a006916.

35. Hemelaar J. The origin and diversity of the HIV-1 pandemic. Trends Mol Med. 2012

Mar;18(3):182–92.

36. Popper SJ, Sarr AD, Travers KU, Guèye-Ndiaye A, Mboup S, Essex ME, et al. Lower Human Immunodeficiency Virus (HIV) Type 2 viral load reflects the difference in pathogenicity of HIV-1 and HIV-2. J Infect Dis. 1999 Oct 1;180(4):1116–21.

37. Levy JA. HIV pathogenesis: 25 years of progress and persistent challenges. AIDS. 2009;23(2):147–60.

38. Solis M, Wilkinson P, Romieu R, Hernandez E, Wainberg MA, Hiscott J. Gene expression profiling of the host response to HIV-1 B, C, or A/E infection in monocyte-derived dendritic cells. Virology. 2006;352(1):86–99.

39. Rambaut A, Robertson DL, Pybus OG, Peeters M, Holmes EC. Phylogeny and the origin of HIV-1. Nature. 2001;410(6832):1047–8.

40. Lau KA, Wong JJL. Current trends of HIV recombination worldwide. Infect Dis Rep. 2013 Jun 6;5(Suppl 1):e4.

41. Korber B, Gaschen B, Yusim K, Thakallapally R, Kesmir C, Detours V. Evolutionary and immunological implications of contemporary HIV-1 variation. Br Med Bull. 2001 Sep 1;58(1):19–42.

42. Los Alamos National Laboratory. HIV circulating recombinant forms (CRFs) [Internet]. HIV Sequence Database. [cited 2019 Apr 26]. Available from: https://www.hiv.lanl.gov/content/sequence/HIV/CRFs/CRFs.html#CRF98

43. Iordanskiy S, Waltke M, Feng Y, Wood C. Subtype-associated differences in HIV-1 reverse transcription affect the viral replication. Retrovirology. 2010;7:85.

44. Imbeault M, Giguère K, Ouellet M, Tremblay MJ. Exon level transcriptomic profiling of HIV-1-infected CD4+ T cells reveals virus-induced genes and host environment favorable for viral replication. PLoS Pathog. 2012;8(8).

45. Ramakrishnan R, Chiang K, Liu H, Budhiraja S, Donahue H, Rice AP. Making a short story long: regulation of P-TEFb and HIV-1 transcriptional elongation in CD4+ T lymphocytes and macrophages. Biology (Basel). 2012 Jun 15;1(3):94–115.

46. Hung M, Patel P, Davis S, Green SR. Importance of ribosomal frameshifting for Human

Immunodeficiency Virus Type 1 particle assembly and replication. Vol. 72, Journal of virology. 1998.

47. Jacks T, Power MD, Masiarz FR, Luciw PA, Barr PJ, Varmus HE. Characterization of ribosomal frameshifting in HIV-1 gag-pol expression. Nature. 1988 Jan;331(6153):280–3.

48. Siliciano RF, Greene WC. HIV latency. Cold Spring Harb Perspect Med. 2011 Sep;1(1):a007096.

49. Jakobsen MR, Ellett A, Churchill MJ, Gorry PR. Viral tropism, fitness and pathogenicity of HIV-1 subtype C. Future Virol. 2010;5(2):219–31.

50. Parczewski M. Genomics and transcriptomics in HIV and HIV/HCV coinfection - Review of basic concepts and genome-wide association studies. HIV AIDS Rev. 2013;12(4):97–101.

51. Ivanoff LA, Dubay JW, Morris JF, Roberts SJ, Gutshall L, Sternberg EJ, et al. V3 loop region of the HIV-1 gp120 envelope protein is essential for virus infectivity. Virology. 1992 Apr;187(2):423–32.

52. Cilliers T, Willey S, Sullivan WM, Patience T, Pugach P, Coetzer M, et al. Use of alternate coreceptors on primary cells by two HIV-1 isolates. Virology. 2005;339(1):136–44.

53. Mörner A, Björndal Å, Albert J, Kewalramani VN, Littman DR, Inoue R, et al. Primary Human Immunodeficiency Virus Type 2 (HIV-2) isolates, like HIV-1 isolates, frequently use CCR5 but show promiscuity in coreceptor usage. J Virol. 1999;73(3):2343–9.

54. Kedzierska K, Crowe S. The role of monocytes and macrophages in the pathogenesis of HIV-1 infection. Curr Med Chem. 2002;9(21):1893–903.

55. Sirois M, Robitaille L, Sasik R, Estaquier J, Fortin J, Corbeil J. R5 and X4 HIV viruses differentially modulate host gene expression in resting CD4 + T cells. AIDS Res Hum Retroviruses. 2008;24(3):485–93.

56. Arrildt KT, LaBranche CC, Joseph SB, Dukhovlinova EN, Graham WD, Ping L-H, et al. Phenotypic correlates of HIV-1 macrophage tropism. J Virol. 2015 Nov 15;89(22):11294–311.

57. Clark SJ, Shaw GM. The acute retroviral syndrome and the pathogenesis of HIV-1 infection. Vol. 5, Seminars in Immunology. 1993. p. 149–55.

58. Badley AD, Pilon AA, Landay A, Lynch DH. Mechanisms of HIV-associated lymphocyte

apoptosis. Blood. 2000;96(9):2951–64.

59. Palmer CS, Cherry CL, Sada-Ovalle I, Singh A, Crowe SM. Glucose metabolism in T cells and monocytes: New perspectives in HIV pathogenesis. EBioMedicine. 2016;6:31–41.

60. Zinkernagel RM, Hengartner H. T-cell-mediated immunopathology versus direct cytolysis by virus: implications for HIV and AIDS. Immunol Today. 1994;15(6):262–8.

61. Espert L, Denizot M, Grimaldi M, Robert-Hebmann V, Gay B, Varbanov M, et al. Autophagy is involved in T cell death after binding of HIV-1 envelope proteins to CXCR4. J Clin Invest. 2006 Aug 1;116(8):2161–72.

62. Vishnu P, Aboulafia DM. Haematological manifestations of human immune deficiency virus infection. Br J Haematol. 2015;171(5):695–709.

63. Brenchley JM, Douek DC. The mucosal barrier and immune activation in HIV pathogenesis. Curr Opin HIV AIDS. 2008;3(3):356–61.

64. Jan V, Cervera P, Maachi M, Baudrimont M, Kim M, Vidal H, et al. Altered fat differentiation and adipocytokine expression are inter-related and linked to morphological changes and insulin resistance in HIV-1-infected lipodystrophic patients. Antivir Ther. 2004;9(4):555–64.

65. Levine AJ, Horvath S, Miller EN, Singer EJ, Shapshak P, Baldwin GC, et al. Transcriptome analysis of HIV-infected peripheral blood monocytes: Gene transcripts and networks associated with neurocognitive functioning. J Neuroimmunol. 2013;265(1–2):96–105.

66. Kumar P. Long term non-progressor (LTNP) HIV infection. Indian J Med Res. 2013 Sep;138(3):291–3.

67. Saag M, Deeks SG. How do HIV elite controllers do what they do? Clin Infect Dis. 2010;51(2):239–41.

68. Yi Y, Rana S, Turner JD, Gaddis N, Collman RG. CXCR-4 is expressed by primary macrophages and supports CCR5-independent infection by dual-tropic but not T-tropic isolates of human immunodeficiency virus type 1. J Virol. 1998;72(1):772–7.

69. Lisziewicz J, Rosenberg E, Lieberman J, Jessen H, Lopalco L, Siliciano R, et al. Control of HIV despite the discontinuation of antiretroviral therapy. N Engl J Med. 1999 May 27;340(21):1683–1683.

70. Rodrigo AG, Shpaer EG, Delwart EL, Iversen AK, Gallo M V, Brojatsch J, et al. Coalescent estimates of HIV-1 generation time in vivo. Proc Natl Acad Sci U S A. 1999 Mar 2;96(5):2187–91.

71. O'Neil PK, Sun G, Yu H, Ron Y, Dougherty JP, Preston BD. Mutational analysis of HIV-1 long terminal repeats to explore the relative contribution of reverse transcriptase and RNA polymerase II to viral mutagenesis. J Biol Chem. 2002 Oct 11;277(41):38053–61.

72. Abram ME, Ferris AL, Shao W, Alvord WG, Hughes SH. Nature, position, and frequency of mutations made in a single cycle of HIV-1 replication. J Virol. 2010 Oct 1;84(19):9864–78.

73. Mansky LM, Temin HM. Lower in vivo mutation rate of human immunodeficiency virus type 1 than that predicted from the fidelity of purified reverse transcriptase. J Virol. 1995 Aug;69(8):5087–94.

74. Cuevas JM, Geller R, Garijo R, López-Aldeguer J, Sanjuán R, Rowland-Jones SL. Extremely high mutation rate of HIV-1 in vivo. 2015;

75. Zanini F, Puller V, Brodin J, Albert J, Neher RA. In vivo mutation rates and the landscape of fitness costs of HIV-1.

76. Roberts JD, Bebenek K, Kunkel TA. The accuracy of reverse transcriptase from HIV-1. Science. 1988 Nov 25;242(4882):1171–3.

77. Yu Q, Landau NR, König R. Vif and the role of antiviral cytidine deaminases in HIV-1 replication.

78. Smyth RP, Davenport MP, Mak J. The origin of genetic diversity in HIV-1. Virus Res. 2012 Nov 1;169(2):415–29.

79. Hu WS, Temin HM. Genetic consequences of packaging two RNA genomes in one retroviral particle: pseudodiploidy and high rate of genetic recombination. Proc Natl Acad Sci U S A. 1990 Feb 1;87(4):1556–60.

80. Jetzt AE, Yu H, Klarmann GJ, Ron Y, Preston BD, Dougherty JP. High rate of recombination throughout the human immunodeficiency virus type 1 genome. J Virol. 2000 Feb;74(3):1234–40.

81. Shriner D, Rodrigo AG, Nickle DC, Mullins JI. Pervasive genomic recombination of HIV-1 in

vivo. Genetics. 2004 Aug;167(4):1573–83.

82. Andino R, Domingo E. Viral quasispecies. Virology. 2015;479–480:46–51.

83. Meyerhans A, Cheynier R, Albert J, Seth M, Kwok S, Sninsky J, et al. Temporal fluctuations in HIV quasispecies in vivo are not reflected by sequential HIV isolations. Cell. 1989;58(5):901–10.

84. Spira S, Wainberg MA, Loemba H, Turner D, Brenner BG. Impact of clade diversity on HIV-1 virulence , antiretroviral drug sensitivity and drug resistance. 2003;229–40.

85. Geretti AM. HIV-1 subtypes : epidemiology and significance for HIV management. 2003;1–7.

86. Lessells RJ, Katzenstein DK, Oliveira T De. Are subtype differences important in HIV drug resistance? Curr Opin Virol. 2012;2(5):636–43.

87. Lai AY, Kondo M. T and B lymphocyte differentiation from hematopoietic stem cell. Semin Immunol. 2008 Aug;20(4):207–12.

88. Mehta AB, Hoffbrand A V. Haemtatology at a Glance. 4th ed. Hoboken, NJ, USA: Blackwell Science; 2005.

89. Hoffbrand A V, Moss PAH. Essential Haematology. 6th ed. Hoboken, NJ, USA: Blackwell Science; 2011.

90. Luckheeram RV, Zhou R, Verma AD, Xia B. CD4+ T cells: Differentiation and functions. Clin Dev Immunol. 2012 Mar 14;2012:1–12.

91. Zhu J, Paul WE. CD4 T cells: fates, functions, and faults. Blood. 2008 Sep 1;112(5):1557–69.

92. Shah DK, Carlos Zúñiga-Pflücker J. An overview of the intrathymic intricacies of T cell development. J Immunol. 2014;192:4017–23.

93. Takahama Y. Journey through the thymus: stromal guides for T-cell development and selection. Nat Rev Immunol. 2006 Feb 1;6(2):127–35.

94. Steinman RM, Pack M, Inaba K. Dendritic cells in the T-cell areas of lymphoid organs. Immunol Rev. 1997 Apr;156:25–37.

95. Golubovskaya V, Wu L. Different subsets of T cells, memory, effector functions, and CAR-T

immunotherapy. Cancers (Basel). 2016 Mar 15;8(3).

96. Kaplan MH, Hufford MM, Olson MR. The development and in vivo function of TH9 cells. Nat Rev Immunol. 2015;15(5):295–307.

97. Boyce JA, Finkelman F, Shearer WT, Vercelli D, Akdis U, Palomares O, et al. TH 17 and TH 22 cells: A confusion of antimicrobial response with tissue inflammation versus protection. J Allergy Clin Immunol. 2012;129:1438–49.

98. Hirahara K, Nakayama T. CD4+ T-cell subsets in inflammatory diseases: beyond the Th1/Th2 paradigm. Int Immunol. 2016 Apr;28(4):163–71.

99. Chang JT, Wherry EJ, Goldrath AW. Molecular regulation of effector and memory T cell differentiation. Nat Immunol. 2014 Dec;15(12):1104–15.

100. Jia L, Wu C. The biology and functions of Th22 cells. Adv Exp Med Biol. 2014;209–30.

101. Crotty S. Follicular Helper CD4 T Cells (TFH). Annu Rev Immunol. 2011 Apr 23;29(1):621–63.

102. Giri MS, Nebozhyn M, Showe L, Montaner LJ. Microarray data on gene modulation by HIV-1 in immune cells: 2000-2006. J Leukoc Biol. 2006;80(5):1031–43.

103. Geiss GK, Bumgarner RE, An MC, Agy MB, Van 't Wout a B, Hammersmark E, et al. Large-scale monitoring of host cell gene expression during HIV-1 infection using cDNA microarrays. Virology. 2000;266(1):8–16.

104. Corbeil J, Sheeter D, Genini D, Rought S, Leoni L, Du P, et al. Temporal gene regulation during HIV-1 infection of human CD4 + T cells. Genome Res. 2001;11:1198–204.

105. Lefebvre G, Desfarges S, Uyttebroeck F, Muñoz M, Beerenwinkel N, Rougemont J, et al. Analysis of HIV-1 expression level and sense of transcription by high-throughput sequencing of the infected cell. J Virol. 2011;85(13):6205–11.

106. Kleinman CL, Doria M, Orecchini E, Giuliani E, Galardi S, De Jay N, et al. HIV-1 infection causes a down-regulation of genes involved in ribosome biogenesis. PLoS One. 2014;9(12):1–18.

107. Xu C, Ye B, Han Z, Huang M, Zhu Y. Comparison of transcriptional profiles between CD4+ and CD8+ T cells in HIV type 1-infected patients. AIDS Res Hum Retroviruses. 2014;30(2):134–41.

108. Sharma A, Yilmaz A, Marsh K, Cochrane A, Boris-Lawrie K. Thriving under stress: selective

translation of HIV-1 structural protein mRNA during Vpr-mediated impairment of eIF4E translation activity. Ross SR, editor. PLoS Pathog. 2012 Mar 22;8(3):e1002612.

109. Chang ST, Sova P, Peng X, Weiss J. Next-generation sequencing reveals HIV-1-mediated suppression of T cell activation and RNA processing and regulation of noncoding RNA expression in a CD4+ T. MBio. 2011;2(5):1–9.

110. Stewart SA, Poon B, Jowett JB, Chen IS. Human immunodeficiency virus type 1 Vpr induces apoptosis following cell cycle arrest. J Virol. 1997 Jul 1;71(7):5579–92.

111. Amini S, Khalili K, Sawaya BE. Effect of HIV-1 Vpr on Cell Cycle Regulators. DNA Cell Biol. 2004 Apr;23(4):249–60.

112. Elder RT, Yu M, Chen M, Zhu X, Yanagida M, Zhao Y. HIV-1 Vpr induces cell cycle G2 arrest in fission yeast (Schizosaccharomyces pombe) through a pathway involving regulatory and catalytic subunits of PP2A and acting on both Wee1 and Cdc25. Virology. 2001 Sep 1;287(2):359–70.

113. Wu JQ, Dwyer DE, Dyer WB, Yang YH, Wang B, Saksena NK. Genome-wide analysis of primary CD4+ and CD8+ T cell transcriptomes shows evidence for a network of enriched pathways associated with HIV disease. Retrovirology. 2011;8(1):18.

114. Simmons A, Aluvihare V, McMichael A. Nef triggers a transcriptional program in T cells imitating single-signal T cell activation and inducing HIV virulence mediators. Immunity. 2001 Jun 1;14(6):763–77.

115. Mohammadi P, Desfarges S, Bartha I, Joos B, Zangger N, Muñoz M, et al. 24 hours in the life of HIV-1 in a T cell line. PLoS Pathog. 2013;9(1):e1003161.

116. Perfettini J-L, Roumier T, Castedo M, Larochette N, Boya P, Raynal B, et al. NF-κB and p53 are the dominant apoptosis-inducing transcription factors elicited by the HIV-1 envelope. J Exp Med. 2004 Mar 1;199(5):629–40.

117. Fenard D, Yonemoto W, Noronha C de, Cavrois M, Williams SA, Greene WC. Nef is physically recruited into the immunological synapse and potentiates T Cell activation early after TCR engagement. J Immunol. 2005 Nov 1;175(9):6050–7.

118. Westendorp M 0, Li-Weber M, Frank RW, Krammeri PH. Human immunodeficiency virus type 1 tat upregulates interleukin-2 secretion in activated T cells. Vol. 68, Journal of virology. 1994.

119. Ott M, Emiliani S, Van Lint C, Herbein G, Lovett J, Chirmule N, et al. Immune hyperactivation of HIV-1-infected T cells mediated by Tat and the CD28 pathway. Science. 1997 Mar 7;275(5305):1481–5.

120. Mehla R, Ayyavoo V. Gene array studies in HIV-1 infection. Curr HIV/AIDS Rep. 2012;9(1):34–43.

121. Bachtel ND, Umviligihozo G, Pickering S, Mota TM, Liang H, Del Prete GQ, et al. HLA-C downregulation by HIV-1 adapts to host HLA genotype. Evans DT, editor. PLOS Pathog. 2018 Sep 4;14(9):e1007257.

122. Ende Z, Deymier MJ, Claiborne DT, Prince JL, Mónaco DC, Kilembe W, et al. HLA Class I downregulation by HIV-1 variants from subtype C transmission pairs. J Virol. 2018 Apr 1;92(7):e01633-17.

123. Liao Q, Wang J, Pei Z, Xu J, Zhang X. Identification of miRNA - mRNA crosstalk in CD4 + T cells during HIV - 1 infection by integrating transcriptome analyses. J Transl Med. 2017;1–11.

124. Rotger M, Dang KK, Fellay J, Heinzen EL, Feng S, Descombes P, et al. Genome-wide mRNA expression correlates of viral control in CD4+ T-Cells from HIV-1-infected individuals. PLoS Pathog. 2010;6(2).

125. Sedaghat AR, German J, Teslovich TM, Cofrancesco J, Jie CC, Talbot CC, et al. Chronic CD4+ T-cell activation and depletion in human immunodeficiency virus type 1 infection: type I interferon-mediated disruption of T-cell dynamics. J Virol. 2008;82(4):1870–83.

126. Schneider WM, Chevillotte MD, Rice CM. Interferon-stimulated genes: a complex web of host defenses. Annu Rev Immunol. 2014;32:513–45.

127. Hyrcza MD, Kovacs C, Loutfy M, Halpenny R, Heisler L, Yang S, et al. Distinct transcriptional profiles in exvVivo CD4+ and CD8+ T cells are established early in Human Immunodeficiency Virus Type 1 infection and are characterized by a chronic interferon response as well as extensive transcriptional changes in CD8+ T cells. J Virol. 2007;81(7):3477–86.

128. Kavanagh Williamson M, Coombes N, Juszczak F, Athanasopoulos M, Khan M, Eykyn T, et al. Upregulation of glucose uptake and hexokinase activity of primary human CD4+ T cells in response to infection with HIV-1. Viruses. 2018 Mar 7;10(3):114.

129. Van't Wout AB, Swain JV, Schindler M, Rao U, Pathmajeyan MS, Mullins JI, et al. Nef induces

multiple genes involved in cholesterol synthesis and uptake in human immunodeficiency virus type 1-infected T cells. J Virol. 2005 Aug;79(15):10053–8.

130. Hawkes D, Jones KL, Smyth RP, Pereira CF, Bittman R, Jaworowski A, et al. Properties of HIV-1 associated cholesterol in addition to raft formation are important for virus infection. Virus Res. 2015 Dec 2;210:18–21.

131. Arendt CW, Littman DR. HIV: master of the host cell. Genome Biol. 2001;2(11).

132. Zheng Y-H, Plemenitas A, Linnemann T, Fackler OT, Peterlin BM. Nef increases infectivity of HIV via lipid rafts. Curr Biol. 2001 Jun 1;11(11):875–9.

133. Rasheed S, Yan JS, Lau A, Chan AS. HIV replication enhances production of free fatty acids, low density lipoproteins and many key proteins involved in lipid metabolism: a proteomics study. Nixon DF, editor. PLoS One. 2008 Aug 20;3(8):e3003.

134. Rose H, Hoy J, Woolley I, Tchoua U, Bukrinsky M, Dart A, et al. HIV infection and high density lipoprotein metabolism. Atherosclerosis. 2008 Jul 1;199(1):79–86.

135. Madge S, Kinloch-de-Loes S, Mercey D, Johnson MA, Weller IVD. Lipodystrophy in patients naive to HIV protease inhibitors. AIDS. 1999;13(6).

136. Wen W, Chen S, Cao Y, Zhu Y, Yamamoto Y. HIV-1 infection initiates changes in the expression of a wide array of genes in U937 promonocytes and HUT78 T cells. Virus Res. 2005;113(1):26–35.

137. Italiani P, Boraschi D. From monocytes to M1/M2 macrophages: phenotypical vs. functional differentiation. Front Immunol. 2014 Oct 17;5.

138. Cassol E, Cassetta L, Rizzi C, Alfano M, Poli G. M1 and M2a polarization of human monocyte-derived macrophages inhibits HIV-1 replication by distinct mechanisms. J Immunol. 2009;182(10):6237–46.

139. Cassol E, Cassetta L, Alfano M, Poli G. Macrophage polarization and HIV-1 infection. J Leukoc Biol. 2010;87(4):599–608.

140. Sieweke MH, Allen JE. Beyond stem cells: Self-renewal of differentiated macrophages. Science (80-). 2013 Nov 22;342(6161):1242974–1242974.

141. Epelman S, Lavine KJ, Randolph GJ. Origin and functions of tissue macrophages. Immunity. 2014 Jul 17;41(1):21–35.

142. Ushach I, Zlotnik A. Biological role of granulocyte macrophage colony-stimulating factor (GM-CSF) and macrophage colony-stimulating factor (M-CSF) on cells of the myeloid lineage. J Leukoc Biol. 2016;100(3):481–9.

143. Koppensteiner H, Brack-Werner R, Schindler M. Macrophages and their relevance in Human Immunodeficiency Virus Type I infection. Retrovirology. 2012;9:82.

144. Murray PJ. Macrophage Polarization. Annu Rev Physiol. 2017 Feb 10;79(1):541–66.

145. Lee B, Sharron M, Montaner LJ, Weissman D, Doms RW. Quantification of CD4, CCR5, and CXCR4 levels on lymphocyte subsets, dendritic cells, and differentially conditioned monocyte-derived macrophages. Proc Natl Acad Sci U S A. 1999;96(9):5215–20.

146. Wang X, Ye L, Hou W, Zhou Y, Wang Y-J, Metzger DS, et al. Cellular microRNA expression correlates with susceptibility of monocytes/macrophages to HIV-1 infection. Blood. 2009 Jan 15;113(3):671–4.

147. Peng G, Greenwell-Wild T, Nares S, Jin W, Lei KJ, Rangel ZG, et al. Myeloid differentiation and susceptibility to HIV-1 are linked to APOBEC3 expression. Blood. 2007 Jul 1;110(1):393–400.

148. Zhu T. HIV-1 in peripheral blood monocytes: an underrated viral source. J Antimicrob Chemother. 2002 Sep;50(3):309–11.

149. Orenstein JM, Fox C, Wahl SM. Macrophages as a source of HIV during opportunistic infections. Science. 1997 Jun 20;276(5320):1857–61.

150. McElrath MJ, Pruett JE, Cohn ZA. Mononuclear phagocytes of blood and bone marrow: comparative roles as viral reservoirs in human immunodeficiency virus type 1 infections. Proc Natl Acad Sci. 1989 Jan 1;86(2):675–9.

151. Rich EA, Chen ISY, Zack JA, Leonard ML, O'Brien WA. Increased susceptibility of differentiated mononuclear phagocytes to productive infection with Human Immunodeficiency Virus-1 (HIV-1). 1992;89:176–83.

152. Van den Bergh R, Florence E, Vlieghe E, Boonefaes T, Grooten J, Houthuys E, et al. Transcriptome analysis of monocyte-HIV interactions. Retrovirology. 2010;7(1):53.

153. Cicala C, Arthos J, Selig SM, Dennis G, Hosack DA, Van Ryk D, et al. HIV envelope induces a cascade of cell signals in non-proliferating target cells that favor virus replication. Proc Natl Acad Sci U S A. 2002;99(14):9380–5.

154. Coberley CR, Kohler JJ, Brown JN, Oshier JT, Baker H V, Popp MP, et al. Impact on genetic networks in human macrophages by a CCR5 strain of Human Immunodeficiency Virus Type 1. J Virol. 2004;78(21):11477–86.

155. Woelk CH, Ottones F, Plotkin CR, Du P, Royer CD, Rought SE, et al. Interferon gene expression following HIV Type 1 infection of monocyte-derived macrophages. AIDS Res Hum Retroviruses. 2004;20(11):1210–22.

156. Zahoor MA, Xue G, Sato H, Murakami T, Takeshima SN, Aida Y. HIV-1 Vpr induces interferon-stimulated genes in human monocyte-derived macrophages. PLoS One. 2014;9(8):e106418.

157. Tilton JC, Johnson AJ, Luskin MR, Manion MM, Yang J, Adelsberger JW, et al. Diminished production of monocyte proinflammatory cytokines during human immunodeficiency virus viremia is mediated by type I interferons. J Virol. 2006;80(23):11486–97.

158. Wu JQ, Ruth Sassé T, Wolkenstein G, Conceicao V, Miranda Saksena M, Soedjono M, et al. Transcriptome analysis of primary monocytes shows global down-regulation of genetic networks in HIV viremic patients versus long-term non-progressors. Virology. 2013;435(2):308–19.

159. Wie SH, Du P, Luong TQ, Rought SE, Beliakova-Bethell N, Lozach J, et al. HIV downregulates interferon-stimulated genes in primary macrophages. J Interf Cytokine Res. 2013;33(2):90–5.

160. Vázquez N, Greenwell-wild T, Marinos NJ, Swaim WD, Nares S, Ott DE, et al. Human Immunodeficiency Virus Type 1-Induced macrophage gene expression includes the p21 gene, a target for viral regulation. J Virol. 2005;79(7):4479–91.

161. Montefiori DC. Protocol for Preparation of Cell Free Stocks of HIV-1 in PBMC [Internet]. 2014 [cited 2019 Feb 4]. Available from: https://www.hiv.lanl.gov/content/nab-reference-strains/html/Protocol-for-Preparation-of-Cell-Free-Stocks-of-HIV-1-in-PBMC-January-2014.pdf

162. Aldovini A, Walker BD, editors. Techniques in HIV research. New York: Stockton Press; 1990.

163. Cecilia D, Kewalramani VN, O'Leary J, Volsky B, Nyambi P, Burda S, et al. Neutralization

profiles of primary Human Immunodeficiency Virus Type 1 isolates in the context of coreceptor usage. J Virol. 1998;72(9):6988–96.

164. Wei X, Decker JM, Liu H, Zhang Z, Arani RB, Kilby JM, et al. Emergence of resistant Human Immunodeficiency Virus Type 1 in patients receiving fusion inhibitor (T-20) monotherapy. Antimicrob Agents Chemother. 2002;46(6):1896–905.

165. Janas AM, Wu L. HIV-1 interactions with cells: from viral binding to cell-cell transmission. Curr Protoc Cell Biol. 2009;Unit–26.5.

166. Wehrly K, Chesebro B. p24 antigen capture assay for quantification of Human Immunodeficiency Virus using readily available inexpensive reagents. Methods. 1997;12(4):288–93.

167. Hong F, Aga E, Cillo AR, Yates AL, Besson G, Fyne E, et al. Novel assays for measurement of total cell-associated HIV-1 DNA and RNA. J Clin Microbiol. 2016;54(4):902–11.

168. Malnati MS, Scarlatti G, Gatto F, Salvatori F, Cassina G, Rutigliano T, et al. A universal real-time PCR assay for the quantification of group-M HIV-1 proviral load. Nat Protoc. 2008;3(7):1240–8.

169. Huang D, Zhuang Y, Zhai S, Song Y, Liu Q, Zhao S, et al. HIV reverse transcriptase activity assay: a feasible surrogate for HIV viral load measurement in China. Diagn Microbiol Infect Dis. 2010;68(3):208–13.

170. Mascola JR, Louder MK, Winter C, Prabhakara R, De Rosa SC, Douek DC, et al. Human Immunodeficiency Virus Type 1 neutralization measured by flow cytometric quantitation of single-round infection of primary human T cells. J Virol. 2002;76(10):4810–21.

171. Baxter AE, Niessl J, Fromentin R, Richard J, Porichis F, Charlebois R, et al. Single-cell characterization of viral translation-competent reservoirs in HIV-infected individuals. Cell Host Microbe. 2016;20(3):368–80.

172. Adan A, Alizada G, Kiraz Y, Baran Y, Nalbant A, Baran Y, et al. Flow cytometry: basic principles and applications. Crit Rev Biotechnol. 2017;37(2):163–76.

173. Cilliers T, Nhlapo J, Coetzer M, Ketas T, Olson WC, Moore JP, et al. The CCR5 and CXCR4 coreceptors are both used by Human Immunodeficiency Virus Type 1. J Virol. 2003;77(7):4449–56.

174. Williamson C, Morris L, Maughan MF, Ping L-H, Dryga S a, Thomas R, et al. Characterization and selection of HIV-1 subtype C isolates for use in vaccine development. AIDS Res Hum Retroviruses. 2003;19(2):133–44.

175. Choge I, Cilliers T, Walker P, Taylor N, Phoswa M, Meyers T, et al. Genotypic and phenotypic characterization of viral isolates from HIV-1 subtype C-infected children with slow and rapid disease progression. AIDS Res Hum Retroviruses. 2006 May;22(5):458–65.

176. Murphy K. Janeway's Immunobiology. 8th ed. New York: Garland Science; 2012.

177. Roederer M. Compensation in flow cytometry. In: Current Protocols in Cytometry. Hoboken, NJ, USA: John Wiley & Sons, Inc.; 2002. p. Unit 1.14.

178. Hulspas R, O'Gorman MRG, Wood BL, Gratama JW, Sutherland DR. Considerations for the control of background fluorescence in clinical flow cytometry. Cytom Part B Clin Cytom. 2009;76B(6):355–64.

179. Andersen MN, Al-Karradi SNH, Kragstrup TW, Hokland M. Elimination of erroneous results in flow cytometry caused by antibody binding to Fc receptors on human monocytes and macrophages. Cytom Part A. 2016;89(11):1001–9.

180. Szalóki G, Goda K. Compensation in multicolor flow cytometry. Cytom Part A. 2015;87(11):982–5.

181. Primrose SB, Twyman RM. Principles of Gene Manipulation and Genomics. 7th ed. Malden: Blackwell Publishing; 2006.

182. Pierce BA. Genetics: A Conceptual Approach. 4th ed. New York: W. H. Freeman and Company; 2012.

183. Geijtenbeek TB., Kwon DS, Torensma R, van Vliet SJ, van Duijnhoven GC., Middel J, et al. DC-SIGN, a dendritic cell–specific HIV-1-binding protein that enhances trans-infection of T cells. Cell. 2000;100(5):587–97.

184. Bounou S, Giguère J, Cantin R, Gilbert C, Imbeault M, Martin G, et al. The importance of virus-associated host ICAM-1 in human immunodeficiency virus type 1 dissemination depends on the cellular context. FASEB J. 2004;18(11):1294–6.

185. Kolte L, Gaardbo JC, Skogstrand K, Ryder LP, Ersbøll AK, Nielsen SD. Increased levels of

regulatory T cells (Tregs) in human immunodeficiency virus-infected patients after 5 years of highly active anti-retroviral therapy may be due to increased thymic production of naive Tregs. Clin Exp Immunol. 2009;155(1):44–52.

186. Nunez R. DNA measurement and cell cycle analysis by flow cytometry. Curr Issues Mol Biol. 2001;3(3):67–70.

187. Vödrös D, Tscherning-Casper C, Navea L, Schols D, De Clercq E, Fenyö EM. Quantitative evaluation of HIV-1 coreceptor use in the GHOST(3) cell assay. Virology. 2001;291(1):1–11.

188. Cronin J, Zhang X-Y, Reiser J. Altering the tropism of lentiviral vectors through pseudotyping. Curr Gene Ther. 2005;5(4):387–98.

189. Fellay J, Shianna K V., Telenti A, Goldstein DB. Host genetics and HIV-1: The final phase? PLoS Pathog. 2010;6(10):1–9.

190. Rato S, Rausell A, Muñoz M, Telenti A, Ciuffi A. Single-cell analysis identifies cellular markers of the HIV permissive cell. PLoS Pathog. 2017;13(10):e1006678.

191. Biancotto A, Iglehart SJ, Vanpouille C, Condack CE, Lisco A, Ruecker E, et al. HIV-1 induced activation of CD4+ T cells creates new targets for HIV-1 infection in human lymphoid tissue ex vivo. Blood. 2008;111(2):699–704.

192. Stevenson M, Stanwick TL, Dempsey MP, Lamonica CA. HIV-1 replication is controlled at the level of T cell activation and proviral integration. EMBO J. 1990;9(5):1551–60.

193. Gowda SD, Stein BS, Mohagheghpour N, Benike CJ, Engleman EG. Evidence that T cell activation is required for HIV-1 entry in CD4+ lymphocytes. J Immunol. 1989;142(3):773–80.

194. Liszewski MK, Yu JJ, O'Doherty U. Detecting HIV-1 integration by repetitive-sampling Alu-gag PCR. Methods. 2009;47(4):254–60.

195. De Spiegelaere W, Malatinkova E, Lynch L, Van Nieuwerburgh F, Messiaen P, O'Doherty U, et al. Quantification of integrated HIV DNA by repetitive-sampling Alu-HIV PCR on the basis of poisson statistics. Clin Chem. 2014;60(6):886–95.

196. Brussel A, Delelis O, Sonigo P. Alu-LTR real-time nested PCR assay for quantifying integrated HIV-1 DNA. Methods Mol Biol. 2005;304:139–54.

197. Imbeault M, Lodge R, Ouellet M, Tremblay MJ. Efficient magnetic bead-based separation of HIV-1-infected cells using an improved reporter virus system reveals that p53 up-regulation occurs exclusively in the virus-expressing cell population. Virology. 2009 Oct 10;393(1):160–7.

198. Sussman JJ, Bonifacino JS, Lippincott-Schwartz J, Weissman AM, Saito T, Klausner RD, et al. Failure to synthesize the T Cell CD3-ζ chain: Structure and function of a partial T cell receptor complex. Cell. 1988 Jan 15;52(1):85–95.

199. Sharpe M, Mount N. Genetically modified T cells in cancer therapy: opportunities and challenges. Dis Model Mech. 2015 Apr 1;8(4):337–50.

200. Hess K, Yang Y, Golech S, Sharov A, Becker KG, Weng N. Kinetic assessment of general gene expression changes during human naive CD4+ T cell activation. Int Immunol. 2004 Dec;16(12):1711–21.

201. Cliff JM, Andrade INJ, Mistry R, Clayton CL, Lennon MG, Lewis AP, et al. Differential gene expression identifies novel markers of CD4+ and CD8+ T cell activation following stimulation by Mycobacterium tuberculosis. J Immunol. 2004 Jul 1;173(1):485–93.

202. Trickett A, Kwan YL. T cell stimulation and expansion using anti-CD3 / CD28 beads. J Immunol Methods. 2003;275:251–5.

203. Maier R, Matilde Bartolomé -Rodríguez M, Moulon C, Weltzien HU, Meyerhans A. Kinetics of CXCR4 and CCR5 up-regulation and human immunodeficiency virus expansion after antigenic stimulation of primary CD4 T lymphocytes. Blood. 2000;96(5):1853–6.

204. Halvorsen R, Leivestad T, Gaudernack G, Thorsby E. Role of accessory cells in the activation of pure T cells via the T Cell Receptor-CD3 complex or with phytohaemagglutinin. 1988;555–63.

205. Tuttle DL, Harrison JK, Anders C, Sleasman JW, Goodenow MM. Expression of CCR5 increases during monocyte differentiation and directly mediates macrophage susceptibility to infection by human immunodeficiency virus type 1. J Virol. 1998;72(6):4962–9.

206. Wang J, Roderiquez G, Oravecz T, Norcross M a. Cytokine regulation of human immunodeficiency virus type 1 entry and replication in human monocytes/macrophages through modulation of CCR5 expression. J Virol. 1998;72(9):7642–7.

207. Naif HM, Li S, Alali M, Sloane A, Wu L, Kelly M, et al. CCR5 expression correlates with susceptibility of maturing monocytes to human immunodeficiency virus type 1 infection. J

Virol. 1998;72(1):830–6.

208. Viola A, Luster AD. Chemokines and their receptors: Drug targets in immunity and inflammation. Annu Rev Pharmacol Toxicol. 2008 Feb;48(1):171–97.

209. Glad C, Borrebaeck CA. Affinity of phytohemagglutinin (PHA) isolectins for serum proteins and regulation of the lectin-induced lymphocyte transformation. J Immunol. 1984 Oct;133(4):2126–32.

210. Rudd CE. Upstream-downstream: CD28 cosignaling pathways and T cell function. Immunity. 1996 Jun 1;4(6):527–34.

211. Duarte RF, Chen FE, Lowdell MW, Potter MN, Lamana ML, Prentice HG, et al. Functional impairment of human T-lymphocytes following PHA-induced expansion and retroviral transduction: implications for gene therapy. Gene. 2002;1359–68.

212. Groot F, Russell RA, Baxter AE, Welsch S, Duncan CJ, Willberg C, et al. Efficient macrophage infection by phagocytosis of dying HIV-1 -infected CD4+T cells. Retrovirology. 2011 Dec 3;8(S2):O31.

213. Bleul CC, Wu L, Hoxie JA, Springer TA, Mackay CR. The HIV coreceptors CXCR4 and CCR5 are differentially expressed and regulated on human T lymphocytes. Immunology. 1997;94:1925–30.

214. Riley JL, Levine BL, Craighead N, Francomano T, Kim D, Carroll RG, et al. Naïve and memory CD4 T cells differ in their susceptibilities to human immunodeficiency virus type 1 infection following CD28 costimulation: implications for transmission and pathogenesis. J Virol. 1998 Oct;72(10):8273–80.

215. Schweighardt B, Roy A-M, Meiklejohn DA, Ii EJG, Moretto WJ, Heymann JJ, et al. R5 Human Immunodeficiency Virus Type 1 (HIV-1) replicates more efficiently in primary CD4 T-cell cultures than X4 HIV-1. J Virol. 2004;78(17):9164–73.

216. Carroll RG, Riley JL, Levine BL, Feng Y, Kaushal S, Ritchey DW, et al. Differential regulation of HIV-1 fusion cofactor expression by CD28 costimulation of CD4+ T cells. Science. 1997;276(5310):273–6.

217. Sato K, Kawasaki H, Nagayama H, Enomoto M, Morimoto C, Tadokoro K, et al. Chemokine receptor expressions and responsiveness of cord blood T cells. J Immunol. 2001 Feb

1;166(3):1659–66.

218. Secchiero P, Zella D, Curreli S, Mirandola P, Capitani S, Gallo RC, et al. Engagement of CD28 modulates CXC Chemokine Receptor 4 surface expression in both resting and CD3-stimulated CD4+ T cells. J Immunol. 2000;164:4018–24.

219. Ebert LM, McColl SR. Up-regulation of CCR5 and CCR6 on distinct subpopulations of antigen-activated CD4+ T lymphocytes. J Immunol. 2002 Jan 1;162(1):186–94.

220. Akagawa KS. Functional heterogeneity of colony-stimulating factor-induced human monocyte-derived macrophages. Int J Hematol. 2002 Jul;76(1):27–34.

221. Leidi M, Gotti E, Bologna L, Miranda E, Rimoldi M, Sica A, et al. M2 macrophages phagocytose rituximab-opsonized leukemic targets more efficiently than M1 cells in vitro. J Immunol. 2009;182:4415–22.

222. Mukherjee R, Kanti Barman P, Kumar Thatoi P, Tripathy R, Kumar Das B, Ravindran B. Non-classical monocytes display inflammatory features: Validation in sepsis and systemic lupus erythematous. Sci Rep. 2015 Nov 11;5(1):13886.

223. Tanaka M, Krutzik SR, Sieling PA, Lee DJ, Rea TH, Modlin RL, et al. Activation of Fc gamma RI on monocytes triggers differentiation into immature dendritic cells that induce autoreactive T cell responses. J Immunol. 2009 Aug 15;183(4):2349–55.

224. Ambarus CA, Krausz S, van Eijk M, Hamann J, Radstake TRDJ, Reedquist KA, et al. Systematic validation of specific phenotypic markers for in vitro polarized human macrophages. J Immunol Methods. 2012 Jan 31;375(1–2):196–206.

225. Lescoat A, Ballerie A, Augagneur Y, Morzadec C, Vernhet L, Fardel O, et al. Distinct properties of human M-CSF and GM-CSF monocyte-derived macrophages to simulate pathological lung conditions in vitro: application to systemic and inflammatory disorders with pulmonary involvement. Int J Mol Sci. 2018 Mar 17;19(3):894.

226. Graziani-Bowering GM, Filion LG. Down regulation of CD4 expression following isolation and culture of human monocytes. Clin Diagn Lab Immunol. 2000 Mar;7(2):182–91.

227. Kazazi F, Mathijs J-M, Foley P, Cunningham AL. Variations in CD4 expression by human monocytes and macrophages and their relationship to infection with the Human Immunodeficiency Virus. J Gen Virol. 1989 Oct 1;70(10):2661–72.

228. Di Marzio P, Tse J, Landau NR. Chemokine receptor regulation and HIV Type 1 tropism in monocyte-macrophages. AIDS Res Hum Retroviruses. 1998 Jan 20;14(2):129–38.

229. Oswald-Richter K, Grill SM, Leelawong M, Unutmaz D. HIV infection of primary human T cells is determined by tunable thresholds of T cell activation. Eur J Immunol. 2004 Jun 1;34(6):1705–14.

230. Sylwester A, Murphy S, Shutt D, Soll DR. HIV-induced T cell syncytia are self-perpetuating and the primary cause of T cell death in culture. J Immunol. 1997 Apr 15;158(8):3996–4007.

231. Pantaleo G, Butini L, Graziosi C, Poli G, Schnittman SM, Greenhouse JJ, et al. Human immunodeficiency virus (HIV) infection in CD4+ T lymphocytes genetically deficient in LFA-1: LFA-1 is required for HIV-mediated cell fusion but not for viral transmission. J Exp Med. 1991;173(2):511–4.

232. Lifson JD, Feinberg MB, Reyes GR, Rabin L, Banapour B, Chakrabarti S, et al. Induction of CD4-dependent cell fusion by the HTLV-III/LAV envelope glycoprotein. Nature. 1986 Oct;323(6090):725–8.

233. Cobos Jiménez V, Booiman T, de Taeye SW, van Dort KA, Rits MAN, Hamann J, et al. Differential expression of HIV-1 interfering factors in monocyte-derived macrophages stimulated with polarizing cytokines or interferons. Sci Rep. 2012 Dec 23;2(1):763.

234. San Segundo-Val I, Sanz-Lozano CS. Introduction to the Gene Expression Analysis. In: Isidoro-García M, editor. Molecular Genetics of Asthma (Methods in Molecular Biology). New York: Humana Press; 2016. p. 29–43.

235. Pfaffl MW. A new mathematical model for relative quantification in real-time RT-PCR. Nucleic Acids Res. 2001;29(9):e45.

236. Wang Z, Gerstein M, Snyder M. RNA-Seq: a revolutionary tool for transcriptomics. Nat Rev Genet. 2009 Jan;10(1):57–63.

237. Iglesias-Ussel M, Vandergeeten C, Marchionni L, Chomont N, Romerio F. High levels of CD2 expression identify HIV-1 latently infected resting memory CD4+ T cells in virally suppressed subjects. J Virol. 2013;87(16):9148–58.

238. Morou AK, Porichis F, Krambovitis E, Sourvinos G, Spandidos D a, Zafiropoulos A. The HIV-1 gp120/V3 modifies the response of uninfected CD4 T cells to antigen presentation: mapping

of the specific transcriptional signature. J Transl Med. 2011;9(1):160.

239. Shin J-M, Yoo K-J, Kim M-S, Kim D, Baek K-H. Hyaluronan-and RNA-binding deubiquitinating enzymes of USP17 family members associated with cell viability. 2006;

240. Lim K-H, Ramakrishna S, Baek K-H. Molecular mechanisms and functions of cytokine-inducible deubiquitinating enzymes. Cytokine Growth Factor Rev. 2013 Oct;24(5):427–31.

241. Masuhara M, Nagao K, Nishikawa M, Kimura T, Nakano T. Enhanced degradation of MDM2 by a nuclear envelope component, mouse germ cell-less. Biochem Biophys Res Commun. 2003 Sep 5;308(4):927–32.

242. Wilkinson JC, Richter BWM, Wilkinson AS, Burstein E, Rumble JM, Balliu B, et al. VIAF, a Conserved Inhibitor of Apoptosis (IAP)-interacting Factor That Modulates Caspase Activation. J Biol Chem. 2004 Dec 3;279(49):51091–9.

243. Van't Wout AB, Lehrman GK, Mikheeva SA, O'Keeffe GC, Katze MG, Bumgarner RE, et al. Cellular gene expression upon human immunodeficiency virus type 1 infection of CD4+-T-cell lines. J Virol. 2003 Jan;77(2):1392–402.

244. Paul S, Schaefer BC. A new look at T cell receptor signaling to nuclear factor-κB. Trends Immunol. 2013 Jun;34(6):269–81.

245. Pande V, Ramos MJ. Nuclear factor kappa B: a potential target for anti-HIV chemotherapy. Curr Med Chem. 2003 Aug;10(16):1603–15.

246. Hedl M, Abraham C. A TPL2 (MAP3K8) disease-risk polymorphism increases TPL2 expression thereby leading to increased pattern recognition receptor-initiated caspase-1 and caspase-8 activation, signalling and cytokine secretion. Gut. 2016;65(11):1799–811.

247. Dhanasekaran DN, Reddy EP. JNK signaling in apoptosis. Oncogene. 2008 Oct 20;27(48):6245–51.

248. Clark AM, Reynolds SH, Anderson M, Wiest JS. Mutational activation of the MAP3K8 protooncogene in lung cancer. Genes Chromosomes Cancer. 2004 Oct;41(2):99–108.

249. Canonne-Hergaux F, Aunis D, Schaeffer E. Interactions of the transcription factor AP-1 with the long terminal repeat of different human immunodeficiency virus type 1 strains in Jurkat, glial, and neuronal cells. J Virol. 1995 Nov;69(11):6634–42.

250. Zhang Y, Feng X-H, Derynck R. Smad3 and Smad4 cooperate with c-Jun/c-Fos to mediate TGF-β-induced transcription. Nature. 1998 Aug 27;394(6696):909–13.

251. Jang C-W, Chen C-H, Chen C-C, Chen J, Su Y-H, Chen R-H. TGF-β induces apoptosis through Smad-mediated expression of DAP-kinase. Nat Cell Biol. 2002 Jan 10;4(1):51–8.

252. Wan X, Helman LJ. Levels of PTEN protein modulate Akt phosphorylation on serine 473, but not on threonine 308, in IGF-II-overexpressing rhabdomyosarcomas cells. Oncogene. 2003 Nov 6;22(50):8205–11.

253. Carnero A, Blanco-Aparicio C, Renner O, Link W, Leal JFM. The PTEN/PI3K/AKT signalling pathway in cancer, therapeutic implications. Curr Cancer Drug Targets. 2008 May;8(3):187–98.

254. Lu X-X, Cao L-Y, Chen X, Xiao J, Zou Y, Chen Q. PTEN inhibits cell proliferation, promotes cell apoptosis, and induces cell cycle arrest via downregulating the PI3K/AKT/hTERT pathway in lung adenocarcinoma A549 cells. Biomed Res Int. 2016;2476842.

255. Kim N, Kukkonen S, Gupta S, Aldovini A. Association of Tat with promoters of PTEN and PP2A subunits is key to transcriptional activation of apoptotic pathways in HIV-infected CD4+ T cells. Rice AP, editor. PLoS Pathog. 2010 Sep 16;6(9):e1001103.

256. Appay V, Sauce D. Immune activation and inflammation in HIV-1 infection: causes and consequences. J Pathol. 2008 Jan 1;214(2):231–41.

257. Williams A, Steffens F, Reinecke C, Meyer D. The Th1/Th2/Th17 cytokine profile of HIV-infected individuals: A multivariate cytokinomics approach. Cytokine. 2013 Feb 1;61(2):521–6.

258. Rhodes DA, Chen H-C, Price AJ, Keeble AH, Davey MS, James LC, et al. Activation of human γδ T cells by cytosolic interactions of BTN3A1 with soluble phosphoantigens and the cytoskeletal adaptor periplakin. J Immunol. 2015 Mar 1;194(5):2390–8.

259. Lee W, Kim S, Baek SY, Lee GR. Transcription factor IRF8 controls Th1-like regulatory T-cell function. 2015;13.

260. Fiscella M, Perry JW, Teng B, Bloom M, Zhang C, Leung K, et al. TIP, a T-cell factor identified using high-throughput screening increases survival in a graft-versus-host disease model. Nat Biotechnol. 2003 Mar 24;21(3):302–7.

261. Mizuma H, Litwin S, Zolla-Pazner S. B-cell activation in HIV infection: relationship of spontaneous immunoglobulin secretion to various immunological parameters. Vol. 71, Clin. exp. Immunol. 1988.

262. Vincent C, Cozon G, Zittoun M, Mellquist M, Kazatchkine MD, Czerkinsky C, et al. Secretory immunoglobulins in serum from human immunodeficiency virus (HIV)-infected patients. J Clin Immunol. 1992 Sep;12(5):381–8.

263. Moretta L, Moretta A. Killer immunoglobulin-like receptors. Curr Opin Immunol. 2004 Oct;16(5):626–33.

264. Wang L, Zhang Y, Xu K, Dong T, Rowland-Jones S, Yindom L-M. Killer-cell immunoglobulin-like receptors associate with HIV-1 infection in a narrow-source Han Chinese cohort. PLoS One. 2018;13(4):e0195452.

265. Boelen L, Debebe B, Silveira M, Salam A, Makinde J, Roberts C h., et al. Inhibitory killer cell immunoglobulin-like receptors strengthen CD8 + T cell–mediated control of HIV-1, HCV, and HTLV-1. Sci Immunol. 2018 Nov 9;3(29):eaao2892.

266. Balasubramaniam M, Pandhare J, Dash C. Are microRNAs important players in HIV-1 infection? An update. Viruses. 2018;10(3):e110.

267. Goodrich JA, Kugel JF. Non-coding-RNA regulators of RNA polymerase II transcription. Nat Rev Mol Cell Biol. 2006 Aug 24;7(8):612–6.

268. Gupta A, Titus Brown C, Zheng Y-H, Adami C. Differentially-expressed pseudogenes in HIV-1 infection. Viruses. 2015;7:5191–5205.

269. Ciuffi A, Rato S, Telenti A, Ciuffi A, Rato S, Telenti A. Single-cell genomics for virology. Viruses. 2016 May 4;8(5):123.

270. Golumbeanu M, Cristinelli S, Rato S, Munoz M, Cavassini M, Beerenwinkel N, et al. Single-cell RNA-Seq reveals transcriptional heterogeneity in latent and reactivated HIV-infected cells. Cell Rep. 2018;23:942–50.

271. Salmon P. Mycoplasma assay [Internet]. [cited 2019 May 11]. Available from: http://lentilab.unige.ch/mycoplasmaassay.html